

Conserving Time Integrators for Nonlinear Elastodynamics

vom Fachbereich Maschinenbau und Verfahrenstechnik
der Technischen Universität Kaiserslautern
zur Verleihung des akademischen Grades
Doktor-Ingenieur (Dr.-Ing.)
genehmigte Dissertation

von Dipl.-Ing. Michael Groß

Hauptreferent:	Prof. Dr.-Ing. Paul Steinmann
Korreferenten:	Prof. Dr.-Ing. Peter Betsch Prof. Dr.-Ing. Karl Schweizerhof
Vorsitzender:	Prof. Dr.-Ing. Bernd Sauer
Dekan:	Prof. Dr.-Ing. Paul Steinmann

Tag der Einreichung: 21. Oktober 2003

Tag der mündl. Prüfung: 10. März 2004

Kaiserslautern, März 2004

D 386

Vorwort

...Der Wert davon, dass man zeitweilig eine strenge Wissenschaft streng betrieben hat, beruht nicht gerade in deren Ergebnissen: denn diese werden, im Verhältnis zum Meere des Wissenswerten, ein verschwindend kleiner Tropfen sein. Aber es ergibt einen Zuwachs an Energie, an Schlußvermögen, an Zähigkeit der Ausdauer; man hat gelernt, einen Zweck zweckmäßig zu erreichen. Insofern ist es sehr schätzbar, in Hinsicht auf Alles, was man später treibt, einmal ein wissenschaftlicher Mensch gewesen zu sein...

Friedrich Nietzsche.

Die vorliegende Arbeit entstand während meiner Tätigkeit als wissenschaftlicher Mitarbeiter am Lehrstuhl für Technische Mechanik (LTM) an der Technischen Universität Kaiserslautern während der Bearbeitung des von der Deutschen Forschungsgemeinschaft (DFG) finanzierten Forschungsprojektes STE 544/13-1 mit dem Titel ‘Galerkin basierte Zeitintegratoren für die nichtlineare Elastodynamik’. Die finanzielle Unterstützung seitens der DFG ermöglichte erst diese Arbeit.

Vor allem möchte ich meinen akademischen Lehrern Prof. Dr.-Ing. P. Steinmann und Prof. Dr.-Ing. P. Betsch für die Anregung zu dieser Arbeit, ihre intensive und konsequente wissenschaftliche Förderung sowie die Übernahme des Hauptreferates beziehungsweise eines Korreferates danken. Herrn Prof. Dr.-Ing. P. Steinmann verdanke ich meine Ausbildung auf den Feldern der Kontinuumsmechanik, und Prof. Dr.-Ing. P. Betsch bildete mich im Bereich numerische Mechanik aus. Herrn Prof. Dr.-Ing. K. Schweizerhof danke ich für die Übernahme eines weiteren Korreferats und für sein sehr großes Interesse an dieser Arbeit.

Allen Mitarbeitern des LTM danke ich für die angenehme und freundliche Arbeitssphäre und für die freundliche Zusammenarbeit. Besonders möchte ich Frau C.E. Jeblick und Herrn Dr.-Ing. F.J. Barth für ihre Unterstützung bei allen Problemen des universitären Lebens danken. Nicht vergessen möchte ich Dipl.-Ing. R. Denzer, Dipl.-Ing. J. Glaser und Dipl.-Math. techn. S. Leyendecker für zahlreiche Anmerkungen zu dieser Arbeit.

Meinen Eltern und Schwiegereltern, insbesondere meiner Frau Marion danke ich für ihren starken Rückhalt und ihre großartige Unterstützung.

Kaiserslautern, März 2004

Michael Groß

Zusammenfassung

...Waren die numerischen Verfahren schon immer von Nutzen, so liegt es auf der Hand, dass nunmehr ihre Rolle in der wissenschaftlichen Forschung eine fundamentale Bedeutung erlangt hat. Kein Mathematiker, der sich der modernen angewandten Mathematik bedient, kein Physiker und kein Ingenieur kann heute entsprechend ausgebildet werden, ohne dass ihm ein gewisses Verständniss für numerische Verfahren vermittelt wird...

[83], Vorwort.

Diese Arbeit beinhaltet einen Beitrag zur rechnergestützten numerischen nichtlinearen Elastodynamik. Es wird eine einheitliche Umgebung zur Entwicklung numerischer Methoden für die Zeitintegration beschrieben. Die betrachteten Methoden vererben Erhaltungseigenschaften des zugrundeliegenden mechanischen Systems an das resultierende Zeitschrittverfahren. Diese Zeitschrittverfahren werden als mechanische Integratoren bezeichnet. Im Rahmen der nichtlinearen Elastodynamik werden ausschließlich die Gesamtenergieerhaltung sowie die Erhaltung von Impulsabbildungen betrachtet. Als konkrete Problemstellungen werden Massenpunktsysteme und die semi-diskrete nichtlineare Elastodynamik behandelt.

Mechanische Integratoren zeichnen sich in der Praxis durch exzellente numerische Stabilität auch bei Langzeitberechnungen von steifen Systemen aus. Ihre dabei erreichte Genauigkeit entspricht der eines Standard-Integrators. Aus diesem Grund sind mechanische Integratoren für eine Zeitintegration sehr attraktiv. Jedoch sind die meisten energie- und drehimpulserhaltenden Integratoren zumeist nur von zweiter Ordnung genau. Ist man an einem kleinen Näherungsfehler interessiert, so muss eine kleine Zeitschrittweite

verwendet werden. Dies ist besonders bei Langzeitberechnungen nicht vorteilhaft. Im Gegensatz dazu können die Zeitschrittweiten bei der Verwendung von Integratoren höherer Genauigkeitsordnung erhöht werden. Als einheitliche Umgebung zur Entwicklung von Integratoren höherer Genauigkeitsordnung hat sich die kontinuierliche Galerkin-Methode erwiesen. Insbesondere ist diese Methode gut geeignet um mechanische Integratoren zu entwickeln. Der Grund ist, dass Erhaltungseigenschaften des zugrundeliegenden Systems an die resultierenden Zeitschrittverfahren vererbt werden.

Das Ziel dieser Arbeit ist eine einheitliche Entwicklungsumgebung für energie- und drehimpulserhaltende Integratoren höherer Genauigkeitsordnung für die nichtlineare Elastodynamik. Dies führt zu dem Problem wie man die vererbten Erhaltungseigenschaften behält, wenn Zeitintegrale im Zeitschrittverfahren durch eine Quadraturregel approximiert werden. Die Erhaltungseigenschaften der entwickelten mechanischen Integratoren werden in einem verallgemeinerten Problem bewiesen. Die Resultate können dann direkt auf Massenpunktsysteme und auf die semi-diskrete nichtlineare Elastodynamik angewandt werden, da beide Problemklassen dem definierten verallgemeinerten Problem untergeordnet sind. Der Unterschied zwischen Massenpunktsystemen und der semi-diskreten nichtlinearen Elastodynamik liegt in der unterschiedlichen Art der inneren Kräfte. Die inneren Kräfte der Massenpunktsysteme hängen von einem skalarwertigen Vektorfeld ab, den Massenpunktabständen, während in der semi-diskreten nichtlinearen Elastodynamik die inneren Kräfte aus einem tensoriellen Spannungsfeld resultieren.

Die dargestellte Entwicklungsumgebung basiert auf der kontinuierlichen Galerkin-Methode in der Zeit. Diese Methode erzeugt eine Familie von k -stufigen Einschrittverfahren. In den Gleichungen dieser Verfahren befinden sich Zeitintegrale. Werden die Zeitintegrale durch eine Quadraturregel angenähert, so zeigt sich dass die Vererbung der Erhaltungseigenschaften auf einer Kollokation in k Quadraturpunkten basiert. Da die betrachteten Impulsabbildungen maximal quadratische Invarianten sind, muss die k -Punkt Gaußregel mit der Genauigkeitsordnung $2k$ verwendet werden. Wir nennen diese Familie von Zeitschrittverfahren verbunden mit einer k -Punkt Gaußregel die $cG(k)$ -Methode. Es werden konservative Systeme mit einer im allgemeinen nichtlinearen potentiellen Energie betrachtet. Im Falle einer approximierten Integration wird deshalb Energieerhal-

tung über eine neue Projektionsmethode erreicht. Diese Projektionsmethode muss die unterschiedliche Art der inneren Kräfte bei den Massensystemen und bei der semi-diskreten Elastodynamik berücksichtigen. Der Unterschied wird verursacht durch die unterschiedlichen Verzerrungsmaße. Aus diesem Grund ist die Projektionsmethode unabhängig von der Form des verwendeten Verzerrungsmaßes gehalten. Die erwähnten Modifikationen der $cG(k)$ -Methode führen letztendlich auf eine erweiterte $cG(k)$ -Methode.

Abstract

...The book is motivated by the rapidly increasing dependence on numerical methods in mathematical modelling driven by the development of powerful computers accessible to everyone...

[44], Preface.

In computational dynamics, energy and momentum conserving time integrators are well established for also integrating stiff mechanical problems for long time periods. However, previously developed energy and momentum conserving integrators are mostly second order accurate. So the error can be only bounded by a very small time step size, which is not worthwhile in respect of long run-times. Higher order integrators however allow for larger time steps, which leads to shorter runs.

The present work is therefore concerned with a unified development of higher order energy and momentum conserving time integrators for nonlinear elastodynamics. The work in particular considers many-particle dynamics and semi-discrete elastodynamics. The developed unified framework is based on the continuous Galerkin (cG) method in time. In the last years, the cG method turned out to be especially well suited for designing energy and momentum conserving time integrators due to its inherent conservation properties.

This work shows that energy conservation can be achieved for all accuracy orders by applying a new projection technique. Total linear and angular momentum is obtained by collocation at Gaussian quadrature points. Numerical examples for the specific problems are presented for illustrating the well performance of the designed higher order conserving time integrators. They exhibit excellent numerical stability in the presence of stiffness without a compromise in accuracy relative to standard integrators of comparable order.

The numerical investigations also includes an efficiency comparison of the developed higher order integrator with a well-known integrator of comparable order. It is shown that in general a higher order integrator renders less CPU time to obtain a constant relative global error, and that the better stability of the developed integrator however must be paid by a more costly matrix assembly.

Contents

Abstract	ix
1 Introduction	1
1.1 Modelling in elastodynamics	2
1.2 Computational dynamics	4
1.3 Motivation for mechanical integrators	6
1.4 Design of mechanical integrators	8
1.5 Outline	10
2 The generalised problem	13
2.1 Lagrangian formulation	14
2.2 Hamiltonian formulation	17
2.3 Total energy conservation	20
2.4 Conservation of momentum maps	21
2.4.1 Noether's theorem	21
2.4.2 Actions of Lie groups	23
2.4.3 Momentum maps	27
2.4.4 Total linear momentum conservation	28
2.4.5 Total angular momentum conservation	29
2.5 Strain measures for deformations	31
2.6 Superimposed rigid body motions	33
3 Galerkin-based time discretisation	35

3.1	Finite element discretisation in time	36
3.2	The continuous Galerkin (cG) method	37
3.2.1	Implicit time stepping schemes	37
3.2.2	Collocation property	39
3.2.3	Total energy conservation	41
3.2.4	Total linear momentum conservation	43
3.2.5	Total angular momentum conservation	44
3.2.6	Iterative solution procedure	44
3.3	The discontinuous Galerkin (dG) method	47
4	One-particle dynamics in a central force field	51
4.1	Hamiltonian formulation	52
4.2	Galerkin-based time discretisation	53
4.3	Design criterion for energy conservation	54
4.4	Enhanced derivative	55
4.5	Assumed distance approximation	58
4.6	Enhanced assumed derivative	59
4.7	The enhanced Galerkin (eG) method	60
4.8	Numerical investigations	61
4.8.1	Linearisation of the algorithms	62
4.8.2	Stiff Neo-Hooke type spring potential	63
4.8.3	Discussion of the results	64
5	Dynamics of many-particle systems	69
5.1	Hamiltonian formulation	70
5.2	Galerkin-based time discretisation	71
5.3	Design criterion for energy conservation	72
5.4	Enhanced derivative	73
5.5	Assumed distance approximation	74
5.6	Enhanced assumed derivative	76
5.7	The enhanced Galerkin (eG) method	77

5.8	Numerical investigations	78
5.8.1	Linearisation of the algorithms	78
5.8.2	Stiff Neo-Hooke type spring potentials	79
5.8.3	Discussion of the results	80
6	Semi-discrete nonlinear elastodynamics	89
6.1	Finite element discretisation in space	90
6.2	Hamiltonian formulation	93
6.3	Galerkin-based time discretisation	96
6.4	Design criterion for energy conservation	97
6.5	Enhanced gradient	98
6.6	Assumed strain approximation	99
6.7	Enhanced assumed gradient	101
6.8	The enhanced Galerkin (eG) method	102
6.9	Numerical investigations	104
6.9.1	Linearisation of the algorithms	104
6.9.2	Compressible Neo-Hooke material	105
6.9.3	Discussion of the results	106
7	Conclusions	121
7.1	The main results	122
7.2	Outlook	123
A	Geometric mechanics	127
A.1	Euclidean spaces	128
A.2	The tangent space	129
A.3	The cotangent space	130
A.4	Bilinear forms on vector spaces	131
A.5	Lie groups	132
A.6	An isoperimetrical problem	133

B	The direct matrix product	137
B.1	The definition	137
B.2	The transpose	138
B.3	The product	138
B.4	The inverse	139
C	Notes on the cG(k) method	141
C.1	Implementation matrices	141
C.1.1	Linear time finite elements ($k = 1$)	141
C.1.2	Quadratic time finite elements ($k = 2$)	142
C.1.3	Cubic time finite elements ($k = 3$)	142
C.1.4	Quartic time finite elements ($k = 4$)	143
C.2	Error estimate for a nodal time interpolation	143
C.3	Accuracy of the cG(k) method at the time nodes	145
D	The assembly operator	147
	Bibliography	149

Chapter 1

Introduction

...Galerkin's principle is flexible enough to apply also to initial-value problems...They still have important advantages over finite differences, for general geometries and for problems which evolve comparatively slowly in time...

[130], Chapter 7: Initial-value problems.

Computer-aided design is nowadays an important component in mechanical engineering. For example, testing of prototypes is increasingly being replaced by computational simulation because this provides a more rapid and less expensive way to evaluate the design. In the field of automotive design, simulation of car motions is replacing test drives and simulation of processes is speeding the design in manufacturing.

Technical systems in mechanical engineering have to satisfy contradictory requirements. High accelerations cause high dynamical forces, which require stiff and heavy constructions. On the other hand, power consumption should be reduced by using lightweight structures, for instance, in wheel suspensions of modern high performance cars or in manipulators of manufacturing robots. Accordingly, if one is interested in simulating motions of such mechanical systems, the elastic deformation of flexible bodies has to be taken into consideration. First the material model of the elastic bodies has to be identified, for example hyperelasticity, and then the flexible body itself has to be modelled, for instance with spatial finite elements or configurations of mass points.

This contribution is concerned with computing motions of hyperelastic continuum bodies. Since the motions are computed in a computational setting, discrete models for elastic bodies are introduced. The dynamical simulation of these models should reproduce the main physical features, which guarantees that the simulation remains qualitatively accurate. The developed numerical integration method has therefore particular properties, which are especially important while integrating mechanical systems.

1.1 Modelling in elastodynamics

Motions of continuum bodies are described by partial differential equations arising from localising the mechanical laws governing the continuum motion. The solutions of these equations of motion depend on the position in the Euclidean space and on the time. Since analytical solutions of these equations only exist for a very limited set of mostly academic problems, the exact solution has to be generally approximated. The approximating solutions are usually determined in a computational setting. These approximating functions can be possibly piecewise interpolating polynomials if we partition the space in which we approximate the solution. This furnishes a finite number of subspaces to which are usually referred to as *elements*. The coefficients of the polynomial basis functions are related to nodal points, the so-called *element nodes*, bordering the considered elements. This kind of approximation is called a *finite element approximation*. Using a finite element approximation for the spatial dependence (see Figure 1.1b), the mass of the body remains homogeneous distributed over the whole space between the nodes. The hyperelastic connection between the nodes emanates from an approximated tensor field. For further details see [17, 148, 14].

A more discrete model of a continuum body is given by a many-particle system arising from a triangulation of the continuum body in imaginary elements. The particles represent the centres of mass pertaining to these imaginary elements of the body (see Figure 1.1c). The mass of the body is then concentrated in these particles [75]. The hyperelasticity of the material is modelled by discrete nonlinear springs between the particles. This problem is included in the so-called *N-body problem* or *many-body problem* which can be described

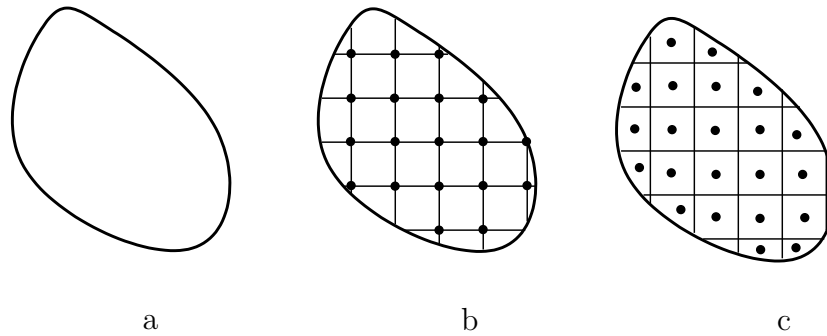


Figure 1.1. Discrete models of the continuum body (a) can be a finite element discretisation with element nodes (b) or a configuration of particles (c).

as follows: Given the initial positions and velocities of a certain number of particles which attract one another by forces of interaction, one has to determine their configuration at any time in the future.

The motions of both above mentioned discrete systems can be divided into small scale and large scale motions, namely deformations of the body and rigid body motions, respectively. Rigid body motions can be translations as well as rotations. A more simple discrete model which can be used to investigate deformations and superimposed rotations is given by a circular pendulum with an elastic rod in the absence of gravitation (see Figure 1.2), which can be often found in the literature as an introduction model for nonlinear elastodynamics. This problem is a special case of the so-called *one-body central force problem* in which one particle is moving under the influence of a force field vectored to the origin of an inertial coordinate system. The one-body central force problem usually emanates from reducing the dynamics of the two-body problem, as mentioned in books on classical mechanics.

The aforementioned discrete models for elastodynamics represent finite-dimensional mechanical systems wherein the motions of the nodes or the particles are described by nonlinear ordinary differential equations in time. These equations of motion are usually derived in the Lagrangian or the Hamiltonian formalism of dynamics, in which first integrals of the equations of motion can be simply deduced by symmetry properties of the underlying system. Symmetries can be based on an invariance with respect to time-reversal or with respect to Lie group actions on each node or each particle, for instance.

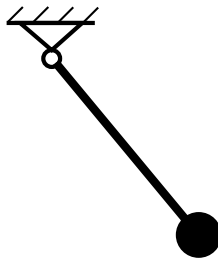


Figure 1.2. Circular pendulum with elastic rod in the absence of gravitation.

The first symmetry leads to total energy conservation and the latter renders conservation of the corresponding momentum maps. For example, a symmetry with respect to translations or rotations renders conservation of linear or angular momentum, respectively.

1.2 Computational dynamics

Considering finite-dimensional mechanical systems, the numerical integration of the corresponding equations of motion can be performed by finite difference schemes [116, 142, 128, 129, 131, 59, 60, 119, 65, 64, 130, 141] and by integrators which are based on numerical quadrature (see [29] for example). The latter include the Runge-Kutta schemes [65, 64, 132, 38, 68] and integrators arising from Galerkin methods in time. We have to distinguish between two different Galerkin methods [44, 86]: The continuous Galerkin method in time [45, 82, 81, 48], which can be traced back at least to [135, 42] for parabolic problems as well as to [82, 81] for ordinary differential equations, and the discontinuous Galerkin method in time [138, 87, 78, 16, 15, 27, 72, 80, 79, 87, 88, 107, 108, 117], which is often accredited to [98]. Finite difference schemes are commonly at most second order accurate whereas Runge-Kutta schemes and schemes arising from Galerkin methods in time are higher order accurate.

In the last decade, numerical integrators have been designed, which inherit major physical properties of the underlying mechanical system. The most considered physical properties are the symplecticity of Hamiltonian flows and the conservation of first integrals of the equations of motion. The conservation of first integrals in particular played a central role in the numerical integration of finite-dimensional mechanical systems. Integrators

preserving one or more of these physical properties have been referred to as *mechanical integrators* [104]. Mechanical integrators are in general either symplectic and momentum conserving or energy and momentum conserving [56, 57, 58, 95, 96, 94, 77, 123, 125, 126, 120, 51, 52, 54, 53]. The reason is that energy conserving integrators cannot be symplectic for a constant time step size according to [145, 146]. In the present work, however, we restrict ourselves to energy and momentum conserving mechanical integrators because they are generally the more practical time integration schemes in the context of elastodynamics [54, 121, 55].

Most of the previously developed energy conserving mechanical integrators are designed by modifying finite difference schemes which are at most second order accurate. A fourth order accurate integrator can be then obtained by the successive application of a second order integrator with different time step sizes, the so-called *sub-stepping procedure* [137, 39]. The design of mechanical integrators by applying a Galerkin method in time has been less noted even though in [48] an energy preserving continuous Galerkin method has been already presented. That has changed in the last few years because the design of higher order mechanical integrators is possible with the continuous Galerkin method in time [22, 19, 20, 21, 18, 67]. The temporal discontinuous Galerkin method, however, does not seem to be as well suited for designing mechanical integrators as the continuous Galerkin method in time [62, 63]. The discontinuous Galerkin method in time is established for solving differential equations with a dissipative or parabolic nature such as diffusion dominated problems which possess a smoothing effect in the solution. (See [44] for the numerical treatment of heat conduction and viscous flow).

In the past, second order accurate integrators have been favoured over higher order accurate integrators for large scale systems of ordinary differential equations. One reason for that can be traced back to a theorem which states the so-called *Dahlquist-barrier* (see [37, 38]). The Dahlquist-barrier restricts the maximum attainable accuracy of A-stable linear multi-step methods to second order. The A-stability refers to the behaviour of the scheme while integrating an linear ordinary differential equation. This concept of stability is based on a condition on the eigenvalues of this differential equation. Another reason are the larger resulting linear systems of higher order implicit schemes. The limit

of A-stability for higher accuracy orders is however confused in [43, 143] for collocation methods based on Gauss points. Examples for collocation methods are implicit Runge-Kutta methods [26] or continuous Galerkin methods in time associated with a certain number of quadrature points [82, 81]. The algebraic stability of Runge-Kutta methods is proved in [30, 10, 25]. This stability is based on conditions on the Butcher-arrays corresponding to the Runge-Kutta methods. An algebraic stable Runge-Kutta method is also A-stable. (See [40] for a detailed discussion of the stability notions of Runge-Kutta methods). The stability of a fourth order accurate mechanical integrator is shown in [137].

1.3 Motivation for mechanical integrators

A numerical solution of the equations of motion is an approximation with an global error $e = C h_n^{p+1}$, where h_n and p denote the time step size and the order of accuracy, respectively. Since the factor C generally grows in time due to rounding and approximation errors [44, 136], a numerical solution may be no longer accurate in long term calculations. Then a fixed error bound at a certain final time T can be achieved by small time steps or by a larger time step size if the accuracy is increased [136, 22]. A higher order accurate integrator, however, may be more costly as a lower order accurate integrator due to a larger linear algebraic system which has to be solved. So one has to investigate the computational cost before one is able to decide which accuracy order p is effective.

The exact reproduction of physical properties however guarantees that the numerical solution remains at least qualitatively accurate because the numerical solution is then embedded in the right solution space [123]. This may be one of the reasons why mechanical integrators perform especially well in long term calculations (see [51, 53, 123, 121], among other papers listed in this work). Conservation laws of mechanical systems in particular play a central role in dynamics because the corresponding first integrals of the motion allow the reduction of the solution space [104, 106, 1]. Conservation of angular momentum and total energy, for example, reduce the dynamics of a free rigid body to a completely integrable one-degree of freedom problem [106, 123] (see Figure 1.3). The exact reproduction of conservation laws is also helpful in the stability analysis of integrators

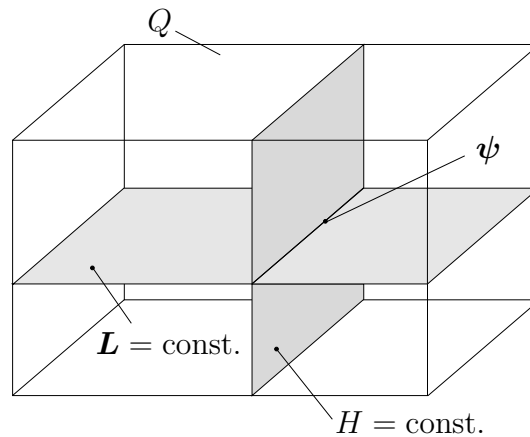


Figure 1.3. The free motion ψ of a body in the configuration space Q is the intersection of the level set of constant angular momentum $\mathbf{L} = \text{const.}$ and the surface of constant energy $H = \text{const.}$

[116, 122, 124]. Nonlinear stability of a solution is often related to the notion of *Lyapunov stability*. A solution is Lyapunov stable if the so-called *Lyapunov function* is bounded. Since the total energy of a system fulfils the requirements for a Lyapunov function [116], energy conserving integrators may be consequently regarded as unconditionally numerically stable [54]. The preservation of momentum maps alleviates the stability analysis further [122, 124, 5, 6] because an additionally preserved momentum map again reduces the dimension of the solution space [54].

The continuous Galerkin method in time is a unified framework for developing higher order accurate integrators for ordinary differential equations [42, 81, 82, 48, 44, 22, 19, 20, 21]. The accuracy depends on the degree of the shape functions and on the quadrature rule used for calculating the remaining integrals. The continuous Galerkin method in time moreover turns out to be especially well suited for designing mechanical integrators due to its inherent conservation properties. The continuous Galerkin method in time associated with a distinct number of Gauss points is a collocation method [82] and leads to the so-called implicit Gauss Runge-Kutta methods [22]. In [118], there has been shown that implicit Gauss Runge-Kutta methods are symplectic and preserve all at most quadratic invariants such as total linear and angular momentum. The conservation of at most quadratic momentum maps has been therefore observed for the continuous Galerkin method in time [22, 19, 20, 21].

In summary, the development of higher order mechanical integrators for large scale systems is currently of interest. A unified framework for designing higher order symplectic and momentum conserving integrators is given by the continuous Galerkin method in time. However, a systematic development of higher order energy and momentum conserving integrators is not available in the currently published literature. The goal of this work is to fill this gap. The newly developed higher order energy and momentum conserving integrators are based on appropriate modifications of a continuous Galerkin method in time.

1.4 Design of mechanical integrators

Two universally applicable approaches for designing energy and momentum conserving integrators can be found in the literature: Projecting the numerical solution of a non-conserving integrator onto a conserving solution space (see Figure 1.4) and deriving a mechanical integrator from a discrete variational principle [140]. In this connection, a number of projection techniques have been proposed:

1. Enforcing conservation laws by a scalar parameter which can be determined by an additional equation in the linear system of equations [77, 125, 126, 147, 99, 136].
2. Modifying quadrature points (in the present context called the collocation parameters) or the weights of a standard quadrature rule so that the conservation law is fulfilled along with a preservation of the original accuracy order of the quadrature rule [123, 48].
3. Replacing the ordinary derivative of a potential with a conserving discrete derivative [56, 57, 58, 95, 96, 94, 51, 52, 54, 53, 120].
4. Determining test functions of a continuous Galerkin method so that the conservation law is satisfied [67].

In the case of the first two techniques, however, there is not clear that a projection by scalars is always possible, especially if several conservation laws are to be simultaneously

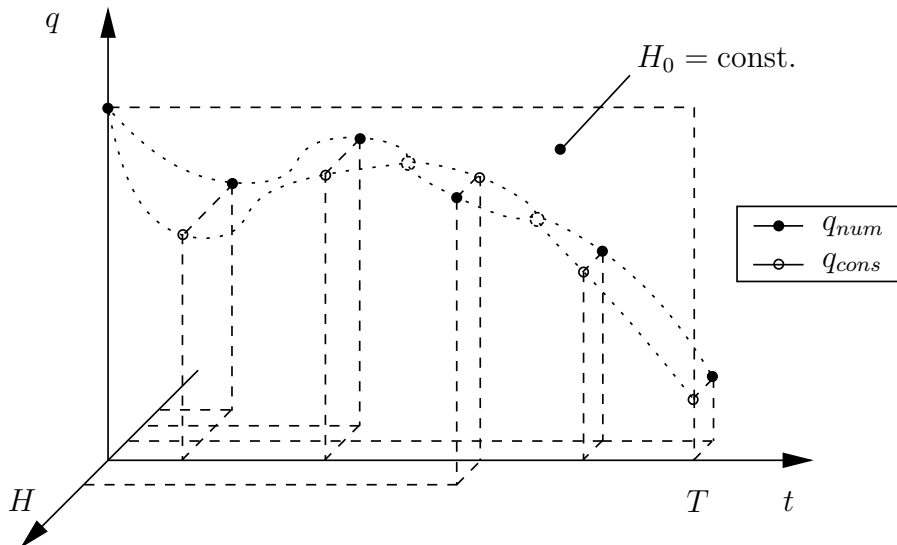


Figure 1.4. The numerical solution q_{num} in the interval $[0, T]$ is projected to the surface $H_0 = \text{const.}$ of a first integral H and results in a H-conserving numerical solution q_{cons} .

satisfied [136], or if the internal forces depend on a tensor field such as in semi-discrete elastodynamics. This can lead to convergence problems in a iterative solution procedure.

Integrators based on discrete variational principles are called *variational integrators* [90], which fulfil the three fundamental properties of autonomous Hamiltonian systems with symmetry, namely the conservation of the symplectic structure as well as the conservation of total energy and momentum maps [89]. This is possible by an adaptively determined time step size according to [146]. This approach is applied to nonlinear elastodynamics in [100] and led to *asynchronous variational integrators*. The term ‘asynchronous’ is based upon the possibility of having different time steps for different elements in the finite element mesh. The resulting algorithms satisfy also the energy and momentum balance for each element.

Mechanical integrators arising from the above mentioned approaches are however at most second order accurate with exception of the mechanical integrators in [48] and [67], which both are applied to scalar problems. Note that in [136, 137], there is demonstrated a possibility for increasing the accuracy from second order to fourth order. In this work, there is presented a further projection technique. The ordinary derivative (or gradient) of a potential is replaced with a continuous *function* which conserves a first integral as constraint. This specific technique leads to mechanical integrators being not bounded in the

accuracy order because no discrete derivatives (or gradients) are used. Since the dimension of the function value and of the function argument is not restricted, the projection method is well suited for problems in several dimensions. This projection technique is applied to the constraint of energy conservation in the context of the continuous Galerkin method in time. The developed approach is specifically applied to the above presented discrete models for elastodynamics, namely particle dynamics and semi-discrete nonlinear elastodynamics. In this way, we designed higher order energy and momentum conserving integrators for both problem classes. We in particular give a detailed account of the computational setting of the designed integrators associated with linear, quadratic, cubic and quartic time finite elements. Consequently, mechanical integrators up to eighth order accuracy have been implemented. The conservation properties are investigated in numerical examples for which accuracy aspects are also investigated in the light of computational effort. The resulting error diagrams can be used to compare the efficiency of a class of integrators related to linear, quadratic and cubic time finite elements.

1.5 Outline

Chapter 2 begins by introducing a generalised problem which covers the considered particle dynamics and semi-discrete elastodynamics. This provides a unified treatment of the major physical properties behind each considered problem.

In Chapter 3, the applied Galerkin-based continuous time discretisation of the equations of motion is presented. Conservation properties of the emanating family of integrators are investigated by applying a main feature of the Galerkin method. Some aspects about the iterative solution procedure for these integrators are also presented. A compact matrix representation allows for a compact description of the algorithmic structure of the whole family of integrators. Finally, a discontinuous time discretisation of the equations of motions is discussed for comparison.

A family of higher order mechanical integrators for dynamics of one particle in a central force field is deduced in Chapter 4. This problem is often used just for illustrating the fundamental difficulties arising in nonlinear elastodynamics or as benchmark problem for

evaluating numerical integrators. The conservation properties, the accuracy as well as the numerical cost of the proposed mechanical integrators are investigated by means of three-dimensional numerical examples. The numerical investigations culminate in a specific diagram which depicts the connection between accuracy and computational effort. In this way, the issue of numerical efficiency is discussed in the context of linear, quadratic and cubic time finite elements.

In Chapter 5, we are concerned with computing three-dimensional motions of many-particle systems. New mechanical integrators for this problem are designed and examined as well. The numerical investigations are analogous to those in the previous chapter.

Higher order mechanical integrators for semi-discrete nonlinear elastodynamics are derived in Chapter 6. The term ‘semi-discrete’ refers to a separate spatial discretisation of a solid continuum body by finite elements. Motions of two-dimensional as well as three-dimensional solid continuum bodies, which exhibits nonlinear hyperelastic material behaviour, are considered in the numerical examples. The spatial discretisation is based on four and eight node Lagrange finite elements, respectively. (See [76] for a definition of these elements).

In Chapter 7, a summary of the main results and some concluding remarks on the presented developments are given.

In an Appendix, additional theoretical as well as numerical aspects, which are relevant to the presented treatment, are summarised for completeness.

Chapter 2

The generalised problem

...The advantage of considering a problem in abstract form is that we can emphasise the essential ingredients and moreover we can apply results for the abstract problem to specific applications, as soon as the assumptions of the abstract problem are satisfied, without having to go through the same type of argument over and over again...

[44], Chapter 21: The Power of Abstraction.

This work is concerned with mechanical integrators for particle dynamics as well as semi-discrete nonlinear elastodynamics. More precisely, we are interested in integrators preserving the conservation laws of these problems. These problems have a common structure because they eventually describe the motion of material points placed in the Euclidean space. In the case of particle dynamics, the material points are the particles and in semi-discrete nonlinear elastodynamics, the spatial nodes represent the material points. Hence the formulations of these problems can be derived from a generalised problem describing motions of a set of material points arranged in a configuration. The kinematic and dynamic aspects of this generalised problem show the distinction of the similarities of particle dynamics as well as semi-discrete nonlinear elastodynamics presented below.

First we present the Lagrangian and Hamiltonian formulation of the generalised problem. We then deduce the conservation laws arising from symmetries of the generalised problem, which are based on an invariance with respect to time-reversal and with respect to Lie group actions on each material point. The first symmetry leads to total energy

conservation and the latter renders conservation of the corresponding momentum maps. These conservation laws will be preserved by the mechanical integrators designed in this work. We are finally investigate deformations and rigid body motions of configurations of material points. These latter investigations prepare for a convenient time approximations of strain measures for the generalised problem in the chapters below.

A more detailed description of the considered formulations can be found in standard books about geometrical methods in mechanics, for example [106, 1, 104, 9, 8, 93, 50]. Further background material about the kinematics are given in books on nonlinear solid mechanics or continuum mechanics such as [74, 105, 110, 103]. A review of the relevant kinematic topics can be found in [17, 142, 23, 113].

2.1 Lagrangian formulation

We define a set $\bar{\mathcal{B}}$ of n_{poi} material points which are arranged in a configuration \mathcal{B}_t at a given time t . The configuration \mathcal{B}_t is embedded in the Euclidean space $\mathbb{R}^{n_{dim}}$ (see Figure 2.1). We identify any material point A , $A = 1, \dots, n_{poi}$, in this configuration \mathcal{B}_t by its position vector $\mathbf{q}^A \in \mathbb{R}^{n_{dim}}$. We assume free motions of the set $\bar{\mathcal{B}}$ such that the number of degrees of freedom reads $n_{dof} = n_{dim}n_{poi}$. The configuration space Q of the material points is then an open set in the n_{dof} -dimensional Euclidean space $\mathbb{R}^{n_{dof}}$. Points in Q are denoted by the vector $\mathbf{q} = (\mathbf{q}^1, \dots, \mathbf{q}^{n_{poi}}) \in Q$ to which we refer to as the *coordinate vector* of the configuration. A motion of the system in a time interval $I_t = [t_a, t_b]$ between two configurations $\mathbf{q}_a = \mathbf{q}(t_a)$ and $\mathbf{q}_b = \mathbf{q}(t_b)$ is the curve $\boldsymbol{\psi} : I_t \ni t \mapsto \mathbf{q}(t) \in Q$. We define a set

$$\mathcal{Q} = \{\boldsymbol{\psi} : I_t \rightarrow Q \mid \boldsymbol{\psi} \text{ smooth, } \boldsymbol{\psi}(t_a) = \mathbf{q}_a \text{ and } \boldsymbol{\psi}(t_b) = \mathbf{q}_b\} \quad (2.1)$$

including all possible motions between the two configurations \mathbf{q}_a and \mathbf{q}_b . Let such a motion be influenced by a conservative force field acting on all material points. This conservative force field is associated with a potential energy $V : Q \rightarrow \mathbb{R}$. We suppose a potential energy $V(\mathbf{q})$ possessing gradients $\nabla_{\mathbf{q}}V$ of the special form

$$\nabla_{\mathbf{q}}V(\mathbf{q}) = \mathbb{Q}(\mathbf{q}) \mathbf{q}. \quad (2.2)$$

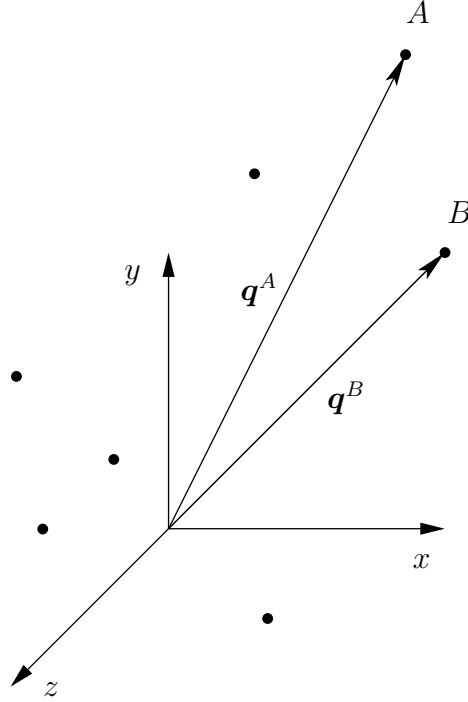


Figure 2.1. The geometry of the generalised problem.

The matrix $\mathbb{Q} \in \mathbb{R}^{n_{dof} \times n_{dof}}$ denotes a nonlinear symmetric stiffness matrix which has a block structure of the form

$$\mathbb{Q}(\mathbf{q}) = \mathbf{Q}(\mathbf{q}) \otimes \mathbf{I}_{n_{dim}}, \quad (2.3)$$

with the structure matrix

$$\mathbf{Q}(\mathbf{q}) = \begin{bmatrix} Q_{11}(\mathbf{q}) & \cdots & Q_{1n_{poi}}(\mathbf{q}) \\ \vdots & & \vdots \\ Q_{n_{poi}1}(\mathbf{q}) & \cdots & Q_{n_{poi}n_{poi}}(\mathbf{q}) \end{bmatrix} \in \mathbb{R}^{n_{poi} \times n_{poi}} \quad (2.4)$$

The matrix $\mathbf{I}_{n_{dim}}$ is the $n_{dim} \times n_{dim}$ identity matrix and the symbol \otimes denotes the direct matrix product.

Let a superimposed dot denote differentiation with respect to time t . We refer to the vector $\dot{\mathbf{q}}$ as the *velocity vector* of the configuration. The velocity vector $\dot{\mathbf{q}}$ is the tangent vector on the configuration space Q at position \mathbf{q} . The corresponding tangent space $T_{\mathbf{q}}Q$ is then given by $T_{\mathbf{q}}Q = \mathbb{R}^{n_{dof}}$. The tangent space $T_{\psi}Q \subset T_{\mathbf{q}}Q$ includes the tangent vectors to the curve ψ . The associated velocity curve $\dot{\psi}$ is given by $\dot{\psi} : I_t \ni t \mapsto \dot{\mathbf{q}}(t) \in T_{\psi}Q$

which is a mapping to the tangent vector $\dot{\mathbf{q}}(t)$ of the motion $\boldsymbol{\psi}$ at time t . The kinetic energy $T : T_{\boldsymbol{\psi}}Q \rightarrow \mathbb{R}$ of the system is a quadratic form in the velocity vector:

$$T(\dot{\mathbf{q}}) = \frac{1}{2} \dot{\mathbf{q}} \cdot \mathbb{M} \dot{\mathbf{q}}, \quad (2.5)$$

with a nonsingular symmetric mass matrix $\mathbb{M} \in \mathbb{R}^{n_{dof} \times n_{dof}}$ which is constant due to conservation of mass and has the following block structure:

$$\mathbb{M} = \mathbf{M} \otimes \mathbf{I}_{n_{dim}}, \quad (2.6)$$

with a structure matrix

$$\mathbf{M} = \begin{bmatrix} M_{11} & \dots & M_{1n_{poi}} \\ \vdots & & \vdots \\ M_{n_{poi}1} & \dots & M_{n_{poi}n_{poi}} \end{bmatrix} \in \mathbb{R}^{n_{poi} \times n_{poi}} \quad (2.7)$$

Note that a diagonal structure matrix \mathbf{M} denotes a concentration of the mass in the material points.

The principle of Hamilton states that an actual motion $\boldsymbol{\psi}$ minimises the functional $\mathcal{S} : \mathcal{Q} \rightarrow \mathbb{R}$ which is defined by $\mathcal{S} = \int_{t_a}^{t_b} L(\mathbf{q}(t), \dot{\mathbf{q}}(t)) dt$, with the function $L : TQ \rightarrow \mathbb{R}$ called the Lagrangian. The space $TQ = Q \times T_{\boldsymbol{\psi}}Q$ designates the tangent bundle of Q with the coordinates $(\mathbf{q}^1, \dots, \mathbf{q}^{n_{poi}}, \dot{\mathbf{q}}^1, \dots, \dot{\mathbf{q}}^{n_{poi}}) \in TQ$ in which the dynamics are described. The necessary condition for this variational problem is given by the following Euler-Lagrange equations:

$$\frac{d}{dt} \nabla_{\dot{\mathbf{q}}} L(\mathbf{q}, \dot{\mathbf{q}}) = \nabla_{\mathbf{q}} L(\mathbf{q}, \dot{\mathbf{q}}). \quad (2.8)$$

The Lagrangian $L(\mathbf{q}, \dot{\mathbf{q}})$ for the considered mechanical system is the difference of the kinetic energy $T(\dot{\mathbf{q}})$ from the potential energy $V(\mathbf{q})$. Employing this Lagrangian and equation (2.5) in the Euler-Lagrange equations (2.8), we obtain the following set of ordinary differential equations:

$$\mathbb{M} \ddot{\mathbf{q}} = -\nabla_{\mathbf{q}} V(\mathbf{q}). \quad (2.9)$$

The equations of motion follow from equations (2.9) by employing the assumed gradi-

ent (2.2) of the potential energy:

$$\boxed{\mathbb{M} \ddot{\mathbf{q}} = -\mathbb{Q}(\mathbf{q})\mathbf{q}} \quad (2.10)$$

Note that if an external force \mathbf{F}^A , which depends explicitly on the time t , acts on the material point \mathbf{q}^A , the equation of motion has to be augmented by the external force vector $\mathbf{F} = (\mathbf{F}^1, \dots, \mathbf{F}^{n_{poi}})$ of the configuration:

$$\mathbb{M} \ddot{\mathbf{q}} = -\mathbb{Q}(\mathbf{q})\mathbf{q} + \mathbf{F}. \quad (2.11)$$

Remark 2.1. The gradient (2.2) generate high and low frequency oscillations, because the matrix $\mathbb{M}^{-\frac{1}{2}} \nabla_{\mathbf{q}}^2 V \mathbb{M}^{-\frac{1}{2}}$ has large and small eigenvalues, respectively [49, 61]. The solution of equation (2.10) therefore has the form of high frequency oscillations superimposed by a low frequency oscillating motion. Mechanical systems with such solutions are called *stiff* [132, 102] or *highly oscillatory* [115, 11, 12, 85, 84]. In the considered mechanical systems, there are accordingly two vastly different time scales present. The faster time scale generally has a negligible effect on the motion of the configuration so that its resolution by the integrator is not important for obtaining an accurate motion.

2.2 Hamiltonian formulation

We consider the configuration \mathcal{B}_t in the phase space $P = T^*Q$ which is an open set in the $2n_{dof}$ -dimensional Euclidean space $\mathbb{R}^{n_{dof}} \times \mathbb{R}^{n_{dof}} \simeq \mathbb{R}^{2n_{dof}}$. Points in P are denoted by the vector $\mathbf{z} = (\mathbf{q}, \mathbf{p}) \in P$, where we refer to $\mathbf{p} = (\mathbf{p}^1, \dots, \mathbf{p}^{n_{poi}}) \in \mathbb{R}^{n_{dof}}$ as *conjugate momentum vector*. The space $T^*Q = Q \times T_{\mathbf{q}}^*Q$ denotes the cotangent bundle of the configuration space Q , which has the coordinates \mathbf{q} and \mathbf{p} . The cotangent space $T_{\mathbf{q}}^*Q$ corresponding to the configuration space Q is given by $T_{\mathbf{q}}^*Q = \mathbb{R}^{n_{dof}}$. A motion ζ_a of the system in a time interval $I_t = [t_a, t_b]$ starting at the point $\mathbf{z}_a = \mathbf{z}(t_a)$ in the phase space P is the curve $\zeta_a : I_t \times P \ni (t, \mathbf{z}_a) \mapsto \mathbf{z}(t) \in P$. The tangent vectors to the curve ζ_a are elements of the tangent space $T_{\zeta_a} P \subset T_{\mathbf{z}} P = \mathbb{R}^{2n_{dof}}$. The associated velocity curve $\dot{\zeta}$ is given by $\dot{\zeta}_a : I_t \ni t \mapsto \dot{\mathbf{z}}(t) \in T_{\zeta_a} P$ which is a mapping to the tangent vector $\dot{\mathbf{z}}(t)$ of the motion ζ_a

at time t . We pass from the coordinates $(\mathbf{q}, \dot{\mathbf{q}})$ of the tangent bundle to the coordinates (\mathbf{q}, \mathbf{p}) of the cotangent bundle by applying the Legendre transformation $\mathbb{F}L : TQ \rightarrow T^*Q$ which is defined by

$$\mathbb{F}L(\mathbf{v}) \cdot \mathbf{w} = \left. \frac{d}{ds} \right|_{s=0} L(\mathbf{q}, \mathbf{v} + s\mathbf{w}), \quad \mathbf{v}, \mathbf{w} \in T_{\mathbf{q}}Q. \quad (2.12)$$

The Legendre transformation $\mathbb{F}L$ is a so-called *fibre derivative* because it maps the fibre $T_{\mathbf{q}}Q$ to the fibre $T_{\mathbf{q}}^*Q$. Applying the Legendre transformation (2.12) to the Lagrange function of the generalised problem, we obtain the relation

$$(\mathbf{q}, \mathbf{p}) = \mathbb{F}L(\mathbf{q}, \dot{\mathbf{q}}) = (\mathbf{q}, \nabla_{\dot{\mathbf{q}}}L(\mathbf{q}, \dot{\mathbf{q}})), \quad (2.13)$$

which is equivalent to the equation

$$\mathbf{p} = \nabla_{\dot{\mathbf{q}}}L(\mathbf{q}, \dot{\mathbf{q}}) = \mathbb{M} \dot{\mathbf{q}}. \quad (2.14)$$

According to Appendix B, the mass matrix (2.6) is invertible. Equation (2.14) can be therefore solved for $\dot{\mathbf{q}}$:

$$\dot{\mathbf{q}} = \mathbb{M}^{-1}\mathbf{p}. \quad (2.15)$$

The inverse \mathbb{M}^{-1} of the mass matrix reads

$$\mathbb{M}^{-1} = \mathbf{M}^{-1} \otimes \mathbf{I}_{n_{dim}}, \quad (2.16)$$

with the structure matrix

$$\mathbf{M}^{-1} = \begin{bmatrix} M_{11}^{-1} & \dots & M_{1n_{poi}}^{-1} \\ \vdots & & \vdots \\ M_{n_{poi}1}^{-1} & \dots & M_{n_{poi}n_{poi}}^{-1} \end{bmatrix} \in \mathbb{R}^{n_{poi} \times n_{poi}}, \quad (2.17)$$

where M_{AB}^{-1} denotes a scalar entry of the structure matrix \mathbf{M}^{-1} . By using the Legendre transformation, we replace the Lagrangian function $L : TQ \rightarrow \mathbb{R}$ with the Hamiltonian

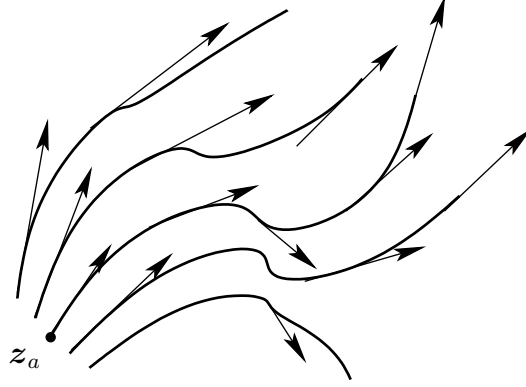


Figure 2.2. Integral curves of a Hamiltonian vector field which is designated by the depicted tangent vectors.

$H : T^*Q \rightarrow \mathbb{R}$ which is given by $H(\mathbf{q}, \mathbf{p}) = \mathbf{p} \cdot \dot{\mathbf{q}}(\mathbf{p}) - L(\mathbf{q}, \dot{\mathbf{q}}(\mathbf{p}))$. Taking equation (2.15) into account, the Hamiltonian takes the form of the total energy of the configuration:

$$H(\mathbf{q}, \mathbf{p}) = T^*(\mathbf{p}) + V(\mathbf{q}), \quad (2.18)$$

with the quadratic form

$$T^*(\mathbf{p}) = \frac{1}{2} \mathbf{p} \cdot \mathbb{M}^{-1} \mathbf{p}, \quad (2.19)$$

defining the kinetic energy $T^* : T_{\mathbf{q}}^*Q \rightarrow \mathbb{R}$ of the system with respect to the cotangent space.

There exists a natural symplectic (canonical) structure $\mathbf{z} \mapsto \Omega$ on the $2n_{dof}$ -dimensional Euclidean space $\mathbb{R}^{n_{dof}} \times \mathbb{R}^{n_{dof}}$, where Ω designates a skew-symmetric bilinear form. This bilinear form on the space $T_{\mathbf{z}}(\mathbb{R}^{n_{dof}} \times \mathbb{R}^{n_{dof}}) = \mathbb{R}^{n_{dof}} \times \mathbb{R}^{n_{dof}}$ is independent of the point \mathbf{z} and given by

$$\Omega(\mathbf{v}, \mathbf{w}) = \mathbf{v} \cdot \mathbb{J} \mathbf{w}, \quad \mathbf{v}, \mathbf{w} \in \mathbb{R}^{n_{dof}} \times \mathbb{R}^{n_{dof}}, \quad (2.20)$$

with the matrix

$$\mathbb{J} = \begin{bmatrix} 0 & 1 \\ -1 & 0 \end{bmatrix} \otimes \mathbf{I}_{n_{dof}}, \quad (2.21)$$

where $\mathbf{I}_{n_{dof}} \in \mathbb{R}^{n_{dof} \times n_{dof}}$ denotes the identity matrix. A natural Hamiltonian system is

characterised by a canonical Hamiltonian vector field $X_H : P \rightarrow T_{\mathbf{z}}P$ defined by

$$X_H(\mathbf{z}) = \Omega^\sharp(\nabla_{\mathbf{z}}H(\mathbf{z})) = \mathbb{J}\nabla_{\mathbf{z}}H(\mathbf{z}). \quad (2.22)$$

An actual motion ζ_a of a natural Hamiltonian system is an integral curve of the canonical Hamiltonian vector field X_H starting at $\mathbf{z}_a \in P$, which is a curve whose tangent space $T_{\zeta_a}P$ is equal to the vector set $\mathcal{V}_{\mathbf{z}} = \{\mathbf{v} \in T_{\mathbf{z}}P | \mathbf{v} = X_H(\mathbf{z}), \mathbf{v}_a = X_H(\mathbf{z}_a)\}$ (see Figure 2.2). The velocity curve $\dot{\zeta}$ is therefore equal to the curve $X_H(\zeta) : I_t \ni t \mapsto \mathbf{v} \in \mathcal{V}_{\zeta}$, which leads to Hamilton's canonical equations of motion being defined by

$$\dot{\mathbf{z}} = X_H(\mathbf{z}) = \mathbb{J}\nabla_{\mathbf{z}}H(\mathbf{z}). \quad (2.23)$$

Using the equations (2.18) and (2.2) in Hamilton's canonical equations (2.23), the equations of motion can be written as the following two ordinary differential equations:

$$\boxed{\begin{aligned} \dot{\mathbf{q}} &= \mathbb{M}^{-1}\mathbf{p}, \\ \dot{\mathbf{p}} &= -\mathbb{Q}(\mathbf{q})\mathbf{q}. \end{aligned}} \quad (2.24)$$

Note that this system of ordinary differential equations does not depend explicitly on the time t . However, if there exist external forces \mathbf{F}^A which depend explicitly on time, the explicitly time-dependent equations of motion read

$$\begin{aligned} \dot{\mathbf{q}} &= \mathbb{M}^{-1}\mathbf{p}, \\ \dot{\mathbf{p}} &= -\mathbb{Q}(\mathbf{q})\mathbf{q} + \mathbf{F}, \end{aligned} \quad (2.25)$$

where $\mathbf{F} = (\mathbf{F}^1, \dots, \mathbf{F}^{n_{poi}})$ denotes the external force vector of the system.

2.3 Total energy conservation

If the Hamiltonian H does not depend explicitly on the time t , then the same motion occurs (but is traced out in reverse order) if t and $-t$ are interchanged. This effect is called the principle of invariance with respect to time-reversal. As consequence, the Hamiltonian

$H(\mathbf{z}(t_a))$ at the starting point $\mathbf{z}(t_a)$ of a motion in an arbitrary time interval $I_t = [t_a, t_b]$ is equal to the Hamiltonian $H(\mathbf{z}(t_b))$ at the end point $\mathbf{z}(t_b)$. Since the total energy of the generalised problem is identical with its Hamiltonian H , the total energy is a constant of the motion as can be easily verified by using the fundamental theorem of calculus:

$$H(\mathbf{z}(t_b)) - H(\mathbf{z}(t_a)) = \int_{t_a}^{t_b} \dot{H}(\mathbf{z}(t)) dt. \quad (2.26)$$

Applying Hamilton's canonical equations (2.23), the time derivative of the Hamiltonian $H(\mathbf{z})$ reads

$$\dot{H}(\mathbf{z}) = \nabla_{\mathbf{z}} H(\mathbf{z}) \cdot \dot{\mathbf{z}} = \nabla_{\mathbf{z}} H(\mathbf{z}) \cdot \mathbb{J} \nabla_{\mathbf{z}} H(\mathbf{z}) = \Omega(\nabla_{\mathbf{z}} H(\mathbf{z}), \nabla_{\mathbf{z}} H(\mathbf{z})). \quad (2.27)$$

The time derivative \dot{H} vanishes owing to the skew-symmetry of Ω and equation (2.26) therefore renders $H(\mathbf{z}(t_b)) = H(\mathbf{z}(t_a))$ which implies total energy conservation.

2.4 Conservation of momentum maps

According to the theorem of E. Noether, there may exist further first integrals in a Hamiltonian system, which are called *momentum maps*. These invariants follow from the eventual symmetry with respect to Lie group actions. In this section, we derive Noether's theorem in the context of the presented generalised problem and introduce the concept of momentum maps to eventually show the conservation of two momentum maps, namely the total linear momentum and the total angular momentum. The introduction of momentum maps therefore shows the derivation and the concept behind the latter both first integrals.

2.4.1 Noether's theorem

The theorem of E. Noether states that to each one-to-one differentiable coordinate transformation which preserves the Lagrangian L of the system, there corresponds a first integral of the equations of motion. If such a coordinate transformation exists one says that this system possesses a *symmetry* [7]. To this end we consider the one-parameter

family of diffeomorphisms $\mathbf{h}_\epsilon : Q \rightarrow Q$, $\epsilon \in \mathbb{R}$, which mean differentiable one-to-one mappings from the configuration space into itself associated with a differentiable inverse. We suppose that this family of mappings form a group with the properties

$$\begin{aligned} \mathbf{h}_0(\mathbf{q}) &= \mathbf{q}, \\ \mathbf{h}_\epsilon^{-1}(\mathbf{q}) &= \mathbf{h}_{-\epsilon}(\mathbf{q}), \quad \text{for any } \epsilon, \epsilon_1, \epsilon_2 \in \mathbb{R}, \mathbf{q} \in Q. \\ \mathbf{h}_{\epsilon_1}(\mathbf{h}_{\epsilon_2}(\mathbf{q})) &= \mathbf{h}_{\epsilon_1+\epsilon_2}(\mathbf{q}), \end{aligned} \quad (2.28)$$

We therefore refer to \mathbf{h}_ϵ as a *one-parameter group of diffeomorphisms*. Here we are only interested in diffeomorphisms \mathbf{h}_ϵ preserving the Lagrangian of the generalised problem, which means $L(\mathbf{q}, \dot{\mathbf{q}}) = L(\mathbf{h}_\epsilon(\mathbf{q}), \dot{\mathbf{h}}_\epsilon(\mathbf{q}))$. The motion $\psi_\epsilon : I_t \ni t \mapsto \mathbf{h}_\epsilon(\mathbf{q}(t)) \in Q$ then also minimises the functional $\mathcal{S}_\epsilon : \mathcal{Q} \rightarrow \mathbb{R}$ given by

$$\mathcal{S}_\epsilon = \int_{t_a}^{t_b} L(\mathbf{h}_\epsilon(\mathbf{q}(t)), \dot{\mathbf{h}}_\epsilon(\mathbf{q}(t))) dt. \quad (2.29)$$

Since the motion $\psi : I_t \ni t \mapsto \mathbf{q}(t) \in Q$ is known by the Euler-Lagrange equations (2.8), the functional \mathcal{S}_ϵ can be considered as a function only depending on the parameter ϵ . The function \mathcal{S}_ϵ then takes a minimum at $\epsilon = 0$ due to the identity property (2.28):

$$\left. \frac{d\mathcal{S}_\epsilon}{d\epsilon} \right|_{\epsilon=0} = 0. \quad (2.30)$$

Taking the chain rule of differentiation into account, the derivative of the function \mathcal{S}_ϵ with respect to ϵ reads

$$\frac{d\mathcal{S}_\epsilon}{d\epsilon} = \int_{t_a}^{t_b} \left[\nabla_{\mathbf{q}} L \cdot \frac{d\mathbf{h}_\epsilon}{d\epsilon} + \nabla_{\dot{\mathbf{q}}} L \cdot \frac{d\dot{\mathbf{h}}_\epsilon}{d\epsilon} \right] dt. \quad (2.31)$$

Using the Euler-Lagrange equation (2.8) in the first term and the permutability of the derivatives in the last term, we obtain

$$\frac{d\mathcal{S}_\epsilon}{d\epsilon} = \int_{t_a}^{t_b} \left[\frac{d}{dt} \nabla_{\dot{\mathbf{q}}} L \cdot \frac{d\mathbf{h}_\epsilon}{d\epsilon} + \nabla_{\dot{\mathbf{q}}} L \cdot \frac{d}{dt} \frac{d\mathbf{h}_\epsilon}{d\epsilon} \right] dt = \int_{t_a}^{t_b} \frac{dJ_\epsilon}{dt} dt, \quad (2.32)$$

where the function $J_\epsilon(\mathbf{q}, \mathbf{p})$ is defined by

$$J_\epsilon(\mathbf{q}, \mathbf{p}) := \mathbf{p} \cdot \frac{d\mathbf{h}_\epsilon(\mathbf{q})}{d\epsilon} \quad (2.33)$$

Note that the dot denotes the dot product of two vectors $\mathbf{u}, \mathbf{v} \in \mathbb{R}^{n_{dof}}$ in the Euclidean space $\mathbb{R}^{n_{dof}}$, which can be also written as

$$\mathbf{u} \cdot \mathbf{v} = \sum_{A=1}^{n_{poi}} \mathbf{u}^A \cdot \mathbf{v}^A, \quad (2.34)$$

where the dot on the right designates the dot product in the Euclidean space $\mathbb{R}^{n_{dim}}$. We now apply the fundamental theorem of calculus to obtain a relation between the function values of J_ϵ at the starting point and the endpoint of the motion:

$$\int_{t_a}^{t_b} \frac{dJ_\epsilon}{dt} dt = J_\epsilon(\mathbf{q}_b, \mathbf{p}_b) - J_\epsilon(\mathbf{q}_a, \mathbf{p}_a), \quad (2.35)$$

where $\mathbf{p}_a = \mathbf{p}(t_a)$ and $\mathbf{p}_b = \mathbf{p}(t_b)$. Taking equation (2.30) into consideration, it follows that the considered dynamical system has the first integral $J : T^*Q \rightarrow \mathbb{R}$ defined by

$$\boxed{J(\mathbf{q}, \mathbf{p}) = \mathbf{p} \cdot \mathbf{X}_h(\mathbf{q})} \quad (2.36)$$

where

$$\mathbf{X}_h(\mathbf{q}) = \left. \frac{d\mathbf{h}_\epsilon(\mathbf{q})}{d\epsilon} \right|_{\epsilon=0} \quad (2.37)$$

is the vector field $\mathbf{X}_h : Q \rightarrow T_{\mathbf{q}}Q$ associated with the one-parameter group \mathbf{h}_ϵ at $\mathbf{q} \in Q$ if the dynamical system *admits the mapping* \mathbf{h}_ϵ which means \mathbf{h}_ϵ preserves the Lagrangian L of the system (see Figure 2.3).

2.4.2 Actions of Lie groups

In the previous section, we considered a one-parameter group $\mathbf{h}_\epsilon : Q \rightarrow Q$, $\epsilon \in \mathbb{R}$, of diffeomorphisms. It turned out that if \mathbf{h}_ϵ preserves the Lagrangian L then there exists a first integral $J : T^*Q \rightarrow \mathbb{R}$ of the equations of motion. For our purposes, we are only interested

in diffeomorphisms \mathbf{h}_ϵ generated by an action of a *Lie group* G with a differentiable binary group operation $\psi : G \times G \rightarrow G$ in an Euclidean space. We consider two Lie groups G throughout our developments. The first group is the *Abelian vector group* $\mathbb{R}^{n_{dim}}$ under the vector addition $\psi(\mathbf{g}_1, \mathbf{g}_2) = \mathbf{g}_1 + \mathbf{g}_2$, for all $\mathbf{g}_1, \mathbf{g}_2 \in \mathbb{R}^{n_{dim}}$. The zero vector $\mathbf{0} \in \mathbb{R}^{n_{dim}}$ is the identity element and the inverse of $\mathbf{g} \in \mathbb{R}^{n_{dim}}$ is $-\mathbf{g}$. The second group is formed from the set of all linear isomorphisms of $\mathbb{R}^{n_{dim}}$ into itself. Taking the matrix multiplication $\psi(\mathbf{g}_1, \mathbf{g}_2) = \mathbf{g}_1 \mathbf{g}_2$, $\forall \mathbf{g}_1, \mathbf{g}_2 \in \mathbb{R}^{n_{dim} \times n_{dim}}$, as binary group operation, we obtain the *general linear group* $GL(n_{dim}, \mathbb{R}^{n_{dim}}) = \{\mathbf{g} \in \mathbb{R}^{n_{dim} \times n_{dim}} \mid \det[\mathbf{g}] \neq 0\}$. The identity element is the $n_{dim} \times n_{dim}$ identity matrix $\mathbf{I}_{n_{dim}}$ and the inverse of the matrix $\mathbf{g} \in \mathbb{R}^{n_{dim} \times n_{dim}}$ is the inverse matrix \mathbf{g}^{-1} .

Let $\phi : G \times Q \rightarrow Q$ be an action of the Lie group G on the configuration space Q . The mapping $\phi_g : Q \rightarrow Q$, $\mathbf{g} \in G$, is then differentiable and there exists an inverse $\phi_g^{-1} = \phi_{g^{-1}}$. We therefore deduce that ϕ_g is one-to-one for each $\mathbf{g} \in G$. Applying the diffeomorphism $\phi_g : Q \rightarrow Q$, we obtain a one-parameter group \mathbf{h}_ϵ of diffeomorphisms if any one-parameter subgroup $\varphi(\epsilon)$ of \mathbf{g} with $\epsilon \in \mathbb{R}$ is given. Therefore, given a curve $\varphi : \mathbb{R} \rightarrow G$ at the identity element $\mathbf{e} \in G$, that is $\varphi(0) = \mathbf{e}$, we call φ a *one-parameter subgroup of G* if $\varphi(\mathbb{R})$ is a subgroup of G and if φ additionally fulfils the following property:

$$\varphi(\epsilon_1 + \epsilon_2) = \psi(\varphi(\epsilon_1), \varphi(\epsilon_2)), \quad \text{for all } \epsilon_1, \epsilon_2 \in \mathbb{R}. \quad (2.38)$$

We can associate a tangent vector $\hat{\xi}$ at the identity $\mathbf{e} \in G$ to each one-parameter subgroup φ , which is defined by

$$\hat{\xi} = \left. \frac{d\varphi(\epsilon)}{d\epsilon} \right|_{\epsilon=0} \in T_{\mathbf{e}}G. \quad (2.39)$$

Conversely, consider any tangent vector $\hat{\xi} \in T_{\mathbf{e}}G$ at $\mathbf{e} \in G$ and for any $\mathbf{g} \in G$ the *left translation map* $\mathbf{L}_g : G \rightarrow G$ which is defined by $\mathbf{L}_g(\mathbf{x}) = \psi(\mathbf{g}, \mathbf{x})$ for all $\mathbf{x} \in G$. The derivative of \mathbf{L}_g at \mathbf{e} is a linear mapping $\nabla_{\mathbf{x}} \mathbf{L}_g(\mathbf{e}) : T_{\mathbf{e}}G \rightarrow T_{\mathbf{g}}G$. Hence we can associate a vector field $\mathbf{X}_{\hat{\xi}} : G \rightarrow T_{\mathbf{e}}G$ to any $\hat{\xi} \in T_{\mathbf{e}}G$. The ordinary differential equation associated with the vector field $\mathbf{X}_{\hat{\xi}}$ and the vector field $\mathbf{X}_{\hat{\xi}}$ itself can be deduced from differentiating the relation $\varphi(\epsilon + \eta) = \psi(\varphi(\epsilon), \varphi(\eta)) = (\mathbf{L}_{\varphi(\epsilon)} \circ \varphi)(\eta)$ at $\eta = 0$. This relation is identical

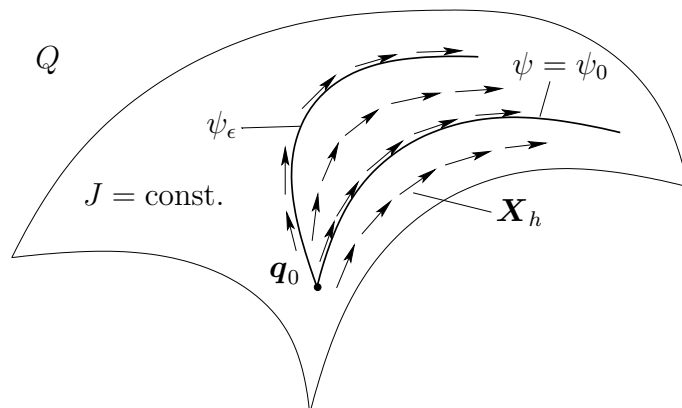


Figure 2.3. The motion ψ_ϵ resulting from the application of the mapping \mathbf{h}_ϵ to the actual motion ψ and ψ itself lie both in the level set of the constant mapping $J(\mathbf{p}, \mathbf{q})$.

to the defining relation (2.38) of a one-parameter subgroup. By differentiating with the chain rule, we obtain

$$\frac{d\varphi(\epsilon)}{d\epsilon} = \left[\nabla_{\mathbf{x}} \mathbf{L}_{\varphi(\epsilon)}(\varphi(\eta)) \cdot \frac{d\varphi(\eta)}{d\eta} \right]_{\eta=0} = \nabla_{\mathbf{x}} \mathbf{L}_{\varphi(\epsilon)}(\mathbf{e}) \cdot \hat{\boldsymbol{\xi}} =: \mathbf{X}_{\hat{\boldsymbol{\xi}}}(\varphi(\epsilon)). \quad (2.40)$$

The vector field $\mathbf{X}_{\hat{\boldsymbol{\xi}}} : G \rightarrow T_{\mathbf{e}}G$ defined in equation (2.40) is called *left invariant* because the diagram in Figure 2.4 commutes.

The tangent space $T_{\mathbf{e}}\mathbb{R}^{n_{dim}}$ of the vector group $\mathbb{R}^{n_{dim}}$ at the identity is isomorphic to $\mathbb{R}^{n_{dim}}$ itself. The left invariant vector field associated with the tangent vector $\hat{\boldsymbol{\xi}} \in T_{\mathbf{e}}\mathbb{R}^{n_{dim}}$ is therefore given by the constant vector field $\mathbf{X}_{\hat{\boldsymbol{\xi}}}(\mathbf{g}) = \hat{\boldsymbol{\xi}}$, for all $\mathbf{g} \in \mathbb{R}^{n_{dim}}$. Considering the general linear group $GL(n_{dim}, \mathbb{R})$, the tangent space $T_{\mathbf{e}}GL(n_{dim}, \mathbb{R})$ is the vector space $L(\mathbb{R}^{n_{dim}}, \mathbb{R}^{n_{dim}})$ of all linear transformations of $\mathbb{R}^{n_{dim}}$ into itself. Hence the left invariant vector field on $GL(n_{dim}, \mathbb{R})$ corresponding to the tangent vector $\hat{\boldsymbol{\xi}} \in L(\mathbb{R}^{n_{dim}}, \mathbb{R}^{n_{dim}})$ is given by the linear vector field $\mathbf{X}_{\hat{\boldsymbol{\xi}}}(\mathbf{g}) = \mathbf{g}\hat{\boldsymbol{\xi}}$, for all $\mathbf{g} \in GL(n_{dim}, \mathbb{R})$.

Let $\varphi(\epsilon)$ be an integral curve of the vector field $\mathbf{X}_{\hat{\boldsymbol{\xi}}} : G \rightarrow T_{\mathbf{e}}G$ with the initial condition $\varphi(0) = \mathbf{e} \in G$. Applying the theory of linear ordinary differential equations, we obtain the solution $\varphi(\epsilon) = \exp[\epsilon\hat{\boldsymbol{\xi}}]$, which is defined in G for all $\epsilon \in \mathbb{R}$. We can thus associate a unique one-parameter subgroup $\varphi_{\hat{\boldsymbol{\xi}}}(\epsilon)$ of G to any $\hat{\boldsymbol{\xi}} \in T_{\mathbf{e}}G$ (see Figure 2.5). Since we can associate a unique element in G via the expression $\varphi_{\hat{\boldsymbol{\xi}}}(1)$ to each $\hat{\boldsymbol{\xi}}$, we can define a mapping $\exp_G : T_{\mathbf{e}}G \rightarrow G$ by the relation $\exp[\hat{\boldsymbol{\xi}}] = \varphi_{\hat{\boldsymbol{\xi}}}(1)$, which is called the *exponential*

$$\begin{array}{ccc}
 TG & \xrightarrow{\nabla L_g} & TG \\
 \uparrow \mathbf{X} & & \uparrow \mathbf{X} \\
 G & \xrightarrow{L_g} & G
 \end{array}$$

Figure 2.4. The commutative diagram of a left invariant vector field \mathbf{X} .

map for G . In particular, \exp_G is a diffeomorphism from a neighbourhood U of $\mathbf{0}$ (zero element) in T_eG onto a neighbourhood V of e in G .

If G is the vector group $\mathbb{R}^{n_{dim}}$ with the tangent space $T_eG \cong \mathbb{R}^{n_{dim}}$, the exponential map $\exp_V : \mathbb{R}^{n_{dim}} \rightarrow \mathbb{R}^{n_{dim}}$ is the identity map. We have therefore a one-parameter subgroup for any $\hat{\xi} \in T_eG$, which is given by $\varphi_{\hat{\xi}}(\epsilon) = \exp_V[\epsilon\hat{\xi}] = \epsilon\hat{\xi}$. The exponential map for the matrix group $GL(n_{dim}, \mathbb{R})$, denoted by $\exp_M : L(\mathbb{R}^{n_{dim}}, \mathbb{R}^{n_{dim}}) \rightarrow GL(n_{dim}, \mathbb{R})$, is given by the matrix exponential

$$\exp_M[\mathbf{A}] = e^{\mathbf{A}} \equiv \sum_{i=0}^{\infty} \frac{\mathbf{A}^i}{i!}, \quad \text{for any } \mathbf{A} \in L(\mathbb{R}^{n_{dim}}, \mathbb{R}^{n_{dim}}). \quad (2.41)$$

Given any $\hat{\xi} \in L(\mathbb{R}^{n_{dim}}, \mathbb{R}^{n_{dim}})$, we can thus construct the following one-parameter subgroup by the matrix exponential:

$$\varphi_{\hat{\xi}}(\epsilon) = \exp_M[\epsilon\hat{\xi}] = e^{\epsilon\hat{\xi}}. \quad (2.42)$$

In this work, we only consider a subgroup of $GL(n_{dim}, \mathbb{R})$ which is called the special orthogonal group $SO(n_{dim})$ defined by

$$SO(n_{dim}) = \{\mathbf{g} \in GL(n_{dim}, \mathbb{R}) \mid \det[\mathbf{g}] = 1 \text{ and } \mathbf{g}^{-1} = \mathbf{g}^T\}. \quad (2.43)$$

One can verify that $T_eSO(n_{dim}) = so(n_{dim}) = \{\mathbf{A} \in \mathbb{R}^{n_{dim} \times n_{dim}} \mid \mathbf{A}^T = -\mathbf{A}\}$ which is the set of all $n_{dim} \times n_{dim}$ real skew-symmetric matrices. The matrix exponential for $SO(n_{dim})$ has a closed-form expression given by the Euler-Rodrigues formula (see in [106]).

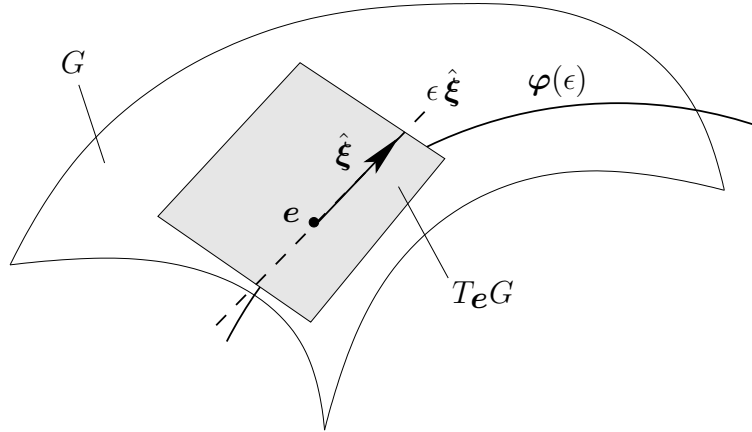


Figure 2.5. Geometrical interpretation of a one-parameter subgroup $\varphi(\epsilon)$ of G .

Now let $\varphi_{\hat{\xi}}(\epsilon)$ be a one-parameter subgroup of G associated with a tangent vector $\hat{\xi} \in T_e G$ and let ϕ be an action of G on Q . A one-parameter group of diffeomorphisms, which is defined by $\mathbf{h}_\epsilon(\mathbf{q}) = \phi(\varphi_{\hat{\xi}}(\epsilon), \mathbf{q})$, is said to be generated by $\hat{\xi}$ and the associated vector field on Q , denoted by

$$\hat{\xi}_Q(\mathbf{q}) = \left. \frac{d\phi(\varphi_{\hat{\xi}}(\epsilon), \mathbf{q})}{d\epsilon} \right|_{\epsilon=0} \quad (2.44)$$

is called the *infinitesimal generator* of the action ϕ corresponding to $\hat{\xi} \in T_e G$.

2.4.3 Momentum maps

According to Noether's theorem, the first integral $J : T^*Q \rightarrow \mathbb{R}$ corresponding to the admitted one-parameter group of diffeomorphisms $\mathbf{h}_\epsilon : Q \rightarrow Q$, $\epsilon \in \mathbb{R}$, is given by

$$J(\mathbf{q}, \mathbf{p}) = \mathbf{p} \cdot \left. \frac{d\mathbf{h}_\epsilon(\mathbf{q})}{d\epsilon} \right|_{\epsilon=0} \quad (2.45)$$

Considering a one-parameter group $\mathbf{h}_\epsilon = \phi_{\varphi_{\hat{\xi}}(\epsilon)}$ generated by $\hat{\xi} \in T_e G$, the first integral is denoted by

$$J_{\hat{\xi}}(\mathbf{q}, \mathbf{p}) = \mathbf{p} \cdot \hat{\xi}_Q(\mathbf{q}) \quad (2.46)$$

where $\hat{\xi}_Q : Q \rightarrow T_{\mathbf{q}}Q$ is the infinitesimal generator of the action ϕ on the configuration space Q . We then say that a map $\mathbf{J} : T^*Q \rightarrow T_e^*G$ is a *momentum map* for the action if we have a first integral $J_{\hat{\xi}} = \mathbf{J} \cdot \hat{\xi}$ for every $\hat{\xi} \in T_eG$. The momentum map \mathbf{J} is thus conserved in the sense that the mapping $J_{\hat{\xi}} : T^*Q \rightarrow \mathbb{R}$, which is defined by equation (2.46), is conserved for any $\hat{\xi} \in T_eG$.

2.4.4 Total linear momentum conservation

If the potential energy V of the generalised problem is independent of the origin of the coordinate frame, the Lagrangian is invariant with respect to a translation of the coordinate frame itself (Galilean invariance). The Lagrangian therefore admits the one-parameter subgroup describing the translation of the whole configuration, and there exists a first integral $J_{\hat{\xi}}(\mathbf{q}, \mathbf{p})$. In the end we obtain as momentum map the total linear momentum. To see this we define the translation of the configuration as an action $\phi : \mathbb{R}^{n_{dim}} \times \mathbb{R}^{n_{dim}} \rightarrow \mathbb{R}^{n_{dim}}$ of the vector group $\mathbb{R}^{n_{dim}}$ on a material point at $\mathbf{q}^A \in \mathbb{R}^{n_{dim}}$ given by

$$\phi(\mathbf{g}, \mathbf{q}^A) = \mathbf{g} + \mathbf{q}^A, \quad \forall \mathbf{g} \in \mathbb{R}^{n_{dim}}. \quad (2.47)$$

Since the identity element of the vector group $\mathbb{R}^{n_{dim}}$ is the zero vector $\mathbf{0}$, we have a one-parameter subgroup $\varphi_{\hat{\xi}}(\epsilon) = \exp_V[\epsilon \hat{\xi}] = \epsilon \hat{\xi}$, $\epsilon \in \mathbb{R}$, for any $\hat{\xi} \in T_{\mathbf{0}}\mathbb{R}^{n_{dim}} \cong \mathbb{R}^{n_{dim}}$ and the infinitesimal generator on Q corresponding to $\hat{\xi}$ reads

$$\hat{\xi}_Q(\mathbf{q}^A) = \left. \frac{d(\epsilon \hat{\xi} + \mathbf{q}^A)}{d\epsilon} \right|_{\epsilon=0} = \hat{\xi}. \quad (2.48)$$

According to Noether's theorem, the first integral $J_{\hat{\xi}} : T^*Q \rightarrow \mathbb{R}$ associated with this infinitesimal generator is given by

$$J_{\hat{\xi}} = \left[\sum_{A=1}^{n_{poi}} \mathbf{p}^A \right] \cdot \hat{\xi} \doteq \mathbf{J} \cdot \hat{\xi}. \quad (2.49)$$

The momentum map $\mathbf{J} : T^*Q \rightarrow T^*\mathbb{R}^{n_{dim}} \cong \mathbb{R}^{n_{dim}}$ associated with the action (2.47) is therefore the total linear momentum of the configuration, which is denoted by

$$\boxed{\mathbf{P} = \sum_{A=1}^{n_{poi}} \mathbf{p}^A} \quad (2.50)$$

Hence we know that the total linear momentum \mathbf{P} is conserved if translations are a so-called *symmetry group*, which means that the corresponding group action conserves the Lagrangian. We finally deduce a condition for the equations of motion which has to be satisfied if translations are admitted and thus \mathbf{P} is conserved. Given the fundamental theorem of calculus, conservation of total linear momentum is a consequence of a vanishing time derivative of the total linear momentum:

$$\mathbf{P}(t_b) - \mathbf{P}(t_a) = \int_{t_a}^{t_b} \dot{\mathbf{P}} dt. \quad (2.51)$$

Differentiating the total linear momentum with respect to time and applying Hamilton's canonical equations of motion (2.24), we obtain

$$\dot{\mathbf{P}} = \sum_{A=1}^{n_{poi}} \dot{\mathbf{p}}^A = \sum_{A,B=1}^{n_{poi}} Q_{AB}(\mathbf{q}) \mathbf{q}^B. \quad (2.52)$$

Accordingly, the time derivative of the total linear momentum vanish if all internal forces arising in the configuration vanish in the sum

$$\boxed{\sum_{A,B=1}^{n_{poi}} Q_{AB}(\mathbf{q}) \mathbf{q}^B = \mathbf{0}} \quad (2.53)$$

A system for which this equation is fulfilled is referred to as *closed* [8].

2.4.5 Total angular momentum conservation

When the potential energy V is independent of the orientation of the coordinate frame, the Lagrangian is invariant with respect to a rotation of the whole configuration \mathcal{B} . Applying Noether's theorem, this symmetry furnishes conservation of total angular mo-

mentum as can be easily verified by using a theorem of Euler, which states that a finite rotation of a vector is given by a linear mapping with a matrix $\mathbf{g} \in SO(n_{dim})$ of the special orthogonal group [106, 127]. Considering the group $SO(n_{dim})$, an action $\phi : SO(n_{dim}) \times \mathbb{R}^{n_{dim}} \rightarrow \mathbb{R}^{n_{dim}}$ rotating each coordinate vector $\mathbf{q}^A \in \mathbb{R}^{n_{dim}}$ of the material point A around the axial vector $\boldsymbol{\xi} \in \mathbb{R}^{n_{dim}}$ going through the origin of the coordinate frame, is therefore defined by

$$\phi(\mathbf{g}, \mathbf{q}^A) = \mathbf{g} \mathbf{q}^A, \quad \forall \mathbf{g} \in SO(n_{dim}). \quad (2.54)$$

Given a $\hat{\boldsymbol{\xi}} \in T_e SO(n_{dim}) = so(n_{dim})$, we have a one-parameter subgroup $\varphi_\xi = \exp_M[\epsilon \hat{\boldsymbol{\xi}}]$. Thus, the infinitesimal generator of the action ϕ corresponding to $\hat{\boldsymbol{\xi}}$ is

$$\hat{\boldsymbol{\xi}}_Q(\mathbf{q}^A) = \left. \frac{d(e^{\epsilon \hat{\boldsymbol{\xi}}} \mathbf{q}^A)}{d\epsilon} \right|_{\epsilon=0} = \hat{\boldsymbol{\xi}} \mathbf{q}^A. \quad (2.55)$$

According to Noether's theorem, a first integral $J_\xi : T^*Q \rightarrow \mathbb{R}$ is related to this infinitesimal generator:

$$J_\xi = \sum_{A=1}^{n_{poi}} \mathbf{p}^A \cdot [\hat{\boldsymbol{\xi}} \mathbf{q}^A]. \quad (2.56)$$

Now we can associate a unique axial vector $\boldsymbol{\xi} \in \mathbb{R}^{n_{dim}}$ to any $\hat{\boldsymbol{\xi}} \in so(n_{dim})$ via the following isomorphism:

$$\hat{\boldsymbol{\xi}} \mathbf{w} = \mathbf{w} \times \boldsymbol{\xi}, \quad \text{for all } \mathbf{w} \in \mathbb{R}^{n_{dim}}, \quad (2.57)$$

where \times denotes the cross vector product in $\mathbb{R}^{n_{dim}}$. The space $so(n_{dim})$ can be therefore identified with $\mathbb{R}^{n_{dim}}$. Employing the above defined isomorphism (2.57) and taking the skew-symmetry of the cross product into account, we obtain

$$J_\xi = \sum_{A=1}^{n_{poi}} \mathbf{p}^A \cdot [\mathbf{q}^A \times \boldsymbol{\xi}] = - \sum_{A=1}^{n_{poi}} [\mathbf{q}^A \times \mathbf{p}^A] \cdot \boldsymbol{\xi} = -\mathbf{J} \cdot \boldsymbol{\xi}. \quad (2.58)$$

The resulting momentum map $\mathbf{J} : T^*Q \rightarrow so(n_{dim})^* \cong \mathbb{R}^{n_{dim}}$ is therefore the total angular momentum of the configuration, which is denoted by

$$\boxed{\mathbf{L} = \sum_{A=1}^{n_{poi}} \mathbf{q}^A \times \mathbf{p}^A} \quad (2.59)$$

We conclude this section with the symmetry conditions for the equations of motion associated with the symmetry group $SO(n_{dim})$. Using the fundamental theorem of calculus, conservation of total angular momentum results if the time derivative $\dot{\mathbf{L}}$ vanishes:

$$\mathbf{L}(t_b) - \mathbf{L}(t_a) = \int_{t_a}^{t_b} \dot{\mathbf{L}} \, dt. \quad (2.60)$$

Differentiating both sides of equation (2.59) with respect to the time t and employing Hamilton's canonical equations (2.24), the time derivative $\dot{\mathbf{L}}$ of the total angular momentum has the form

$$\dot{\mathbf{L}} = \sum_{A=1}^{n_{poi}} [\dot{\mathbf{q}}^A \times \mathbf{p}^A + \mathbf{q}^A \times \dot{\mathbf{p}}^A] = \sum_{A,B=1}^{n_{poi}} [M_{AB}^{-1} \mathbf{p}^B \times \mathbf{p}^A + Q_{AB}(\mathbf{q}) \mathbf{q}^A \times \mathbf{q}^B]. \quad (2.61)$$

Owing to the symmetry of the mass and the stiffness matrix in conjunction with the skew-symmetry of the cross product, all terms related to the same matrix annihilate each other and yield a vanishing time derivative $\dot{\mathbf{L}}$. Consequently, the total angular momentum is conserved in the sense $\mathbf{L}(t_b) = \mathbf{L}(t_a)$ by definition of the mass and the stiffness matrix of the generalised problem.

2.5 Strain measures for deformations

In this section, we introduce strain measures for the generalised problem, which are well-known from books on nonlinear solid mechanics or continuum mechanics mentioned in the preamble of this chapter.

A deformation of the configuration \mathcal{B} is indicated by the variation of the distances between neighbouring material points [74]. A quantitative measure of strains in the

deformed configuration \mathcal{B} can be therefore derived from the distance between neighbouring material points. To this end we determine the change in length between two neighbouring material points A and B in the configuration \mathcal{B} after a deformation (see Figure 2.6). The geometry of neighbouring material points in the initial configuration \mathcal{B}_0 is given by

$$\mathbf{X}^B = \mathbf{X}^A + (\mathbf{X}^B - \mathbf{X}^A) = \mathbf{X}^A + \|\mathbf{X}^B - \mathbf{X}^A\| \mathbf{E}^{AB} = \mathbf{X}^A + d\mathbf{X}^A, \quad (2.62)$$

where

$$\mathbf{E}^{AB} = \frac{\mathbf{X}^B - \mathbf{X}^A}{\|\mathbf{X}^B - \mathbf{X}^A\|} = \frac{d\mathbf{X}^A}{\|d\mathbf{X}^A\|} \quad (2.63)$$

is the unit vector in the direction of the initial connecting line. Similarly, the geometry of neighbouring material points in the current configuration \mathcal{B}_t reads

$$\mathbf{x}^B = \mathbf{x}^A + (\mathbf{x}^B - \mathbf{x}^A) = \mathbf{x}^A + \|\mathbf{x}^B - \mathbf{x}^A\| \mathbf{e}^{AB} = \mathbf{x}^A + d\mathbf{x}^A, \quad (2.64)$$

where

$$\mathbf{e}^{AB} = \frac{\mathbf{x}^B - \mathbf{x}^A}{\|\mathbf{x}^B - \mathbf{x}^A\|} = \frac{d\mathbf{x}^A}{\|d\mathbf{x}^A\|} \quad (2.65)$$

is the unit vector in the direction of the current connecting line. The stretch ratio or simply the *stretch* λ is defined by

$$\lambda^2 = \frac{\|d\mathbf{x}^A\|^2}{\|d\mathbf{X}^A\|^2} = \frac{d\mathbf{x}^A \cdot d\mathbf{x}^A}{d\mathbf{X}^A \cdot d\mathbf{X}^A} \quad (2.66)$$

The stretch λ therefore measures how much an initial line element $d\mathbf{X}^A$ has stretched to the current line element $d\mathbf{x}^A$. Taking the deformation mapping φ into account, we obtain by Taylor's theorem

$$\mathbf{x}^B = \varphi(\mathbf{X}^A + d\mathbf{X}^A) = \varphi(\mathbf{X}^A) + \nabla_{\mathbf{X}} \varphi(\mathbf{X}^A) d\mathbf{X}^A + \mathcal{O}(\|\mathbf{X}^B - \mathbf{X}^A\|^2). \quad (2.67)$$

The gradient $\nabla_{\mathbf{X}} \varphi(\mathbf{X}_A)$ of the deformation map is called the *deformation gradient* \mathbf{F} so that equation (2.67) leads to $d\mathbf{x}^A = \mathbf{F} d\mathbf{X}^A$ if nonlinear terms are neglected, which is a

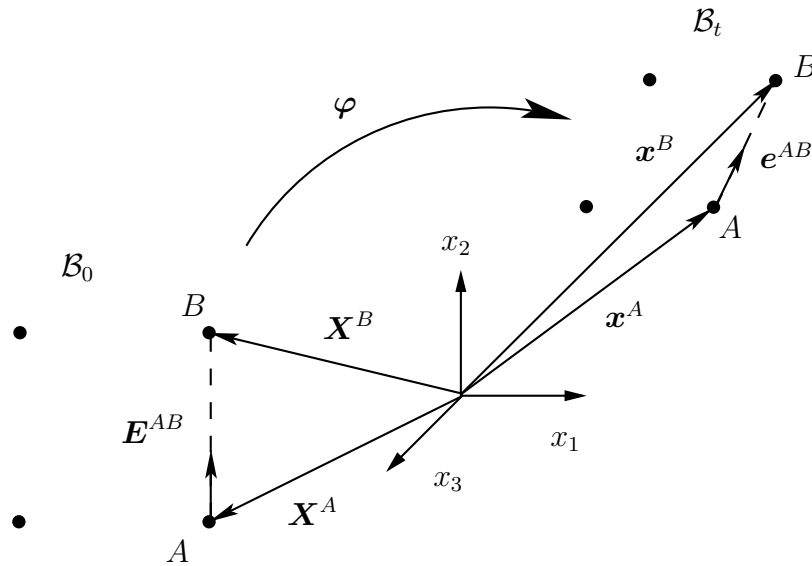


Figure 2.6. The geometry of two neighbouring material points in the configuration \mathcal{B} .

good approximation the smaller $d\mathbf{X}^A$ is. The squared stretch therefore reads

$$\boxed{\lambda^2 = \mathbf{E}^{AB} \cdot \mathbf{C} \mathbf{E}^{AB}} \quad (2.68)$$

where $\mathbf{C} = \mathbf{F}^T \mathbf{F}$ denotes the so-called *right Cauchy-Green tensor*. The right Cauchy-Green tensor is a symmetric and positive definite tensor and an important strain measure in nonlinear elastodynamics. In particle dynamics, equation (2.66) is preferred as formulation for the stretch.

2.6 Superimposed rigid body motions

Within this section, we are concerned with rigid body motions in the context of the generalised problem. To this end we summarise the relevant topics from the books mentioned in the preamble.

If the configuration is moved without a change in its shape, which means rigid body motions, the applied strain measure must not indicate a stretch. A strain measure having this property is called *consistent* with respect to rigid body motions. In this section, we show the consistency of the strain measures considered in the previous section with

respect to superimposed rigid body motions. This property proves to be important in view of the subsequent time discretisation of the strain measures.

Each motion φ^+ of the configuration \mathcal{B} is a composition of a motion φ associated with a deformation and a superimposed rigid body motion χ such that $\varphi^+ = \chi \circ \varphi$. The deformation is identified by changed distances between the material points and is therefore indicated by a changed value of the chosen strain measure. A rigid body motion of the configuration is however characterised by no variation of the distances between the material points and therefore given by an Euclidean transformation $\mathbf{x}^+ = \chi(\mathbf{x}, t) \equiv \mathbf{a}(t) + \mathbf{R}(t) \mathbf{x}$, with $\mathbf{a}(t) \in \mathbb{R}^{n_{dim}}$ and $\mathbf{R}(t) \in SO(n_{dim})$. The vector $\mathbf{a}(t)$ is associated with a rigid body translation and the tensor $\mathbf{R}(t)$ renders a rigid body rotation. The rotation tensor $\mathbf{R}(t)$ naturally fulfils the equation $[\mathbf{R}(t)]^T \mathbf{R}(t) = \mathbf{I}_{n_{dim}}$. Taking the previous section into account, line elements associated with closely neighbouring points are then related by $d\mathbf{x}^+ = \mathbf{R}(t) d\mathbf{x}$. By using of this relation, the stretch λ associated with a deformation which is superimposed by a rigid body motion take the form

$$[\lambda^+]^2 = \frac{d\mathbf{x}^+ \cdot d\mathbf{x}^+}{d\mathbf{X} \cdot d\mathbf{X}} = \frac{d\mathbf{x} \cdot [\mathbf{R}^T(t)\mathbf{R}(t)] d\mathbf{x}}{d\mathbf{X} \cdot d\mathbf{X}} = \lambda^2, \quad (2.69)$$

where λ denotes the stretch only associated with the deformation. Consequently, a rigid body motion of the system does not affect the stretch because an Euclidean transformation give not rise to a change in the stretch λ . The particle distance or the right Cauchy-Green tensor are therefore consistent strain measures for the generalised problem. This invariance of the strain measure with respect to rigid body motions, however, have to be maintained if the strain measure is discretised in time.

Chapter 3

Galerkin-based time discretisation

...Mathematically, one property that can be guaranteed is that if energy is conserved in the true problem, then it is conserved in Galerkin's method, and that if it is decreasing with time in the true problem, then it is decreasing in the Galerkin approximation...

[130], Chapter 7: Initial-value Problems.

We obtain a numerical solution of the equations of motion by discretising them with respect to the time t . We apply the Galerkin method in time which is based on a piecewise polynomial approximation of Hamilton's canonical equations. More precisely, we use Galerkin finite element methods which rely on continuous or discontinuous trial functions. To this end we introduce finite elements in time and a corresponding master element. The equations of motion are then related to an initial value problem on this reference element. We apply the continuous Galerkin finite element method along the way described in [22, 19, 20] for solving this initial value problem. We obtain a family of higher order implicit time stepping schemes which possesses some properties when applied a certain kind of quadrature. The first property is the collocation property which states that this family of time stepping schemes provides a continuous approximation which exactly satisfies the underlying differential equation at a finite number of quadrature points [28, 129]. The collocation property proves to be important for conserving first integrals of the underlying equations of motion. Applying this collocation property, we then investigate the conservation of the first integrals of Hamilton's canonical equations pertaining to the

generalised problem. We conclude the examination of the continuous Galerkin method in time by depicting the iterative solution procedure of this family of time stepping schemes in a compact description. At the end we present the discontinuous Galerkin method in time according to [62]. However, it turned out that the temporal discontinuous Galerkin method is not convenient to design mechanical integrators because the discontinuous approximation introduces a kind of energy dissipation (see more details in [62, 63]). We therefore concentrate in the further chapters on the continuous Galerkin method in time.

3.1 Finite element discretisation in time

We divide the time interval $\mathcal{T} = [t_0, T]$ of interest into $N_\tau - 1$ nonoverlapping subintervals \mathcal{T}_n of length h_n , $n = 1, \dots, N_\tau - 1$, such that

$$\mathcal{T} = \bigcup_{n=1}^{N_\tau-1} \mathcal{T}_n. \quad (3.1)$$

This partition of \mathcal{T} is related with a mesh of time points $t_0 < t_1 < \dots < t_{N_\tau} = T$. We subsequently transform each subinterval $\mathcal{T}_n = [t_{n-1}, t_n]$ to a master element $\mathcal{I}_\alpha = [0, 1]$ corresponding to the normalised coordinate

$$\alpha = \frac{t - t_{n-1}}{h_n}, \quad (3.2)$$

where $h_n = t_n - t_{n-1}$ denotes the length of \mathcal{T}_n . Accordingly, the motion in each subinterval \mathcal{T}_n is determined by the following initial-value problem with respect to the master element: Given the initial value $\mathbf{z}_0 = \mathbf{z}(t_{n-1})$, find the motion $\zeta_0 : \mathcal{I}_\alpha \times P \ni (\alpha, \mathbf{z}_0) \mapsto \mathbf{z}(\alpha) \in P$ in the phase space P which is determined by the ordinary differential equation

$$\boxed{\frac{d\mathbf{z}(\alpha)}{d\alpha} = h_n \mathbb{J} \nabla_{\mathbf{z}} H(\mathbf{z}(\alpha))} \quad (3.3)$$

Where appropriate, we indicate differentiation with respect to α by using a prime.

3.2 The continuous Galerkin (cG) method

In this section, we apply the continuous Galerkin method to the initial value problem (3.3) emanating from the finite element discretisation of Hamilton's canonical equations. The continuous Galerkin method is defined using continuous trial functions of degree k and test functions of degree $k - 1$. The finite element approximation of the test functions accordingly leads to possible discontinuities across the element boundaries. More details can be found in [44, 22, 19, 20]. The continuous Galerkin method can be traced back at least to [135, 42] for parabolic problems and to [82, 81] for ordinary differential equations.

3.2.1 Implicit time stepping schemes

An implicit *time stepping scheme* is a system of nonlinear equations which relates the nodal values \mathbf{z}_I , $I = 1, \dots, k + 1$, to the initial value \mathbf{z}_0 . Galerkin's method determines the nodal values \mathbf{z}_I such that the residual error of the considered differential equation is orthogonal to all functions in the test space. The residual error of the ordinary differential equation (3.3) reads

$$\mathbf{R}(\mathbf{z}) = \frac{d\mathbf{z}}{d\alpha} - h_n \mathbb{J}\nabla_{\mathbf{z}}H(\mathbf{z}). \quad (3.4)$$

The Galerkin orthogonality condition for the trial function $\mathbf{z}(\alpha)$, the weak form of the residual error (3.4), takes the form

$$\int_0^1 \Omega(\mathbf{R}(\mathbf{z}(\alpha)), \delta\mathbf{z}(\alpha)) d\alpha = \int_0^1 \mathbb{J}\delta\mathbf{z}(\alpha) \cdot \mathbf{R}(\mathbf{z}(\alpha)) d\alpha = 0, \quad (3.5)$$

where the test function $\delta\mathbf{z}(\alpha)$ and the trial function are polynomials of degree $k - 1$ and k , respectively, and given by

$$\delta\mathbf{z}(\alpha) = \sum_{I=1}^k \tilde{M}_I(\alpha) \delta\mathbf{z}_I, \quad \mathbf{z}(\alpha) = \sum_{J=1}^{k+1} M_J(\alpha) \mathbf{z}_J, \quad (3.6)$$

where $\delta\mathbf{z}_I = \delta\mathbf{z}((I - 1)/(k - 1))$, $I = 1, \dots, k$ and $\mathbf{z}_J = \mathbf{z}((J - 1)/k)$, $J = 1, \dots, k + 1$ denote the nodal values at the equidistant nodes of the polynomials. We have to state the continuity condition $\mathbf{z}_1 = \mathbf{z}_0$ at the beginning of each time step for global continuity

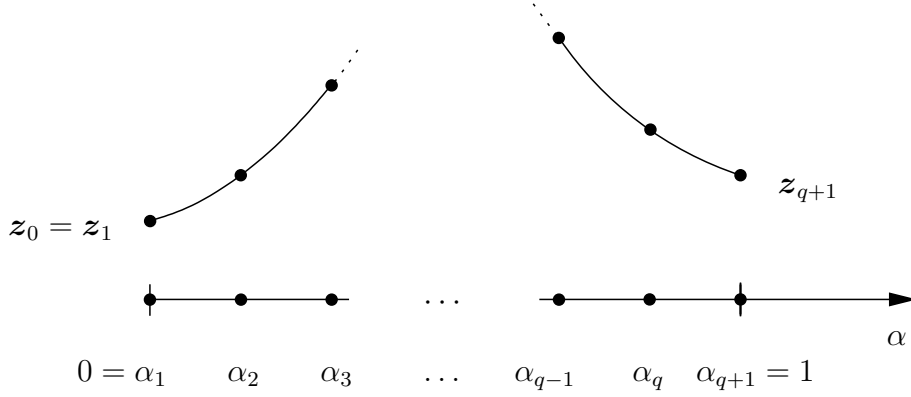


Figure 3.1. The $q + 1$ nodes of a continuous Lagrange polynomial of degree q .

of the trial functions. The functions \tilde{M}_I and M_J denote Lagrange polynomials of degree $k - 1$ and degree k , respectively, with respect to the equidistant nodes on the master element. Lagrange polynomials $L_I(\alpha)$, $I = 1, \dots, q + 1$, of degree q with respect to $q + 1$ equidistant nodes $\alpha_I = (I - 1)/q$ (see Figure 3.1) generally have the following form [44]:

$$L_I(\alpha) = \prod_{\substack{J=1 \\ J \neq I}}^{q+1} \frac{\alpha - \alpha_J}{\alpha_I - \alpha_J}, \quad I = 1, \dots, q+1. \quad (3.7)$$

Employing the test as well as the trial functions in the weak form (3.5) and taking the fundamental theorem of variational calculus into account, we obtain

$$\sum_{J=1}^{k+1} \int_0^1 \tilde{M}_I M_J' d\alpha z_J - h_n \int_0^1 \tilde{M}_I(\alpha) \mathbb{J} \nabla_{\mathbf{z}} H(\mathbf{z}(\alpha)) d\alpha = \mathbf{0}, \quad I = 1, \dots, k. \quad (3.8)$$

The first term is an integral over a polynomial of degree $2(k - 1)$ and can be exactly determined, however the second integrand includes the Jacobian of the arbitrary Hamiltonian and generally has to be determined by numerical quadrature. We generally apply interpolatory quadrature formulas (see [83, 81]) given by

$$I_h\{f\} = \sum_{l=1}^{N_q^\alpha} f(\xi_l) w_l, \quad (3.9)$$

where ξ_l and w_l denote the quadrature points and the associated weights, respectively.

However, we limit our considerations to the Gaussian quadrature rules with the accuracy order $\mathcal{O}(h_n^{2N_q^\alpha})$ (see [13, 38, 66] for details) and obtain

$$\boxed{\sum_{J=1}^{k+1} \int_0^1 \tilde{M}_I M_J' d\alpha \mathbf{z}_J - h_n \sum_{l=1}^{N_q^\alpha} \tilde{M}_I(\xi_l) \mathbb{J} \nabla_{\mathbf{z}} H(\mathbf{z}(\xi_l)) w_l = \mathbf{0}} \quad I = 1, \dots, k. \quad (3.10)$$

These equations represent a family of higher order integrators with the parameters k and N_q^α (see [22, 19, 20]). Essentially two additional steps have to be performed to obtain a particular integrator. First the selection of the degree k of the finite elements in time and second the number of quadrature points N_q^α for calculating the integral including the Jacobian of the Hamiltonian.

3.2.2 Collocation property

In this section, we show that the integrators (3.10) is able to provide a continuous approximation of the motion, which exactly satisfies Hamilton's equations at the Gauss points. To this end we consider the integrator (3.10), however, we also apply a N_q^α -point Gauss rule to the integral in the first term. Nevertheless, this integral is supposed to be exactly calculated. Since the corresponding integrand is a polynomial of degree $2(k-1)$, the integral is exactly calculated by $N_q^\alpha \geq k-1$ Gauss points. Hence we require in the following at least $k-1$ Gauss points. Taking the definition (3.4) into account, we obtain the equations (3.10) in the form of the following homogeneous linear system of equations:

$$\left[\tilde{\mathbf{W}}(\xi_1, \dots, \xi_{N_q^\alpha}) \otimes \mathbf{I}_{2n_{dof}} \right] \begin{bmatrix} \mathbf{R}(\mathbf{z}(\xi_1)) w_1 \\ \vdots \\ \mathbf{R}(\mathbf{z}(\xi_{N_q^\alpha})) w_{N_q^\alpha} \end{bmatrix} = \begin{bmatrix} \mathbf{0} \\ \vdots \\ \mathbf{0} \end{bmatrix} \quad (3.11)$$

with the structure matrix

$$\tilde{\mathbf{W}}(\xi_1, \dots, \xi_{N_q^\alpha}) = \begin{bmatrix} \tilde{\mathbf{w}}(\xi_1) & \dots & \tilde{\mathbf{w}}(\xi_{N_q^\alpha}) \end{bmatrix}, \quad \text{where } \tilde{\mathbf{w}}(\alpha) = \begin{bmatrix} \tilde{M}_1(\alpha) \\ \vdots \\ \tilde{M}_k(\alpha) \end{bmatrix} \quad (3.12)$$

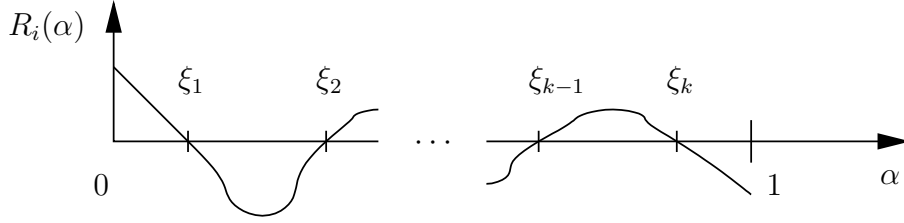


Figure 3.2. One component $R_i(\alpha)$ of the residual $\mathbf{R}(\mathbf{z}(\alpha))$ in the case of collocation at the Gauss points ξ_l , $l = 1, \dots, k$.

The solution of the system (3.11) is unique if $N_q^\alpha = k$. In this case, we obtain the trivial solution if the coefficient matrix is additionally invertible. According to Appendix B, the inverse of a direct product of matrices is given by the direct product of the inverse matrices. Since the inverse of the $2n_{dof} \times 2n_{dof}$ identity matrix $\mathbf{I}_{2n_{dof}}$ exists, we only have to verify that the structure matrix (3.12) is non-singular. Accordingly, the Lagrange polynomial basis of the test space has to satisfy the so-called *Haar condition* (see [114]).

A family of Lagrange polynomials generally satisfies the Haar condition if it is a polynomial basis. This can be easily verified by relating this family of Lagrange polynomials to a monomial basis because the Haar matrix $\tilde{\mathbf{W}}$ corresponding to a monomial basis is the well-known Vandermonde matrix. For this purpose we write the monomials α^j , $j = 0, \dots, k-1$, by using the Lagrange polynomials \tilde{M}_I , $I = 1, \dots, k$. The monomials result from an interpolation over the time nodes α_I associated with the Lagrange polynomials. This leads to the equations $\alpha^j = \sum_{I=1}^k \tilde{M}_I(\alpha)(\alpha_I)^j$ (see [73, 44, 66]). In matrix notation, we obtain a linear algebraic system of the form

$$\tilde{\mathbf{v}}(\alpha) = \tilde{\mathbf{V}}(\alpha_1, \dots, \alpha_k) \tilde{\mathbf{w}}(\alpha), \quad (3.13)$$

with the Vandermonde matrix given by (see [66, 73, 13])

$$\tilde{\mathbf{V}}(\alpha_1, \dots, \alpha_k) = \begin{bmatrix} \tilde{\mathbf{v}}(\alpha_1) & \dots & \tilde{\mathbf{v}}(\alpha_k) \end{bmatrix}, \quad \text{where } \tilde{\mathbf{v}}(\alpha) = \begin{bmatrix} 1 \\ \vdots \\ \alpha^{k-1} \end{bmatrix} \quad (3.14)$$

The structure matrix $\tilde{\mathbf{W}}(\xi_1, \dots, \xi_k)$ can be therefore written as a product of Vander-

monde matrices: $\tilde{\mathbf{W}}(\xi_1, \dots, \xi_k) = \tilde{\mathbf{V}}^{-1}(\alpha_1, \dots, \alpha_k) \tilde{\mathbf{V}}(\xi_1, \dots, \xi_k)$. The determinant of the structure matrix can be thus expressed by the so-called *Vandermonde determinant*. The corresponding formula can be found in [66], for instance. Applying this determinant formula, we obtain the following relation:

$$\det \tilde{\mathbf{W}}(\xi_1, \dots, \xi_k) = \prod_{I=1}^{k-1} \prod_{J=I+1}^k \frac{\xi_I - \xi_J}{\alpha_I - \alpha_J} \quad (3.15)$$

Hence the determinant of the structure matrix cannot vanish because the time nodes and the Gauss points are pairwise distinct so that the structure matrix is therefore non-singular.

Since the Haar condition for the test space is fulfilled by using k Gauss points, the system (3.11) has only the trivial solution which can be written as

$$\boxed{\begin{aligned} \frac{d\mathbf{q}(\xi_l)}{d\alpha} &= h_n \mathbb{M}^{-1} \mathbf{p}(\xi_l) \\ \frac{d\mathbf{p}(\xi_l)}{d\alpha} &= -h_n \nabla_{\mathbf{q}} V(\mathbf{q}(\xi_l)) \end{aligned}} \quad \text{for } l = 1, \dots, k. \quad (3.16)$$

The time stepping schemes (3.10) associated with k -point Gaussian quadrature therefore exactly fulfil Hamilton's canonical equations at the Gauss points ξ_l , which means that the determined residual has roots at the Gauss points (see Figure 3.2). We call this combination the *cG(k) method*. Note that the cG(k) method leads to k -stage Gauss Runge-Kutta methods (see [82, 81, 22, 132] for example) for which the collocation property is satisfied [143].

3.2.3 Total energy conservation

This section investigates the total energy conservation of the cG(k) method. For this purpose we determine the total energy at the endpoint of the interval \mathcal{I}_α in dependence on the total energy at the given initial point. Since the approximation of the total energy is continuous, we relate the energies at the boundaries of \mathcal{I}_α by applying the fundamental

theorem of calculus (see also [4, 22]):

$$H(\mathbf{z}(1)) - H(\mathbf{z}(0)) = \int_0^1 \frac{dT^*(\mathbf{p}(\alpha))}{d\alpha} d\alpha + \int_0^1 \frac{dV(\mathbf{q}(\alpha))}{d\alpha} d\alpha, \quad (3.17)$$

Employing the kinetic energy T^* of the generalised problem, the first integrand is a polynomial of degree $2k - 1$. The corresponding integral is exactly calculated by a k -point Gauss rule. Thus the fundamental theorem of calculus applied to the kinetic energy T^* can be written as

$$T^*(\mathbf{p}(1)) - T^*(\mathbf{p}(0)) = \sum_{l=1}^k \frac{d\mathbf{p}(\xi_l)}{d\alpha} \cdot \mathbb{M}^{-1} \mathbf{p}(\xi_l) w_l. \quad (3.18)$$

The potential energy is assumed to be an arbitrary nonlinear function. The corresponding fundamental theorem of calculus is satisfied by a quadrature rule which fulfils the following equation:

$$\boxed{V(\mathbf{q}(1)) - V(\mathbf{q}(0)) = \sum_{l=1}^k \nabla_{\mathbf{q}} V(\mathbf{q}(\xi_l)) \cdot \frac{d\mathbf{q}(\xi_l)}{d\alpha} w_l} \quad (3.19)$$

Now we take the collocation property of the cG(k) method into account and additionally suppose that equation (3.19) is fulfilled. Employing equations (3.16a) and (3.16b) in the equations (3.19) and (3.18), respectively, summation of the resulting two equations leads to $H(\mathbf{z}(1)) = H(\mathbf{z}(0))$ independent of a finite time step size h_n . Accordingly, the cG(k) method is an energy conserving integrator if the condition (3.19) is satisfied. We refer to this equation as the *energy conservation condition* for the cG(k) method.

Remark 3.1. The energy conservation condition (3.19) can be interpreted as the discrete version of the gradient theorem which states

$$V(\mathbf{q}(1)) - V(\mathbf{q}(0)) = \int_{\psi} \nabla_{\mathbf{q}} V \cdot d\mathbf{q}, \quad (3.20)$$

where ψ is a path starting at $\mathbf{q}(0)$ and ending at $\mathbf{q}(1)$ (see Figure 3.3). The gradient theorem describes a fundamental property of a potential function $V(\mathbf{q})$, namely the path-independence of the line integral $\int_{\psi} \nabla_{\mathbf{q}} V \cdot d\mathbf{q}$ [144, 139]. The path-independence of the

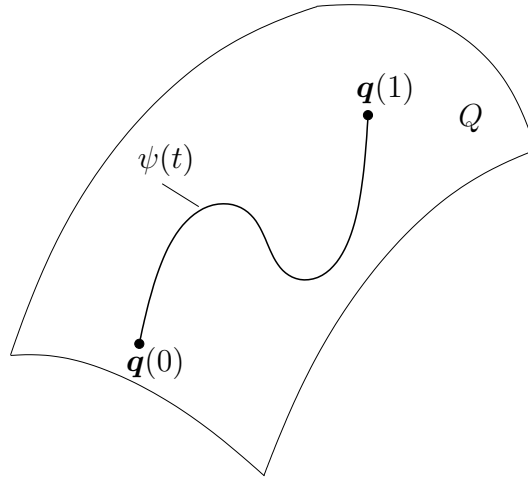


Figure 3.3. The work done by a force field along a path ψ in the configuration space Q only depends on the initial point and the end point.

work done by the conservative force field $-\nabla_{\mathbf{q}}V$ follows from this property. The work is then equal to the difference between the final and the initial value of the potential $V(\mathbf{q})$. The energy conservation condition (3.19) guarantees that this fundamental property of a conservative force field is retained in spite of applying quadrature for calculating integrals.

3.2.4 Total linear momentum conservation

This section verifies the total linear momentum conservation of the cG(k) method applied to the generalised problem. Since the motion is continuously approximated by the cG(k) method, we also apply the fundamental theorem of calculus to relate the total linear momenta at neighbouring points in the partition of the interesting time interval. The fundamental theorem of calculus with respect to the total linear momentum reads

$$\mathbf{P}(\mathbf{z}(1)) - \mathbf{P}(\mathbf{z}(0)) = \int_0^1 \frac{d\mathbf{P}(\mathbf{z}(\alpha))}{d\alpha} d\alpha = \int_0^1 \sum_{A=1}^{n_{poi}} \frac{d\mathbf{p}^A(\alpha)}{d\alpha} d\alpha. \quad (3.21)$$

The integrand in equation (3.21) is a sum of polynomials of degree $k - 1$. The corresponding integral is exactly determined by Gaussian quadrature with k Gauss points. In addition, the collocation property of the cG(k) method provides that the equations of

motion (2.10) are satisfied at k Gauss points. Hence we obtain

$$\mathbf{P}(\mathbf{z}(1)) - \mathbf{P}(\mathbf{z}(0)) = -h_n \sum_{l=1}^k \sum_{A,B=1}^{n_{poi}} Q_{AB}(\mathbf{q}(\xi_l)) \mathbf{q}^B(\xi_l) w_l. \quad (3.22)$$

Taking equation (2.53) into account, the cG(k) method leads to total linear momentum conservation $\mathbf{P}(\mathbf{z}(1)) = \mathbf{P}(\mathbf{z}(0))$ independent of the time step size.

3.2.5 Total angular momentum conservation

A further invariant of the generalised problem is the total angular momentum whose conservation is examined in this section. We apply the fundamental theorem of calculus to determine the total angular momentum at the endpoint of the master element:

$$\mathbf{L}(\mathbf{z}(1)) - \mathbf{L}(\mathbf{z}(0)) = \int_0^1 \frac{d\mathbf{L}(\mathbf{z}(\alpha))}{d\alpha} d\alpha = \int_0^1 \sum_{A=1}^{n_{poi}} \frac{d}{d\alpha} [\mathbf{q}^A(\alpha) \times \mathbf{p}^A(\alpha)] d\alpha. \quad (3.23)$$

In accordance with the kinetic energy T^* , the integral in the fundamental theorem of calculus applied to the total angular momentum \mathbf{L} is exactly calculated by applying k Gauss points:

$$\mathbf{L}(\mathbf{z}(1)) - \mathbf{L}(\mathbf{z}(0)) = \sum_{l=1}^k \sum_{A=1}^{n_{node}} \left[\frac{d\mathbf{q}^A(\xi_l)}{d\alpha} \times \mathbf{p}^A(\xi_l) + \mathbf{q}^A(\xi_l) \times \frac{d\mathbf{p}^A(\xi_l)}{d\alpha} \right] w_l. \quad (3.24)$$

Taking equations (3.16) in conjunction with equation (2.2) into account, total angular momentum conservation $\mathbf{L}(\mathbf{z}(1)) = \mathbf{L}(\mathbf{z}(0))$ independent of the used time step size follows from the same argumentation as in Section 2.4.5.

3.2.6 Iterative solution procedure

This section describes the procedure for solving the equations of the cG(k) method in a computational setting. Taking the definition $\mathbf{z} = (\mathbf{q}, \mathbf{p})$ into account, the cG(k) method

of the generalised problem takes the form

$$\begin{aligned} \sum_{J=1}^{k+1} \int_0^1 \tilde{M}_I M'_J \, d\alpha \, \mathbf{q}_J - h_n \int_0^1 \tilde{M}_I \mathbb{M}^{-1} \mathbf{p} \, d\alpha &= \mathbf{0}, \\ \sum_{J=1}^{k+1} \int_0^1 \tilde{M}_I M'_J \, d\alpha \, \mathbf{p}_J + h_n \sum_{l=1}^k \tilde{M}_I(\xi_l) \mathbb{Q}(\mathbf{q}(\xi_l)) \mathbf{q}(\xi_l) w_l &= \mathbf{0}, \end{aligned} \quad I = 1, \dots, k. \quad (3.25)$$

We collect the unknown coordinates and momenta in the vectors $\mathbf{x}_q = (\mathbf{q}_2, \dots, \mathbf{q}_{k+1})$ and $\mathbf{x}_p = (\mathbf{p}_2, \dots, \mathbf{p}_{k+1})$, respectively. The $2k$ vector equations of the cG(k) method can be then expressed in matrix notation as

$$\mathbf{b}' \otimes \mathbf{q}_1 + [\mathbf{A}' \otimes \mathbf{I}_{n_{dof}}] \mathbf{x}_q - h_n \mathbf{b} \otimes [\mathbb{M}^{-1} \mathbf{p}_1] - h_n [\mathbf{A} \otimes \mathbb{M}^{-1}] \mathbf{x}_p = \mathbf{0}, \quad (3.26)$$

$$\mathbf{b}' \otimes \mathbf{p}_1 + [\mathbf{A}' \otimes \mathbf{I}_{n_{dof}}] \mathbf{x}_p + h_n [\tilde{\mathbf{W}}(\xi_1, \dots, \xi_k) \otimes \mathbf{I}_{n_{dof}}] \mathbf{f}(\mathbf{x}_q) = \mathbf{0}, \quad (3.27)$$

where we introduced the following matrices for a compact description:

$$\mathbf{A} = \begin{bmatrix} A_{11} & \dots & A_{1k} \\ \vdots & & \vdots \\ A_{k1} & \dots & A_{kk} \end{bmatrix} \quad \mathbf{A}' = \begin{bmatrix} A'_{11} & \dots & A'_{1k} \\ \vdots & & \vdots \\ A'_{k1} & \dots & A'_{kk} \end{bmatrix} \quad \mathbf{b} = \begin{bmatrix} b_1 \\ \vdots \\ b_k \end{bmatrix} \quad \mathbf{b}' = \begin{bmatrix} b'_1 \\ \vdots \\ b'_k \end{bmatrix} \quad (3.28)$$

Here the prime at the matrices \mathbf{A}' and \mathbf{b}' does not indicate differentiation of the matrices \mathbf{A} and \mathbf{b} with respect to α , which can be seen by the corresponding coefficients of these matrices:

$$A_{IJ} = \int_0^1 \tilde{M}_I M_{J+1} \, d\alpha, \quad b_I = \int_0^1 \tilde{M}_I M_1 \, d\alpha, \quad (3.29)$$

$$A'_{IJ} = \int_0^1 \tilde{M}_I M'_{J+1} \, d\alpha, \quad b'_I = \int_0^1 \tilde{M}_I M'_1 \, d\alpha. \quad (3.30)$$

and the force vector \mathbf{f} reads

$$\mathbf{f}(\mathbf{x}_q) = \begin{bmatrix} \mathbb{Q}(\mathbf{q}(\xi_1)) \mathbf{q}(\xi_1) w_1 \\ \vdots \\ \mathbb{Q}(\mathbf{q}(\xi_k)) \mathbf{q}(\xi_k) w_k \end{bmatrix} \quad (3.31)$$

Since the unknown momenta are linear combinations of the unknown coordinates, we eliminate the vector \mathbf{x}_p such that we obtain the residual

$$\boxed{\mathbf{R}(\mathbf{x}_q) = \frac{1}{h_n} [\mathbf{A}_m^R \otimes \mathbb{M}] \mathbf{x}_q + \frac{1}{h_n} \mathbf{A}_q^R \otimes [\mathbb{M} \mathbf{q}_1] + \mathbf{A}_p^R \otimes \mathbf{p}_1 + h_n [\tilde{\mathbf{W}}(\boldsymbol{\xi}) \otimes \mathbf{I}_{n_{dof}}] \mathbf{f}(\mathbf{x}_q)}$$
(3.32)

with the Gauss points $\boldsymbol{\xi} = (\xi_1, \dots, \xi_k)$ and the matrices

$$\mathbf{A}_m^R = \mathbf{A}' \mathbf{A}^{-1} \mathbf{A}', \quad \mathbf{A}_q^R = \mathbf{A}' \mathbf{A}^{-1} \mathbf{b}', \quad \mathbf{A}_p^R = \mathbf{b}' - \mathbf{A}' \mathbf{A}^{-1} \mathbf{b}. \quad (3.33)$$

Accordingly, to determine the unknown coordinates \mathbf{q}_A , $A = 2, \dots, k+1$, we have to solve the nonlinear equations $\mathbf{R}(\mathbf{x}_q) = \mathbf{0}$. As we iteratively solve this nonlinear system of equations by using the Newton-Raphson method, we perform a linearisation. Using i as iteration index, we therefore obtain the iteration formula

$$\mathbf{x}_q^{(i+1)} = \mathbf{x}_q^{(i)} - \mathbf{K}_T^{-1}(\mathbf{x}_q^{(i)}) \mathbf{R}(\mathbf{x}_q^{(i)}), \quad (3.34)$$

where $\mathbf{K}_T(\mathbf{x}_q) = \nabla_{\mathbf{x}_q} \mathbf{R}(\mathbf{x}_q)$ indicates the tangent operator corresponding to the residual (3.32), which reads

$$\boxed{\mathbf{K}_T(\mathbf{x}_q) = \frac{1}{h_n} [\mathbf{A}_m^R \otimes \mathbb{M}] + h_n [\tilde{\mathbf{W}}(\boldsymbol{\xi}) \otimes \mathbf{I}_{n_{dof}}] \mathbf{K}(\mathbf{x}_q)}$$
(3.35)

where

$$\mathbf{K}(\mathbf{x}_q) = \nabla_{\mathbf{x}_q} \mathbf{f}(\mathbf{x}_q) = \begin{bmatrix} \mathbf{K}_2(\xi_1) w_1 & \dots & \mathbf{K}_{k+1}(\xi_1) w_1 \\ \vdots & & \vdots \\ \mathbf{K}_2(\xi_k) w_k & \dots & \mathbf{K}_{k+1}(\xi_k) w_k \end{bmatrix} \quad (3.36)$$

We initialise the unknown coordinates for the first iteration by the following equation:

$$\boxed{\mathbf{x}_q = -\mathbf{A}_q^q \otimes \mathbf{q}_1 - h_n \mathbf{A}_p^q \otimes [\mathbb{M}^{-1} \mathbf{p}_1]}$$
(3.37)

with

$$\mathbf{A}_q^q = [\mathbf{A}']^{-1} \mathbf{b}' = -\mathbf{e}_k, \quad \mathbf{A}_p^q = [\mathbf{A}']^{-1} \mathbf{A} [\mathbf{A}']^{-1} \mathbf{b}' - [\mathbf{A}']^{-1} \mathbf{b}, \quad (3.38)$$

where $\mathbf{e}_k = (1, \dots, 1) \in \mathbb{R}^k$ (see Appendix C.3). Finally, the momenta \mathbf{x}_p are determined by the following equation with the now known coordinates \mathbf{q}_A , $A = 1, \dots, k + 1$:

$$\boxed{\mathbf{x}_p = \frac{1}{h_n} [\mathbf{A}_m^p \otimes \mathbb{M}] \mathbf{x}_q + \frac{1}{h_n} \mathbf{A}_q^p \otimes [\mathbb{M} \mathbf{q}_1] - \mathbf{A}_p^p \otimes \mathbf{p}_1} \quad (3.39)$$

with the matrices

$$\mathbf{A}_m^p = \mathbf{A}^{-1} \mathbf{A}', \quad \mathbf{A}_q^p = \mathbf{A}^{-1} \mathbf{b}', \quad \mathbf{A}_p^p = \mathbf{A}^{-1} \mathbf{b}. \quad (3.40)$$

Remark 3.2. In this work, we decide to check in the stopping criterion of the iterative solution procedure the Euclidean norm of the residual. For this purpose we choose a tolerance ϵ which has to be fulfilled by the Euclidean norm. Another possible stopping criterion is to check whether the residual is virtually stayed constant (see [41]). Moreover, we have only applied an iterative solution procedure associated with a consistent tangent which can be also unsymmetric. A direct solver based on Gaussian elimination in conjunction with sparse matrices is employed. We can avoid an unsymmetric tangent by applying a symmetric nested iterative procedure proposed in [6]. The condition for this numerical implementation, however, is an additive structure of the internal force vector $\mathbf{f}(\mathbf{x}_q)$ which leads to the split of the tangent in a symmetric part and an unsymmetric part. In the inner loop of this solution procedure, one considers the internal forces corresponding to the unsymmetric tangent at a fixed deformation and iterates in the internal forces associated with the symmetric tangents. Once this symmetric iterative process converges, the internal forces associated with the unsymmetric tangents are updated with the computed deformation in the outer loop and the iteration is repeated. These nested iterations are taken to convergence.

3.3 The discontinuous Galerkin (dG) method

In this section, we apply the discontinuous Galerkin method in time to the initial value problem (3.3). The trial as well as the test functions of the discontinuous Galerkin method in time are piecewise polynomials of equal degree. Both functions are generally discon-

tinuous across the element boundaries. This turns out to be an advantage in the error analysis and it improves the stability for parabolic problems in comparison to the continuous Galerkin method in time (see [44, 138]).

We take as trial functions for the discontinuous Galerkin method in time the same as for the continuous Galerkin method. For this reason the test functions take here the form:

$$\delta \mathbf{z}(\alpha) = \sum_{I=1}^{k+1} M_I(\alpha) \delta \mathbf{z}_I, \quad (3.41)$$

where $\delta \mathbf{z}_I = \delta \mathbf{z}((I-1)/k)$, $I = 1, \dots, k+1$, denotes the values at the equidistant nodes of the polynomials. The weak form of the discontinuous Galerkin method in time is given by the equation

$$\int_0^1 \Omega(\mathbf{R}(\mathbf{z}(\alpha)), \delta \mathbf{z}(\alpha)) \, d\alpha + \Omega(\llbracket \mathbf{z} \rrbracket, \delta \mathbf{z}_1) = 0. \quad (3.42)$$

Here the initial condition \mathbf{z}_0 is introduced in a variational sense through an additional term because otherwise the coefficients \mathbf{z}_I , $I = 1, \dots, k+1$, of the trial functions are over-determined. In general, one therefore gets a jump $\llbracket \mathbf{z} \rrbracket := \mathbf{z}_1 - \mathbf{z}_0 \neq \mathbf{0}$ (discontinuity) in the master element \mathcal{I}_α at $\alpha = 0$. We finally obtain a generally discontinuous approximation of the test and the trial functions.

Employing the trial functions and the test functions in the weak form, the fundamental theorem of variational calculus renders the equations

$$\sum_{J=1}^{k+1} \int_0^1 M_I M'_J \, d\alpha \, \mathbf{z}_J - h_n \int_0^1 M_I(\alpha) \mathbb{J} \nabla_{\mathbf{z}} H(\mathbf{z}(\alpha)) \, d\alpha + \delta_{1I} \llbracket \mathbf{z} \rrbracket = \mathbf{0}, \quad I = 1, \dots, k+1. \quad (3.43)$$

The integrand in the first term coincides with a polynomial of order $2k-1$. The corresponding integral can be then exactly computed. However, the integral in the second term generally has to be approximated. By using interpolatory quadrature of the form (3.9), one obtains the following higher order integrator (compare [44, 62, 63]):

$$\boxed{\sum_{J=1}^{k+1} \int_0^1 M_I M'_J \, d\alpha \, \mathbf{z}_J - h_n \sum_{l=1}^{N_q^\alpha} M_I(\xi_l) \mathbb{J} \nabla_{\mathbf{z}} H(\mathbf{z}(\xi_l)) w_l + \delta_{1I} \llbracket \mathbf{z} \rrbracket = \mathbf{0}} \quad I = 1, \dots, k+1. \quad (3.44)$$

$k = 1$	Quadratic potential			Arbitrary potentials	
H	exact	sym. quadrature		sym. quadrature	
	D	$N_q = 1$	$1 < N_q < \infty$	$N_q = 1$	$1 < N_q < \infty$
		C	D	NC	
L	exact	sym. quadrature		sym. quadrature	
	D	$N_q = 1$	$1 < N_q < \infty$	$N_q = 1$	$1 < N_q < \infty$
		C	D	C	NC

Figure 3.4. Conservation properties of the dG(1) method. ‘C’ denotes conservation, ‘D’ denotes decay and ‘NC’ denotes nonconservation, in general. An empty space signifies the absence of a corresponding evidence or counterevidence. ‘exact’ means exact integration and ‘sym. quadrature’ denotes the application of a symmetric quadrature rule, that is a rule with symmetric quadrature points in the master element.

By applying $N_q^\alpha = k + 1$ quadrature points, this family of time stepping schemes is of the order $k + 1 \leq p \leq 2k + 1$ accurate and equivalent to an implicit Runge-Kutta method (see [98]).

Remark 3.3. A nonvanishing jump $[[\mathbf{z}]]$ renders nonconservation of first integrals (see [62, 63]). In these references, there has been shown a total energy decay associated with an arbitrary convex Hamiltonian for constant time finite elements ($k=0$) and associated with a quadratic convex Hamiltonian for higher order time finite elements. The conservation of total angular momentum for constant and linear finite elements in time is discussed in [62]. In Figure 3.4, we have summarised the conservation properties for linear time finite elements ($k=1$). It is remarkable that there is conservation by using *one* symmetric quadrature point (reduced integration). The reason is that the jump $[[\mathbf{z}]]$ in the equations (3.44) associated with $k = 1$ vanishes by applying one Gaussian quadrature point. The resulting integrator is then equivalent to the cG(1) method and leads to total angular momentum conservation in general and total energy conservation in the integrable case.

Chapter 4

One-particle dynamics in a central force field

...the problem was constructed so as to exhibit key features typical of more complex systems with symmetry such as those arising in nonlinear solid mechanics, namely, the presence of large (and relatively slow) overall motions together with high-frequency internal motions...

[54], Abstract.

Dynamics of a single particle under the influence of a central force field is a concrete example of the generalised problem with $n_{poi} = 1$ moving material points. The Hamiltonian formulation of the generalised problem can be therefore applied to this problem. The central force field is based on a potential energy which does not depend on the orientation of the inertial coordinate system associated with the Euclidean space. The angular momentum is consequently a constant of the motion. However, the potential energy depends on the origin of the inertial coordinate system, which prevents a symmetry with respect to translations. Hence the total linear momentum is not conserved. More details about this so-called *one-body problem* can be found in standard books on classical mechanics, for instance [9, 50].

The one-body problem typically results from reducing the motion of two particles under the influence of a mutual central force. In this so-called *two-body central force*

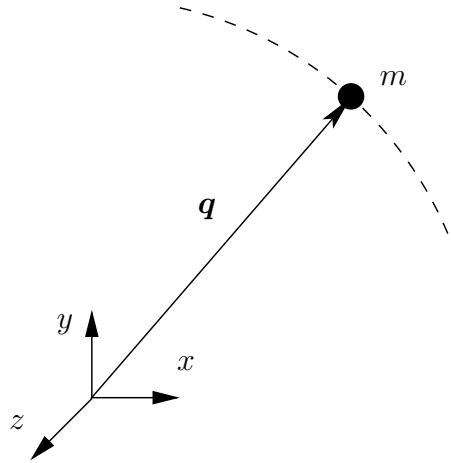


Figure 4.1. The geometry of the one-body problem.

problem, we obtain two independent equations of motion if the three components of the radius vector to the centre of mass as well as the three components of the difference vector between the particles are treated as coordinates. The first equation of motion then states that the centre of mass is either at rest or moving uniformly. The second equation describes the motion of a single particle of a reduced mass, which is positioned at a distance from a fixed centre of force. This central force motion of two particles about their centre of mass can be therefore reduced to an equivalent one-body problem.

4.1 Hamiltonian formulation

We consider a single particle of mass m in the configuration space $Q \subset \mathbb{R}^{n_{dim}}$. The particle moves about a fixed centre of force in the origin of an inertial coordinate system (see Figure 4.1). The current position of the particle is denoted by the position vector $\mathbf{q} \in Q$. The potential energy $V : \mathbb{R}^{n_{dim}} \rightarrow \mathbb{R}$ is only a function of the radial distance $\|\mathbf{q}\|$. Hence we introduce a function $\hat{V} : \mathbb{R}_+ \rightarrow \mathbb{R}$ to describe the potential energy as follows: $V = \hat{V}(\|\mathbf{q}\|)$. The gradient $\nabla_{\mathbf{q}}V$ of this potential energy therefore has to be determined by the chain rule of differentiation:

$$\nabla_{\mathbf{q}}V(\mathbf{q}) = D\hat{V}(\|\mathbf{q}\|)\nabla_{\mathbf{q}}\|\mathbf{q}\| = \frac{D\hat{V}(\|\mathbf{q}\|)}{\|\mathbf{q}\|} \mathbf{I}_{n_{dim}} \mathbf{q} = \mathbb{Q}(\mathbf{q}) \mathbf{q}, \quad (4.1)$$

where the stiffness matrix $\mathbb{Q}(\mathbf{q})$ is given by the equation (2.3) and the corresponding structure matrix reads

$$\mathbf{Q}(\mathbf{q}) = \left[\frac{D\hat{V}(\|\mathbf{q}\|)}{\|\mathbf{q}\|} \right] \quad (4.2)$$

Since the stiffness matrix \mathbb{Q} only depends on $\|\mathbf{q}\|$, it can be rewritten as $\mathbb{Q} = \hat{\mathbb{Q}}(\|\mathbf{q}\|)$.

The inverse mass matrix \mathbb{M}^{-1} has the form (2.16) with the structure matrix

$$\mathbf{M}^{-1} = \left[\frac{1}{m} \right] \quad (4.3)$$

We obtain no conservation of the linear momentum \mathbf{p} because the internal forces do not vanish for an arbitrary motion. However, the angular momentum $\mathbf{L} = \mathbf{q} \times \mathbf{p}$ is conserved.

4.2 Galerkin-based time discretisation

The starting point for designing higher order mechanical integrators is a time discretisation. We now perform a time discretisation of the equations of motion pertaining to the one-body problem by using the cG(k) method:

$$\begin{aligned} \sum_{J=1}^{k+1} \int_0^1 \tilde{M}_I M'_J \, d\alpha \mathbf{q}_J - h_n \int_0^1 \tilde{M}_I(\alpha) \mathbb{M}^{-1} \mathbf{p}(\alpha) \, d\alpha &= \mathbf{0}, \\ \sum_{J=1}^{k+1} \int_0^1 \tilde{M}_I M'_J \, d\alpha \mathbf{p}_J + h_n \sum_{l=1}^k \tilde{M}_I(\xi_l) \hat{\mathbb{Q}}(r^h(\xi_l)) \mathbf{q}(\xi_l) w_l &= \mathbf{0}, \end{aligned} \quad I = 1, \dots, k, \quad (4.4)$$

where $r^h : \mathcal{I}_\alpha \rightarrow \mathbb{R}_+$ denotes an arbitrary time approximation of the radial distance $\|\mathbf{q}\|$. One possible approximation of the radial distance is the Euclidean norm of the approximated position vector \mathbf{q} . We call this time approximation $r = \|\mathbf{q}\|$ of the radial distance the *cG approximation* which only relies on the approximation \mathbf{q} of the position vector. However, the cG approximation of the radial distance has a disadvantage when computing rigid body rotations because it generates an artificial stretch λ at the Gauss points (see Figure 4.2). We have a considerable artificial compression at the midpoint of the master element for $k = 1$ ($\lambda(\xi_1) = 0.7071$), small artificial compressions at both Gauss points for $k = 2$ ($\lambda(\xi_1) = \lambda(\xi_2) = 0.9904$) and both a small artificial compression ($\lambda(\xi_2) = 0.9983$)

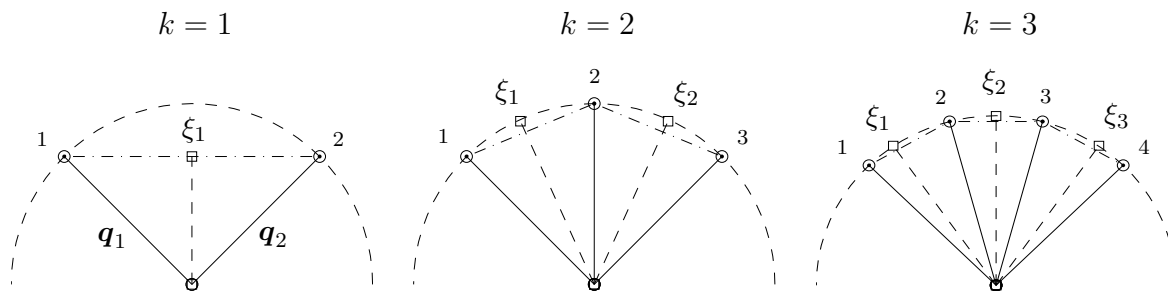


Figure 4.2. Position vector $\mathbf{q}(\alpha)$ at the time nodes I , $I = 1, \dots, k + 1$, and at the Gauss points ξ_l , $l = 1, \dots, k$, on the master element during a rigid body rotation determined by the cG approximation r of the radial distance for $k=1,2,3$.

and extensions ($\lambda(\xi_1) = \lambda(\xi_3) = 1.0027$) for $k = 3$. We refer to the cG(k) method corresponding to the cG approximation r as *standard cG(k) method* or *simple cG(k) method*. The cG(k) method can be related to implicit Gauss Runge-Kutta methods (see [22]) which are known to be a family of symplectic integrators (compare [118]). These integrators preserve the symplectic structure of the integral curves, which leads to a volume preservation in phase space (Liouville's theorem). Thus the property of being symplectic refers to families of integral curves, wherefore it is difficult to interpret its consequence for individual integral curves of the Hamiltonian vector field (for example, see [123, 132] and references therein). We obtain with linear time finite elements ($k = 1$) the symplectic implicit midpoint rule for the one-body problem, which takes the form

$$\begin{aligned} \mathbf{q}_2 - \mathbf{q}_1 - \frac{h_n}{2} \mathbb{M}^{-1} [\mathbf{p}_1 + \mathbf{p}_2] &= \mathbf{0}, \\ \mathbf{p}_2 - \mathbf{p}_1 + \frac{h_n}{2} \hat{\mathbb{Q}} \left(\left\| \frac{\mathbf{q}_1 + \mathbf{q}_2}{2} \right\| \right) [\mathbf{q}_1 + \mathbf{q}_2] &= \mathbf{0}. \end{aligned} \tag{4.5}$$

For instance, this time stepping scheme is investigated in [11, 54].

4.3 Design criterion for energy conservation

In this section, we deduce a criterion for designing mechanical integrators for the one-body problem from the energy conservation condition for the cG(k) method. We employ the gradient (4.1) of the potential energy pertaining to the one-body problem in the energy

conservation condition (3.19) for the $cG(k)$ method and obtain the relation

$$\hat{V}(r^h(1)) - \hat{V}(r^h(0)) = \sum_{l=1}^k D\hat{V}(r^h(\xi_l)) \frac{\mathbf{q}(\xi_l)}{r^h(\xi_l)} \cdot \frac{d\mathbf{q}(\xi_l)}{d\alpha} w_l. \quad (4.6)$$

We now suppose that the approximated position vector \mathbf{q} and the approximation r^h of the radial distance are related at all Gauss points ξ_l , $l = 1, \dots, k$, as follows:

$$\frac{\mathbf{q}(\xi_l)}{r^h(\xi_l)} \cdot \frac{d\mathbf{q}(\xi_l)}{d\alpha} = \frac{dr^h(\xi_l)}{d\alpha} \quad (4.7)$$

Taking equation (4.7) into account, the total energy H is conserved if the following equation holds:

$$\boxed{\hat{V}(r^h(1)) - \hat{V}(r^h(0)) = \sum_{l=1}^k D\hat{V}(r^h(\xi_l)) \frac{dr^h(\xi_l)}{d\alpha} w_l} \quad (4.8)$$

We refer to equation (4.8) as the *design criterion* for an energy conserving integrator for the one-body problem.

Remark 4.1. Since the potential energy V is given by the potential function \hat{V} which only depends on the radial distance, the gradient $\nabla_{\mathbf{q}}V$ is determined by the chain rule of differentiation (see equation (4.1)). Hence equation (4.7) maintains the gradient form (2.2) of the internal forces at the Gauss points. We therefore have to bear in mind that relation (4.7) is satisfied. In Section 3.2.3, we have mentioned that the energy conservation condition can be considered as a discrete version of the gradient theorem. The design criterion (4.8) can be viewed as a discrete version of the gradient theorem in polar coordinates.

4.4 Enhanced derivative

We consider the design criterion (4.8) as constraint on the ordinary derivative $D\hat{V}$. We obtain the problem of finding a function with a minimal distance to the ordinary derivative, which satisfies the design criterion as constraint. This problem leads to an additive enhanced derivative, as we can see in this section. This kind of variational problem with

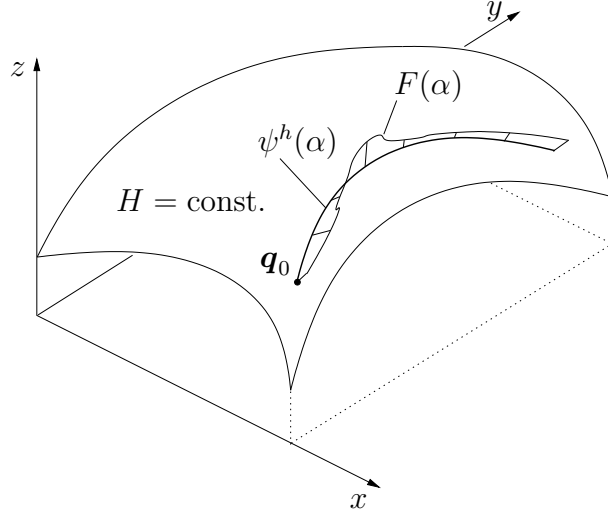


Figure 4.3. Generalised force $F(\alpha)$ associated with the constraint of energy conservation along the approximated motion $\psi^h(\alpha)$ starting at \mathbf{q}_0 and lying in the surface $H = \text{const.}$

constraint can be classified as *isoperimetrical problem* in view of the specific constraint. (See [47, 31, 91, 69, 46] for further details about isoperimetrical problems. For completeness, a summary of the main features of solving isoperimetrical problems is given in Appendix A.6). The minimisation of the distance to the ordinary derivative is equivalent to minimising the functional

$$\mathcal{F}(D\hat{V}) = \frac{1}{2} \int_0^1 \left[D\hat{V}(\alpha) - D\hat{V}(r^h(\alpha)) \right]^2 d\alpha. \quad (4.9)$$

Since the design criterion has to be simultaneously satisfied while minimising \mathcal{F} , we have to introduce the constraint $\mathcal{G} = 0$, where

$$\mathcal{G}(D\hat{V}) = \hat{V}(r^h(1)) - \hat{V}(r^h(0)) - \int_0^1 D\hat{V}(\alpha) \frac{dr^h(\alpha)}{d\alpha} d\alpha. \quad (4.10)$$

We now augment \mathcal{F} with the constraint \mathcal{G} through a Lagrange multiplier $\lambda \in \mathbb{R}$ and obtain the Lagrange functional $\mathcal{L} = \mathcal{F} + \lambda \mathcal{G}$. The minimisation of this Lagrange functional then results in the corresponding Euler-Lagrange equation. Taking the constraint into account, the solution of this Euler-Lagrange equation is given by an additive enhanced derivative of the form

$$\boxed{D\hat{V}(\alpha) = D\hat{V}(r^h(\alpha)) + \frac{\mathcal{G}(D\hat{V})}{\mathcal{N}} \frac{dr^h(\alpha)}{d\alpha}} \quad (4.11)$$

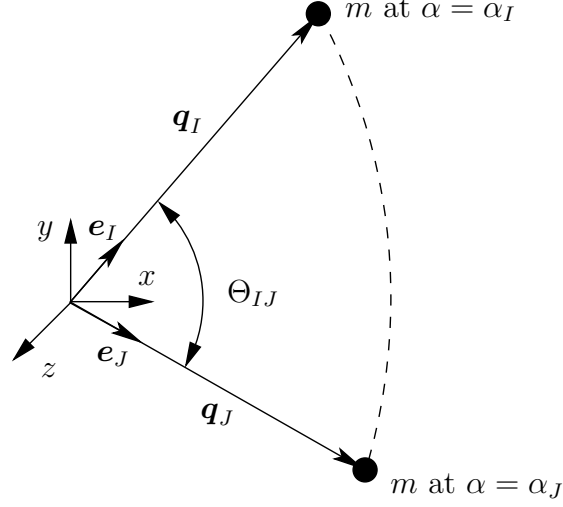


Figure 4.4. The geometry of the two positions of a particle m at the time nodes α_I and α_J .

where

$$\mathcal{N} = \int_0^1 \frac{dr^h(\alpha)}{d\alpha} \frac{dr^h(\alpha)}{d\alpha} d\alpha. \quad (4.12)$$

In the computational setting, we apply a k -point Gaussian quadrature rule with the accuracy $\mathcal{O}(h_n^{2k})$ for solving the integrals. The design criterion is then determined such that

$$\mathcal{G}(D\hat{V}) = \hat{V}(r^h(1)) - \hat{V}(r^h(0)) - \left[\hat{V}(r^h(1)) - \hat{V}(r^h(0)) + \mathcal{O}(h_n^{2k}) \right]. \quad (4.13)$$

This implies that the distance of the enhanced derivative to the ordinary derivative is within the error bounds of the Gaussian quadrature in the cG(k) method. The accuracy of the cG(k) method is therefore not deteriorated by the enhanced derivative.

Remark 4.2. The last term of the enhanced derivative in equation (4.11) can be regarded as a generalised force $F(\alpha)$ for the enforcement of the constraint of energy conservation (compare Lagrange equations for holonomic constraints in standard books on classical mechanics). Note that in the case of exact quadrature this force vanishes due to the intrinsic energy conservation of the one-body problem, however in the case of numerical quadrature this generalised force $F(\alpha)$ does generally not vanish (see Figure 4.3).

4.5 Assumed distance approximation

The enhanced derivative (4.11) gives rise to the question for an appropriate time approximation r^h of the radial distance. Since the radial distance is invariant with respect to an occurring rigid body rotation, we seek for a time approximation r^h which retains this property. Further, the invariance with respect to rigid body motions should be numerically preserved because this property can be related to the numerical stability of the time stepping scheme (see [54] and [5] for instance). We start from the cG approximation r of the radial distance and separate that part which satisfies the invariance property. For this purpose, let $r_I = \|\mathbf{q}_I\|$ denote the absolute value of the position vector $\mathbf{q}_I = r_I \mathbf{e}_I$ at the time node α_I , where \mathbf{e}_I is the associated directional unit vector. The squared absolute value of the cG approximation r is then given by

$$\mathbf{q} \cdot \mathbf{q} = \sum_{I,J=1}^{k+1} M_I M_J \mathbf{q}_I \cdot \mathbf{q}_J = \sum_{I,J=1}^{k+1} M_I M_J r_I r_J \cos \Theta_{IJ}, \quad (4.14)$$

where $\cos \Theta_{IJ} = \mathbf{e}_I \cdot \mathbf{e}_J$ (see Figure 4.4). It follows from the dependence on the angle Θ_{IJ} that the cG approximation r is affected by a rigid body rotation through a scaling with a factor, however the squared absolute value of r can be split into two terms:

$$\mathbf{q} \cdot \mathbf{q} = r^2 + 2 \sum_{I=1}^k \sum_{J=I+1}^{k+1} M_I M_J r_I r_J (\cos \Theta_{IJ} - 1), \quad (4.15)$$

where

$$r^2 = \sum_{I,J=1}^{k+1} M_I M_J r_I r_J. \quad (4.16)$$

Taking the square root of r^2 , we obtain an interpolation formula over the distances r_I at the time nodes of the master element:

$$\boxed{r(\alpha) = \sum_{I=1}^{k+1} M_I(\alpha) r_I} \quad (4.17)$$

This interpolation formula is called the *assumed distance approximation* of the radial distance (see [19]). The assumed distance approximation r is not affected by a rigid body

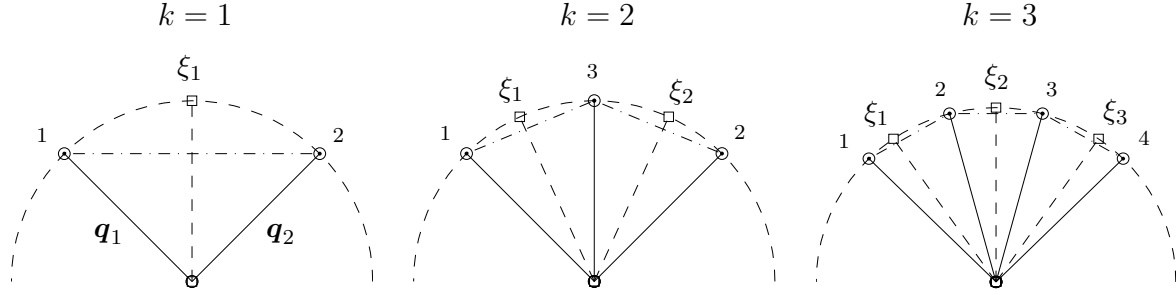


Figure 4.5. Position vector $\mathbf{q}(\alpha)$ at the time nodes I , $I = 1, \dots, k + 1$, and at the Gauss points ξ_l , $l = 1, \dots, k$, on the master element during a rigid body rotation determined by the assumed distance approximation r of the radial distance for $k=1,2,3$.

rotation due to the absence of the angle Θ_{IJ} (compare [54]) and it therefore preserves the symmetry of the one-body problem with respect to rigid body rotations on the whole master element. This property is due to the completeness condition of the Lagrange polynomials M_I , $I = 1, \dots, k + 1$. The assumed distance approximation is also a consistent time approximation of the radial distance because the approximation order is the same as that of the cG approximation of the position vector (compare Appendix C.2). Accordingly, the assumed distance approximation can be applied as physically consistent time approximation of the radial distance.

Remark 4.3. The application of the assumed distance approximation can be interpreted as an approximation of the position vector with respect to the corotational directional unit vector $\mathbf{e}(\alpha) = \mathbf{q}(\alpha)/\|\mathbf{q}(\alpha)\|$, whereby the length of the position vector is approximated by the assumed distance approximation. Accordingly, the position vector is approximated by the vector $\mathbf{q}(\alpha) = r(\alpha) \mathbf{e}(\alpha)$ which does not change its length during rigid body rotations (see Figure 4.5). On the contrary, the cG approximation is an approximation with respect to the inertial coordinate frame (x, y, z) with the directional unit vectors \mathbf{e}_x , \mathbf{e}_y and \mathbf{e}_z (compare [36, 112, 32, 35]).

4.6 Enhanced assumed derivative

In this section, we apply the assumed distance approximation r to the enhanced derivative (4.11) while retaining its total energy conservation property. The application of the

assumed distance approximation to the enhanced derivative is restricted by the condition (4.7) which has to be fulfilled at all Gauss points in those terms where the chain rule of differentiation is used. In the special case $k = 1$, the assumed distance approximation and the cG approximation \mathbf{r} satisfies this condition at the one Gauss point $\alpha = 1/2$. However, generally the chain rule of differentiation can be preserved only by the cG approximation for which the condition (4.7) is fulfilled for arbitrary k . In other terms, however, we apply the assumed distance approximation such that the design criteria in the enhanced derivatives take the following form:

$$\underline{\mathcal{G}} = \hat{V}(\mathbf{r}(1)) - \hat{V}(\mathbf{r}(0)) - \sum_{l=1}^k D\hat{V}(\mathbf{r}(\xi_l)) \frac{d\mathbf{r}(\xi_l)}{d\alpha} w_l. \quad (4.18)$$

This composite approximation is possibly due to the same accuracy order of both distance approximations. By using Gaussian quadrature for calculating all integrals, the enhanced derivative associated with the design criterion (4.18) reads

$$\boxed{\underline{D}\hat{V} = D\hat{V}(\mathbf{r}) + \frac{\underline{\mathcal{G}}}{\underline{\mathcal{N}}} \frac{d\mathbf{r}}{d\alpha}} \quad (4.19)$$

where

$$\underline{\mathcal{N}} = \sum_{l=1}^k \frac{d\mathbf{r}(\xi_l)}{d\alpha} \frac{d\mathbf{r}(\xi_l)}{d\alpha} w_l. \quad (4.20)$$

The cG approximation is only applied in the Lagrange multiplier $\lambda = \underline{\mathcal{G}}/\underline{\mathcal{N}}$ which scales the length of the generalised force associated with the energy conservation. The generalised force direction, which is represented by the derivative $d\mathbf{r}/d\alpha$, is invariant with respect to rigid body rotations.

4.7 The enhanced Galerkin (eG) method

A mechanical integrator is a time integration method preserving the physical structure of the underlying mechanical system. We are essentially interested in preserving first integrals. The first integrals of the one-body problem are the total energy $H(\mathbf{q}, \mathbf{p})$ and the angular momentum $\mathbf{L} = \mathbf{q} \times \mathbf{p}$. The cG(k) method preserves the angular momen-

tum by collocation at k Gauss points . The total energy is preserved by the enhanced derivative. By using the assumed distance approximation, we also conserve the symmetry with respect to rigid body rotations. We therefore recommend as higher order accurate mechanical integrator the $cG(k)$ method in conjunction with the enhanced derivative and the assumed distance approximation. We refer to this mechanical integrator as the *enhanced $cG(k)$ method* or short *enhanced Galerkin ($eG(k)$) method*, which applied to the one-body problem reads

$$\boxed{\begin{aligned} \sum_{J=1}^{k+1} \int_0^1 \tilde{M}_I M'_J \, d\alpha \, \mathbf{q}_J - \frac{h_n}{m} \int_0^1 \tilde{M}_I(\alpha) \mathbf{p}(\alpha) \, d\alpha &= \mathbf{0}, \\ \sum_{J=1}^{k+1} \int_0^1 \tilde{M}_I M'_J \, d\alpha \, \mathbf{p}_J + h_n \sum_{l=1}^k \tilde{M}_I(\xi_l) \frac{\mathbf{D}\hat{V}(\xi_l)}{\mathbf{r}(\xi_l)} \mathbf{q}(\xi_l) w_l &= \mathbf{0}, \end{aligned}} \quad I = 1, \dots, k. \quad (4.21)$$

The $eG(1)$ method for the one-body problem is identical to a well known mechanical integrator proposed in [51, 52, 54], which is given by

$$\begin{aligned} \mathbf{q}_2 - \mathbf{q}_1 - \frac{h_n}{2m} [\mathbf{p}_1 + \mathbf{p}_2] &= \mathbf{0}, \\ \mathbf{p}_2 - \mathbf{p}_1 + h_n \frac{\hat{V}(\|\mathbf{q}_2\|) - \hat{V}(\|\mathbf{q}_1\|)}{\|\mathbf{q}_2\| - \|\mathbf{q}_1\|} \frac{\mathbf{q}_1 + \mathbf{q}_2}{\|\mathbf{q}_1\| + \|\mathbf{q}_2\|} &= \mathbf{0}. \end{aligned} \quad (4.22)$$

This scheme is occasionally referred to as *Simo-Gonzalez method* (see [11] for instance).

4.8 Numerical investigations

In this section, we compare the conservation properties, accuracy as well as computational costs of the $eG(k)$ method and the $cG(k)$ method by means of a numerical example. Further, the efficiency of higher order finite elements in time is investigated for both methods. To this end we begin by describing the linearisation of both methods and we conclude with the discussion of the numerical results.

4.8.1 Linearisation of the algorithms

The solution of the cG(k) as well the eG(k) method is performed according to Section 3.2.6. In the Newton-Raphson method, we have set the tolerance ϵ of the stopping criteria to $\epsilon = 10^{-10}$. The blocks \mathbf{K}_J , $J = 2, \dots, k+1$ of the tangent operator \mathbf{K} pertaining to the cG(k) and the eG(k) method can be divided in two parts: $\mathbf{K}_J = \mathbf{K}_{\text{Geo}_J} + \mathbf{K}_{\text{Mat}_J}$, where the matrix $\mathbf{K}_{\text{Geo}_J}$ is called the geometrical part associated with the node J and the matrices $\mathbf{K}_{\text{Mat}_J}$ are called the material parts. In general, the geometrical parts of the tangent are defined to be those parts which are associated with the linearisation of the so-called *B-matrices* of the nonlinear problem and the material parts result from linearising the algorithmic constitutive law. Note that in the nonlinear case the B-matrices are those matrices which are used to formulate the conservative forces as product with the algorithmic constitutive law. Here we have thus the following B-matrices:

$$\mathbf{B} = \frac{\mathbf{q}}{\mathbf{r}} \qquad \mathbf{B}_J = \frac{\mathbf{q}_J}{r_J} \qquad (4.23)$$

The symmetric geometrical parts then follow from linearising the matrix \mathbf{B} . The geometrical as well as the material parts associated with the cG method take the form

$$\mathbf{K}_{\text{Geo}_J} = M_J \frac{D\hat{V}(\mathbf{r})}{\mathbf{r}} [\mathbf{I}_{n_{dim}} - \mathbf{B} \otimes \mathbf{B}], \qquad (4.24)$$

$$\mathbf{K}_{\text{Mat}_J} = M_J D^2\hat{V}(\mathbf{r}) \mathbf{B} \otimes \mathbf{B}.$$

Since the cG approximation of the radial distance is also applied in the eG method, the geometrical parts associated with the eG method are similar to those of the cG method, however the corresponding material parts are more difficult as those of the cG method:

$$\begin{aligned} \underline{\mathbf{K}}_{\text{Geo}_J} &= M_J \frac{D\hat{V}}{\mathbf{r}} [\mathbf{I}_{n_{dim}} - \mathbf{B} \otimes \mathbf{B}], \\ \underline{\mathbf{K}}_{\text{Mat}_J} &= \left[\left[M_J D^2\hat{V}(\mathbf{r}) + M'_J \frac{\underline{\mathcal{G}}}{\underline{\mathcal{N}}} \right] + \delta_{J,k+1} \left[\frac{1}{\underline{\mathcal{N}}} D\hat{V}(r_J) \frac{d\mathbf{r}}{d\alpha} \right] \right] \mathbf{B} \otimes \mathbf{B}_J - \\ &- \left[\frac{1}{\underline{\mathcal{N}}} \frac{d\mathbf{r}}{d\alpha} \underline{\mathbf{L}}_1 \right] \mathbf{B} \otimes \mathbf{B}_J - \left[\frac{1}{\underline{\mathcal{N}}} \frac{d\mathbf{r}}{d\alpha} \right] \mathbf{B} \otimes \underline{\mathbf{L}}_2, \end{aligned} \qquad (4.25)$$

where

$$\begin{aligned}\underline{\mathbf{L}}_1 &= \sum_{l=1}^k \frac{dr(\xi_l)}{d\alpha} \left[M_J(\xi_l) D^2 \hat{V}(r(\xi_l)) + M'_J(\xi_l) \frac{\underline{\mathcal{G}}}{\underline{\mathcal{N}}} \right] w_l, \\ \underline{\mathbf{L}}_2 &= \sum_{l=1}^k D\hat{V}(r(\xi_l)) \left[M'_J \mathbf{B}(\xi_l) + M_J \frac{d\mathbf{B}(\xi_l)}{d\alpha} \right] w_l.\end{aligned}\tag{4.26}$$

Note that the material parts of the cG method are symmetric and those of the eG method are unsymmetric.

4.8.2 Stiff Neo-Hooke type spring potential

We consider a particle with the mass $m = 10$ and the initial position $\mathbf{q}_0 = (2, 1, 1)$ in the three-dimensional Euclidean space (see Figure 4.6). We initiate the particle motion by an initial angular velocity vector $\boldsymbol{\omega}_0 = (0.5, -2, 1)$. The initial velocity \mathbf{v}_0 has been determined by $\mathbf{v}_0 = \boldsymbol{\omega}_0 \times \mathbf{q}_0$. The particle can be thought of as connected with the origin via a stiff nonlinear spring with stiffness $c = 10^3$ and a spring length $\bar{r} = 4$ in the force free configuration. The potential energy of the spring is derived from a one-dimensional compressible Neo-Hooke material and has the form (also see [19])

$$\hat{V}(r) = \frac{c}{6} \bar{r}^2 \left[\left(\frac{r}{\bar{r}} \right)^2 + 2 \frac{\bar{r}}{r} - 3 \right]\tag{4.27}$$

The first integrals of the motion are the angular momentum $\mathbf{L} = \mathbf{q} \times \mathbf{p}$ and the total energy $H = T + \hat{V}$. The angular momentum \mathbf{L}_0 of the particle at the initial state is given by

$$\mathbf{L}_0 = m \mathbf{q}_0 \times (\boldsymbol{\omega}_0 \times \mathbf{q}_0) = m r_0^2 \boldsymbol{\omega}_0 = (30, -120, 60)\tag{4.28}$$

and the corresponding total energy H_0 of the particle reads

$$H_0 = T(\mathbf{v}_0) + \hat{V}(r_0) = \frac{1}{2} m r_0^2 \|\boldsymbol{\omega}_0\|^2 + \hat{V}(r_0) = 1866.8,\tag{4.29}$$

where $r_0 = \|\mathbf{q}_0\|$ denotes the absolute value of the initial position vector.

4.8.3 Discussion of the results

In Figure 4.7, we depict the particle orbits which are determined by the eG method. A comparison of the orbits reveals that the final position of the motion depends on the accuracy of the method (compare the orbits within the dotted circles). The difference between $k = 2$ and $k = 3$ is thereby smaller as between $k = 1$ and $k = 2$. Total angular momentum and total energy is depicted in Figure 4.7 and Figure 4.8, respectively. The first integrals which are computed by the eG method stay at the initial values independent of the family parameter k and the chosen time step size h_n . The total angular momentum corresponding to the cG method is also constant over the whole time interval. The total energy of the cG method however oscillates between two bounds which are associated with the inner and the outer turning points of the orbit. Moreover, we see that the cG method tends to instabilities after a perturbation, since its total energy no longer periodically oscillates after changing the time step size. The last diagram in Figure 4.8 depicts the residual error of the energy conservation condition (3.19) pertaining to $k = 3$. The cG method particularly violates the energy conservation condition at the turning points of the orbit, whereas the residual error corresponding to the eG method is below the Newton-Raphson tolerance ϵ . We summarise that the total energy of the cG method depends on the family parameter k , on the time step size h_n as well as on the motion itself. This is in opposition to the total energy evolution of the eG method.

The left diagram of Figure 4.9 shows the graphs of the relative global error in the position at time T versus the time step size. This relative error is defined by

$$e_{\mathbf{q}} = \frac{\|\mathbf{q}(T) - \mathbf{q}^{ref}(T)\|}{\|\mathbf{q}^{ref}(T)\|} \quad (4.30)$$

where $\mathbf{q}^{ref}(T)$ denotes a reference solution at time T . The reference solution is computed by the eG(4) method with a time step size $h_n = 0.01$. The graphs have the shape of lines due to the logarithmic scale for both axes. The slopes of these lines specify the accuracy order $\mathcal{O}(h^{2k})$ of the continuous Galerkin method (compare [82]). Since both methods show similar accuracy properties, we observe for both methods the same behaviour if k is increased; we observe increasing slopes of the lines and decreasing line intercepts.

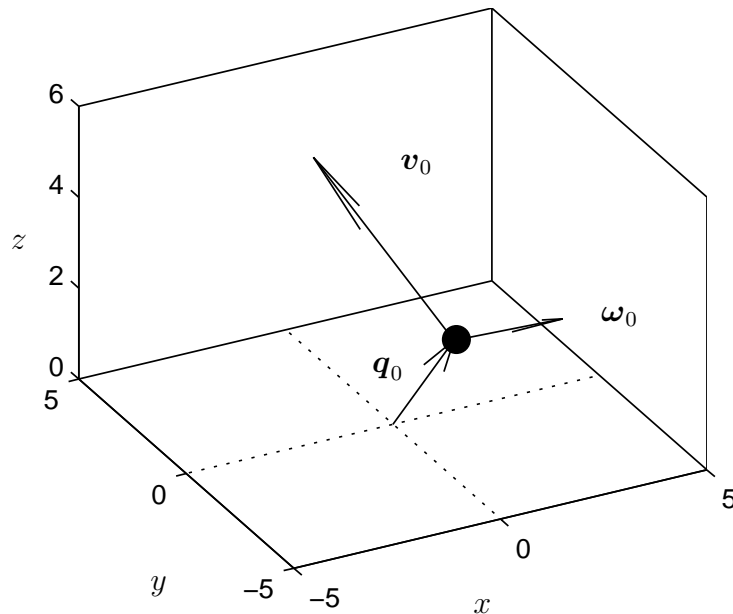


Figure 4.6. Initial velocity vector \mathbf{v}_0 and initial angular velocity vector $\boldsymbol{\omega}_0$ of a mass point at initial position \mathbf{q}_0 .

Considering a relative global error achievable with $k = 1, 2, 3$, the corresponding time step size is increasing by increasing the parameter k . Hence a greater family parameter is associated with allowing a greater time step size to obtain the solution at time T .

In the right diagram of Figure 4.9, the relative global error is depicted versus the corresponding CPU time in a double logarithmic scale. We also obtained lines by virtue of a least square curve fitting. First we compare the CPU time of a specific method by increasing k . We observe that with a greater k , less CPU time is required to achieve a prescribed accuracy. This observation holds for both cG and eG method. The saving of CPU time with a greater family parameter is related to larger time steps and to a smaller iteration number within the Newton-Raphson iteration. The smaller iteration number is a direct consequence of the higher accuracy. Comparing both methods for a fixed k , the CPU time of the eG method is generally longer in comparison with the cG method because of the more extensive internal force and the corresponding tangent operator. The advantage of the eG method in comparison with the cG method is a better stability because the eG method allows for time steps larger as those for the cG method. This is evident if the time step size h_n has been set larger as the largest depicted in Figure 4.9.

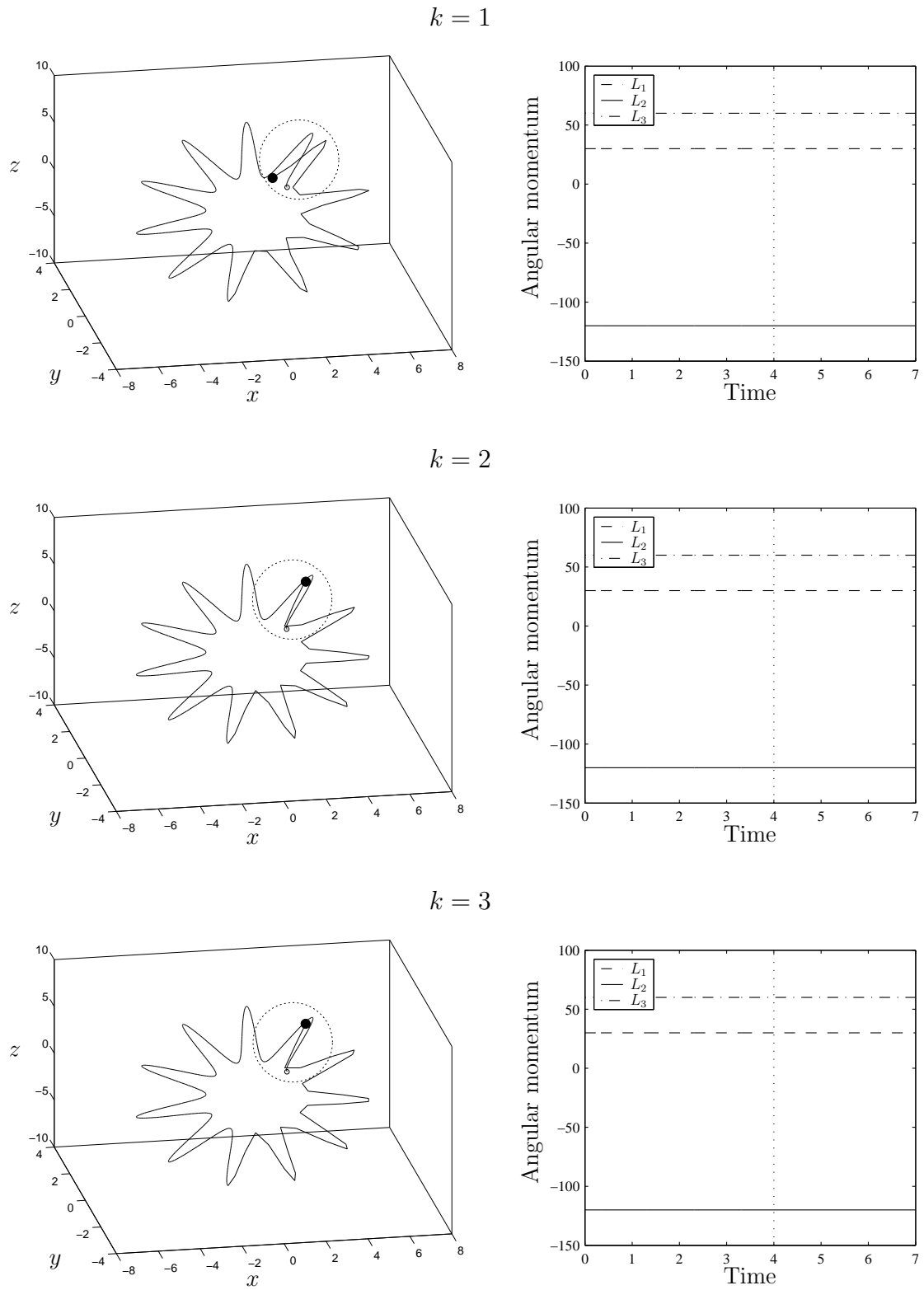


Figure 4.7. Orbit and total angular momentum of a particle (mass $m = 10$, spring stiffness $c = 10^3$) computed with the eG method ($k = 1$, $k = 2$ and $k = 3$). The time step size h_n has been set to 0.01 for $T \leq 4$ and to 0.1 for $T > 4$.

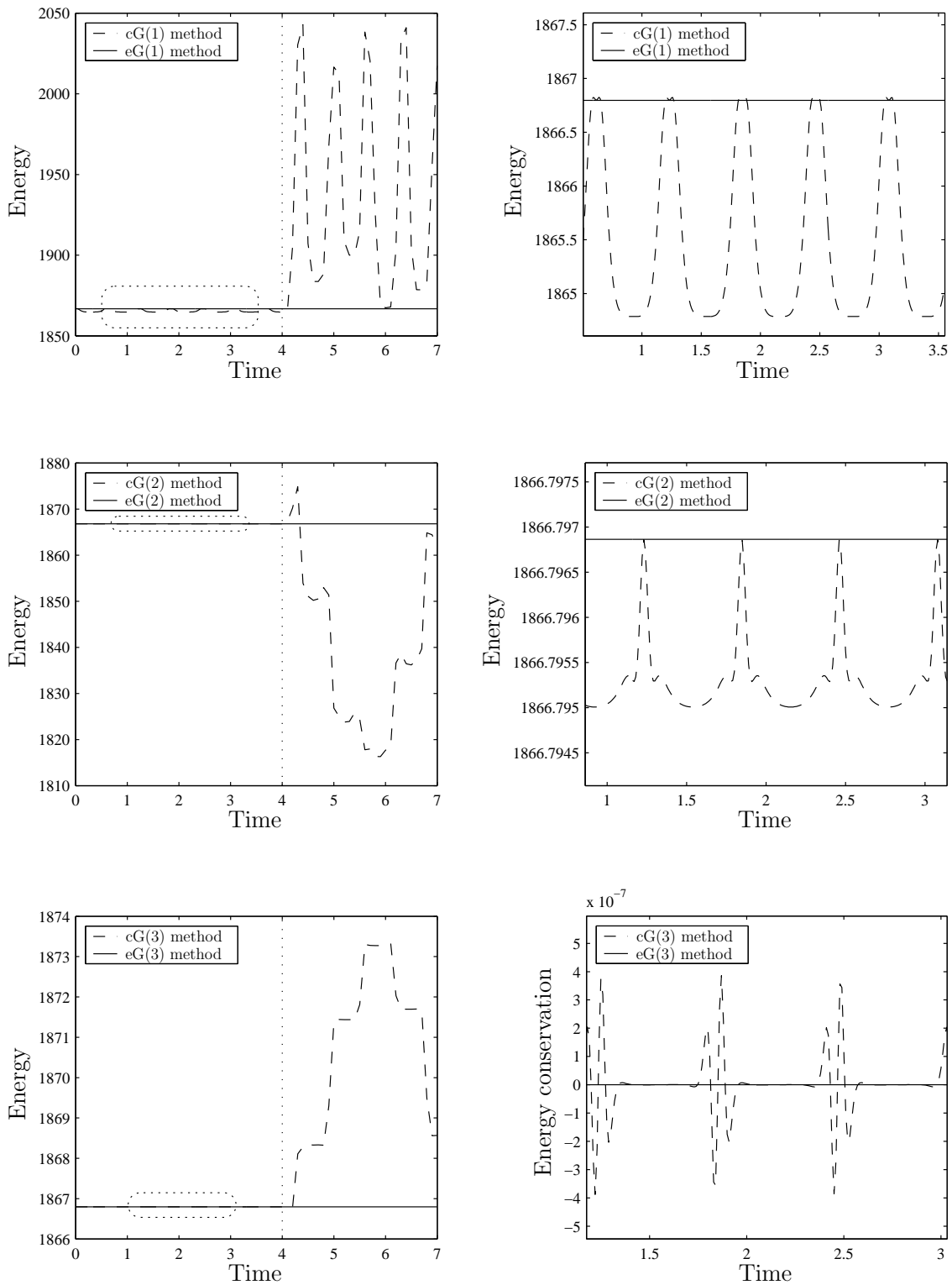


Figure 4.8. Total energy of a particle (mass $m = 10$, spring stiffness $c = 10^3$) computed with the cG method as well as with the eG method. The time step size h_n has been set to 0.01 for $T \leq 4$ and to 0.1 for $T > 4$.

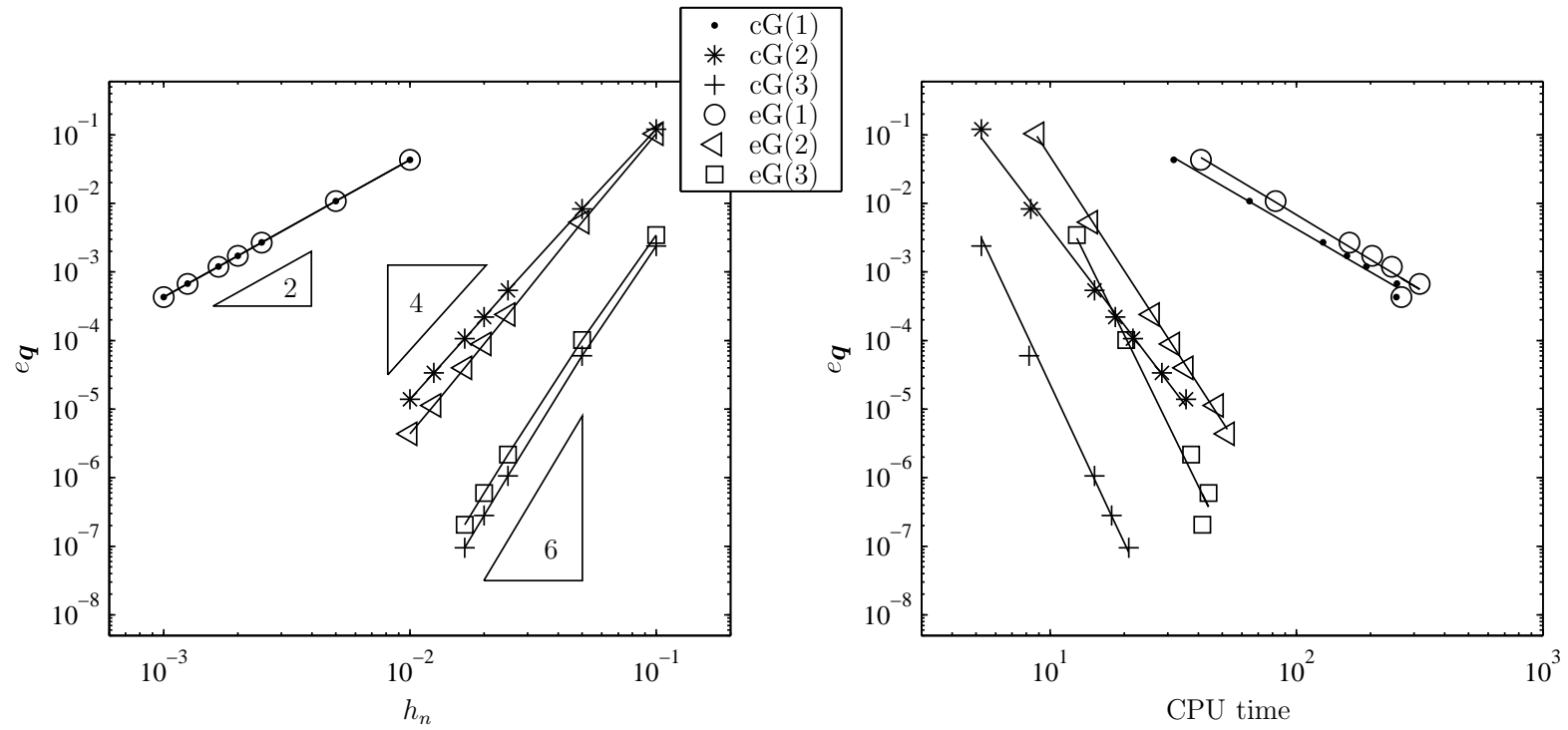


Figure 4.9. Relative global error in the position (on the left) and corresponding CPU time (on the right) of a particle motion (mass $m = 10$, spring stiffness $c = 10^3$) at time $T = 10$ pertaining to the cG and the eG method for $k = 1, 2, 3$.

Chapter 5

Dynamics of many-particle systems

...We do not need exact classical trajectories to do this, but must lay great emphasis on energy conservation as being of primary importance for this reason. Momentum conservation is also important, but this can usually be easily arranged...

[3], Chapter 3: Molecular Dynamics.

Many-particle dynamics are also covered by the generalised problem in Section 2. The material points of the configuration are particles with mass. In contrast to the one-body problem, the potential energy in many-particle dynamics depends neither on the orientation nor on the origin of an inertial coordinate system. Translations as well as rotations of a many-particle configuration are therefore symmetry groups and the total linear momentum is preserved along with the total angular momentum. We here suppose that the interaction forces are large enough to prevent collisions during the motions.

In standard books of classical mechanics, the problem of moving many-particle configurations is often called *N-body problem* or *many-body problem* (see [9, 50, 106] for example). The many-body problem is typically mentioned in connection with motions in the outer solar system and molecular dynamics. In the outer solar system, the potential energy is associated with the so-called *Kepler potential* due to the gravitational forces between the planets. Astronomers have studied the motions of the outer solar system in long term computations and have observed a chaotic evolution [134]. In molecular dynamics, the Lennard-Jones potential is very popular to describe the repulsive and attractive forces

between molecules [71]. This potential is a special case of the Mie potential (see also [133] for an overview). Computations in molecular dynamics usually aim at macroscopic quantities such as temperature, pressure or energy and more or less using the trajectories of the atoms [3].

5.1 Hamiltonian formulation

We consider a configuration of n_{par} particles of masses m_A , $A = 1, \dots, n_{par}$, moving in the Euclidean space $\mathbb{R}^{n_{dim}}$. The potential energy V of the configuration is related to all potentials $V^{AB} = V^{BA}$ corresponding to interactional forces between the particles A and B :

$$V(\mathbf{q}) = \sum_{A=1}^{n_{par}-1} \sum_{B=A+1}^{n_{par}} V^{AB}(\mathbf{q}^A, \mathbf{q}^B). \quad (5.1)$$

We refer to the vectors $\mathbf{r}^{AB} = \mathbf{q}^B - \mathbf{q}^A$, $B \neq A$, as the radius vector from particle A to particle B . The potentials of interaction only depend on the distances $r^{AB} = \|\mathbf{r}^{AB}\|$ between the particles. For this reason we define functions $\hat{V}^{AB} : \mathbb{R}_+ \rightarrow \mathbb{R}$ and write the potentials of interaction as $V^{AB} = \hat{V}^{AB}(\|\mathbf{r}^{AB}\|)$. The gradients $\nabla_{\mathbf{q}^A} V^{AB}$ of the potentials of interaction accordingly take the form

$$\nabla_{\mathbf{q}^A} V^{AB} = D\hat{V}^{AB} \nabla_{\mathbf{r}^{AB}} \|\mathbf{r}^{AB}\| \cdot \nabla_{\mathbf{q}^A} \mathbf{r}^{AB} = -\frac{D\hat{V}^{AB}}{\|\mathbf{r}^{AB}\|} \mathbf{r}^{AB}. \quad (5.2)$$

Thus the coefficients of the symmetric stiffness structure matrix (2.4) have the form

$$Q_{AB} = \begin{cases} -\frac{D\hat{V}^{AB}(\|\mathbf{r}^{AB}\|)}{\|\mathbf{r}^{AB}\|} & \text{if } A \neq B, \\ \sum_{\substack{C=1 \\ C \neq A}}^{n_{par}} \frac{D\hat{V}^{AC}(\|\mathbf{r}^{AC}\|)}{\|\mathbf{r}^{AC}\|} & \text{if } A = B. \end{cases} \quad (5.3)$$

Since the potential energy only depends on the particle distances $r^{AB} \in \mathbb{R}_+$, we redefine the stiffness matrix as $\mathbb{Q} = \hat{\mathbb{Q}}(\mathbf{r})$, where \mathbf{r} denotes the following matrix including the

particle distances r^{AB} as components:

$$\mathbf{r} = \begin{bmatrix} 0 & r^{12} & \dots & r^{1n_{par}} \\ r^{21} & 0 & \dots & r^{2n_{par}} \\ \vdots & & & \vdots \\ r^{n_{par}1} & \dots & \dots & 0 \end{bmatrix} \quad (5.4)$$

The mass matrix of the many-body problem is associated with a diagonal structure matrix with coefficients $M_{AB} = m_A \delta_{AB}$, where δ_{AB} designates the Kronecker delta. The inversion of the structure matrix then leads to the coefficients $M_{AB}^{-1} = 1/m_A \delta_{AB}$ of the inverse structure matrix (2.17). We have a closed particle system due to the coefficients (5.3):

$$\sum_{A,B=1}^{n_{par}} Q_{AB} \mathbf{q}^B = \sum_{\substack{A,B=1 \\ B \neq A}}^{n_{par}} Q_{AB} \mathbf{q}^B + \sum_{A=1}^{n_{par}} Q_{AA} \mathbf{q}^A = \mathbf{0}. \quad (5.5)$$

Therefore, the total linear momentum is conserved. Moreover, we have total angular momentum conservation because the mass and the stiffness matrix are symmetric.

5.2 Galerkin-based time discretisation

We perform a temporal discretisation of Hamilton's equations of motion for the many-body problem by applying the cG(k) method. On the basis of this family of time stepping schemes we derive mechanical integrators by incorporating the energy conservation condition (3.19) in the following sections. We obtain the following schemes:

$$\begin{aligned} \sum_{J=1}^{k+1} \int_0^1 \tilde{M}_I M'_J \, d\alpha \mathbf{q}_J - h_n \int_0^1 \tilde{M}_I \mathbb{M}^{-1} \mathbf{p} \, d\alpha &= \mathbf{0}, \\ \sum_{J=1}^{k+1} \int_0^1 \tilde{M}_I M'_J \, d\alpha \mathbf{p}_J + h_n \sum_{l=1}^k \tilde{M}_I(\xi_l) \hat{\mathbb{Q}}(\mathbf{r}^h(\xi_l)) \mathbf{q}(\xi_l) w_l &= \mathbf{0}, \end{aligned} \quad I = 1, \dots, k, \quad (5.6)$$

where $\mathbf{r}^h : \mathcal{I}_\alpha \rightarrow \mathbb{R}_+^{n_{par} \times n_{par}}$ is an arbitrary time approximation of the matrix (5.4). For example, a time approximation of this matrix can be generated by the absolute val-

ues $r^{AB} = \|\mathbf{r}^{AB}\|$ of the approximated distance vectors $\mathbf{r}^{AB} = \sum_{I=1}^{k+1} M_I(\alpha) \mathbf{r}_I^{AB}$, where $\mathbf{r}_I^{AB} = \mathbf{q}_I^B - \mathbf{q}_I^A$. We refer to the matrix \mathbf{r} corresponding to the particle distances r^{AB} as the *cG approximation* of the matrix (5.4). Note that this time approximation is leading to artificial strains between the time nodes during a rigid body rotation (compare Section 4.2). Then we call the cG(k) method associated with the cG approximation \mathbf{r} the *standard cG(k) method* or simple *cG(k) method*. This method is leading to implicit Gauss Runge-Kutta schemes (see [22]) which are identified as symplectic and momentum conserving in [118]. In the special case of linear time finite elements ($k = 1$), we obtain the implicit midpoint rule which is given by

$$\begin{aligned} \mathbf{q}_2 - \mathbf{q}_1 - \frac{h_n}{2} \mathbb{M}^{-1} [\mathbf{p}_1 + \mathbf{p}_2] &= \mathbf{0}, \\ \mathbf{p}_2 - \mathbf{p}_1 + \frac{h_n}{2} \hat{\mathbb{Q}} \left(\mathbf{r} \left(\frac{1}{2} \right) \right) [\mathbf{q}_1 + \mathbf{q}_2] &= \mathbf{0}. \end{aligned} \quad (5.7)$$

This integrator is second order accurate and can be also derived by finite differences (see [123, 19]).

5.3 Design criterion for energy conservation

In this section, we deduce a criterion for designing mechanical integrators for the many-body problem. Since the potential energy of the particle configuration results from summing over the potentials of interaction, we are able to localise the energy conservation condition (3.19) with respect to an arbitrary particle pair (A, B). The resulting equation is then formulated in the corresponding interaction potential \hat{V}^{AB} :

$$\hat{V}^{AB} \left(r^{AB^h}(1) \right) - \hat{V}^{AB} \left(r^{AB^h}(0) \right) = \sum_{l=1}^k D\hat{V}^{AB} \left(r^{AB^h}(\xi_l) \right) \frac{\mathbf{r}^{AB}(\xi_l)}{r^{AB^h}(\xi_l)} \cdot \frac{d\mathbf{r}^{AB}(\xi_l)}{d\alpha} w_l. \quad (5.8)$$

We now suppose that the approximation r^{AB^h} and the corresponding approximated distance vector are related by the following equation at all Gauss points ξ_l :

$$\frac{\mathbf{r}^{AB}(\xi_l)}{r^{AB^h}(\xi_l)} \cdot \frac{d\mathbf{r}^{AB}(\xi_l)}{d\alpha} = \frac{dr^{AB^h}(\xi_l)}{d\alpha} \quad (5.9)$$

Employing condition (5.9) in equation (5.8), we obtain a local energy conservation condition which reads

$$\boxed{\hat{V}^{AB}(r^{AB^h}(1)) - \hat{V}^{AB}(r^{AB^h}(0)) = \sum_{l=1}^k D\hat{V}^{AB}(r^{AB^h}(\xi_l)) \frac{dr^{AB^h}(\xi_l)}{d\alpha} w_l} \quad (5.10)$$

This equation is a *design criterion* for energy conserving integrators for the many-body problem and has to apply in accordance with equation (5.9). Since the gradient of the potential energy is determined by the chain rule of differentiation, relation (5.9) guarantees the gradient form (2.2) for the approximated internal force vector of the configuration at the Gauss points.

5.4 Enhanced derivative

In this section, we consider the design criterion (5.10) as constraint on the ordinary derivatives $D\hat{V}^{AB}$. By using the variational calculus we then determine functions $D\hat{V}^{AB}$ with a minimal distance to these ordinary derivatives, which also satisfy the total energy constraint. A variational problem with a constraint of this form is called an *isoperimetrical problem* in the relevant literature [47, 31, 91, 69, 46]. (See also Appendix A.6). We therefore search for functions $D\hat{V}^{AB}(\alpha)$ minimising the functionals

$$\mathcal{F}^{AB}(D\hat{V}^{AB}) = \frac{1}{2} \int_0^1 \left[D\hat{V}^{AB}(\alpha) - D\hat{V}^{AB}(r^{AB^h}(\alpha)) \right]^2 d\alpha \quad (5.11)$$

on the master element \mathcal{I}_α and satisfying the design criteria

$$\mathcal{G}^{AB}(D\hat{V}^{AB}) = \hat{V}^{AB}(r^{AB^h}(1)) - \hat{V}^{AB}(r^{AB^h}(0)) - \int_0^1 D\hat{V}^{AB}(\alpha) \frac{dr^{AB^h}(\alpha)}{d\alpha} d\alpha. \quad (5.12)$$

Solutions of this minimisation problem with constraint are functions which minimise the Lagrange functionals $\mathcal{L}^{AB} = \mathcal{F}^{AB} + \lambda^{AB} \mathcal{G}^{AB}$, where λ^{AB} denotes the associated Lagrange multiplier. One obtains the minimising functions by solving the corresponding Euler-Lagrange equations. Taking the constraint into account, the solutions of the Euler-

Lagrange equations are represented by the enhanced derivatives

$$\boxed{D\hat{V}^{AB}(\alpha) = D\hat{V}^{AB}\left(r^{AB^h}(\alpha)\right) + \frac{\mathcal{G}^{AB}(D\hat{V}^{AB})}{\mathcal{N}^{AB}} \frac{dr^{AB^h}(\alpha)}{d\alpha}} \quad (5.13)$$

where

$$\mathcal{N}^{AB} = \int_0^1 \frac{dr^{AB^h}(\alpha)}{d\alpha} \frac{dr^{AB^h}(\alpha)}{d\alpha} d\alpha. \quad (5.14)$$

In the computational setting, we apply k -point Gaussian quadrature for calculating the remaining integrals in the cG(k) method. We therefore also apply this quadrature rule to the integrals in the enhanced derivatives. Taking the accuracy $\mathcal{O}(h_n^{2k})$ of the Gaussian quadrature into account, the design criterion differs from the fundamental theorem of calculus by $\mathcal{O}(h_n^{2k})$. Since the enhancement of the ordinary derivatives has thus the same accuracy order as the quadrature rule applied in the cG(k) method, the accuracy of this integrator is also maintained with the enhanced derivatives.

5.5 Assumed distance approximation

In the enhanced derivatives $D\hat{V}^{AB}$, we have to choose a time approximation r^{AB^h} of the particle distances r^{AB} , which fulfils the requirements of a consistent strain measure for particle dynamics, namely the invariance with respect to a rigid body motion of the particle configuration (see Section 2.6). We here deduce a time approximation of the particle distances maintaining this property. We start from the natural radial distance approximation r^{AB} arising from the cG approximation \mathbf{q}^A of the position vectors. Considering the motion of two neighbouring particles A and B (see Figure 5.1), the squared absolute value pertaining to the cG approximation \mathbf{r}^{AB} of the radius vector reads

$$\mathbf{r}^{AB} \cdot \mathbf{r}^{AB} = \sum_{I,J=1}^{k+1} M_I M_J \mathbf{r}_I^{AB} \cdot \mathbf{r}_J^{AB} = \sum_{I,J=1}^{k+1} M_I M_J r_I^{AB} r_J^{AB} \cos \Theta_{IJ}^{AB}, \quad (5.15)$$

where $\cos \Theta_{IJ}^{AB} = \mathbf{e}_I^{AB} \cdot \mathbf{e}_J^{AB}$. The distances $r_I^{AB} = \|\mathbf{r}_I^{AB}\|$ denote the absolute values of the distance vectors \mathbf{r}_I^{AB} between the particles A and B . The vectors \mathbf{e}_I^{AB} designate the corresponding directional unit vectors. The cG approximation is affected by a rigid body

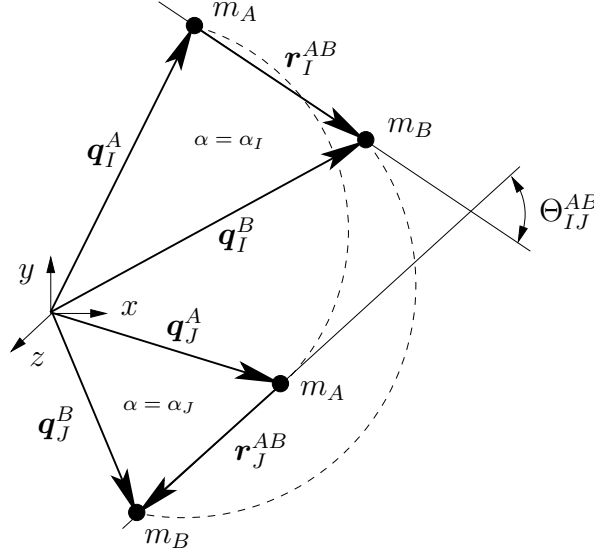


Figure 5.1. Geometry of the motion of two neighbouring particles A and B

rotation due to the dependence on the angle Θ_{IJ}^{AB} . However, one can split this squared cG approximation r^{AB} into two parts by using the completeness condition for the Lagrange basis functions M_I , $I = 1, \dots, k+1$:

$$\mathbf{r}^{AB} \cdot \mathbf{r}^{AB} = \sum_{I,J=1}^{k+1} M_I M_J r_I^{AB} r_J^{AB} + 2 \sum_{I=1}^k \sum_{J=I+1}^{k+1} M_I M_J r_I^{AB} r_J^{AB} (\cos \Theta_{IJ}^{AB} - 1). \quad (5.16)$$

The square root of the first term is an interpolation formula over the particle distances r_I^{AB} at the time nodes of the master element \mathcal{I}_α , which reads

$$\boxed{r^{AB}(\alpha) = \sum_{I=1}^{k+1} M_I(\alpha) r_I^{AB}} \quad (5.17)$$

One refers to this interpolation formula as the *assumed distance approximation* of the particle distances (see [19]). The assumed distance approximation is a consistent approximation of the particle distances because the approximation order is the same as that of the cG approximation (compare Appendix C.2). The assumed distance approximation r^{AB} is not affected by a rigid body rotation due to the absence of a dependence on the angle Θ_{IJ}^{AB} (compare [120]). The assumed distance approximation is consequently that part of the cG approximation, which is indifferent with respect to rigid body motions.

Note that the assumed distance approximation can be interpreted as approximation of the radius vector with respect to the corresponding corotational directional unit vector (compare Section 4.5).

5.6 Enhanced assumed derivative

The assumed distance approximation in the previous section is not influenced by rigid body motions and can be therefore recommended for using in the enhanced derivatives. The constraint of energy conservation, however, generally prevents the application of the assumed distance approximation in each term of the enhanced derivatives because of equation (5.9). This equation has to be fulfilled at all Gauss points in those terms where the chain rule of differentiation is used. For example, equation (5.9) is satisfied by the cG approximations r^{AB} of the particle distances for arbitrary k . Only in the case $k = 1$, equation (5.9) is also satisfied by the assumed distance approximation. In the argument of the ordinary derivatives $D\hat{V}^{AB}$ and in the directional part of the enhanced derivatives, we can use the assumed distance approximation without affecting the energy conservation condition. Taking into account the assumed distance approximation, the design criteria in the enhanced derivatives are given by

$$\underline{\mathcal{G}}^{AB} = \hat{V}^{AB}(r^{AB}(1)) - \hat{V}^{AB}(r^{AB}(0)) - \sum_{l=1}^k D\hat{V}^{AB}(r^{AB}(\xi_l)) \frac{dr^{AB}(\xi_l)}{d\alpha} w_l. \quad (5.18)$$

The corresponding enhanced derivatives associated with Gaussian quadrature for calculating the integrals have the following form:

$$\boxed{\underline{D}\hat{V}^{AB} = D\hat{V}^{AB}(r^{AB}) + \frac{\underline{\mathcal{G}}^{AB}}{\underline{\mathcal{N}}^{AB}} \frac{dr^{AB}}{d\alpha}} \quad (5.19)$$

where

$$\underline{\mathcal{N}}^{AB} = \sum_{l=1}^k \frac{dr^{AB}(\xi_l)}{d\alpha} \frac{dr^{AB}(\xi_l)}{d\alpha} w_l. \quad (5.20)$$

This composite approximation is possibly due to the same accuracy order of both distance approximations.

5.7 The enhanced Galerkin (eG) method

A mechanical integrator for many-particle dynamics has to conserve all invariants of the motion. The collocation property of the cG(k) method leads to conservation of total linear and total angular momentum. We obtain total energy conservation by incorporating the enhanced derivatives associated with Gaussian quadrature. The employed assumed distance approximation of the particle distances is indifferent with respect to rigid body motions. We therefore recommend as higher order accurate mechanical integrator the cG(k) method in conjunction with the enhanced assumed derivatives. The resulting time stepping scheme is given by

$$\boxed{\begin{aligned} \sum_{J=1}^{k+1} \int_0^1 \tilde{M}_I M'_J \, d\alpha \, \mathbf{q}_J - h_n \int_0^1 \tilde{M}_I \mathbb{M}^{-1} \mathbf{p} \, d\alpha &= \mathbf{0}, \\ \sum_{J=1}^{k+1} \int_0^1 \tilde{M}_I M'_J \, d\alpha \, \mathbf{p}_J + h_n \sum_{l=1}^k \tilde{M}_I(\xi_l) \underline{\mathbf{Q}}(\xi_l) \mathbf{q}(\xi_l) w_l &= \mathbf{0}. \end{aligned}} \quad I = 1, \dots, k, \quad (5.21)$$

The corresponding stiffness matrix $\underline{\mathbf{Q}} = \mathbf{Q} \otimes \mathbf{I}_{n_{dim}}$ has a structure matrix \mathbf{Q} with coefficients

$$\mathbf{Q}_{AB} = \begin{cases} -\frac{\underline{\mathbf{D}} \hat{V}^{AB}}{r^{AB}} & \text{if } A \neq B, \\ \sum_{\substack{C=1 \\ C \neq A}}^{n_{par}} \frac{\underline{\mathbf{D}} \hat{V}^{AC}}{r^{AC}} & \text{if } A = B. \end{cases} \quad (5.22)$$

We refer to this mechanical integrator as the *enhanced cG(k) method* or short *enhanced Galerkin (eG(k)) method* corresponding to the many-body problem. The eG(1) method for the many-body problem can be written in a more explicit form as the following equations:

$$\begin{aligned} \mathbf{q}_2^A - \mathbf{q}_1^A - \frac{h_n}{2 m_A} [\mathbf{p}_1^A + \mathbf{p}_2^A] &= \mathbf{0}, \\ \mathbf{p}_2^A - \mathbf{p}_1^A - h_n \sum_{\substack{B=1 \\ B \neq A}}^{n_{par}} \frac{\hat{V}^{AB}(r_2^{AB}) - \hat{V}^{AB}(r_1^{AB})}{r_2^{AB} - r_1^{AB}} \frac{\mathbf{r}_1^{AB} + \mathbf{r}_2^{AB}}{r_1^{AB} + r_2^{AB}} &= \mathbf{0}, \quad A = 1, \dots, n_{par}. \end{aligned} \quad (5.23)$$

This time-stepping scheme is identical with the energy and momentum conserving second order accurate integrators investigated in [58, 120, 19].

5.8 Numerical investigations

We now present numerical results of the eG(k) method as well as the cG(k) method for many-particle dynamics in order to compare conservation properties, accuracy and computational costs. The numerical example is calculated by linear, quadratic as well as by cubic time finite elements.

5.8.1 Linearisation of the algorithms

We begin by describing the linearisation of both methods. The procedure for solving the time stepping schemes follows directly from Section 3.2.6. In the stopping criteria of the iterative solution procedure, the tolerance ϵ is set to 10^{-8} . The block matrices \mathbf{K}_J , $J = 2, \dots, k+1$, of the tangent operator themselves have a block structure which takes the form

$$\mathbf{K}_J = \begin{bmatrix} -\sum_{\substack{C=1 \\ C \neq 1}}^{n_{par}} \mathbf{K}_J^{1C} & \dots & \mathbf{K}_J^{1n_{par}} \\ \vdots & & \vdots \\ \mathbf{K}_J^{n_{par}1} & \dots & -\sum_{\substack{C=1 \\ C \neq n_{par}}}^{n_{par}} \mathbf{K}_J^{n_{par}C} \end{bmatrix} \quad (5.24)$$

The blocks \mathbf{K}_J^{AB} in turn can be written as a sum of a geometrical part associated with linearising the corresponding B-matrix and a material part associated with the linearisation of the algorithmic constitutive law: $\mathbf{K}_J^{AB} = \mathbf{K}_{GeoJ}^{AB} + \mathbf{K}_{MatJ}^{AB}$. We have the following B-matrices to formulate the conservative forces:

$$\mathbf{B}^{AB} = \frac{\mathbf{r}^{AB}}{r^{AB}} \quad \mathbf{B}_J^{AB} = \frac{\mathbf{r}_J^{AB}}{r_J^{AB}} \quad (5.25)$$

The geometrical and the material parts associated with the cG method then take the following forms:

$$\begin{aligned}\mathbf{K}_{\text{Geo}_J^{AB}} &= -M_J \frac{D\hat{V}^{AB}(\mathbf{r}^{AB})}{\mathbf{r}^{AB}} [\mathbf{I}_{n_{dim}} - \mathbf{B}^{AB} \otimes \mathbf{B}^{AB}], \\ \mathbf{K}_{\text{Mat}_J^{AB}} &= -M_J D^2\hat{V}^{AB}(\mathbf{r}^{AB}) \mathbf{B}^{AB} \otimes \mathbf{B}^{AB}.\end{aligned}\quad (5.26)$$

Determining the geometrical parts associated with the eG method, one obtains a similar form as for the cG method, however in consequence of the additional terms in the enhanced derivatives, the material parts associated with the eG method are more complicated:

$$\begin{aligned}\underline{\mathbf{K}}_{\text{Geo}_J^{AB}} &= -M_J \frac{\underline{\mathbf{D}}\hat{V}^{AB}}{\mathbf{r}^{AB}} [\mathbf{I}_{n_{dim}} - \mathbf{B}^{AB} \otimes \mathbf{B}^{AB}], \\ \underline{\mathbf{K}}_{\text{Mat}_J^{AB}} &= \left[\frac{1}{\underline{\mathcal{N}}^{AB}} \frac{d\mathbf{r}^{AB}}{d\alpha} \underline{\mathbf{L}}_1^{AB} - M_J D^2\hat{V}^{AB}(\mathbf{r}^{AB}) - M'_J \frac{\underline{\mathcal{G}}^{AB}}{\underline{\mathcal{N}}^{AB}} \right] \mathbf{B}^{AB} \otimes \mathbf{B}_J^{AB} - \\ &- \delta_{J,k+1} \left[\frac{1}{\underline{\mathcal{N}}^{AB}} D\hat{V}^{AB}(\mathbf{r}_J^{AB}) \frac{d\mathbf{r}^{AB}}{d\alpha} \right] \mathbf{B}^{AB} \otimes \mathbf{B}_J^{AB} + \left[\frac{1}{\underline{\mathcal{N}}^{AB}} \frac{d\mathbf{r}^{AB}}{d\alpha} \right] \mathbf{B}^{AB} \otimes \underline{\mathbf{L}}_2^{AB},\end{aligned}\quad (5.27)$$

where

$$\begin{aligned}\underline{\mathbf{L}}_1^{AB} &= \sum_{l=1}^k \frac{d\mathbf{r}^{AB}(\xi_l)}{d\alpha} \left[M_J(\xi_l) D^2\hat{V}^{AB}(\mathbf{r}^{AB}(\xi_l)) + M'_J(\xi_l) \frac{\underline{\mathcal{G}}^{AB}}{\underline{\mathcal{N}}^{AB}} \right] w_l, \\ \underline{\mathbf{L}}_2^{AB} &= \sum_{l=1}^k D\hat{V}^{AB}(\mathbf{r}^{AB}(\xi_l)) \left[M'_J \mathbf{B}^{AB}(\xi_l) + M_J \frac{d\mathbf{B}^{AB}(\xi_l)}{d\alpha} \right] w_l.\end{aligned}\quad (5.28)$$

It is obviously that the material parts corresponding to the eG method are unsymmetric and those corresponding to the cG method are symmetric.

5.8.2 Stiff Neo-Hooke type spring potentials

We consider configurations with $n_{par} = k + 2$ particles which all have the mass $m_A = 10$, $A = 1, \dots, n_{par}$. The particles are arranged in deltahedra which means polyhedra whose faces are congruent equilateral triangles. The length of the edges is $L = 2$. The deltahedra are positioned with their barycentre in the origin of the three-dimensional Euclidean space. The particles can be thought of as connected by stiff nonlinear springs with stiffness

$c = 10^3$ and spring length $\bar{r}^{AB} = L$ in the force free configuration. We initiate the motions of the configurations with an initial angular velocity vector $\boldsymbol{\omega}_0 = (0, 0.7, 0.7)$. The initial velocity vectors \mathbf{v}_0^A of the particles are determined by the equation $\mathbf{v}_0^A = \mathbf{v}_T + \boldsymbol{\omega}_0 \times \mathbf{q}_0^A$, where $\mathbf{v}_T = (2.5, -0.3, -0.2)$ denotes a constant translation velocity vector. The potentials of interaction are derived from a one-dimensional compressible Neo-Hooke material and take the form

$$\hat{V}^{AB}(r^{AB}) = \frac{c}{6} (\bar{r}^{AB})^2 \left[\left(\frac{r^{AB}}{\bar{r}^{AB}} \right)^2 + 2 \frac{\bar{r}^{AB}}{r^{AB}} - 3 \right] \quad (5.29)$$

(see also [19]).

5.8.3 Discussion of the results

In the Figures 5.2, 5.6 and 5.10, the initial velocities of the configurations are depicted. The diagrams on the left show a three-dimensional view and the diagrams on the right a top view on the configurations. The three-dimensional motions are shown in the Figures 5.3, 5.7 and 5.11. The particles are indicated by different markers for a better tracing of the motion. Comparing the graphs of the momentum maps and the total energy depicted in the Figures 5.4, 5.8, 5.12 and in the Figures 5.5, 5.9, 5.13, respectively, we see that the first integrals computed by the eG method are constant over the whole time interval independent of the family parameter k and the chosen time step size h_n . The total linear and angular momentum computed by the cG method is also constant over the whole time interval, however the corresponding total energy oscillates about its initial value. The diagrams verify that the total energy computed by the cG method depends on k as well as on the time step size h_n . Since the total energy oscillations of the cG method are pronouncedly aperiodic after the change of the time step size, the cG method tends to be instable in contrast to the eG method.

The left diagram in Figure 5.14 shows the graphs of the relative global error in the position at time T versus the time step size. This relative error at time T is given by

$$e_{\mathbf{q}} = \frac{\|\mathbf{q}(T) - \mathbf{q}^{ref}(T)\|}{\|\mathbf{q}^{ref}(T)\|} \quad (5.30)$$

where $\mathbf{q}^{ref}(T)$ denotes the reference solution at time T . The reference solution is computed by the eG(4) method with a time step size $h_n = 0.001$. The graphs have the shape of lines due to the logarithmic scale of both axes. The slopes of these lines specify the accuracy $\mathcal{O}(h^{2k})$ of the continuous Galerkin method (compare [82]). The cG and the eG method show a similar behaviour with respect to the accuracy, namely the intercept of the lines is decreasing with increasing k . It follows that the time step size corresponding to a relative global error achievable with $k = 1, 2, 3$ is increasing with increasing k . A greater k therefore enables larger time steps for calculating the solution at time T .

In the right diagram in Figure 5.14, the relative global error versus the CPU time is depicted in a double logarithmic plot. By virtue of a least square curve fitting, we also obtained lines. First we consider the CPU time for one method corresponding to the family parameter $k = 1, 2, 3$. We observed for both methods that a greater k leads to less CPU time for computing a solution with a prescribed accuracy. This saving of CPU time is related to a smaller number of time steps and to a smaller iteration number in the Newton-Raphson iteration. We now compare both methods for a fixed family parameter k . The CPU time of the eG method is generally greater in comparison with the cG method because of the more extensive internal forces and the associated tangent operator. The advantage of the eG method is the better stability compared to the cG method because the eG method allows for time steps which are larger as those for the cG method. This is obviously when we use a time step size h_n larger as the largest depicted in Figure 5.14.

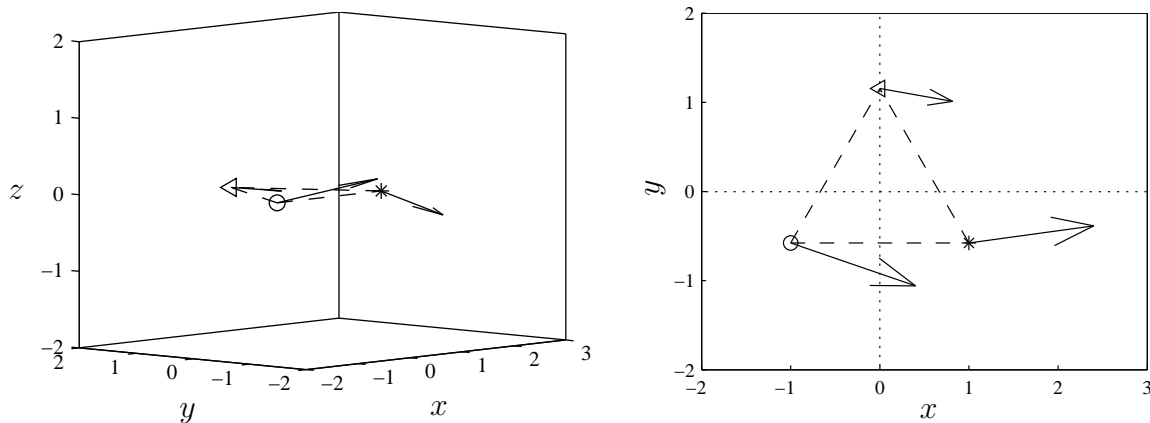


Figure 5.2. Initial velocity vectors of an equilateral triangle with an edge length $L = 2$.

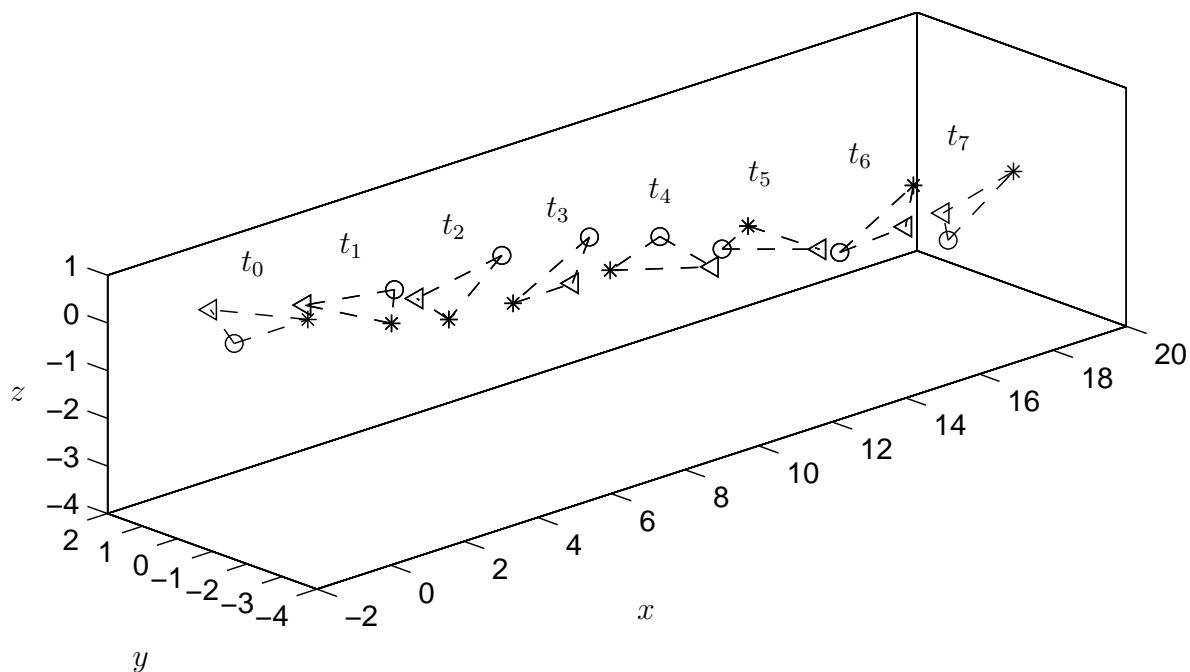


Figure 5.3. Motion of a stiff equilateral triangle (spring stiffness $c = 10^3$, point masses $m = 10$) computed with the eG(1) method. The time step size h_n has been set to 0.1 for $T \leq 3$ and to 0.2 for $T > 3$.

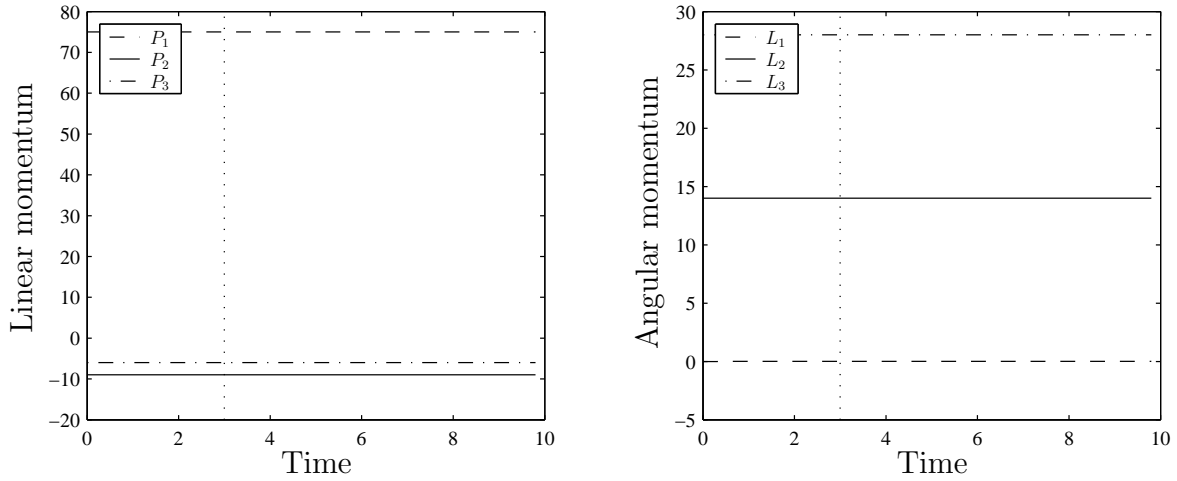


Figure 5.4. Momentum maps of a stiff equilateral triangle (spring stiffness $c = 10^3$, point masses $m = 10$) computed with the cG(1) method as well as with the eG(1) method. The time step size h_n has been set to 0.1 for $T \leq 3$ and to 0.2 for $T > 3$.

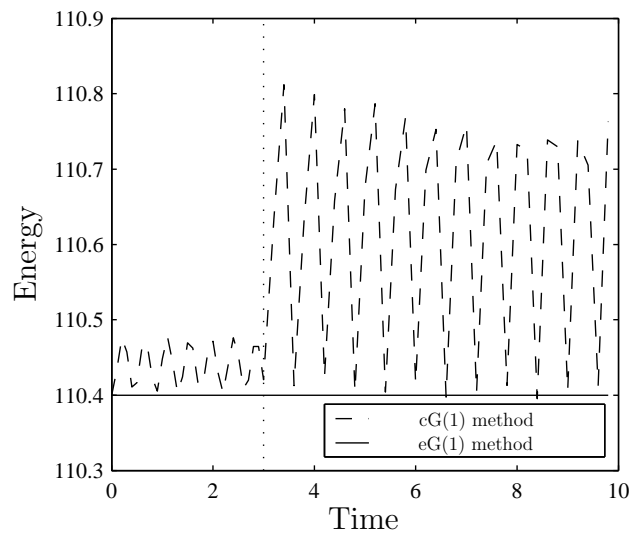


Figure 5.5. Total energy of a stiff equilateral triangle (spring stiffness $c = 10^3$, point masses $m = 10$) computed with the cG(1) method as well as with the eG(1) method. The time step size h_n has been set to 0.1 for $T \leq 3$ and to 0.2 for $T > 3$.

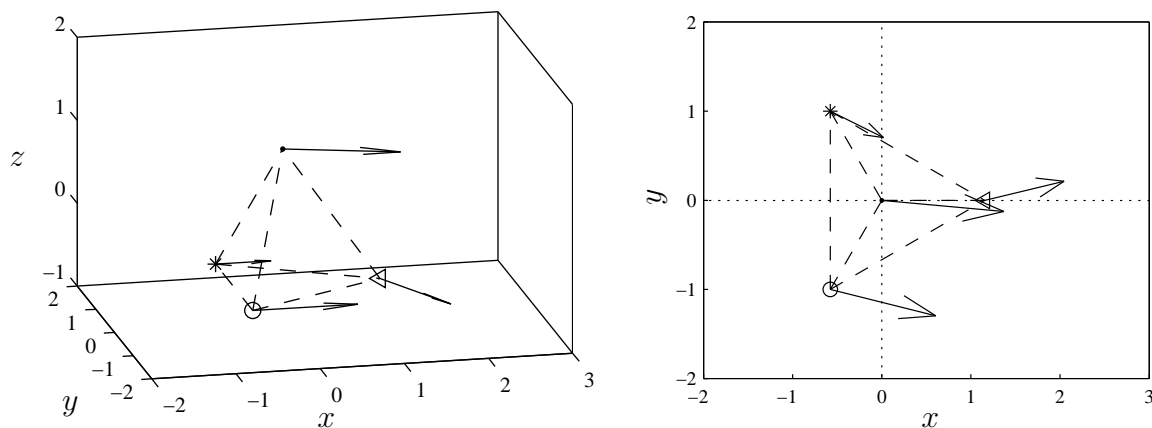


Figure 5.6. Initial velocity vectors of a tetrahedron with an edge length $L = 2$.

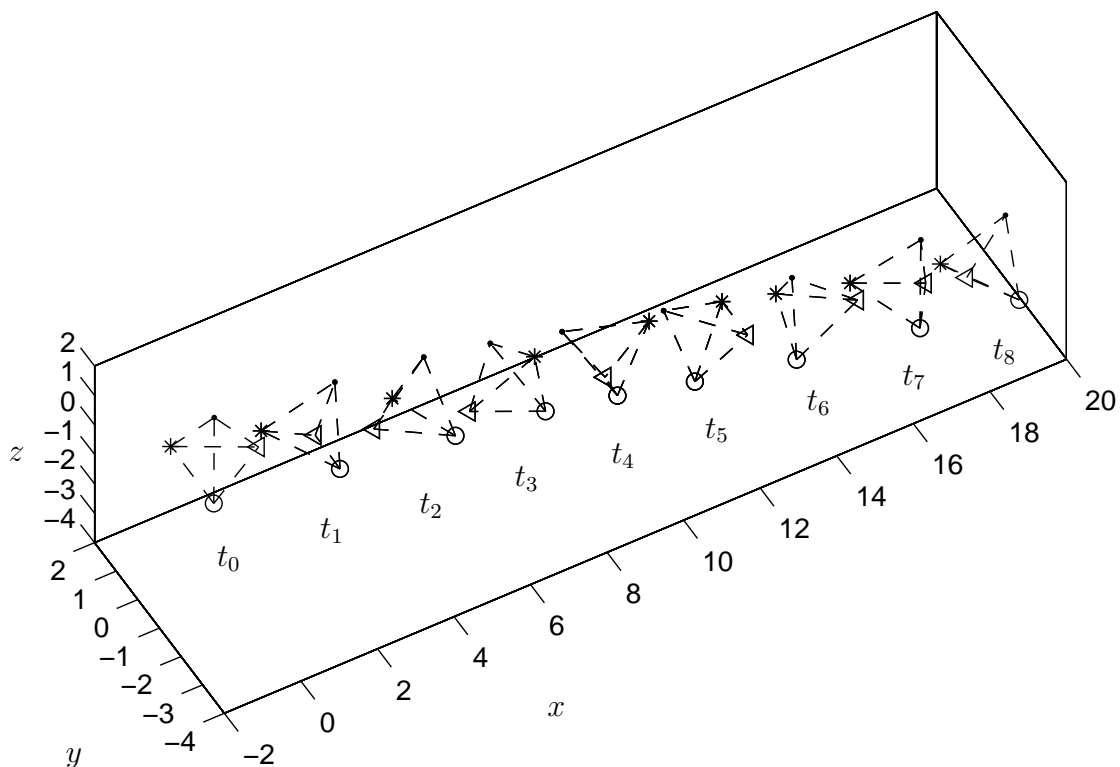


Figure 5.7. Motion of a stiff tetrahedron (spring stiffness $c = 10^3$, point masses $m = 10$) computed with the eG(2) method. The time step size h_n has been set to 0.1 for $T \leq 3$ and to 0.2 for $T > 3$.

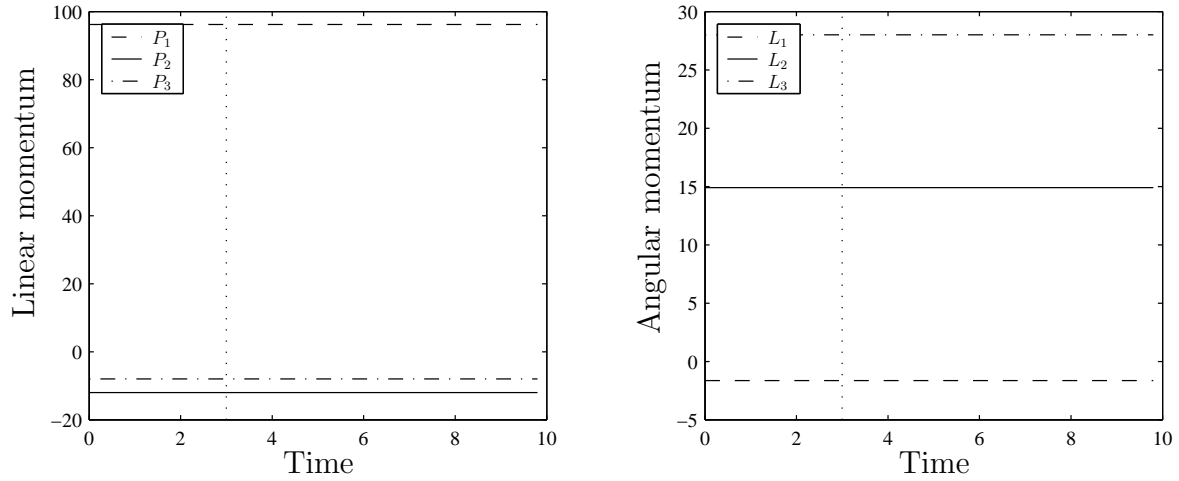


Figure 5.8. Momentum maps of a stiff tetrahedron (spring stiffness $c = 10^3$, point masses $m = 10$) computed with the cG(2) method as well as with the eG(2) method. The time step size h_n has been set to 0.1 for $T \leq 3$ and to 0.2 for $T > 3$.

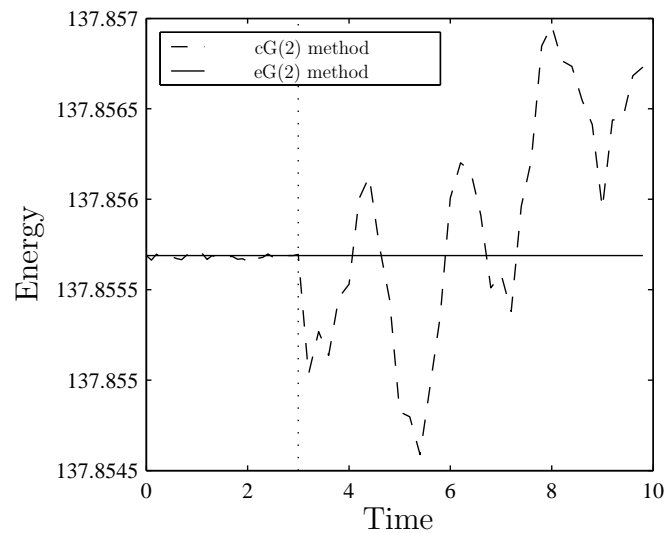


Figure 5.9. Total energy of a stiff tetrahedron (spring stiffness $c = 10^3$, point masses $m = 10$) computed with the cG(2) method as well as with the eG(2) method. The time step size h_n has been set to 0.1 for $T \leq 3$ and to 0.2 for $T > 3$.

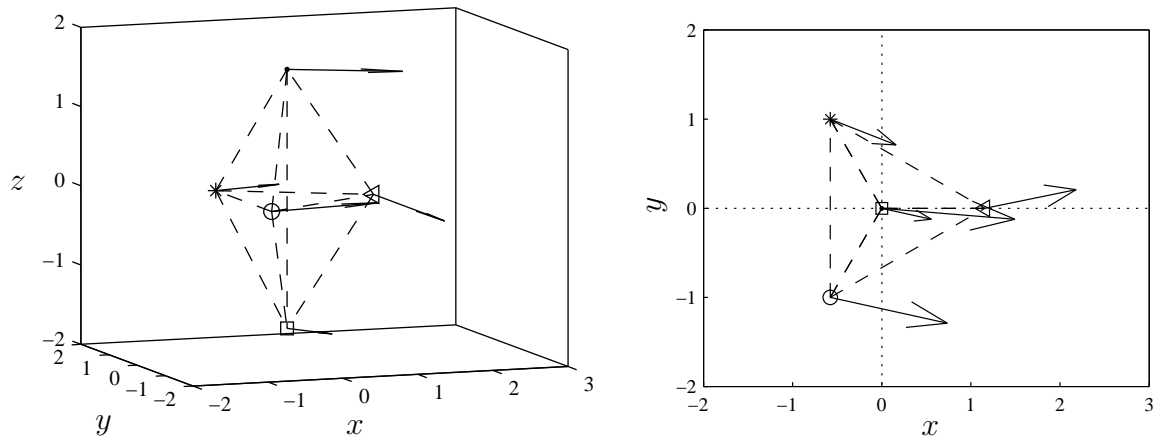


Figure 5.10. Initial velocity vectors of a triangular dipyrmaid with an edge length $L = 2$.

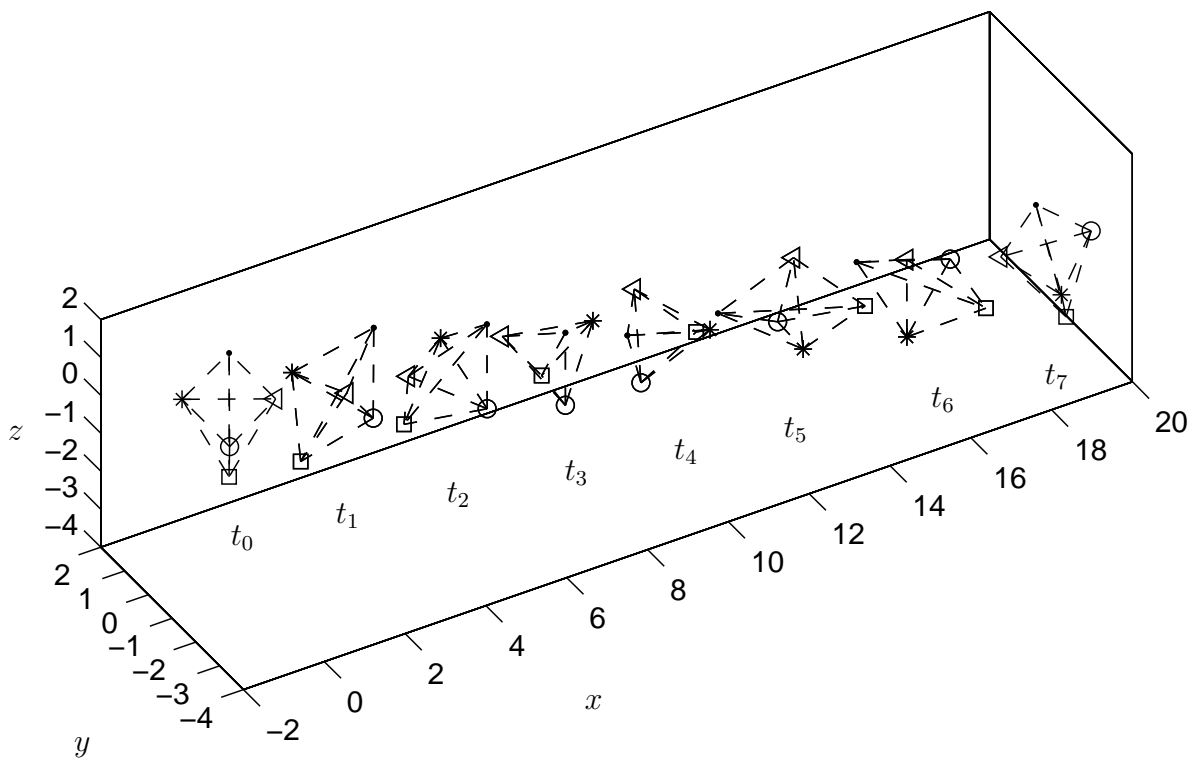


Figure 5.11. Motion of a stiff triangular dipyrmaid (spring stiffness $c = 10^3$, point masses $m = 10$) computed with the eG(3) method. The time step size h_n has been set to 0.1 for $T \leq 3$ and to 0.2 for $T > 3$.

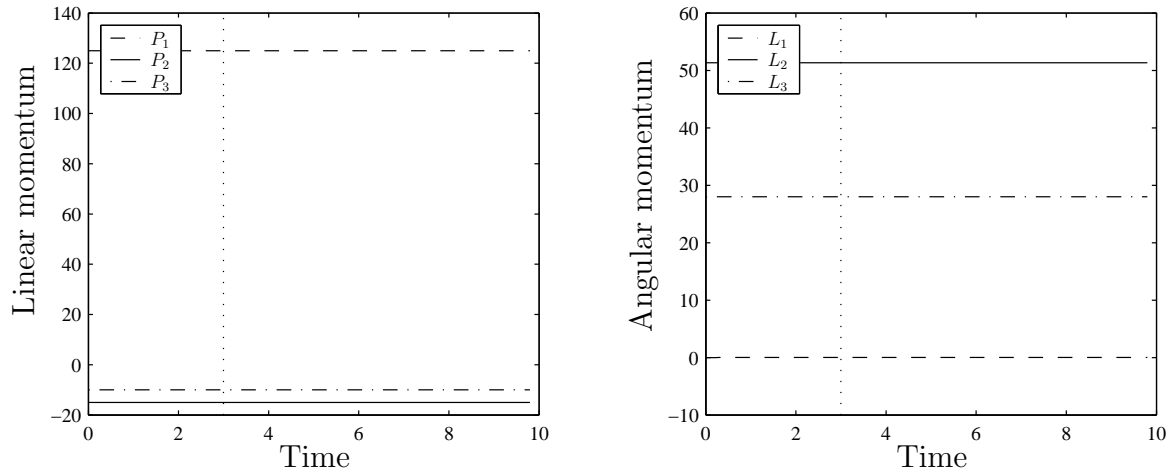


Figure 5.12. Momentum maps of a stiff triangular dipyrmaid (spring stiffness $c = 10^3$, point masses $m = 10$) computed with the cG(3) method as well as with the eG(3) method. The time step size h_n has been set to 0.1 for $T \leq 3$ and to 0.2 for $T > 3$.

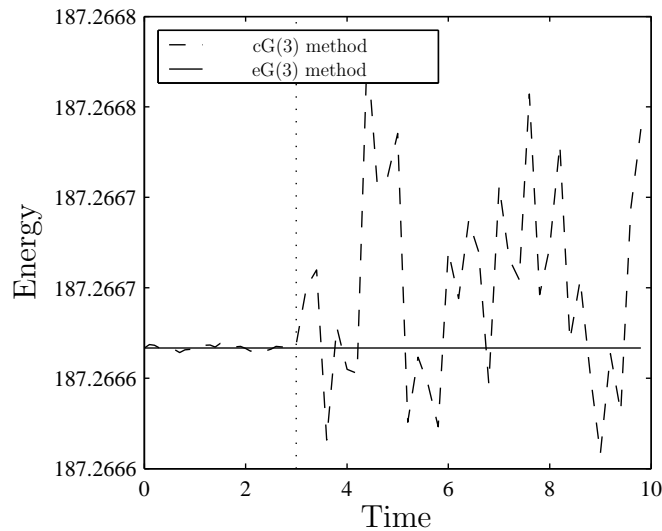


Figure 5.13. Total energy of a stiff triangular dipyrmaid (spring stiffness $c = 10^3$, point masses $m = 10$) computed with the cG(3) method as well as with the eG(3) method. The time step size h_n has been set to 0.1 for $T \leq 3$ and to 0.2 for $T > 3$.

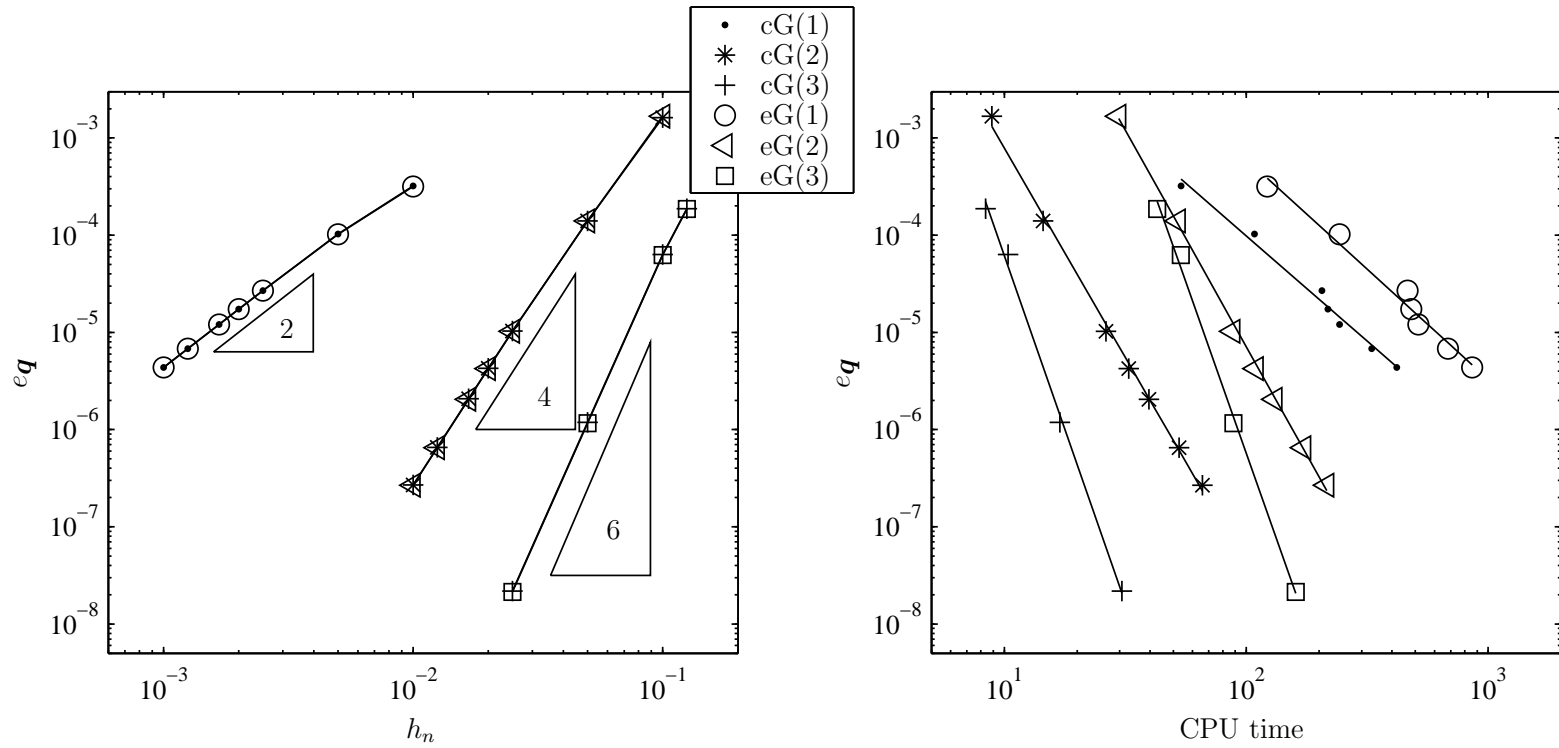


Figure 5.14. Relative global error in the position (on the left) and CPU time (on the right) corresponding to the motion of a stiff tetrahedron (spring stiffness $c = 10^3$, point masses $m = 10$) at time $T = 10$ pertaining to the cG and the eG method for $k = 1, 2, 3$.

Chapter 6

Semi-discrete nonlinear elastodynamics

...Given that stiffness is an issue and that one is interested in long term simulations it is then natural to search for implicit schemes which are unconditionally stable and which preserve as much as possible the intrinsic properties of the underlying system. Namely, conservation laws such as that of energy and angular momentum...

[121], Chapter 1: Introduction.

We now deal with a hyperelastic solid continuum body embedded in a n_{dim} -dimensional Euclidean space. A spatial finite element discretisation in a Lagrangian description of the motion generates the so-called *semi-discrete equations of motion*. This system of ordinary differential equations describes motions of spatial nodes which are together coincident with a configuration of material points pertaining to the solid continuum body. The dynamics of the spatial discretised hyperelastic body in a Lagrangian description is therefore a further example of the generalised problem in Section 2.

In continuum mechanics, a distinction is drawn between the Lagrangian description of motion and the Eulerian description. These descriptions are different in the choice of independent variables for the kinematics and the equations of motion. In the Lagrangian description, the motion is described by coordinates indicating continuum points of the

body. The nodes in a Lagrangian mesh are therefore coincident with material points. Consequently, no material passes between the elements and element quadrature points also remain coincident with continuum points. In contrast, Eulerian coordinates specify the location of a point in the Euclidean space. Eulerian mesh nodes are thus fixed and continuum points cross element interfaces. Moreover, the continuum point at a given quadrature point changes with time. Since we are interested in trajectories of material points of a solid continuum body, we apply the Lagrangian description of motion. A detailed description of nonlinear finite element methods for solid continuum bodies can be found in [109, 17, 33, 34, 142].

6.1 Finite element discretisation in space

We consider a partition of a solid continuum body $\mathcal{B} \subset \mathbb{R}^{n_{dim}}$ into nonoverlapping sub-domains \mathcal{B}^e , $e = 1, \dots, n_{el}$, such that

$$\mathcal{B} = \bigcup_{e=1}^{n_{el}} \mathcal{B}^e. \quad (6.1)$$

The sub-domain $\mathcal{B}^e \subset \mathcal{B}$ is called the *e-th element* which is defined by a set of material points called the *element nodes*. The positions of the element nodes in the initial configuration \mathcal{B}_0^e at time $t = 0$ are denoted by $\mathbf{X}_e^a \in \overline{\mathcal{B}}_0^e$, $a = 1, \dots, n_{en}$, and their positions in the current configuration \mathcal{B}_t^e at time $t \in \mathbb{I} =]0, T]$ are denoted by $\mathbf{x}_e^a \in \overline{\mathcal{B}}_t^e$ (see Figure 6.1). The positions \mathbf{x}_e^a are given by the mappings $\mathbf{q}_e^a : \mathbb{I} \rightarrow \mathbb{R}^{n_{dim}}$ such that $\mathbf{x}_e^a = \mathbf{q}_e^a(t)$. We refer to the vector \mathbf{q}_e^a as the *position vector* of the node a in the element \mathcal{B}^e .

This discretisation of \mathcal{B} renders a configuration $\overline{\mathcal{B}}$ of n_{np} material points which we call in this context the spatial nodes. The positions of these nodes in the initial configuration \mathcal{B}_0 at time $t = 0$ are denoted by $\mathbf{X}^A \in \overline{\mathcal{B}}_0$, $A = 1, \dots, n_{np}$, and their positions in the current configuration \mathcal{B}_t at time $t \in \mathbb{I}$ are denoted by $\mathbf{x}^A \in \overline{\mathcal{B}}_t$. The positions \mathbf{x}^A are given by the mappings $\mathbf{q}^A : \mathbb{I} \rightarrow \mathbb{R}^{n_{dim}}$ such that $\mathbf{x}^A = \mathbf{q}^A(t)$. We refer to the vector \mathbf{q}^A as the position vector of the node A in the configuration $\overline{\mathcal{B}}_t$ and to the vector $\mathbf{q} = (\mathbf{q}^1, \dots, \mathbf{q}^{n_{np}})$ as the corresponding coordinate vector of the configuration.

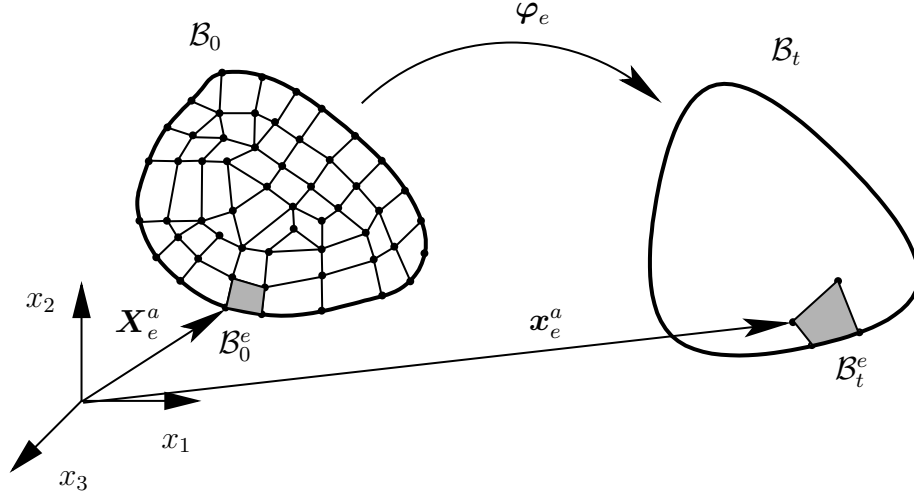


Figure 6.1. Motion of a solid continuum body \mathcal{B} embedded in the n_{dim} -dimensional Euclidean space $\mathbb{R}^{n_{dim}}$ and partitioned into nonoverlapping sub-domains \mathcal{B}^e , $e = 1, \dots, n_{el}$.

In semi-discrete elastodynamics, the Euclidean space between the spatial nodes is continuously approximated. The position \mathbf{X}_e of a continuum point in the initial configuration \mathcal{B}_0^e is parameterised by the mapping $\Psi_e : \square \rightarrow \mathcal{B}_0^e$ and its position \mathbf{x}_e in the current configuration \mathcal{B}_t^e is parameterised by the mapping $\psi_e : \square \times \mathbb{I} \rightarrow \mathcal{B}_t^e$. According to a standard isoparametric discretisation (see Figure 6.2) these mappings are given by (see [142])

$$\mathbf{X}_e = \Psi_e(\boldsymbol{\eta}_e) = \sum_{a=1}^{n_{en}} N_a(\boldsymbol{\eta}_e) \mathbf{X}_e^a, \quad \mathbf{x}_e = \psi_e(\boldsymbol{\eta}_e, t) = \sum_{a=1}^{n_{en}} N_a(\boldsymbol{\eta}_e) \mathbf{q}_e^a(t). \quad (6.2)$$

The set $\square \subset \mathbb{R}^{n_{dim}}$ is the unit n_{dim} -hypercube called the parent domain and $N_a : \square \rightarrow \mathbb{R}$ denotes a Lagrangian shape function which satisfies the condition $N_a(\boldsymbol{\eta}_e^b) = \delta_a^b$, where $\boldsymbol{\eta}_e^b \in \bar{\square}$, $b = 1, \dots, n_{en}$, are the element nodes of the e -th element in the parent domain.

The physical fields in the isoparametric concept are approximated analogously to the geometry. The motion of a continuum point at the initial position $\mathbf{X}_e \in \mathcal{B}_0^e$ to its current position $\mathbf{x}_e \in \mathcal{B}_t^e$ is approximated by the field $\varphi_e : \mathcal{B}^e \times \mathbb{I} \rightarrow \mathcal{B}_t^e$ defined by

$$\mathbf{x}_e = \varphi_e(\mathbf{X}_e, t) = \psi_e \circ (\Psi_e)^{-1}(\mathbf{X}_e)(t) = \sum_{a=1}^{n_{en}} N_a(\boldsymbol{\eta}_e(\mathbf{X}_e)) \mathbf{q}_e^a(t). \quad (6.3)$$

The Lagrangian velocity of a continuum point in the element \mathcal{B}^e is given by the partial

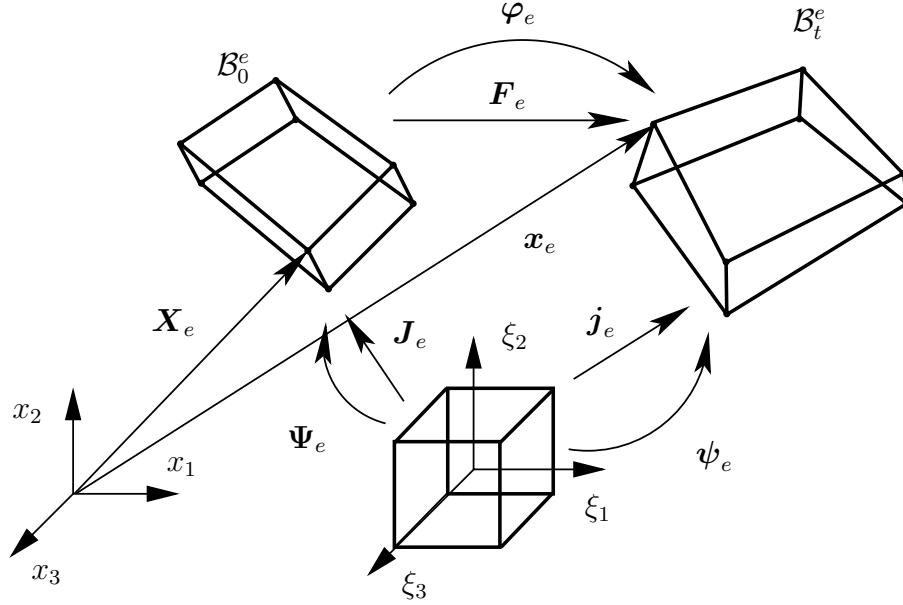


Figure 6.2. Standard isoparametric parameterisation of the motion of an element \mathcal{B}^e .

time derivative $\mathbf{v}_e(\mathbf{X}_e, t) = \partial \varphi_e(\mathbf{X}_e, t) / \partial t$. The linear tangent map of the field φ_e is given by the deformation gradient

$$\mathbf{F}_e = \nabla_{\mathbf{X}_e} \varphi_e = \sum_{a=1}^{n_{en}} \mathbf{q}_e^a \otimes \mathbf{J}_e^{-T} \cdot \nabla_{\eta} N_a, \quad (6.4)$$

with the Jacobian

$$\mathbf{J}_e = \nabla_{\eta} \mathbf{X}_e = \sum_{a=1}^{n_{en}} \mathbf{X}_e^a \otimes \nabla_{\eta} N_a. \quad (6.5)$$

We consider isotropic hyperelastic materials for which the second Piola-Kirchhoff stress tensor corresponding to the element \mathcal{B}^e is defined as the gradient $\mathbf{S}_e = 2 \nabla_{\mathbf{C}_e} W_e$ of the scalar-valued isotropic strain energy density function $W_e = W_e(\mathbf{C}_e)$ with the right Cauchy-Green strain tensor $\mathbf{C}_e = \mathbf{F}_e^T \mathbf{F}_e$ as argument. This right Cauchy-Green tensor with respect to the above discretisation reads

$$\mathbf{C}_e = \sum_{a,b=1}^{n_{en}} [\mathbf{q}_e^a \cdot \mathbf{q}_e^b] \mathbf{N}_{ab}^e, \quad (6.6)$$

where

$$\mathbf{N}_{ab}^e = \mathbf{J}_e^{-T} \cdot [\nabla_{\eta} N_a \otimes \nabla_{\eta} N_b] \cdot \mathbf{J}_e^{-1}. \quad (6.7)$$

6.2 Hamiltonian formulation

The potential energy V of the configuration $\bar{\mathcal{B}}$ is equal to the strain energy of the body \mathcal{B} . The strain energy results from summing over the strain energies $V_e = \int_{\mathcal{B}_0^e} W_e(\mathbf{C}_e) \, dV$ of the elements. The gradient $\nabla_{\mathbf{q}} V$ of the strain energy takes the form of equation (2.2). The corresponding global stiffness matrix \mathbb{Q} follows from assembling the element stiffness matrices $\hat{\mathbb{Q}}_e(\mathbf{C}_e)$ denoted by

$$\mathbb{Q} = \mathbf{A} \begin{matrix} n_{el} \\ \hat{\mathbb{Q}}_e(\mathbf{C}_e) \end{matrix}. \quad (6.8)$$

The element stiffness matrices have a block structure of the form $\hat{\mathbb{Q}}_e = \hat{\mathbf{Q}}_e(\mathbf{C}_e) \otimes \mathbf{I}_{ndim}$ which are based on structure matrices

$$\hat{\mathbf{Q}}_e = \begin{bmatrix} \hat{Q}_{11}^e & \cdots & \hat{Q}_{1n_{en}}^e \\ \vdots & & \vdots \\ \hat{Q}_{n_{en}1}^e & \cdots & \hat{Q}_{n_{en}n_{en}}^e \end{bmatrix} \quad (6.9)$$

where the coefficients of these matrices depend on the second Piola-Kirchhoff stress tensor corresponding to the element \mathcal{B}^e :

$$\hat{Q}_{ab}^e(\mathbf{C}_e) = \int_{\mathcal{B}_0^e} \mathbf{s}_e(\mathbf{C}_e) : \mathbf{N}_{ab}^e \, dV. \quad (6.10)$$

Remark 6.1. The global stiffness matrix \mathbb{Q} is also symmetric because the assembly operator \mathbf{A} is a symmetry preserving matrix transformation which depends on the connectivity matrices associated with the spatial discretisation of the body \mathcal{B} (see Appendix D).

The kinetic energy T of the configuration $\bar{\mathcal{B}}$ is defined as the union of all kinetic element energies T_e which in turn are defined as volume integrals over the squared velocity field. In connection with the approximated deformation, the kinetic energy T_e takes the form

$$T_e = \frac{1}{2} \int_{\mathcal{B}_0^e} \rho_0 \mathbf{v}_e \cdot \mathbf{v}_e \, dV = \frac{1}{2} \sum_{a,b=1}^{n_{en}} M_{ab}^e \dot{\mathbf{q}}_e^a \cdot \dot{\mathbf{q}}_e^b = \frac{1}{2} \dot{\mathbf{q}}_e \cdot \mathbb{M}_e \dot{\mathbf{q}}_e, \quad (6.11)$$

with the element coordinate vector $\mathbf{q}_e = (\mathbf{q}_e^1, \dots, \mathbf{q}_e^{n_{en}})$ and the following coefficients of the element mass matrix \mathbb{M}_e pertaining to the e -th element:

$$M_{ab}^e = \int_{\mathcal{B}_0^e} \rho_0 N_a N_b \, dV. \quad (6.12)$$

The matrices \mathbb{M}_e have a block structure of the form $\mathbb{M}_e = \mathbf{M}_e \otimes \mathbf{I}_{n_{dim}}$, where the corresponding structure matrix \mathbf{M}_e reads

$$\mathbf{M}_e = \begin{bmatrix} M_{11}^e & \dots & M_{1n_{en}}^e \\ \vdots & & \vdots \\ M_{n_{en}1}^e & \dots & M_{n_{en}n_{en}}^e \end{bmatrix} \quad (6.13)$$

A matrix assembly of the element mass matrices \mathbb{M}_e furnishes a symmetric global consistent mass matrix

$$\mathbb{M} = \mathbf{A} \begin{matrix} n_{el} \\ \mathbf{M}_e, \\ e=1 \end{matrix} \quad (6.14)$$

such that the kinetic energy T and the linear momentum vector $\mathbf{p} = (\mathbf{p}^1, \dots, \mathbf{p}^{n_{np}})$ of the configuration is given by equation (2.5) and (2.14), respectively.

Remark 6.2. The mass matrix is not diagonal as in a configuration of particles because the mass is continuously distributed over the whole space between the spatial nodes. In contrast to many-particle dynamics, a force at element node a can therefore generate accelerations at element node b .

Remark 6.3. In the computational setting, there exist possibilities to diagonalise or to lump the mass matrix [76, 14, 142]. For example, one can use a nodal quadrature rule instead of the naturally chosen Gauss rule (see [55]) or the row-sum technique. *Lumped mass matrices* are often applied due to their economy, but they possibly lead to difficulties such as negative masses or zero masses at nodes along symmetry axes. In [70], there can be found a lumping procedure which has been shown to work well in many structural and solid mechanical problems. In the present work, however, the consistent mass matrix is employed.

The total linear momentum of the configuration is defined by summing the total linear momenta \mathbf{P}_e of all elements. In the Lagrangian description of motions, the total linear momenta \mathbf{P}_e take the forms

$$\mathbf{P}_e = \int_{\mathcal{B}_0^e} \rho_0 \mathbf{v}_e \, dV = \sum_{a=1}^{n_{en}} \int_{\mathcal{B}_0^e} \rho_0 N_a \, dV \dot{\mathbf{q}}_e^a. \quad (6.15)$$

Taking the completeness condition $\sum_{a=1}^{n_{en}} N_a = 1$ into account, we obtain the total linear momenta \mathbf{P}_e as the sum over all linear momenta \mathbf{p}_e^a pertaining to the element nodes in $\overline{\mathcal{B}}_t^e$:

$$\mathbf{P}_e = \sum_{a,b=1}^{n_{en}} M_{ab}^e \dot{\mathbf{q}}_e^a = \sum_{b=1}^{n_{en}} \mathbf{p}_e^b. \quad (6.16)$$

A further summation over the elements furnishes the total linear momentum of the configuration as in the generalised problem:

$$\mathbf{P} = \sum_{A=1}^{n_{np}} \mathbf{p}^A \quad (6.17)$$

We see that a linear momentum vector \mathbf{p}^A of a spatial node A leads to contributions in the adjoining elements \mathcal{B}^e . The total linear momentum \mathbf{P} is conserved if equation (2.53) is fulfilled for each element \mathcal{B}^e :

$$\sum_{a,b=1}^{n_{en}} \hat{Q}_{ab}^e(\mathbf{C}_e) \mathbf{q}_e^b = \sum_{b=1}^{n_{en}} \int_{\mathcal{B}_0^e} \nabla_\xi \left[\sum_{a=1}^{n_{en}} N_a \right] \cdot [\mathbf{J}_e^{-1} \cdot \mathbf{S}_e(\mathbf{C}_e) \cdot \mathbf{J}_e^{-T}] \cdot \nabla_\xi N_b \, dV \mathbf{q}_e^b = \mathbf{0}. \quad (6.18)$$

Employing the completeness condition for the spatial Lagrangian shape functions N_a , $a = 1, \dots, n_{en}$, equation (6.18) shows total linear momentum conservation of the spatial finite element discretisation.

The total angular momentum \mathbf{L} of the configuration results from summing over all angular momenta \mathbf{L}_e of the spatial elements. In the Lagrangian description, the total angular momentum of each element is given by

$$\mathbf{L}_e = \int_{\mathcal{B}_0^e} \rho_0 \boldsymbol{\varphi}_e \times \mathbf{v}_e \, dV = \sum_{a,b=1}^{n_{en}} \mathbf{q}_e^a \times M_{ab}^e \dot{\mathbf{q}}_e^b = \sum_{a=1}^{n_{en}} \mathbf{q}_e^a \times \mathbf{p}_e^a. \quad (6.19)$$

The further summation over all elements results in $\mathbf{L} = \sum_{A=1}^{nnp} \mathbf{q}^A \times \mathbf{p}^A$. Since the total angular momentum has the form as in the generalised problem, the total angular momentum is conserved due to the symmetry of the mass and stiffness matrix (see Section 2).

6.3 Galerkin-based time discretisation

We use the cG(k) method as time discretisation of the semi-discrete equations of motion. These higher order integrators are the basis for designing energy and momentum conserving integrators in the following sections. The cG(k) method for the semi-discrete nonlinear elastodynamics reads

$$\begin{aligned} \sum_{J=1}^{k+1} \int_0^1 \tilde{M}_I M'_J \, d\alpha \, \mathbf{q}_J - h_n \int_0^1 \tilde{M}_I \mathbb{M}^{-1} \mathbf{p} \, d\alpha &= \mathbf{0}, \\ \sum_{J=1}^{k+1} \int_0^1 \tilde{M}_I M'_J \, d\alpha \, \mathbf{p}_J + h_n \sum_{l=1}^k \tilde{M}_I(\xi_l) \mathbb{Q}^h(\xi_l) \mathbf{q}(\xi_l) w_l &= \mathbf{0}, \end{aligned} \quad I = 1, \dots, k. \quad (6.20)$$

The time approximation $\mathbb{Q}^h(\alpha)$ of the global stiffness matrix is given by the element stiffness matrices $\hat{\mathbb{Q}}_e^h = \hat{\mathbb{Q}}_e(\mathbf{C}_e^h(\alpha))$, where $\mathbf{C}_e^h : \mathcal{I}_\alpha \rightarrow \mathbb{R}^{n_{dim} \times n_{dim}}$ denotes an arbitrary time approximation of the right Cauchy-Green tensor of the element \mathcal{B}^e . We refer to the approximation $\mathbf{F}_e = \sum_{I=1}^{k+1} M_I(\alpha) \mathbf{F}_I^e$ of the deformation gradient pertaining to the element e as the cG approximation, where \mathbf{F}_I^e denote the deformation gradients at the time nodes α_I . This approximation only relies on the cG approximation \mathbf{q}_e of the position vector. The cG approximation of the right Cauchy-Green tensor is then given by $\mathbf{C}_e = \mathbf{F}_e^T \mathbf{F}_e$. This approximation of the right Cauchy-Green tensor however has a disadvantage when computing rigid body rotations because it generates artificial strains at the Gauss points (see in Figure 6.3 the stretch $\lambda(\alpha)$ in direction of a symmetry axis of the depicted body). There is considerable artificial compression at the midpoint of the master element for $k = 1$ ($\lambda(\xi_1) = 0.7071$), small artificial compressions at both Gauss points for $k = 2$ ($\lambda(\xi_1) = \lambda(\xi_2) = 0.9904$) and both a small artificial compression ($\lambda(\xi_2) = 0.9983$) and extensions ($\lambda(\xi_1) = \lambda(\xi_3) = 1.0027$) for $k = 3$. We call the cG(k) method associated with the cG approximation \mathbf{C}_e as the *standard cG(k) method* or simple cG(k) method.

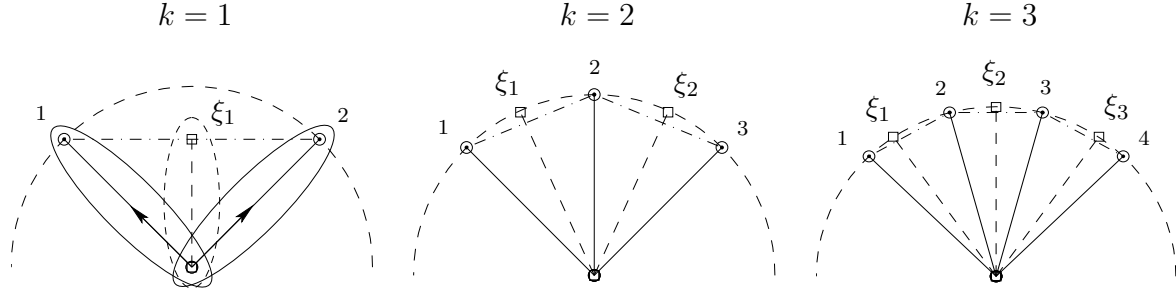


Figure 6.3. Stretch $\lambda(\alpha)$ in direction of the depicted directional unit vectors during a rigid body rotation determined by the cG approximation \mathbf{C} of the right Cauchy-Green tensor for $k = 1, 2, 3$. The numbered points and the points ξ_l , $l = 1, \dots, k$, denote the time nodes and the Gauss points on the master element, respectively.

According to [22], the cG(k) method is identical with implicit Gauss Runge-Kutta methods which are symplectic and momentum conserving [118]. One obtains as particular case for $k = 1$, the second order accurate implicit midpoint rule:

$$\begin{aligned} \mathbf{q}_2 - \mathbf{q}_1 - \frac{h_n}{2} \mathbb{M}^{-1} [\mathbf{p}_1 + \mathbf{p}_2] &= \mathbf{0}, \\ \mathbf{p}_2 - \mathbf{p}_1 + \frac{h_n}{2} \mathbb{Q}^h \left(\frac{1}{2} \right) [\mathbf{q}_1 + \mathbf{q}_2] &= \mathbf{0}. \end{aligned} \quad (6.21)$$

In the context of nonlinear elastodynamics, the implicit midpoint rule has been also derived by a finite difference approximation in [125, 53, 121], for instance.

6.4 Design criterion for energy conservation

We now deduce a criterion for designing mechanical integrators by localising the energy conservation condition for the cG(k) method. In the case of semi-discrete nonlinear elastodynamics, we localise with respect to the spatial discretisation and obtain an energy conservation condition for each element of the mesh. We subsequently localise with respect to the spatial quadrature and obtain the following condition for each continuum point in the element e :

$$W_e(\mathbf{C}_e^h(1)) - W_e(\mathbf{C}_e^h(0)) = \sum_{l=1}^k \nabla_{\mathbf{C}_e} W_e(\mathbf{C}_e^h(\xi_l)) : \sum_{a,b=1}^{n_{en}} 2 N_{ab}^e \left[\mathbf{q}_e^b(\xi_l) \cdot \frac{d\mathbf{q}_e^a(\xi_l)}{d\alpha} \right] w_l. \quad (6.22)$$

We suppose that the temporal approximation \mathbf{C}_e^h of the right Cauchy-Green tensor fulfils the following condition at all the Gauss points:

$$2 \mathbb{I}_{\text{sym}} : \sum_{a,b=1}^{n_{en}} \mathbf{N}_{ab}^e \left[\mathbf{q}_e^b(\xi_l) \cdot \frac{d\mathbf{q}_e^a(\xi_l)}{d\alpha} \right] = \frac{\partial \mathbf{C}_e^h(\xi_l)}{\partial \alpha}, \quad (6.23)$$

where \mathbb{I}_{sym} denotes the symmetric fourth-order identity tensor. Taking the last equation into account, the pointwise condition leads to the equation

$$\boxed{W_e(\mathbf{C}_e^h(1)) - W_e(\mathbf{C}_e^h(0)) = \sum_{l=1}^k \nabla_{\mathbf{C}_e} W_e(\mathbf{C}_e^h(\xi_l)) : \frac{\partial \mathbf{C}_e^h(\xi_l)}{\partial \alpha} w_l} \quad (6.24)$$

We refer to equation (6.24) as the *design criterion* for an energy conserving integrator. Note that this equation has to be applied in conjunction with equation (6.23) to maintain the gradient form (2.2) of the internal force vector at the Gauss points ξ_l , $l = 1, \dots, k$.

Remark 6.4. It is a consequence of an existing strain energy density function W that the work done on a hyperelastic or Green elastic material is independent of the deformation path. The strain energy stored in the material thus only depends on the initial and the final state of the deformation path because the following relation on the strain energy density holds:

$$W(\mathbf{C}_1) - W(\mathbf{C}_0) = \int_{\varphi} \nabla_{\mathbf{C}} W : d\mathbf{C}, \quad (6.25)$$

where φ designates a deformation path starting with a reference configuration \mathcal{B}_0 and ending in a current configuration \mathcal{B}_1 . Equation (6.24) can be therefore regarded as a discrete counterpart of the gradient theorem (6.25).

6.5 Enhanced gradient

We now regard the design criterion (6.24) as condition for the gradient of the strain energy density function. We then have to determine new tensor-valued functions $DW_e(\alpha)$ satisfying the design criterion as constraint and possessing a minimal distance to the approximated ordinary gradients $\nabla_{\mathbf{C}_e} W_e(\mathbf{C}_e^h(\alpha))$. This is a variational problem with

constraint, which is called an *isoperimetrical problem* due to the specific form of the constraint [47, 31, 91, 69, 46]. (See also Appendix A.6 for more details). We consequently minimise the functionals

$$\mathcal{F}_e(DW_e) = \frac{1}{2} \int_0^1 \|DW_e(\alpha) - \nabla_{\mathbf{C}_e} W_e(\mathbf{C}_e^h(\alpha))\|^2 d\alpha \quad (6.26)$$

on the master element \mathcal{I}_α under the constraint

$$\mathcal{G}_e(DW_e) = W_e(\mathbf{C}_e^h(1)) - W_e(\mathbf{C}_e^h(0)) - \int_0^1 DW_e(\alpha) : \frac{\partial \mathbf{C}_e^h(\alpha)}{\partial \alpha} d\alpha. \quad (6.27)$$

To this end we augment the functionals \mathcal{F}_e with the constraints \mathcal{G}_e through Lagrange multipliers $\lambda_e \in \mathbb{R}$. We obtain Lagrange functionals $\mathcal{L}_e = \mathcal{F}_e + \lambda_e \mathcal{G}_e$ and the corresponding Euler-Lagrange equations as necessary condition for a minimum. Taking the design criterion into account, the solution of the present isoperimetrical problem is the following enhanced gradient:

$$\boxed{DW_e(\alpha) = \nabla_{\mathbf{C}_e} W_e(\mathbf{C}_e^h(\alpha)) + \frac{\mathcal{G}_e(\nabla_{\mathbf{C}_e} W_e)}{\mathcal{N}_e} \frac{\partial \mathbf{C}_e^h(\alpha)}{\partial \alpha}} \quad (6.28)$$

where

$$\mathcal{N}_e = \int_0^1 \frac{\partial \mathbf{C}_e^h(\alpha)}{\partial \alpha} : \frac{\partial \mathbf{C}_e^h(\alpha)}{\partial \alpha} d\alpha. \quad (6.29)$$

In a computational setting, we also apply k -point Gaussian quadrature with an accuracy $\mathcal{O}(h_n^{2k})$ for computing the time integrals in the enhanced gradient. In consequence, the distance of the enhanced gradient to the approximated ordinary gradient is of the same accuracy. The ordinary gradient is thus modified within the error bounds of the cG(k) method and the accuracy order of this integrator is therefore retained.

6.6 Assumed strain approximation

In the enhanced gradients DW_e , we have to employ an appropriate time approximation \mathbf{C}_e^h of the right Cauchy-Green tensor which is a consistent strain measure (see Section 2.5). This consistency, however, is generally lost in a time approximation. Starting from the

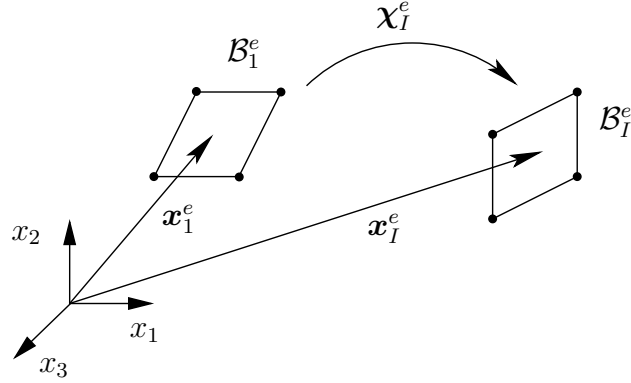


Figure 6.4. Rigid body motion χ_I^e of an element \mathcal{B}^e . The initial element domain is denoted by \mathcal{B}_1^e , whereas the element domain at time node α_I is denoted by \mathcal{B}_I^e .

cG approximation \mathbf{C}_e of the right Cauchy-Green tensor associated to an element \mathcal{B}^e , we separate that part of \mathbf{C}_e which is invariant with respect to rigid body motions. For these purposes we consider a general rigid body motion χ_e of an element \mathcal{B}^e , which is given by an Euclidean transformation (see Figure 6.4). The deformation gradient at each time node α_I , $I = 2, \dots, k+1$, pertaining to the motion χ_I^e is given by $\mathbf{F}_I^e = \mathbf{R}_I^e \mathbf{F}_1^e$, where \mathbf{F}_1^e denotes the deformation gradient of the motion to the initial configuration and $\mathbf{R}_I^e \in SO(n_{dim})$ designate orthogonal rotation tensors with the property $(\mathbf{R}_I^e)^T \mathbf{R}_I^e = \mathbf{I}_{n_{dim}}$. The cG approximation \mathbf{C}_e of the right Cauchy-Green tensor can be written as

$$\mathbf{F}_e^T \mathbf{F}_e = \sum_{I=1}^{k+1} M_I \mathbf{C}_I^e - \sum_{I=1}^k \sum_{J=I+1}^{k+1} M_I M_J [\mathbf{F}_I^e - \mathbf{F}_J^e]^T [\mathbf{F}_I^e - \mathbf{F}_J^e], \quad (6.30)$$

where $\mathbf{C}_I^e = (\mathbf{F}_I^e)^T \mathbf{F}_I^e$ is the right Cauchy-Green tensor at the time node α_I . Since the tensors \mathbf{R}_I^e are elements of the special orthogonal group $SO(n_{dim})$ which has a matrix multiplication as group operation, the difference of two orthogonal tensors is generally not an orthogonal tensor. The last term of equation (6.30) is therefore affected by a rigid body motion. Taking the orthogonality property into account, the first term is not influenced by a rigid body motion. The first term in equation (6.30) is called the *assumed strain approximation* of the right Cauchy-Green tensor (compare [20]):

$$\boxed{\mathbf{C}_e(\alpha) = \sum_{I=1}^{k+1} M_I(\alpha) \mathbf{C}_I^e} \quad (6.31)$$

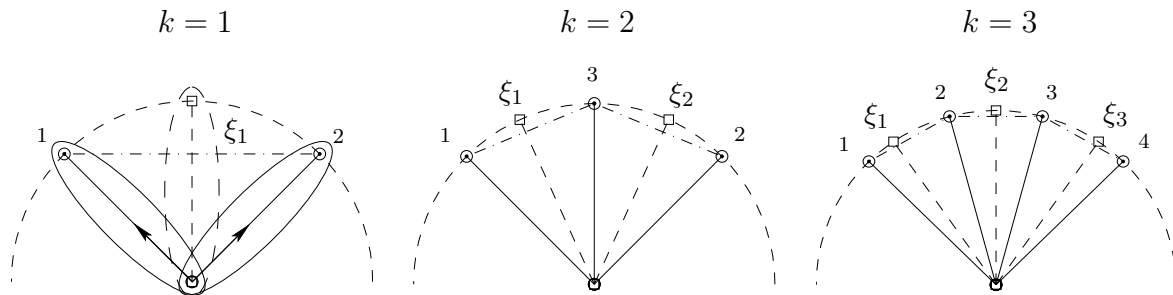


Figure 6.5. Stretch $\lambda(\alpha)$ in direction of the depicted directional unit vectors during a rigid body rotation determined by the assumed strain approximation \mathbf{C} of the right Cauchy-Green tensor for $k = 1, 2, 3$. The numbered points and the points ξ_l , $l = 1, \dots, k$, denote the time nodes and the Gauss points on the master element, respectively.

Hence the assumed strain approximation can be viewed as that part of the cG approximation, which is indifferent with respect to rigid body motions. According to Appendix C.2, the assumed strain approximation is also a consistent time approximation of the right Cauchy-Green tensor because the approximation order is the same as for the cG approximation \mathbf{C}_e .

Remark 6.5. The application of the assumed strain approximation can be interpreted as the approximation $d\mathbf{x}(\alpha)$ of a line element in the current configuration with respect to the corotational directional unit vector $\mathbf{n}(\alpha)$ defined by $d\mathbf{x}(\alpha) = d\|\mathbf{x}\|(\alpha) \mathbf{n}(\alpha)$, where $d\mathbf{x}(\alpha) = \mathbf{F}(\alpha) d\mathbf{X}$, with a separate approximation of the length of the line element. The approximated line element in the current configuration can be then written as $d\mathbf{x}(\alpha) = [d\mathbf{X} \cdot \mathbf{C}(\alpha) d\mathbf{X}]^{\frac{1}{2}} \mathbf{n}(\alpha)$ which does not change its length after a rigid body rotation (see Figure 6.5). By using the cG approximation a line element in the same direction has the length $[d\mathbf{X} \cdot \mathbf{C}(\alpha) d\mathbf{X}]^{\frac{1}{2}}$ with the cG approximation $\mathbf{C} = \mathbf{F}^T \mathbf{F}$ of the right Cauchy-Green tensor. The line element is then approximated with respect to the inertial coordinate frame.

6.7 Enhanced assumed gradient

The assumed strain approximation in the previous section is not affected by rigid body motions. We can therefore recommend this time approximation of the right Cauchy-Green

tensor to conserve the objectivity of this strain tensor. However, the constraint of energy conservation prevents the application of the assumed strain approximation in each term of the enhanced gradients. The reason is equation (6.23) which has to be fulfilled at all Gauss points in those terms where the chain rule of differentiation is used. This equation is satisfied by the cG approximation \mathbf{C}_e for arbitrary k . However, the assumed strain approximation only satisfies this condition in the special case $k = 1$. In the argument of the ordinary gradients and in the directional part of the enhanced gradients, we can use the assumed strain approximation without affecting the energy conservation condition. Taking the assumed strain approximation into account, the design criteria in the enhanced gradients are thus given by

$$\underline{\mathcal{G}}_e = W_e(\mathbf{C}_e(1)) - W_e(\mathbf{C}_e(0)) - \sum_{l=1}^k \nabla_{\mathbf{C}_e} W_e(\mathbf{C}_e(\xi_l)) : \frac{\partial \mathbf{C}_e(\xi_l)}{\partial \alpha} w_l. \quad (6.32)$$

The design criteria are fulfilled by the following enhanced gradients associated with k -point Gaussian quadrature:

$$\boxed{\underline{D}W_e = \nabla_{\mathbf{C}_e} W_e(\mathbf{C}_e) + \frac{\underline{\mathcal{G}}_e}{\underline{\mathcal{N}}_e} \frac{\partial \mathbf{C}_e}{\partial \alpha}} \quad (6.33)$$

where

$$\underline{\mathcal{N}}_e = \sum_{l=1}^k \frac{\partial \mathbf{C}_e(\xi_l)}{\partial \alpha} : \frac{\partial \mathbf{C}_e(\xi_l)}{\partial \alpha} w_l. \quad (6.34)$$

This composite approximation is possibly due to the same accuracy order of both time approximations of the right Cauchy-Green tensor.

6.8 The enhanced Galerkin (eG) method

A mechanical integrator for semi-discrete elastodynamics should conserve all first integrals of the motion. The collocation at k Gauss points furnishes the conservation of total linear and total angular momentum. Conservation of total energy is enforced by the enhanced gradients with Gaussian quadrature. Moreover, we used in the enhanced gradients the objective assumed strain approximation of the right Cauchy-Green tensor. The application

of a rotationally invariant strain measure is recommended for improving the numerical stability of the integrator (see [53]). We therefore recommend as higher order accurate mechanical integrator the cG(k) method in conjunction with the enhanced gradient and assumed strain approximation given by

$$\boxed{\begin{aligned} \sum_{J=1}^{k+1} \int_0^1 \tilde{M}_I M'_J \, d\alpha \mathbf{q}_J - h_n \int_0^1 \tilde{M}_I \mathbb{M}^{-1} \mathbf{p} \, d\alpha &= \mathbf{0}, \\ \sum_{J=1}^{k+1} \int_0^1 \tilde{M}_I M'_J \, d\alpha \mathbf{p}_J + h_n \sum_{l=1}^k \tilde{M}_I(\xi_l) \underline{\mathbb{Q}}(\xi_l) \mathbf{q}(\xi_l) w_l &= \mathbf{0}, \end{aligned}} \quad I = 1, \dots, k. \quad (6.35)$$

The time approximation $\underline{\mathbb{Q}}(\alpha)$ of the stiffness matrix is given by the element stiffness matrices $\underline{\mathbb{Q}}_e(\alpha)$ corresponding to the coefficients

$$\underline{\mathbb{Q}}_{ab}^e(\alpha) = \int_{\mathcal{B}_0^e} 2 \underline{\mathbb{D}}W_e(\alpha) : \mathbf{N}_{ab}^e \, dV \quad (6.36)$$

of the structure element stiffness matrix $\underline{\mathbb{Q}}_{ab}^e$. We refer to this mechanical integrator as the *enhanced cG(k) method* or simple as the *enhanced Galerkin (eG(k)) method* for semi-discrete elastodynamics. The eG(1) method for semi-discrete elastodynamics is given by

$$\begin{aligned} \mathbf{q}_2 - \mathbf{q}_1 - \frac{h_n}{2} \mathbb{M}^{-1} [\mathbf{p}_1 + \mathbf{p}_2] &= \mathbf{0}, \\ \mathbf{p}_2 - \mathbf{p}_1 + \frac{h_n}{2} \underline{\mathbb{Q}}\left(\frac{1}{2}\right) [\mathbf{q}_1 + \mathbf{q}_2] &= \mathbf{0}, \end{aligned} \quad (6.37)$$

where the gradient of the strain energy density function restricted to the element e is approximated by the following finite difference quotient:

$$\underline{\mathbb{D}}W_e\left(\frac{1}{2}\right) = \nabla_{\mathbf{C}_e} W_e\left(\frac{\mathbf{C}_1^e + \mathbf{C}_2^e}{2}\right) + \frac{\underline{\mathcal{G}}_e}{\underline{\mathcal{N}}_e} [\mathbf{C}_2^e - \mathbf{C}_1^e], \quad (6.38)$$

with the expressions

$$\begin{aligned} \underline{\mathcal{G}}_e &= W_e(\mathbf{C}_2^e) - W_e(\mathbf{C}_1^e) - \nabla_{\mathbf{C}_e} W_e\left(\frac{\mathbf{C}_1^e + \mathbf{C}_2^e}{2}\right) : [\mathbf{C}_2^e - \mathbf{C}_1^e], \\ \underline{\mathcal{N}}_e &= \|\mathbf{C}_2^e - \mathbf{C}_1^e\|^2. \end{aligned} \quad (6.39)$$

This integrator is equivalent to the total energy and momentum conserving integrator in [53], which is based on a second order accurate finite difference approximation.

6.9 Numerical investigations

In this section, we present the linearisation of the cG(k) and the eG(k) method in nonlinear elastodynamics. We then verify the conservation properties stated for the eG(k) method in numerical examples and draw a comparison between the cG(k) and the eG(k) method with respect to conservation of first integrals, accuracy and numerical costs. Finally, the efficiency of higher order time finite elements is also discussed in the light of computation time.

6.9.1 Linearisation of the algorithms

The implementation of the cG(k) as well as the eG(k) method follows directly from Section 3.2.6. We have used the $\epsilon = 10^{-8}$ as tolerance for the residual in the stopping criteria of the Newton-Raphson method. The blocks \mathbf{K}_J , $J = 2, \dots, k+1$, of the tangent operator themselves have again a block structure:

$$\mathbf{K}_J = \underset{e=1}{\overset{n_{el}}{\mathbf{A}}} \begin{bmatrix} {}^e\mathbf{K}_J^{11} & \dots & {}^e\mathbf{K}_J^{1n_{en}} \\ \vdots & & \vdots \\ {}^e\mathbf{K}_J^{n_{en}1} & \dots & {}^e\mathbf{K}_J^{n_{en}n_{en}} \end{bmatrix} \quad (6.40)$$

The blocks can be also divided in symmetric geometrical parts associated with linearising B-matrices and material parts following from the linearisation of the algorithmic constitutive law: ${}^e\mathbf{K}_J^{ab} = {}^e\mathbf{K}_{\text{Geo}J}^{ab} + {}^e\mathbf{K}_{\text{Mat}J}^{ab}$. Here we have the following B-matrices to formulate the conservative forces and the corresponding tangent matrices:

$$\mathbf{B}_a^e(\alpha) = \mathbf{F}_e(\alpha) \otimes \nabla_\xi N_a \cdot \mathbf{J}_e^{-1}, \quad [{}^e\mathbf{B}_J^b]^T = \mathbf{J}_e^{-T} \cdot \nabla_\xi N_b \otimes [\mathbf{F}_J^e]^T. \quad (6.41)$$

The geometrical and the material parts associated with the cG method read with these B-matrices

$$\begin{aligned} {}^e\mathbf{K}_{\text{Geo}J}^{ab} &= M_J \mathbf{Q}_{ab}^e \mathbf{I}_{n_{dim}}, \\ {}^e\mathbf{K}_{\text{Mat}J}^{ab} &= M_J \int_{\mathcal{B}_0^e} \mathbf{B}_a^e : \left[4 \nabla_{\mathbf{C}_e}^2 W_e(\mathbf{C}_e) \right] : [\mathbf{B}_b^e]^T \, dV. \end{aligned} \quad (6.42)$$

The geometrical parts of the eG method take similar forms as those of the cG method because the B-matrices \mathbf{B}_a^e also determines the internal nodal force direction in the eG method. However, the corresponding material parts are more complicated due to the additional terms of the enhanced gradient:

$$\begin{aligned} {}^e\mathbf{K}_{\text{Geo}J}^{ab} &= M_J \underline{\mathbf{Q}}_{ab}^e \mathbf{I}_{n_{dim}}, \\ {}^e\mathbf{K}_{\text{Mat}J}^{ab} &= \int_{\mathcal{B}_0^e} \mathbf{B}_a^e : \left[M_J 4 \nabla_{\mathbf{C}_e}^2 W_e(\mathbf{C}_e) + M_J' 4 \frac{\underline{\mathcal{G}}_e}{\underline{\mathcal{N}}_e} \mathbb{1}_{\text{sym}} \right] : [{}^e\mathbf{B}_J^b]^T \, dV + \\ &+ \int_{\mathcal{B}_0^e} \mathbf{B}_a^e : \left[\delta_{J,k+1} \frac{2}{\underline{\mathcal{N}}_e} \frac{\partial \mathbf{C}_e(\alpha)}{\partial \alpha} \otimes \mathbf{S}_J^e - \frac{4}{\underline{\mathcal{N}}_e} \frac{\partial \mathbf{C}_e(\alpha)}{\partial \alpha} \otimes \underline{\mathbf{L}}_1^e \right] : [{}^e\mathbf{B}_J^b]^T \, dV - \\ &- \int_{\mathcal{B}_0^e} \mathbf{B}_a^e : \left[\frac{4 \underline{\mathcal{G}}_e}{\underline{\mathcal{N}}_e^2} \frac{\partial \mathbf{C}_e}{\partial \alpha} \otimes \underline{\mathbf{L}}_2^e \right] \, dV, \end{aligned} \quad (6.43)$$

where

$$\begin{aligned} \underline{\mathbf{L}}_1^e &= \sum_{l=1}^k M_J(\xi_l) \frac{\partial \mathbf{C}_e(\xi_l)}{\partial \alpha} : \nabla_{\mathbf{C}_e}^2 W_e(\mathbf{C}_e(\xi_l)) w_l + \\ &+ \sum_{l=1}^k M_J'(\xi_l) \left[\nabla_{\mathbf{C}_e} W_e(\mathbf{C}_e(\xi_l)) + \frac{\underline{\mathcal{G}}_e}{\underline{\mathcal{N}}_e} \frac{\partial \mathbf{C}_e(\xi_l)}{\partial \alpha} \right] w_l, \\ \underline{\mathbf{L}}_2^e &= \sum_{l=1}^k \frac{\partial \mathbf{C}_e(\xi_l)}{\partial \alpha} : \left[M_J' [\mathbf{B}^e(\xi_l)]^T + M_J \left[\frac{\partial \mathbf{B}^e(\xi_l)}{\partial \alpha} \right]^T \right] w_l. \end{aligned} \quad (6.44)$$

Note that the material parts corresponding to the eG method are unsymmetric and those corresponding to the cG method are symmetric.

6.9.2 Compressible Neo-Hooke material

We consider k -blade planar and spatial propellers discretised by four-node and eight node Lagrange elements, respectively. The propellers are positioned with their centre in the origin of the corresponding Euclidean space. Given an initial angular velocity

vector $\boldsymbol{\omega}_0$ and an initial translation velocity vector \mathbf{v}_T , the initial velocity vectors \mathbf{v}_0^A , $A = 1, \dots, n_{np}$, of the nodes are determined by $\mathbf{v}_0^A = \mathbf{v}_T + \boldsymbol{\omega}_0 \times \mathbf{q}_0^A$. The propellers consist of compressible Neo-Hooke material with the Lamé constants $\lambda = 3000$, $\mu = 750$ in the flexible case and $\lambda = 30000$, $\mu = 7500$ in the stiff case. The motion starts in the stress free reference configuration with a homogenous mass density $\rho_0 = 8.93$. The strain energy density function of the compressible Neo-Hooke material is as follows:

$$W_e(\mathbf{C}_e) = \frac{\mu}{2} [\text{tr } \mathbf{C}_e - 3] + \frac{\lambda}{2} [\ln J_e]^2 - \mu \ln J_e, \quad (6.45)$$

where $J_e = \sqrt{\mathbf{C}_e}$ (see also [20]).

6.9.3 Discussion of the results

In the Figures 6.6, 6.14 and 6.22, the initial states of the planar motions depicted in the Figures 6.7, 6.15 and 6.23 are shown. The motions of the planar propellers are such that the centre of mass moves parallel to the x-axis. The figures 6.10, 6.18 and 6.26 show the initial conditions for the spatial motions plotted in the Figures 6.11, 6.19 and 6.27.

In the Figures 6.8, 6.16, 6.24, the momentum maps of the planar motions are depicted and the Figures 6.12, 6.20, 6.28 shows the momentum maps associated with the spatial motions. The corresponding total energies as well as a nodal distance of the mesh are plotted in the Figures 6.9, 6.17, 6.25 and in the Figures 6.13, 6.21, 6.29, respectively. It is obviously that the eG method fulfils the conservation laws independently of the family parameter k and the chosen time step size h_n . The total linear and angular momentum computed by the cG method is also constant over the time in contrast to the corresponding total energy. The cG method shows a blow-up behaviour because its total energy increases after the change of the time step size. The blow up is also shown in the nodal distance plots. The total energy computed by the cG method further depends on k as well as on the time step size h_n .

The left diagram of Figure 6.30 depicts the logarithm of the relative global error in the position at time T versus the logarithm of the associated time step sizes h_n . This

relative error is determined by

$$e_{\mathbf{q}} = \frac{\|\mathbf{q}(T) - \mathbf{q}^{ref}(T)\|}{\|\mathbf{q}^{ref}(T)\|} \quad (6.46)$$

where $\mathbf{q}^{ref}(T)$ denotes the reference solution at time T computed by the eG(4) method with a time step size $h_n = 0.001$. The graphs are lines due to the logarithmic scale of both axes. The slopes of the lines indicate the accuracy order $\mathcal{O}(h_n^{2k})$ of both methods under consideration. We observe increasing slopes of the lines and decreasing intercepts of the lines while increasing the parameter k for both methods. For this reason a greater k leads to a greater time step size h_n for calculating the solution at the time T with a prescribed accuracy.

The right diagram in Figure 6.30 is a double logarithmic plot showing the relative global error versus the corresponding CPU time. We also obtained lines due to a least square curve fitting. Firstly, we compare the CPU time consumed by one method corresponding to $k = 1, 2, 3$. We see that a greater k renders less CPU time to obtain a constant relative global error for both methods. A greater k accordingly leads to a saving of CPU time, which is due to larger time steps as well as less Newton-Raphson iterations. Secondly, comparing the CPU time of both methods for a fixed family parameter k , we observe that the CPU time of the eG method is generally greater in comparison with the cG method. The reason for this observation is the more extensive internal force vector and the associated unsymmetric tangent operator of the eG method. The advantage of the eG method is a better stability because the eG method allows for larger time steps compared to the cG method in the same problem.

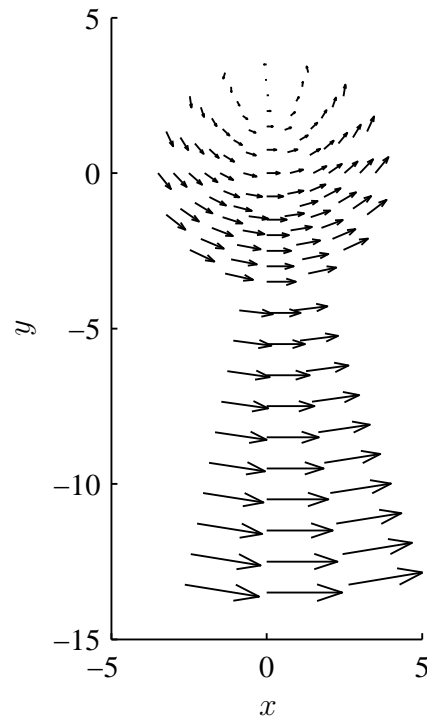


Figure 6.6. Initial velocity vectors of a planar 1-blade propeller discretised by $n_{np} = 119$ nodes in $n_{el} = 100$ four-node elements. The initial angular velocity vector and the translational velocity vector are given by $\boldsymbol{\omega}_0 = (0, 0, 0.7)$ and $\boldsymbol{v}_T = (2, 0, 0)$, respectively.

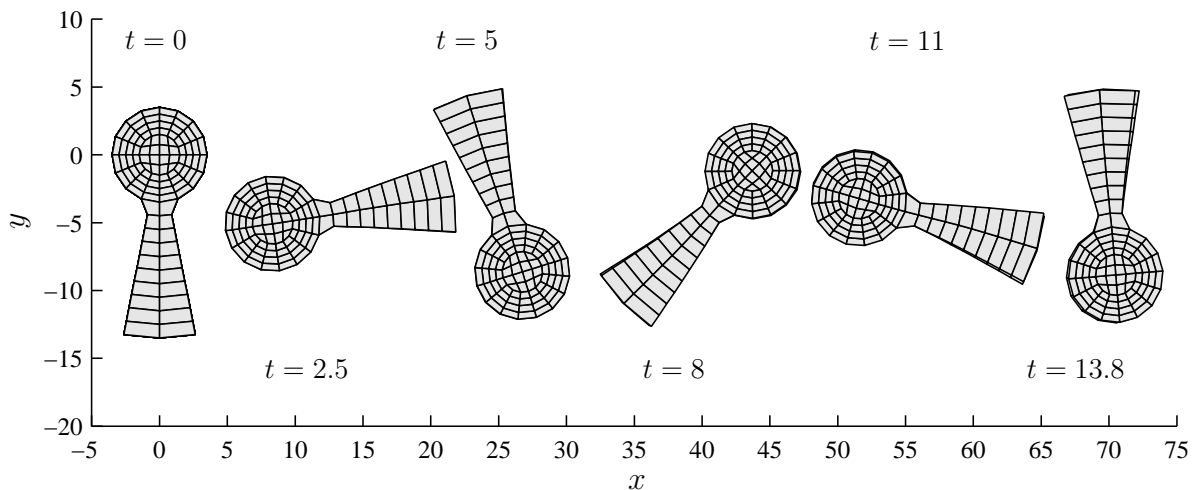


Figure 6.7. Motion of a planar 1-blade propeller (Neo Hooke material with $\lambda = 30000$, $\mu = 7500$, $\rho_0 = 8.93$) discretised by $n_{np} = 119$ nodes in $n_{el} = 100$ four-node elements and computed with the cG(1) method as well as with the eG(1) method. The time step size h_n has been set to 0.1 for $T \leq 5$ and to 0.2 for $T > 5$. The propellers pertaining to the eG(1) method are depicted on top.

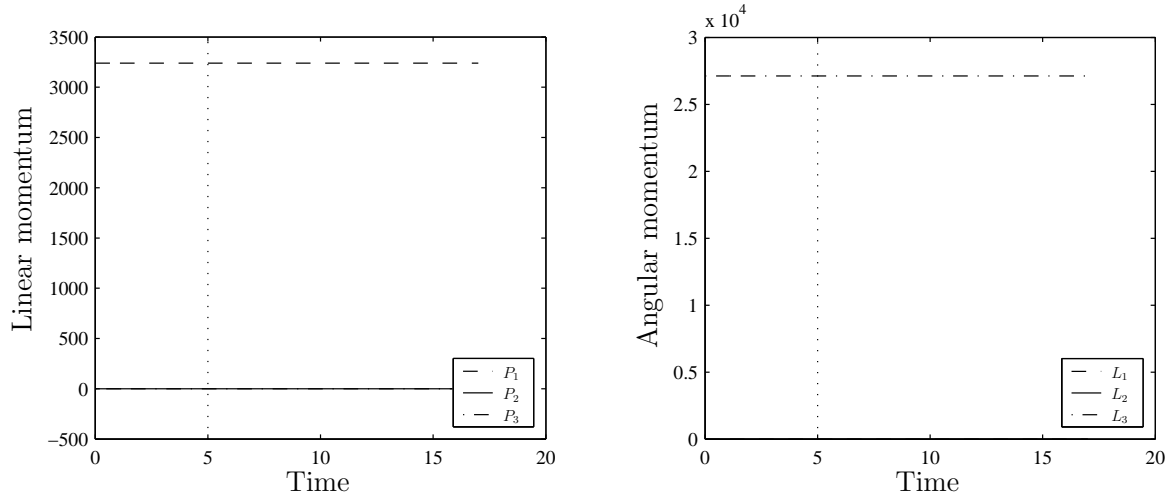


Figure 6.8. Momentum maps of a planar 1-blade propeller (Neo Hooke material with $\lambda = 30000$, $\mu = 7500$, $\rho_0 = 8.93$) discretised by $n_{np} = 119$ nodes in $n_{el} = 100$ four-node elements and computed with the cG(1) method as well as with the eG(1) method. The time step size h_n has been set to 0.1 for $T \leq 5$ and to 0.2 for $T > 5$.

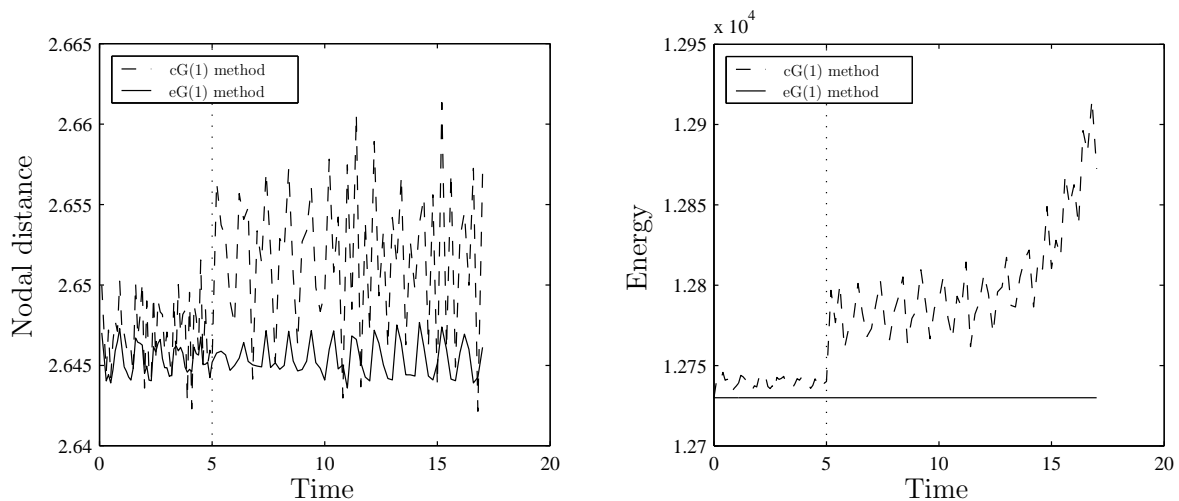


Figure 6.9. Nodal distance and total energy of a planar 1-blade propeller (Neo Hooke material with $\lambda = 30000$, $\mu = 7500$, $\rho_0 = 8.93$) discretised by $n_{np} = 119$ nodes in $n_{el} = 100$ four-node elements and computed with the cG(1) method as well as with the eG(1) method. The time step size h_n has been set to 0.1 for $T \leq 5$ and to 0.2 for $T > 5$.

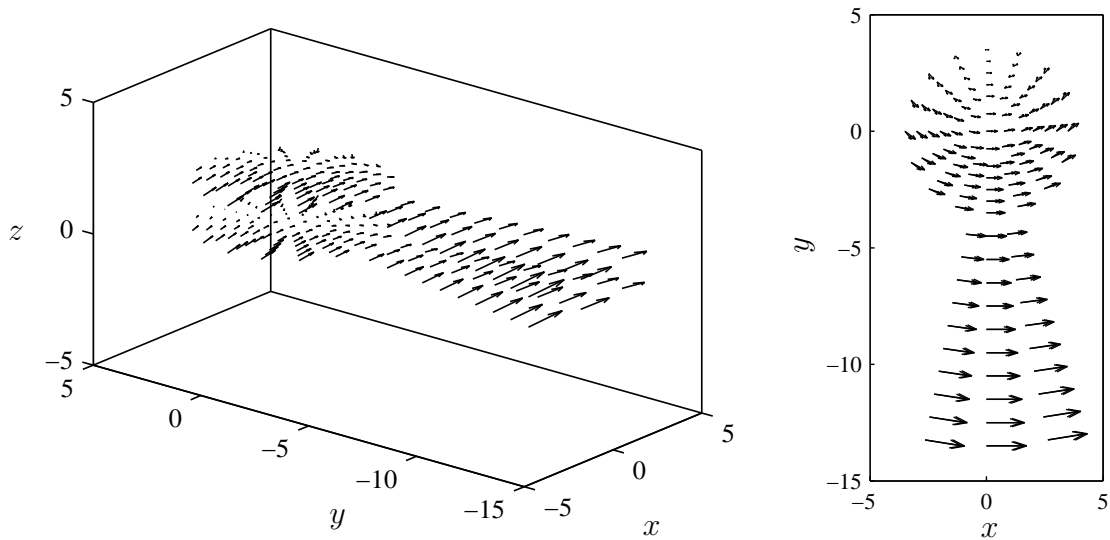


Figure 6.10. Initial velocity vectors of a spatial 1-blade propeller discretised by $n_{np} = 238$ nodes in $n_{el} = 100$ eight-node elements. The initial angular velocity vector and the translational velocity vector are given by $\boldsymbol{\omega}_0 = (0, 0.7, 0.7)$ and $\mathbf{v}_T = (2, 0, -0.1)$, respectively.

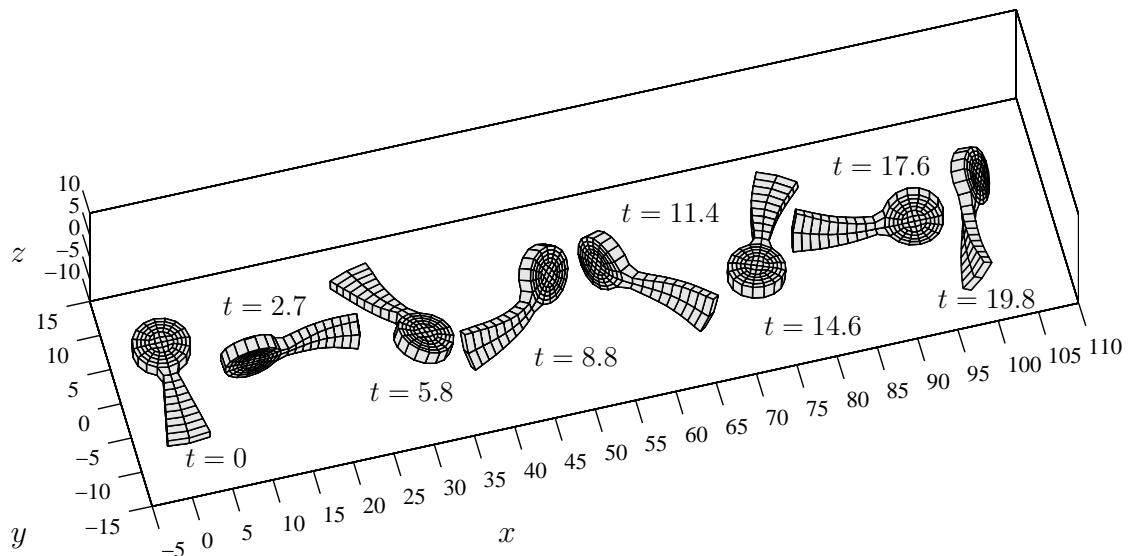


Figure 6.11. Motion of a spatial 1-blade propeller (Neo Hooke material with $\lambda = 3000$, $\mu = 750$, $\rho_0 = 8.93$) discretised by $n_{np} = 238$ nodes in $n_{el} = 100$ eight-node elements and computed with the eG(1) method. The time step size h_n has been set to 0.1 for $T \leq 5$ and to 0.2 for $T > 5$.

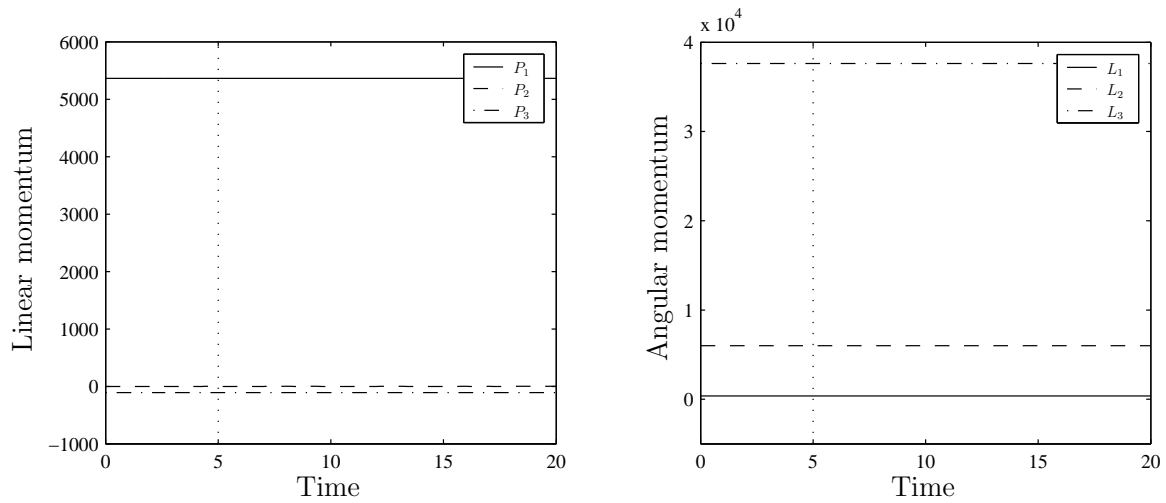


Figure 6.12. Momentum maps of a spatial 1-blade propeller (Neo Hooke material with $\lambda = 3000$, $\mu = 750$, $\rho_0 = 8.93$) discretised by $n_{np} = 238$ nodes in $n_{el} = 100$ eight-node elements and computed with the eG(1) method. The time step size h_n has been set to 0.1 for $T \leq 5$ and to 0.2 for $T > 5$.

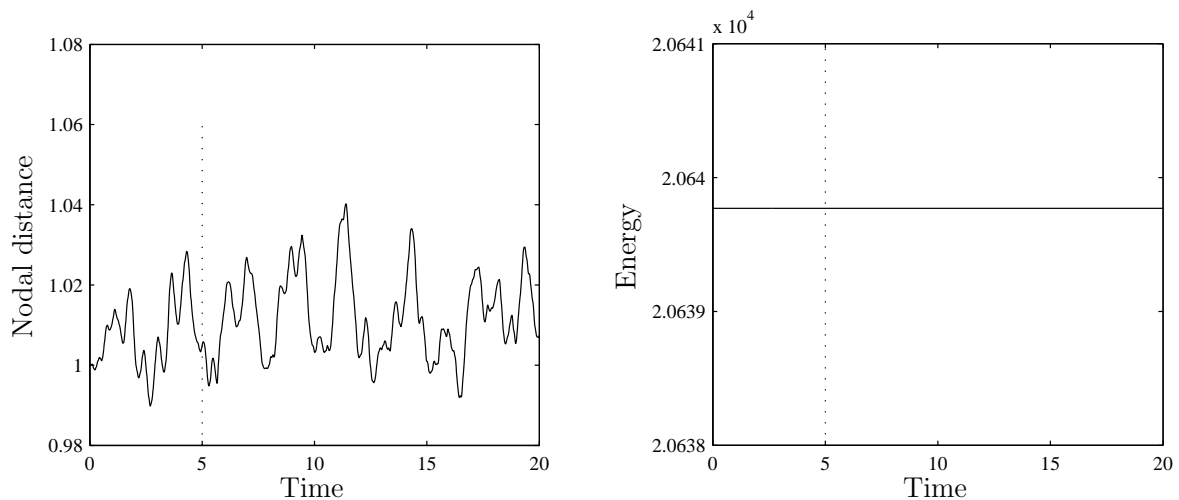


Figure 6.13. Nodal distance and total energy of a spatial 1-blade propeller (Neo Hooke material with $\lambda = 3000$, $\mu = 750$, $\rho_0 = 8.93$) discretised by $n_{np} = 238$ nodes in $n_{el} = 100$ eight-node elements and computed with the eG(1) method. The time step size h_n has been set to 0.1 for $T \leq 5$ and to 0.2 for $T > 5$.

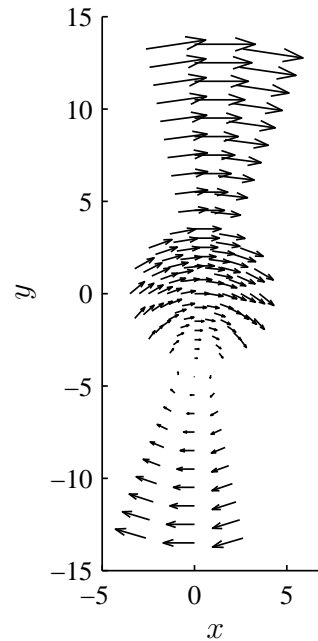


Figure 6.14. Initial velocity vectors of a planar 2-blade propeller discretised by $n_{np} = 149$ nodes in $n_{el} = 120$ four-node elements. The initial angular velocity vector and the translational velocity vector are given by $\boldsymbol{\omega}_0 = (0, 0, -0.7)$ and $\mathbf{v}_T = (3, 0, 0)$, respectively.

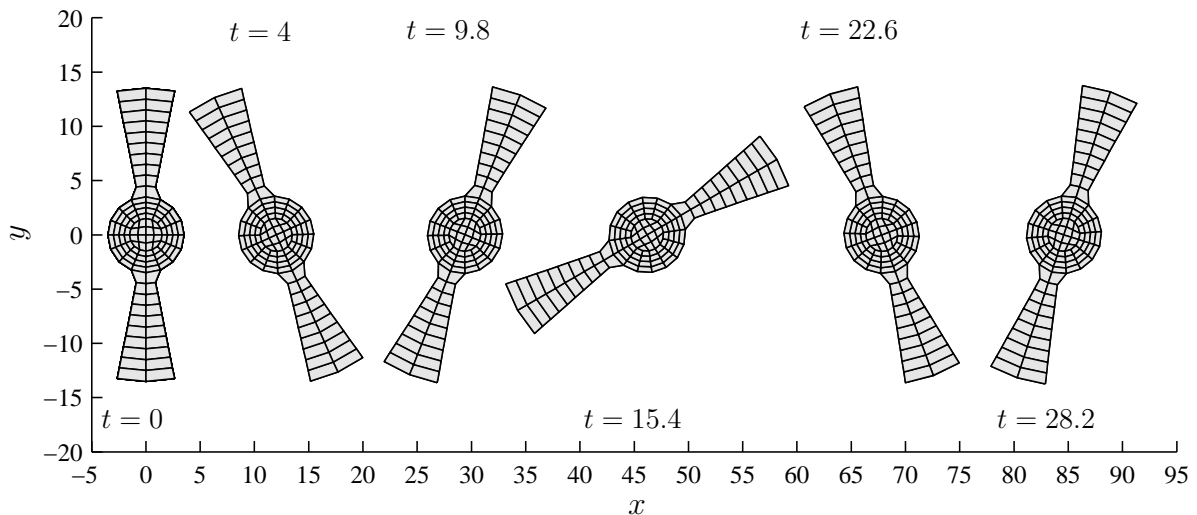


Figure 6.15. Motion of a planar 2-blade propeller (Neo Hooke material with $\lambda = 30000$, $\mu = 7500$, $\rho_0 = 8.93$) discretised by $n_{np} = 149$ nodes in $n_{el} = 120$ four-node elements and computed with the cG(2) method as well as with the eG(2) method. The time step size h_n has been set to 0.1 for $T \leq 5$ and to 0.2 for $T > 5$. The propellers pertaining to the eG(2) method are depicted on top.

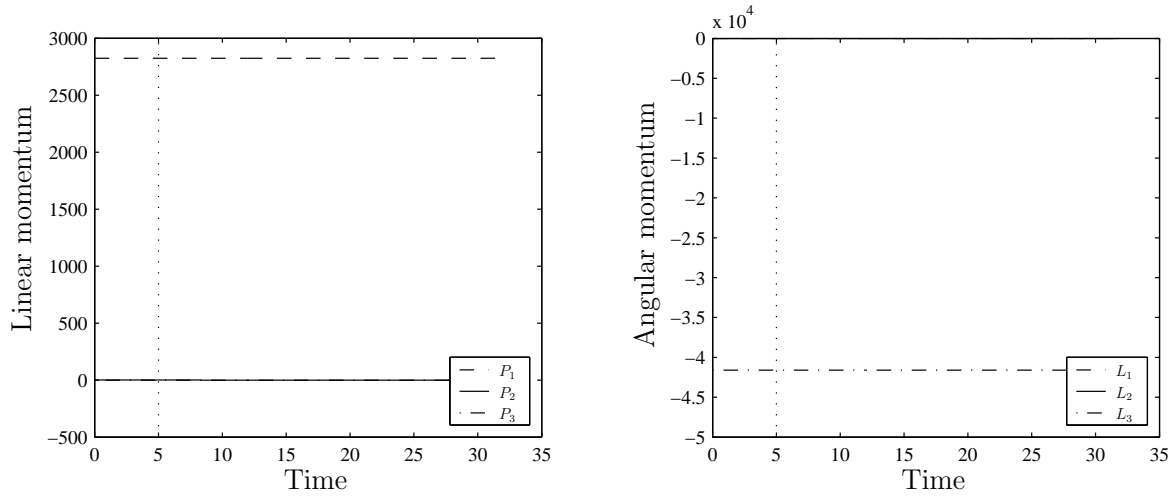


Figure 6.16. Momentum maps of a planar 2-blade propeller (Neo Hooke material with $\lambda = 30000$, $\mu = 7500$, $\rho_0 = 8.93$) discretised by $n_{np} = 149$ nodes in $n_{el} = 120$ four-node elements and computed with the cG(2) method as well as with the eG(2) method. The time step size h_n has been set to 0.1 for $T \leq 5$ and to 0.2 for $T > 5$.

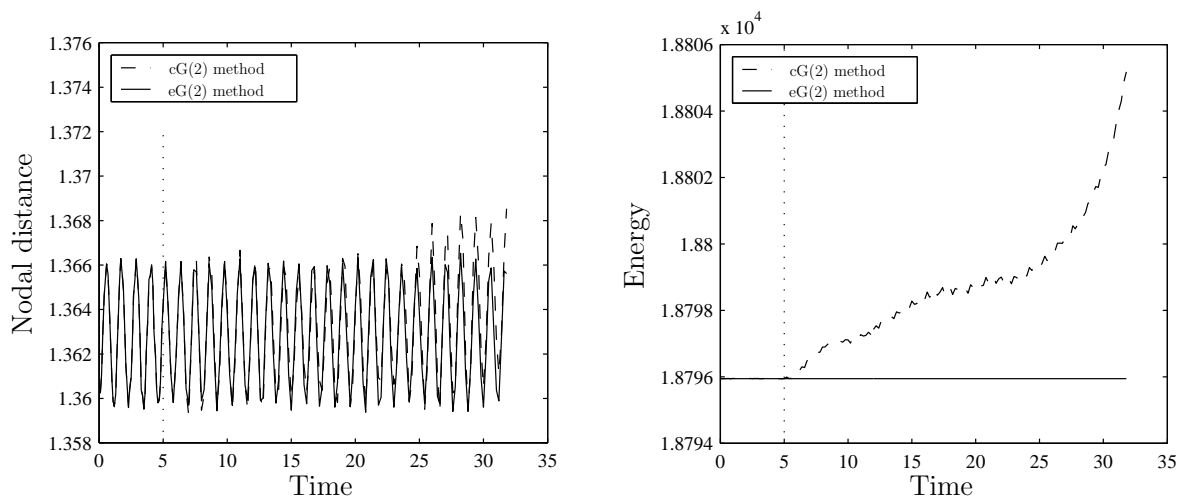


Figure 6.17. Nodal distance and total energy of a planar 2-blade propeller (Neo Hooke material with $\lambda = 30000$, $\mu = 7500$, $\rho_0 = 8.93$) discretised by $n_{np} = 149$ nodes in $n_{el} = 120$ four-node elements and computed with the cG(2) method as well as with the eG(2) method. The time step size h_n has been set to 0.1 for $T \leq 5$ and to 0.2 for $T > 5$.

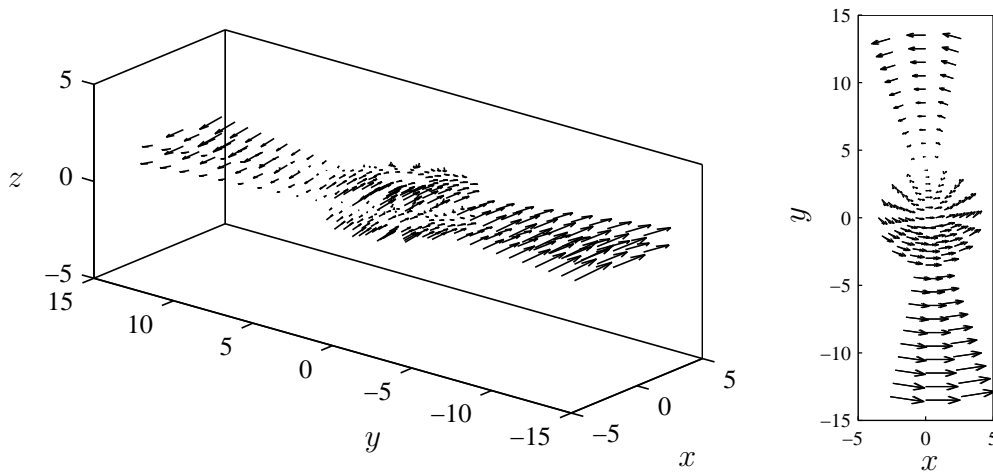


Figure 6.18. Initial velocity vectors of a spatial 2-blade propeller discretised by $n_{np} = 298$ nodes in $n_{el} = 120$ eight-node elements. The initial angular velocity vector and the translational velocity vector are given by $\boldsymbol{\omega}_0 = (0, 0.7, 0.7)$ and $\mathbf{v}_T = (2, 0, -0.1)$, respectively.

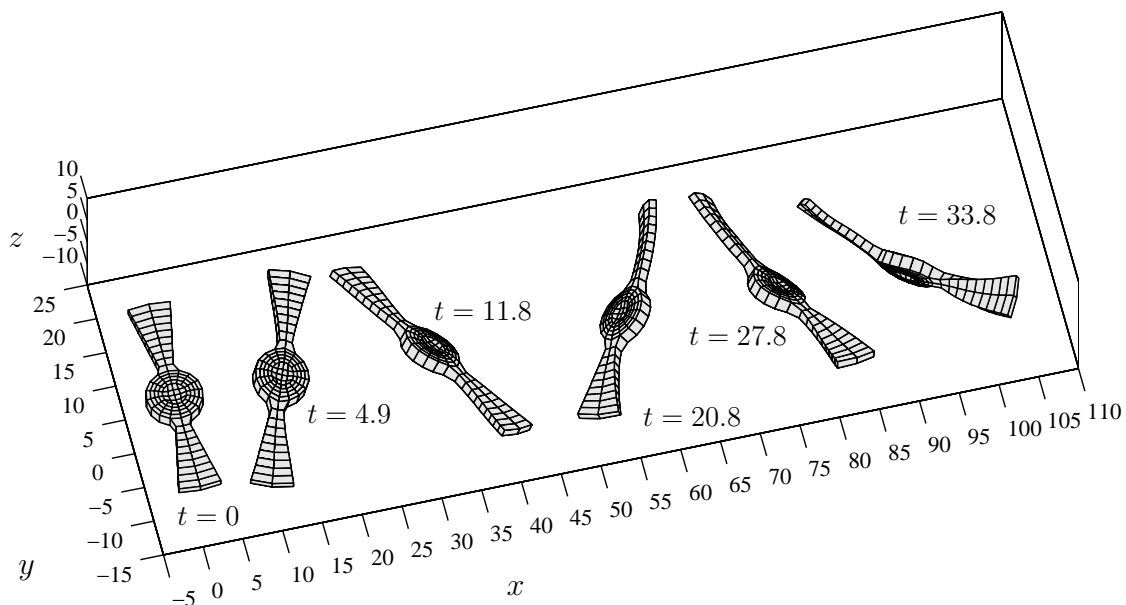


Figure 6.19. Motion of a spatial 2-blade propeller (Neo Hooke material with $\lambda = 3000$, $\mu = 750$, $\rho_0 = 8.93$) discretised by $n_{np} = 298$ nodes in $n_{el} = 120$ eight-node elements and computed with the eG(2) method. The time step size h_n has been set to 0.1 for $T \leq 5$ and to 0.2 for $T > 5$.

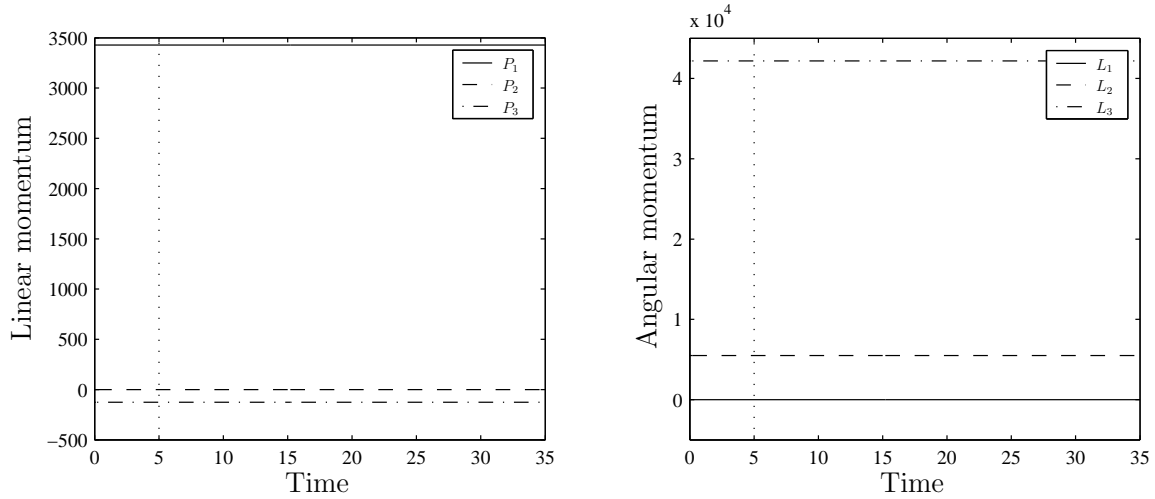


Figure 6.20. Momentum maps of a spatial 2-blade propeller (Neo Hooke material with $\lambda = 3000$, $\mu = 750$, $\rho_0 = 8.93$) discretised by $n_{np} = 298$ nodes in $n_{el} = 120$ eight-node elements and computed with the eG(2) method. The time step size h_n has been set to 0.1 for $T \leq 5$ and to 0.2 for $T > 5$.

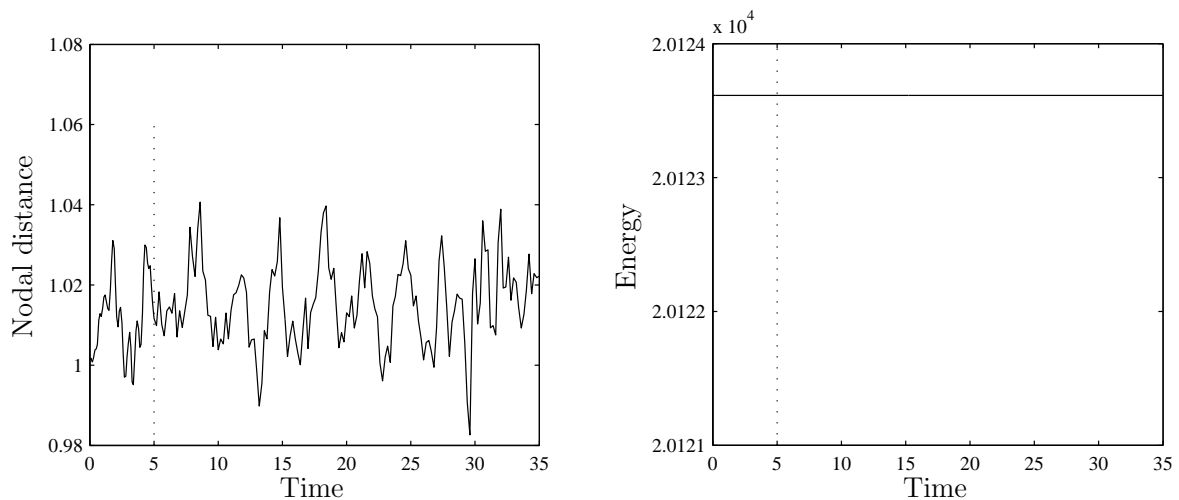


Figure 6.21. Nodal distance and total energy of a spatial 2-blade propeller (Neo Hooke material with $\lambda = 3000$, $\mu = 750$, $\rho_0 = 8.93$) discretised by $n_{np} = 298$ nodes in $n_{el} = 120$ eight-node elements and computed with the eG(2) method. The time step size h_n has been set to 0.1 for $T \leq 5$ and to 0.2 for $T > 5$.

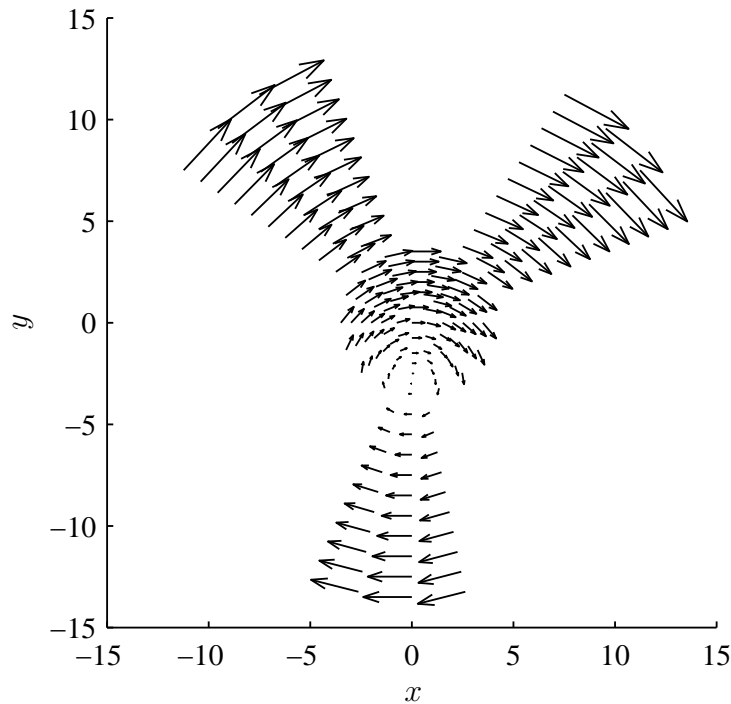


Figure 6.22. Initial velocity vectors of a planar 3-blade propeller discretised by $n_{np} = 179$ nodes in $n_{el} = 140$ four-node elements. The initial angular velocity vector and the translational velocity vector are given by $\boldsymbol{\omega}_0 = (0, 0, -0.7)$ and $\mathbf{v}_T = (2, 0, 0)$, respectively.

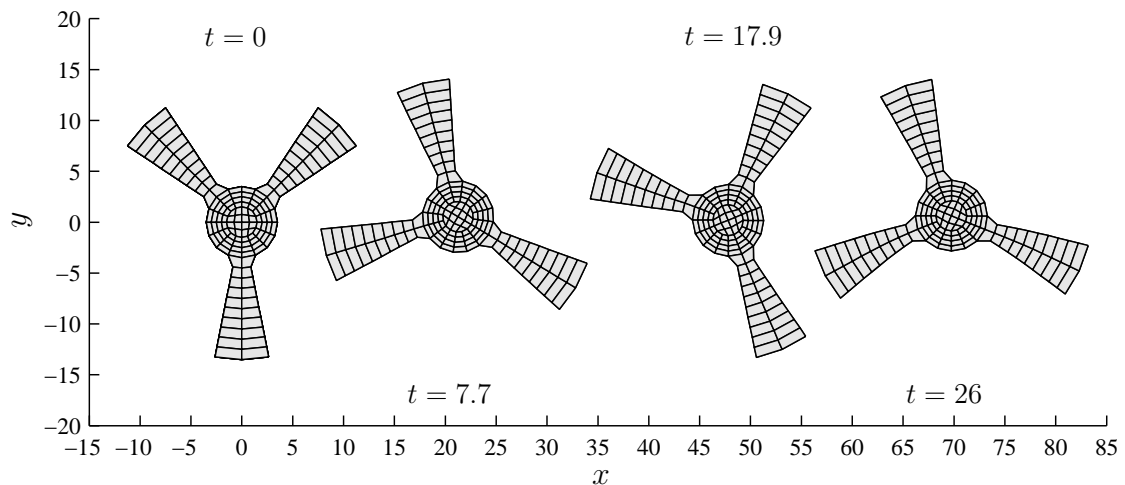


Figure 6.23. Motion of a planar 3-blade propeller (Neo Hooke material with $\lambda = 30000$, $\mu = 7500$, $\rho_0 = 8.93$) discretised by $n_{np} = 179$ nodes in $n_{el} = 140$ four-node elements and computed with the cG(3) method as well as with the eG(3) method. The time step size h_n has been set to 0.1 for $T \leq 5$ and to 0.3 for $T > 5$. The propellers pertaining to the eG(3) method are depicted on top.

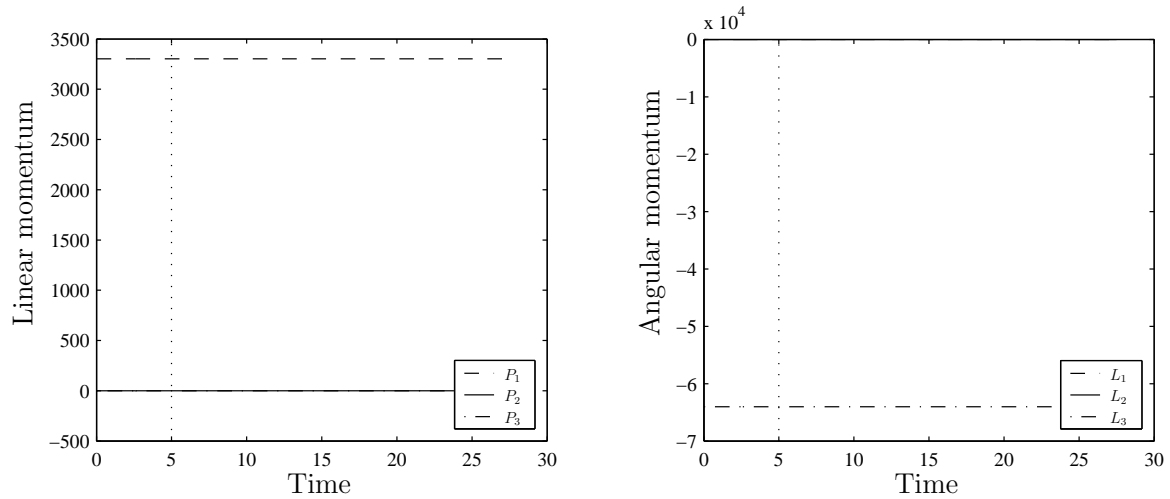


Figure 6.24. Momentum maps of a planar 3-blade propeller (Neo Hooke material with $\lambda = 30000$, $\mu = 7500$, $\rho_0 = 8.93$) discretised by $n_{np} = 179$ nodes in $n_{el} = 140$ four-node elements and computed with the cG(3) method as well as with the eG(3) method. The time step size h_n has been set to 0.1 for $T \leq 5$ and to 0.3 for $T > 5$.

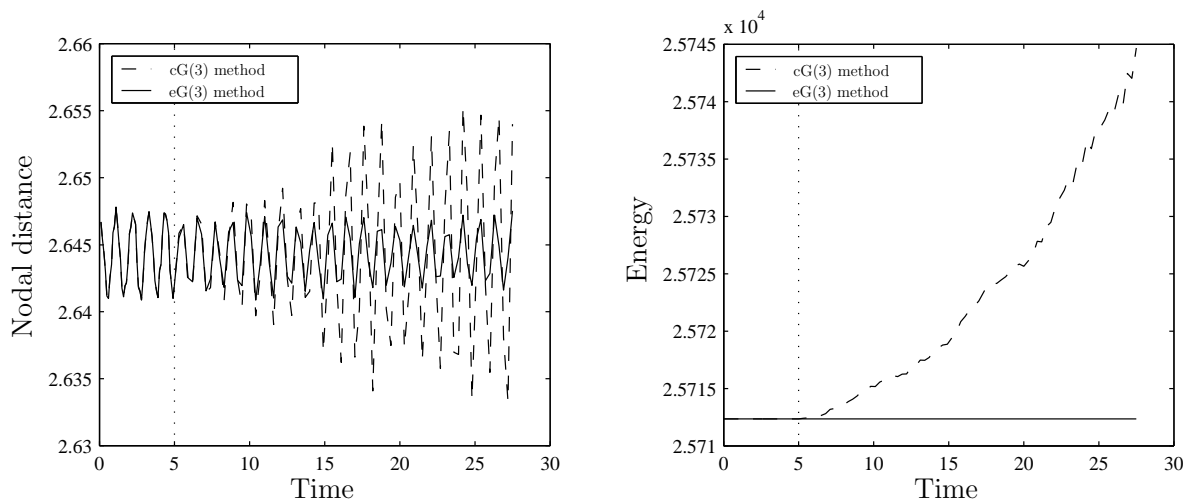


Figure 6.25. Nodal distance and total energy of a planar 3-blade propeller (Neo Hooke material with $\lambda = 30000$, $\mu = 7500$, $\rho_0 = 8.93$) discretised by $n_{np} = 179$ nodes in $n_{el} = 140$ four-node elements and computed with the cG(3) method as well as with the eG(3) method. The time step size h_n has been set to 0.1 for $T \leq 5$ and to 0.3 for $T > 5$.

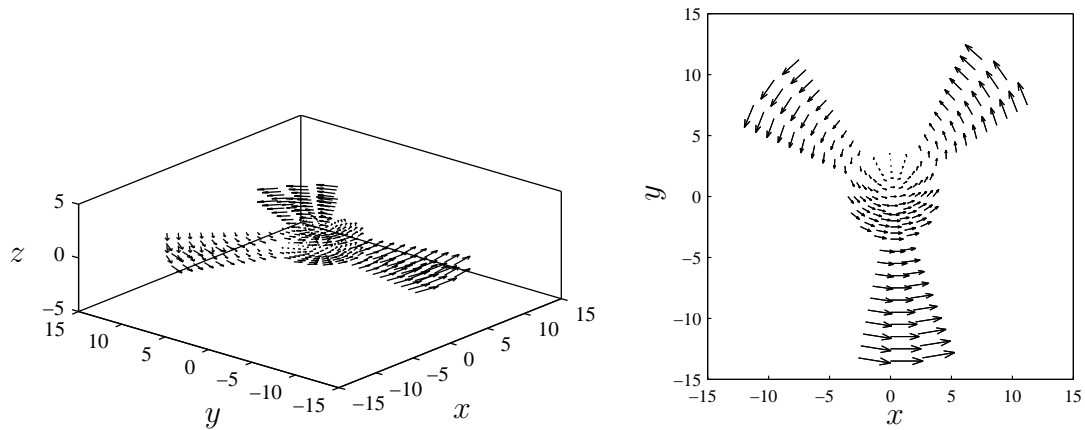


Figure 6.26. Initial velocity vectors of a spatial 3-blade propeller discretised by $n_{np} = 358$ nodes in $n_{el} = 140$ eight-node elements. The initial angular velocity vector and the translational velocity vector are given by $\boldsymbol{\omega}_0 = (0, 0, 0.7)$ and $\mathbf{v}_T = (2, 0, -0.1)$, respectively.

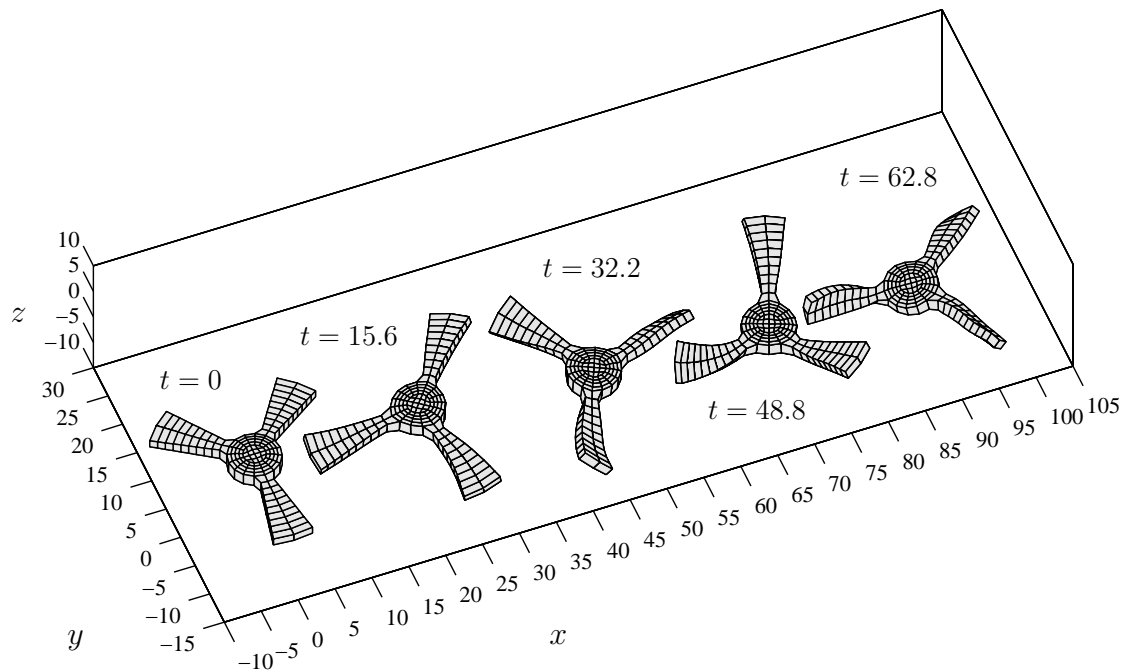


Figure 6.27. Motion of a spatial 3-blade propeller (Neo Hooke material with $\lambda = 3000$, $\mu = 750$, $\rho_0 = 8.93$) discretised by $n_{np} = 358$ nodes in $n_{el} = 140$ eight-node elements and computed with the eG(3) method. The time step size h_n has been set to 0.1 for $T \leq 5$ and to 0.2 for $T > 5$.

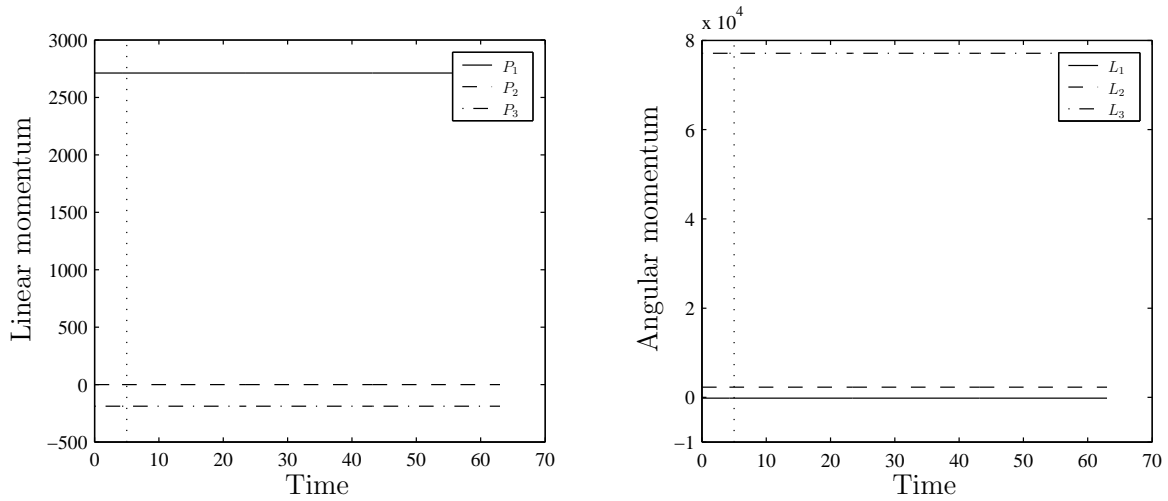


Figure 6.28. Momentum maps of a spatial 3-blade propeller (Neo Hooke material with $\lambda = 3000$, $\mu = 750$, $\rho_0 = 8.93$) discretised by $n_{np} = 358$ nodes in $n_{el} = 140$ eight-node elements and computed with the eG(3) method. The time step size h_n has been set to 0.1 for $T \leq 5$ and to 0.2 for $T > 5$.

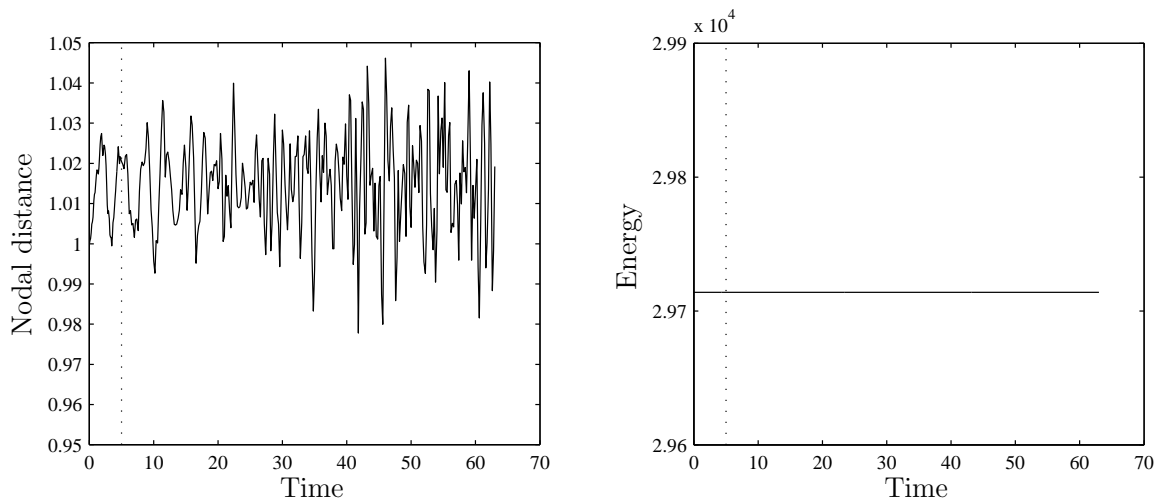


Figure 6.29. Nodal distance and total energy of a spatial 3-blade propeller (Neo Hooke material with $\lambda = 3000$, $\mu = 750$, $\rho_0 = 8.93$) discretised by $n_{np} = 358$ nodes in $n_{el} = 140$ eight-node elements and computed with the eG(3) method. The time step size h_n has been set to 0.1 for $T \leq 5$ and to 0.2 for $T > 5$.

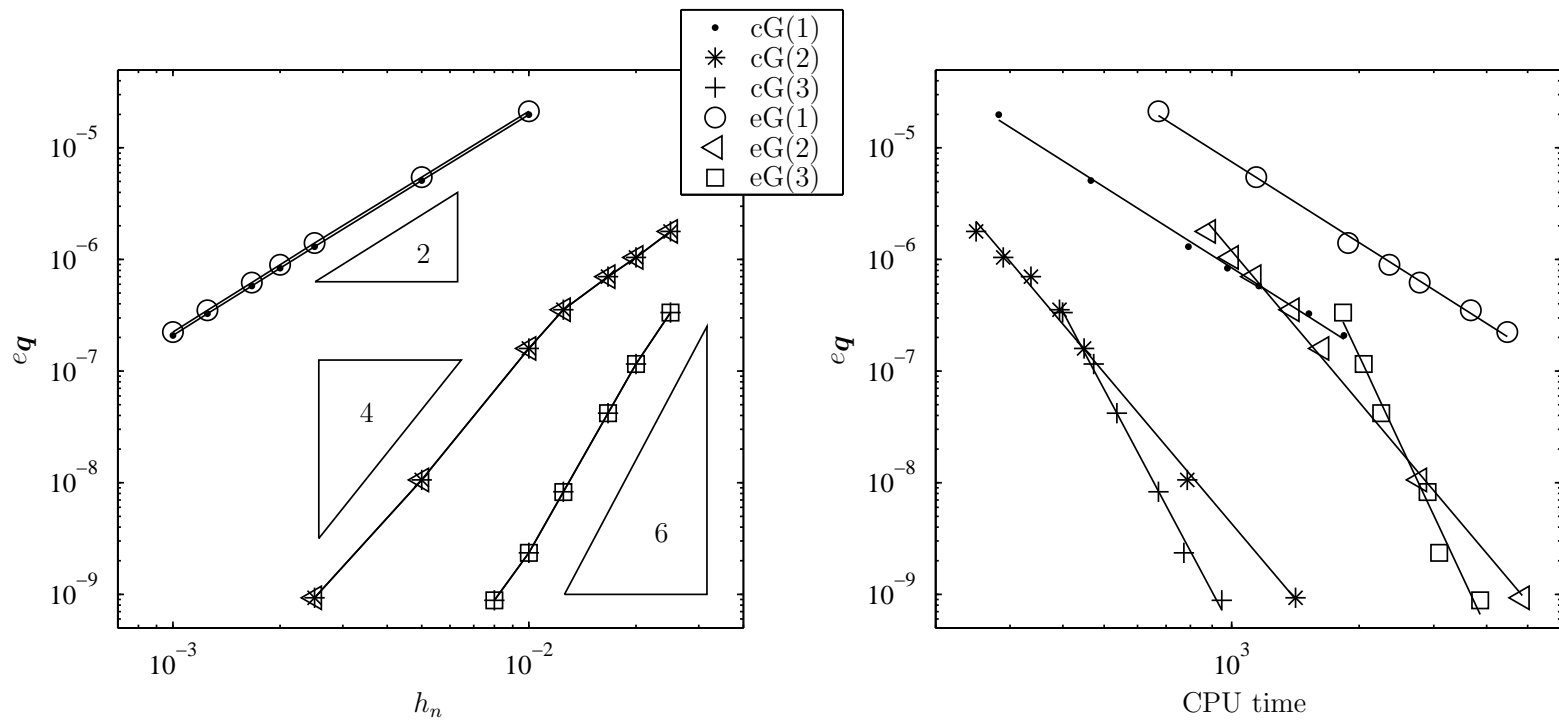


Figure 6.30. Relative global error in the position (on the left) and CPU time (on the right) of the cG method and the eG method for $k = 1, 2, 3$ determined at time $T = 1$ of the motion of the planar 1-blade propeller (Neo Hooke material with $\lambda = 3000$, $\mu = 750$, $\rho_0 = 8.93$) discretised by $n_{np} = 119$ nodes in $n_{el} = 100$ four-node elements.

Chapter 7

Conclusions

...This thesis is no way the last word on conserving schemes for Hamiltonian systems. There are many issues which were not addressed herein and are well worth investigation...the question arise as to whether or not higher order one-step conserving schemes can be constructed...

[51], Chapter 9: Summary & Conclusions.

This work includes a contribution to the computational treatment of nonlinear elastodynamics. In particular, we have been concerned with the unified development of higher order numerical time integration methods. We considered methods which inherit the physical properties of the underlying mechanical system. Such numerical time integration methods are called mechanical integrators. We restricted ourselves to the treatment of first integrals of the equations of motion. The total energy as well as the total linear and angular momentum play the role of first integrals in the context of nonlinear elastodynamics. Mechanical integrators possess excellent numerical stability in computing stiff problems and in long term calculations. Their achieved accuracy is thereby indistinguishable from standard integrators. Mechanical integrators are therefore especially attractive for time integration. Energy and momentum conserving integrators which are previously developed are however mostly second order accurate. Thus to bound the global error one has to take a very small time step size, which is expensive in long term calculations. In contrast, higher order integrators can decrease the computational costs because they

allow for larger time steps. A unified framework for designing higher order time integrators is the continuous Galerkin method in time. This method is particularly well suited for designing mechanical integrators because the resulting time stepping schemes inherit physical properties as symplecticity or first integrals from the equations of motion.

The goal of this work was to develop a unified framework for designing higher order accurate energy and momentum conserving time integration schemes for nonlinear elastodynamics. This led to the problem how the inherited invariants can be conserved if time integrals in the integration scheme are determined by a quadrature rule. We restricted our considerations to finite-dimensional mechanical systems emanating from a spatial discretisation of continuum bodies. The conservation properties of the designed mechanical integrators have been proved independent of the applied spatial discretisation by setting up a generalised problem. These results have been directly applied to many-particle dynamics and nonlinear semi-discrete elastodynamics because both problem classes are included in the generalised problem. The distinction between many-particle dynamics and semi-discrete elastodynamics can be traced back to different kinds of internal forces. In many-particle dynamics, the internal forces depend on a scalar-valued vector field, namely the particle distances. The internal forces in semi-discrete elastodynamics however emanate from a stress tensor field.

7.1 The main results

The proposed unified framework for designing higher order mechanical integrators is the continuous Galerkin method in time. In the resulting family of k -stage time stepping schemes, time integrals have to be evaluated. The conservation properties have been related to *collocation* at k quadrature points due to the application of numerical quadrature for evaluating these integrals. Since the momentum maps are at most quadratic invariants, we had to choose a k -point *Gaussian* rule with accuracy order $2k$. We called this family of time stepping schemes associated with k -point *Gaussian* quadrature the $cG(k)$ method. Energy conservation has been additionally achieved for arbitrary nonlinear conservative systems by devising a new *projection technique*. The projection had

to take into account the difference between the internal forces in particle dynamics and in semi-discrete elastodynamics. In particle dynamics, the newly developed projection approach only affects a scalar-valued function, however in semi-discrete elastodynamics each stress component is influenced by the projection technique. The distinction is caused by different strain measures. To this end the projection technique is *independent* of the form of the strain measure. We have further shown that the usual time approximations of the used strain measures are leading to approximation errors for large rigid body rotations. We have therefore designed an objective time approximation and applied it in the projection approach.

The aforementioned modifications of the $cG(k)$ method led to a *new method* called $eG(k)$ method which turned out to be well suited in long time calculations and also in computing stiff systems. The presented numerical examples allocated this conclusion. The relative global error of the solution and the computational cost of the $cG(k)$ as well as of the $eG(k)$ method are also investigated within the numerical examples. We have shown that the relative global error of the $eG(k)$ method is similar to that of the $cG(k)$ method for the same parameter k . We have also shown that a greater k renders less CPU time to obtain a constant relative global error for both methods. The advantage of the eG method is a better stability because it allows for larger time steps compared to the cG method in the same problem, however, the eG method is more costly due to the unsymmetric tangent operator.

7.2 Outlook

We have deduced the conservation conditions for the $cG(k)$ method from a generalised problem. We have, however, considered specific problems for designing the $eG(k)$ methods. One reason was the different strain measures which are used in the specific problems. On the other hand, the transformations of the energy conservation condition (3.19) into the projection equation have been specifically described for each problem. The mathematical description of the $eG(k)$ method could be completed by formalising this transformation according to [51]. The formalism described herein based on the fact that the

projection equation is exactly the gradient theorem with respect to a generalised *density* of the potential energy. In [51], the functional dependence on the distinct consistent strain measures is moreover generalised by taking the feature of each consistent strain measure into account. Since a consistent strain measure is invariant with respect to Euclidean transformations, each consistent strain measure can be viewed as an invariant of the group of translations ($G = \mathbb{R}^{n_{poi}}$) as well as of the group of rotations ($G = SO(n_{dim})$). These abstractions end in an G -equivariant derivative (or gradient) for the density of the potential energy. By using this formalism in conjunction with the projection method proposed in this work, one is able to describe a higher order mechanical integrator for the generalised problem. It even should be possible to formulate in this manner higher order mechanical integrators which preserve the Hamiltonian as well as each at most quadratic momentum map pertaining to an arbitrary Hamiltonian system with symmetry.

We restricted ourselves to the treatment of energy conserving systems. The used projection should be extended to dissipative systems associated with a given dissipation function, for instance systems with Rayleigh damping. The dissipative part can be then included in the Hamiltonian formulation in the form of generalised forces. Energy conservation is thus a special case in which the dissipation function identically vanishes. Numerical damping is introduced in a similar manner in [5, 6].

In respect to the numerical investigations, the error analysis could be enhanced. In this work, we only investigated the relative global error at the final time. The curves of the error versus the time step size pertaining to the eG(k) method were therefore nearly indistinguishable from those of the cG(k) method. In [19, 20], the mean square norm of the solution error is calculated for the cG(k) method as well as for mechanical integrators under consideration. This L_2 -error plotted versus the time step size also led to parallel lines. In computing stiff systems, however, the L_2 -error of the cG(k) method was a constant value greater as the L_2 -error of the mechanical integrator under consideration. This locking behaviour in time may be also observed in relation to the eG(k) method.

In this work, we have only applied an usual Newton-Raphson iterative process associated with the consistent tangent. A direct solver based on Gaussian elimination in conjunction with sparse matrices has been employed. Our comparison of numerical costs

within the context of specific examples has shown that the $eG(k)$ method is more expensive compared to the $cG(k)$ method because of the extensive internal force vector of the $eG(k)$ method. Further the material tangent matrices of the $eG(k)$ method are unsymmetric and much costly. To avoid the added costs of the $eG(k)$ method by these drawbacks, a symmetric nested iterative procedure is proposed in [6]. The additive structure of the internal force vector corresponding to the $eG(k)$ method becomes the key for this efficient numerical implementation. Since the first terms of the enhanced derivatives (gradients) lead to a symmetric material tangent, one considers the rest of the terms at a fixed deformation. Once this symmetric iterative process converges, the conserving terms are updated with the computed deformation and the iteration is repeated. These nested iterations are taken to convergence. According to [6], the symmetric nested iteration halve the CPU time for less degrees of freedom, where the computational cost is dominated by the matrix assembly, as well as for much degrees of freedom, where the solver dominates the total computational cost. This is despite the fact that a nested iteration can double the number of iterations (that is, solver calls) for large time steps. For relatively small time steps, the number of iterations is not affected.

Appendix A

Geometric mechanics

...The Hamiltonian methods are not particularly superior to Lagrangian techniques for the *direct* solution of mechanical problems. Rather, the usefulness of the Hamiltonian viewpoint lies in providing a framework for theoretical extensions in many areas of physics...

[50], Chapter 8: The Hamilton Equations of Motion.

Several mathematical models can be used to describe motions of mechanical systems. The simplest model for motions of real bodies is Newtonian mechanics which deal with a configuration of point masses in the three-dimensional Euclidean space on which acts the Euclidean transformations. We are interested in Newtonian potential systems which are specified by the masses of the points and by their potential energy. Group motions leaving the potential energy invariant correspond to conservation laws.

Lagrangian mechanics describe motions of a mechanical system by means of the configuration space. This space has the structure of a differentiable manifold on which acts a group of diffeomorphisms. We consider differentiable manifolds embedded in the Euclidean space. A Lagrangian mechanical system is given by a manifold (the configuration space) and a function on its tangent bundle (the Lagrangian). Each one-parameter group of diffeomorphisms acting on the configuration space and thereby preserving the Lagrangian is associated with a conservation law. A Newtonian potential system is a particular case of a Lagrangian system in which the configuration space is the Euclidean space and the Lagrangian is the difference between kinetic and potential energy.

Hamiltonian mechanics is geometry in the phase space. This space has the structure of a symplectic manifold which is an even-dimensional manifold with a symplectic structure. On the phase space acts the group of symplectic diffeomorphisms. A Hamiltonian mechanical system is given by a symplectic manifold (the phase space) and a function on it (the Hamiltonian). Every one-parameter group of symplectic diffeomorphisms on the phase space preserving the Hamiltonian is associated with a first integral of the equations of motion. Lagrangian mechanics is contained in Hamiltonian mechanics as a special case in which the phase space is the cotangent bundle of the configuration space and the Hamiltonian is the Legendre transform of the Lagrangian.

Geometric mechanics mean mechanics on a manifold, that is Lagrangian and Hamiltonian mechanics. In this appendix, we abstract notions of geometric mechanics used in the previous chapters. More details can be found in books on geometric mechanics, for example in [111, 8, 9, 1, 106, 104, 24].

A.1 Euclidean spaces

Let \mathbb{R} denote the field of real numbers. \mathbb{R}^n then denotes the set of all ordered n -tuples $\mathbf{x} = (x^1, \dots, x^n) \in \mathbb{R}^n$ of real numbers x^A , $A = 1, \dots, n$. We refer to \mathbb{R}^n as the *n-dimensional real linear vector space* with vectors $\mathbf{x} \in \mathbb{R}^n$. This space is also an inner product space (\mathbb{R}^n, \cdot) by the dot product $\mathbf{x} \cdot \mathbf{y}$ of two vectors $\mathbf{x}, \mathbf{y} \in \mathbb{R}^n$, which is given by

$$\mathbf{x} \cdot \mathbf{y} = \sum_{A=1}^n x^A y^A. \quad (\text{A.1})$$

\mathbb{R}^n is further a complete metric space $(\mathbb{R}^n, \|\cdot\|)$, the so-called *Euclidean space* \mathbb{R}^n , by the Euclidean norm which is defined by

$$\|\mathbf{x} - \mathbf{y}\| := \sum_{A=1}^n \sqrt{(x^A - y^A)(x^A - y^A)}. \quad (\text{A.2})$$

We refer to $\mathbb{R}^{n \times n}$ as the *set of all square matrices*

$$\mathbf{M} = \begin{bmatrix} M_{11} & \dots & M_{1n} \\ \vdots & & \vdots \\ M_{n1} & \dots & M_{nn} \end{bmatrix} \in \mathbb{R}^{n \times n} \quad (\text{A.3})$$

of real numbers M_{AB} , $A, B = 1, \dots, n$. The set $\mathbb{R}^{n \times n}$ is also a n^2 -dimensional real linear vector space with ‘vectors’ \mathbf{M} and an inner product space $(\mathbb{R}^{n \times n}, \cdot)$ by the double dot product of two matrices $\mathbf{M}, \mathbf{N} \in \mathbb{R}^{n \times n}$, given by

$$\mathbf{M} : \mathbf{N} = \sum_{A,B=1}^n M_{AB} N_{AB}. \quad (\text{A.4})$$

$\mathbb{R}^{n \times n}$ is a complete metric space $(\mathbb{R}^{n \times n}, \|\cdot\|)$, the so-called *Euclidean space* $\mathbb{R}^{n \times n}$, by the Euclidean norm for matrices, which is defined by

$$\|\mathbf{M} - \mathbf{N}\| := \sum_{A,B=1}^n \sqrt{(M_{AB} - N_{AB})(M_{AB} - N_{AB})}. \quad (\text{A.5})$$

Further details can be found in standard books on linear algebra or geometry such as [4, 24].

A.2 The tangent space

Let $I \subset \mathbb{R}$ be an open interval which contains the origin of the one-dimensional Euclidean space \mathbb{R} . A curve γ in $U \subset \mathbb{R}^n$ at \mathbf{x} is a smooth mapping $\gamma : I \rightarrow U$ with $\gamma(0) = \mathbf{x}$. A tangent vector \mathbf{v} to the curve γ at \mathbf{x} is a vector with coordinates

$$v^A = \left. \frac{d\gamma^A(t)}{dt} \right|_{t=0} \in \mathbb{R}. \quad (\text{A.6})$$

The tangent space $T_{\mathbf{x}}U$ to U at $\mathbf{x} \in U$ is a n -dimensional real vector space over the set of all tangent vectors \mathbf{v} to all curves in U at \mathbf{x} (see Figure A.1). The elements of $T_{\mathbf{x}}U$ are therefore contravariant 1-tensors. We can choose the standard basis $\{\mathbf{e}_1, \dots, \mathbf{e}_n\}$ as basis

for the tangent space $T_{\mathbf{x}}U$. With respect to the standard basis a tangent vector $\mathbf{v} \in T_{\mathbf{x}}U$ reads $\mathbf{v} = v^A \mathbf{e}_A$. We identify the tangent space $T_{\mathbf{x}}U$ with the vector space \mathbb{R}^n by viewing a tangent vector as a vector $\mathbf{v} = (v^1, \dots, v^n) \in \mathbb{R}^n$. The tangent bundle TU to U denotes the union of the tangent spaces at the various points of the subspace U , which means

$$TU = \bigcup_{\mathbf{x} \in U} T_{\mathbf{x}}U \quad (\text{A.7})$$

and can be identified with the vector space $U \times \mathbb{R}^n$. Considering a smooth mapping $\mathbf{f} : U \rightarrow V$ with $V \subset \mathbb{R}^m$, the linear mapping $\nabla_{\mathbf{x}}\mathbf{f}(\mathbf{x}) : T_{\mathbf{x}}U \rightarrow T_{\mathbf{f}(\mathbf{x})}V$ between two tangent spaces is defined by

$$\mathbf{v} = \left. \frac{d}{dt}(\mathbf{f} \circ \gamma)(t) \right|_{t=0} = \left[\nabla_{\mathbf{x}}\mathbf{f}(\gamma(t)) \cdot \frac{d\gamma(t)}{dt} \right]_{t=0} = \nabla_{\mathbf{x}}\mathbf{f}(\mathbf{x}) \cdot \mathbf{u}. \quad (\text{A.8})$$

The corresponding mapping between the tangent bundles TU and TV , the so-called *tangent map* $\nabla\mathbf{f} : TU \rightarrow TV$, is then given by $TU \ni (\mathbf{x}, \mathbf{u}) \mapsto (\mathbf{f}(\mathbf{x}), \nabla_{\mathbf{x}}\mathbf{f}(\mathbf{x}) \cdot \mathbf{u}) \in TV$. A detailed description can be found in [8, 9, 1, 106, 104].

A.3 The cotangent space

A cotangent vector \mathbf{p} of a tangent vector $\mathbf{v} \in T_{\mathbf{x}}U$ is a linear functional $\mathbf{p} : T_{\mathbf{x}}U \rightarrow \mathbb{R}$ which is defined by $\mathbf{p}(\mathbf{v}) = p_A v^A$ with $p_A \in \mathbb{R}$. We refer to the *cotangent space* $T_{\mathbf{x}}^*U$ to U at $\mathbf{x} \in U$ as the n -dimensional real vector space over the set of all cotangent vectors \mathbf{p} . Elements of $T_{\mathbf{x}}^*U$ are therefore covariant 1-tensors. A basis $\{\mathbf{e}^1, \dots, \mathbf{e}^n\}$ of the cotangent space $T_{\mathbf{x}}^*U$ can be derived from the basis $\{\mathbf{e}_1, \dots, \mathbf{e}_n\}$ of the tangent space $T_{\mathbf{x}}U$ as follows:

$$\mathbf{p}(\mathbf{v}) = \mathbf{p}(v^A \mathbf{e}_A) = p_B \mathbf{e}^B(v^A \mathbf{e}_A) = p_B v^A \mathbf{e}^B(\mathbf{e}_A) \doteq p_A v^A \quad (\text{A.9})$$

The basis $\{\mathbf{e}^1, \dots, \mathbf{e}^n\}$ is thus defined by $\mathbf{e}^B(\mathbf{e}_A) = \delta_A^B$. A cotangent vector $\mathbf{p} \in T_{\mathbf{x}}^*U$ with respect to the basis $\{\mathbf{e}^1, \dots, \mathbf{e}^n\}$ reads $\mathbf{p} = p_A \mathbf{e}^A$. We identify $T_{\mathbf{x}}^*U$ with the \mathbb{R}^n by viewing a cotangent vector \mathbf{p} as a vector $\mathbf{p} = (p_1, \dots, p_n) \in \mathbb{R}^n$ and by using the dot product as

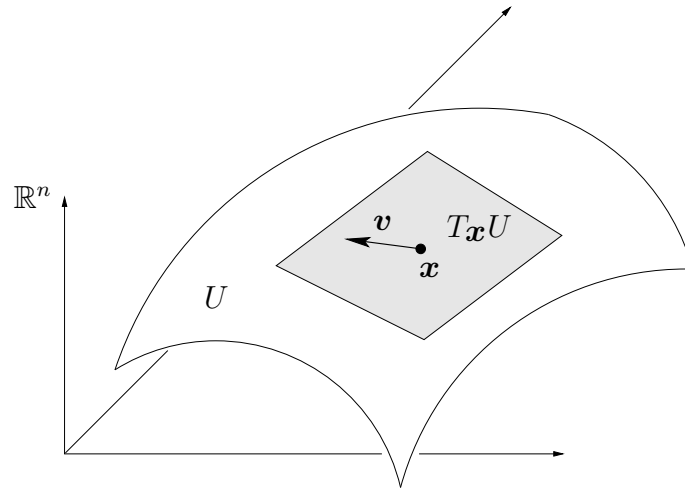


Figure A.1. The tangent space $T_{\mathbf{x}}U$ at the point $\mathbf{x} \in U \subset \mathbb{R}^n$ includes the tangent vector \mathbf{v} .

linear functional: $\mathbf{p}(\mathbf{v}) = \mathbf{p} \cdot \mathbf{v} = (p_1, \dots, p_n) \cdot (v^1, \dots, v^n) = p_A v^A$. The cotangent bundle T^*U denotes the union of the cotangent spaces to U at all of its points $\mathbf{x} \in U$:

$$T^*U = \bigcup_{\mathbf{x} \in U} T_{\mathbf{x}}^*U. \quad (\text{A.10})$$

We therefore identify T^*U with the vector space $U \times \mathbb{R}^n$. For example, the derivative $\nabla_{\mathbf{x}} f(\mathbf{x})$ at a point $\mathbf{x} \in U$ of a smooth function $f : U \rightarrow \mathbb{R}$ is an element of the cotangent space $T_{\mathbf{x}}^*U$. Consider a smooth mapping $\mathbf{f} : U \rightarrow V$ between Euclidean spaces. The linear mapping

$$\nabla_{\mathbf{x}} \mathbf{f}(\mathbf{x})^{-T} : T_{\mathbf{x}}^*U \rightarrow T_{\mathbf{f}(\mathbf{x})}^*V \quad (\text{A.11})$$

is a mapping between cotangent spaces. The cotangent map $\nabla \mathbf{f}^{-T} : T^*U \rightarrow T^*V$ is therefore given by $T^*U \ni (\mathbf{x}, \mathbf{a}) \mapsto (\mathbf{f}(\mathbf{x}), \nabla_{\mathbf{x}} \mathbf{f}(\mathbf{x})^{-T} \cdot \mathbf{a}) \in T^*V$. More details can be found in [8, 9, 1, 106, 104].

A.4 Bilinear forms on vector spaces

A bilinear form B on the tangent space $T_{\mathbf{x}}U$ is called a mapping $B : T_{\mathbf{x}}U \times T_{\mathbf{x}}U \rightarrow \mathbb{R}$ which is linear in both arguments and given by $B(\mathbf{v}, \mathbf{u}) = \mathbf{v} \cdot \mathbf{B}\mathbf{u} = v^A B_{AB} u^B$. The coordinates B_{AB} of the matrix \mathbf{B} associated with the bilinear form B are given by

$B_{AB} = B(\mathbf{e}_A, \mathbf{e}_B)$. One can relate a linear map $B^b : T_{\mathbf{x}}U \rightarrow T_{\mathbf{x}}^*U$ between the tangent space $T_{\mathbf{x}}U$ and the cotangent space $T_{\mathbf{x}}^*U$ to the bilinear form B , which is defined by $\mathbf{p}(\mathbf{u}) = B^b(\mathbf{v})(\mathbf{u}) := B(\mathbf{v}, \mathbf{u}) = v^A B_{AB} u^B$. We have therefore the relation $p_B = B_{AB} v^A$ in terms of coordinates, which is equivalent to the equation $\mathbf{p} = B^b(\mathbf{v}) = \mathbf{B}^T \mathbf{v}$. A bilinear form B^* on the cotangent space $T_{\mathbf{x}}^*U$ is a mapping $B^* : T_{\mathbf{x}}^*U \times T_{\mathbf{x}}^*U \rightarrow \mathbb{R}$ given by $B^*(\mathbf{p}, \mathbf{a}) = \mathbf{p} \cdot \mathbf{B}^* \mathbf{a} = p_A B^{AB} a_B$, which is also linear in both arguments. A linear mapping $B^\sharp : T_{\mathbf{x}}^*U \rightarrow T_{\mathbf{x}}U$ associated with the bilinear form B^* is similarly in terms of coordinates given by $v^B = B^{AB} p_A$. The coordinates B^{AB} of the matrix \mathbf{B}^* associated with the bilinear form B^* are given by the coordinates of the inverse of \mathbf{B}^T :

$$v^A = B_{AB}^{-1} p_B \doteq B^{BA} p_B \rightsquigarrow B_{AB}^{-1} = B^{BA}, \quad (\text{A.12})$$

where B_{AB}^{-1} denotes the coordinates of the inverse of \mathbf{B} . We thus obtain in vector notation the relations $\mathbf{v} = B^\sharp(\mathbf{p}) = [\mathbf{B}^*]^T \mathbf{p} = \mathbf{B}^{-1} \mathbf{p}$. Further details are presented in [2, 106].

A.5 Lie groups

A *group* consists of a set G together with a binary operation $\psi : G \times G \rightarrow G$ with certain required properties. The operation ψ associates to any ordered pair (g_1, g_2) of elements from G a unique element $\psi(g_1, g_2)$ of G . The required properties are thereby the following:

1. *Associativity*: We require $\psi(\psi(g_1, g_2), g_3) = \psi(g_1, \psi(g_2, g_3))$ for any $g_1, g_2, g_3 \in G$.
2. *Existence of an identity element* $e \in G$: There exists an element e in G such that we have $\psi(e, g) = \psi(g, e) = g$ for each g in G .
3. *Existence of an inverse*: There is an element $g^{-1} \in G$ such that $\psi(g, g^{-1}) = e$ and $\psi(g^{-1}, g) = e$ for each $g \in G$.

The group is called *Abelian* or commutative under the binary operation ψ if the elements commute which means $\psi(g_1, g_2) = \psi(g_2, g_1)$. It therefore follows that a group G has exactly one identity element e and each element g is associated with only one inverse g^{-1} .

The group G is a *Lie group* provided that the mapping $\psi : G \times G \rightarrow G$ and the mapping $G \rightarrow G$ defined by $g \mapsto g^{-1}$ are both smooth.

Let Q be an open set in some Euclidean space. We call a smooth map $\phi : G \times Q \rightarrow Q$ an *action* of a group G on a set Q if the following relations hold:

1. $\phi(e, \mathbf{q}) = \mathbf{q}$ for all $\mathbf{q} \in Q$.
2. $\phi(g_1, \phi(g_2, \mathbf{q})) = \phi(\psi(g_1, g_2), \mathbf{q})$ for all $\mathbf{q} \in Q$ and any $g_1, g_2 \in G$.

A *group homomorphism* of a group (G, ψ) into a group (H, Ψ) is a map $f : G \rightarrow H$ which preserves the group operation, which means we have $f(\psi(g_1, g_2)) = \Psi(f(g_1), f(g_2))$ for all $g_1, g_2 \in G$. If the homomorphism f is a bijection then its inverse is also a group homomorphism and f is called a *group isomorphism*. In this case, the groups G and H are called *isomorphic*. Further details can be found in books on linear algebra, geometry or geometric mechanics [92, 101, 24, 104, 1, 106].

A.6 An isoperimetrical problem

...Da nahmlich der Plan des Universums der vollkommene ist, kann kein Zweifel bestehen, dass alle Wirkungen in der Welt aus den Ursachen mit Hilfe der Methode der Maxima und Minima gleich gut bestimmt werden konnen...

Leonhard Euler (1707-1783).

Variational calculus is a fundamental tool in geometric mechanics. In particular, variations under a given constraint occur in dynamics. One of the simplest constraint involves an integral as in the functional itself. Such a variational problem is called *isoperimetrical problem* [47, 31, 91, 69, 46] and described as follows: Given a function $f(\alpha)$, $\alpha \in \mathcal{I}_\alpha = [0, 1]$ and a functional

$$\mathcal{F}(f) = \int_0^1 F(f(\alpha)) \, d\alpha, \quad (\text{A.13})$$

we search for a function $\bar{f}(\alpha)$ minimising \mathcal{F} and satisfying a constraint $\mathcal{G}(f) = 0$ as well as boundary conditions $f(0) = f_0$ and $f(1) = f_1$. We are interested in determining a

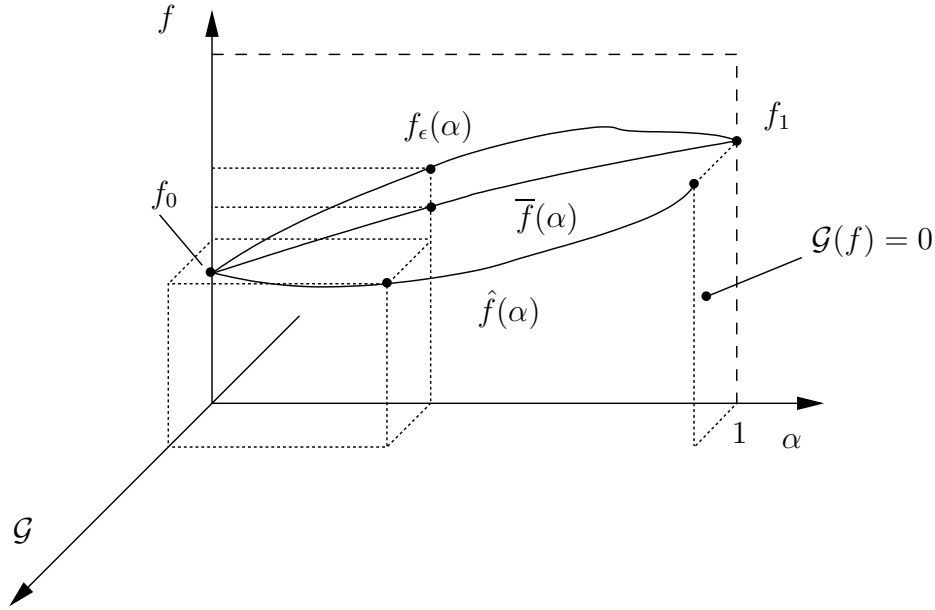


Figure A.2. Variational problem on $\mathcal{I}_\alpha = [0, 1]$ with constraint $\mathcal{G}(f) = 0$.

function $\bar{f}(\alpha)$ which minimise the distance

$$F(f) = \frac{1}{2} \langle f - \hat{f}, f - \hat{f} \rangle \quad (\text{A.14})$$

of the function $f(\alpha)$ to the function $\hat{f}(\alpha)$ in the whole Interval $\mathcal{I}_\alpha = [0, 1]$ under satisfaction of the constraint

$$\mathcal{G}(f) := c - \int_0^1 G(f(\alpha)) \, d\alpha = 0, \quad (\text{A.15})$$

with $c \in \mathbb{R}$ and

$$G(f) = \langle f, g \rangle, \quad (\text{A.16})$$

where $\langle \cdot, \cdot \rangle$ denotes the scalar product with a function on \mathcal{I}_α in the corresponding Euclidean space. Following the procedure of Euler, we assume that the function $\bar{f}(\alpha)$ has been found and construct a one-parameter family of functions with the parameter $\epsilon \in [-\epsilon_0, \epsilon_0]$, which is given by $f_\epsilon(\alpha) = \bar{f}(\alpha) + \epsilon \tilde{f}(\alpha) = \bar{f}(\alpha) + \delta \tilde{f}(\alpha)$. Herein is $\tilde{f}(\alpha)$ an arbitrary function only satisfying the conditions $\tilde{f}(0) = 0 = \tilde{f}(1)$ so that the boundary conditions are fulfilled (see Figure A.2).

The optimal solution is given for $\epsilon = 0$ which means a vanishing variation $\delta \tilde{f}(\alpha)$. A variational problem with constraint can be considered as an ordinary variational problem with respect to the augmented Lagrange functional $\mathcal{L} = \mathcal{F} + \lambda \mathcal{G}$, where $\lambda \in \mathbb{R}$ denotes a Lagrange multiplier. Employing the constraint and $f_\epsilon(\alpha)$, we obtain a function \mathcal{L}_ϵ which only depends on the parameter ϵ because the functions $\bar{f}(\alpha)$ and $\tilde{f}(\alpha)$ are assumed to be known. Since the optimal solution is included in the one-parameter family for $\epsilon = 0$, the function \mathcal{L}_ϵ take a minimum at $\epsilon = 0$, which implies

$$\left. \frac{d\mathcal{L}_\epsilon}{d\epsilon} \right|_{\epsilon=0} = 0. \quad (\text{A.17})$$

We obtain the following Euler-Lagrange equation because $\tilde{f}(\alpha)$ is assumed to be arbitrary:

$$\frac{\partial F(\bar{f})}{\partial f} - \lambda \frac{\partial G(\bar{f})}{\partial f} = 0. \quad (\text{A.18})$$

This Euler-Lagrange equation is the necessary condition for the optimal solution which is given by $\bar{f}(\alpha) = \hat{f}(\alpha) + \lambda g(\alpha)$. The Lagrange multiplier λ is determined by the constraint (A.15) and reads

$$\lambda = \frac{\mathcal{G}(\hat{f})}{\mathcal{N}} \quad \text{with} \quad \mathcal{N} = \int_0^1 \langle g(\alpha), g(\alpha) \rangle d\alpha. \quad (\text{A.19})$$

We finally employ equation (A.19) and obtain the optimal solution $\bar{f}(\alpha)$ for the given problem:

$$\boxed{\bar{f}(\alpha) = \hat{f}(\alpha) + \frac{\mathcal{G}(\hat{f})}{\mathcal{N}} g(\alpha)} \quad (\text{A.20})$$

Appendix B

The direct matrix product

The direct matrix product or the Kronecker product of matrices is a brief notation for writing a special block matrix. In this appendix, we show the transposition, the multiplication and the inversion of such a matrix, which occurs in this work at different places. For more details see [97, 132, 40].

B.1 The definition

Given two matrices $\mathbf{A} \in \mathbb{R}^{m \times n}$ and $\mathbf{B} \in \mathbb{R}^{p \times q}$ of the form

$$\mathbf{A} = \begin{bmatrix} a_{11} & \dots & a_{1n} \\ \vdots & & \vdots \\ a_{m1} & \dots & a_{mn} \end{bmatrix} \quad \mathbf{B} = \begin{bmatrix} b_{11} & \dots & b_{1q} \\ \vdots & & \vdots \\ b_{p1} & \dots & b_{pq} \end{bmatrix} \quad (\text{B.1})$$

the direct matrix product of \mathbf{A} and \mathbf{B} is defined to be the real $mp \times nq$ dimensional matrix

$$\mathbf{A} \otimes \mathbf{B} = \begin{bmatrix} a_{11}\mathbf{B} & \dots & a_{1n}\mathbf{B} \\ \vdots & & \vdots \\ a_{m1}\mathbf{B} & \dots & a_{mn}\mathbf{B} \end{bmatrix} \quad (\text{B.2})$$

B.2 The transpose

Given the direct product $\mathbb{C} = \mathbf{A} \otimes \mathbf{B} \in \mathbb{R}^{mp \times nq}$ of the matrices $\mathbf{A} \in \mathbb{R}^{m \times n}$ and $\mathbf{B} \in \mathbb{R}^{p \times q}$ of the form (B.1), the transpose $\mathbb{C}^T \in \mathbb{R}^{nq \times mp}$ reads

$$\mathbb{C}^T = \begin{bmatrix} a_{11}\mathbf{B} & \dots & a_{1n}\mathbf{B} \\ \vdots & & \vdots \\ a_{m1}\mathbf{B} & \dots & a_{mn}\mathbf{B} \end{bmatrix}^T = \begin{bmatrix} a_{11}\mathbf{B}^T & \dots & a_{m1}\mathbf{B}^T \\ \vdots & & \vdots \\ a_{1n}\mathbf{B}^T & \dots & a_{mn}\mathbf{B}^T \end{bmatrix} \quad (\text{B.3})$$

Hence the transpose of a direct matrix product is given by

$$\boxed{(\mathbf{A} \otimes \mathbf{B})^T = \mathbf{A}^T \otimes \mathbf{B}^T} \quad (\text{B.4})$$

B.3 The product

Let $\mathbb{C} = \mathbf{A} \otimes \mathbf{B} \in \mathbb{R}^{mp \times nq}$ be the direct product of the matrices $\mathbf{A} \in \mathbb{R}^{m \times n}$ and $\mathbf{B} \in \mathbb{R}^{p \times q}$ of the form (B.1). Let $\mathbb{C}' = \mathbf{A}' \otimes \mathbf{B}' \in \mathbb{R}^{nq \times rs}$ be a further direct product of the matrices $\mathbf{A}' \in \mathbb{R}^{n \times r}$ and $\mathbf{B}' \in \mathbb{R}^{q \times s}$ given by

$$\mathbf{A}' = \begin{bmatrix} a'_{11} & \dots & a'_{1r} \\ \vdots & & \vdots \\ a'_{n1} & \dots & a'_{nr} \end{bmatrix} \quad \mathbf{B}' = \begin{bmatrix} b'_{11} & \dots & b'_{1s} \\ \vdots & & \vdots \\ b'_{q1} & \dots & b'_{qs} \end{bmatrix} \quad (\text{B.5})$$

Multiplying the matrices \mathbb{C} and \mathbb{C}' , the matrix product $\mathbb{C}\mathbb{C}' \in \mathbb{R}^{mp \times rs}$ is given by

$$\mathbb{C}\mathbb{C}' = \begin{bmatrix} a_{11}\mathbf{B} & \dots & a_{1n}\mathbf{B} \\ \vdots & & \vdots \\ a_{m1}\mathbf{B} & \dots & a_{mn}\mathbf{B} \end{bmatrix} \begin{bmatrix} a'_{11}\mathbf{B}' & \dots & a'_{1r}\mathbf{B}' \\ \vdots & & \vdots \\ a'_{n1}\mathbf{B}' & \dots & a'_{nr}\mathbf{B}' \end{bmatrix} \quad (\text{B.6})$$

The matrix product of two direct matrix products is therefore given by the direct matrix product of the product matrices:

$$\boxed{(\mathbf{A} \otimes \mathbf{B})(\mathbf{A}' \otimes \mathbf{B}') = \mathbf{A}\mathbf{A}' \otimes \mathbf{B}\mathbf{B}'} \quad (\text{B.7})$$

B.4 The inverse

Let $\mathbb{C} = \mathbf{A} \otimes \mathbf{B} \in \mathbb{R}^{mn \times mn}$ be a quadratic matrix, where $\mathbf{A} \in \mathbb{R}^{m \times m}$ and $\mathbf{B} \in \mathbb{R}^{n \times n}$ are also quadratic matrices of the form

$$\mathbf{A} = \begin{bmatrix} a_{11} & \dots & a_{1m} \\ \vdots & & \vdots \\ a_{m1} & \dots & a_{mm} \end{bmatrix} \quad \mathbf{B} = \begin{bmatrix} b_{11} & \dots & b_{1n} \\ \vdots & & \vdots \\ b_{n1} & \dots & b_{nn} \end{bmatrix} \quad (\text{B.8})$$

The inverse of the matrix \mathbb{C} has the form $\mathbb{C}^{-1} = \mathbf{A}' \otimes \mathbf{B}^{-1} \in \mathbb{R}^{mn \times mn}$, where $\mathbf{A}' \in \mathbb{R}^{m \times m}$ is a quadratic matrix

$$\mathbf{A}' = \begin{bmatrix} a'_{11} & \dots & a'_{1m} \\ \vdots & & \vdots \\ a'_{m1} & \dots & a'_{mm} \end{bmatrix} \quad (\text{B.9})$$

The matrix \mathbf{A}' are then determined by the following matrix equation:

$$\mathbb{C} \mathbb{C}^{-1} = [\mathbf{A} \mathbf{A}'] \otimes [\mathbf{B} \mathbf{B}^{-1}] = \mathbf{A} \mathbf{A}' \otimes \mathbf{I}_n \doteq \mathbf{I}_{mn} = \mathbf{I}_m \otimes \mathbf{I}_n \quad (\text{B.10})$$

This matrix equation is obviously equivalent to the matrix equation $\mathbf{A} \mathbf{A}' = \mathbf{I}_m$ which means \mathbf{A}' is the inverse of \mathbf{A} . The inverse of a direct matrix product $\mathbf{A} \otimes \mathbf{B}$ is consequently the direct matrix product of the inverse matrices:

$$\boxed{(\mathbf{A} \otimes \mathbf{B})^{-1} = \mathbf{A}^{-1} \otimes \mathbf{B}^{-1}} \quad (\text{B.11})$$

Appendix C

Notes on the cG(k) method

In this appendix, we give more information about the implementation and error analysis of the cG(k) method. More precisely, we give the matrices required for the implementation and details for proving the approximation error bounds at the time nodes and between the time nodes of the master element.

C.1 Implementation matrices

This appendix include the matrices required for the implementation of the cG(k) method for $k = 1, \dots, 4$.

C.1.1 Linear time finite elements ($k = 1$)

$$\begin{aligned} \mathbf{A}_m^R &= [+2] & \mathbf{A}_q^R &= [-2] & \mathbf{A}_p^R &= [-2] \\ \mathbf{A}_m^p &= [+2] & \mathbf{A}_q^p &= [-2] & \mathbf{A}_p^p &= [+1] \\ & & \mathbf{A}_q^q &= [-1] & \mathbf{A}_p^q &= [-1] \end{aligned} \tag{C.1}$$

C.1.2 Quadratic time finite elements ($k = 2$)

$$\begin{aligned}
 \mathbf{A}_m^R &= \begin{bmatrix} 0 & 1 \\ -8 & 3 \end{bmatrix} & \mathbf{A}_q^R &= \begin{bmatrix} -1 \\ 5 \end{bmatrix} & \mathbf{A}_p^R &= \begin{bmatrix} -1 \\ 1 \end{bmatrix} \\
 \mathbf{A}_m^p &= \begin{bmatrix} 2 & \frac{1}{2} \\ -8 & 4 \end{bmatrix} & \mathbf{A}_q^p &= \begin{bmatrix} -\frac{5}{2} \\ 4 \end{bmatrix} & \mathbf{A}_p^p &= \begin{bmatrix} \frac{1}{2} \\ -1 \end{bmatrix} \\
 & & \mathbf{A}_q^q &= \begin{bmatrix} -1 \\ -1 \end{bmatrix} & \mathbf{A}_p^q &= \begin{bmatrix} -\frac{1}{2} \\ -1 \end{bmatrix}
 \end{aligned} \tag{C.2}$$

C.1.3 Cubic time finite elements ($k = 3$)

$$\begin{aligned}
 \mathbf{A}_m^R &= \begin{bmatrix} \frac{3}{2} & \frac{3}{2} & -\frac{1}{2} \\ -3 & -3 & 3 \\ 15 & -12 & 4 \end{bmatrix} & \mathbf{A}_q^R &= \begin{bmatrix} -\frac{5}{2} \\ 3 \\ -7 \end{bmatrix} & \mathbf{A}_p^R &= \begin{bmatrix} -1 \\ 0 \\ -1 \end{bmatrix} \\
 \mathbf{A}_m^p &= \begin{bmatrix} \frac{13}{6} & \frac{7}{6} & -\frac{5}{54} \\ -\frac{20}{3} & \frac{10}{3} & \frac{16}{27} \\ \frac{27}{2} & -\frac{27}{2} & \frac{13}{2} \end{bmatrix} & \mathbf{A}_q^p &= \begin{bmatrix} -\frac{175}{54} \\ \frac{74}{27} \\ -\frac{13}{2} \end{bmatrix} & \mathbf{A}_p^p &= \begin{bmatrix} \frac{11}{27} \\ -\frac{11}{27} \\ 1 \end{bmatrix} \\
 & & \mathbf{A}_q^q &= \begin{bmatrix} -1 \\ -1 \\ -1 \end{bmatrix} & \mathbf{A}_p^q &= \begin{bmatrix} -\frac{1}{3} \\ -\frac{2}{3} \\ -1 \end{bmatrix}
 \end{aligned} \tag{C.3}$$

C.1.4 Quartic time finite elements ($k = 4$)

$$\begin{aligned}
\mathbf{A}_m^R &= \begin{bmatrix} 4 & \frac{3}{5} & -\frac{4}{5} & \frac{3}{10} \\ -\frac{44}{5} & -\frac{3}{5} & \frac{28}{5} & -\frac{17}{10} \\ \frac{28}{5} & -\frac{3}{5} & -\frac{44}{5} & \frac{11}{2} \\ -\frac{332}{15} & \frac{123}{15} & -\frac{52}{3} & \frac{157}{30} \end{bmatrix} & \mathbf{A}_q^R &= \begin{bmatrix} -\frac{41}{10} \\ \frac{11}{2} \\ -\frac{17}{10} \\ \frac{289}{30} \end{bmatrix} & \mathbf{A}_p^R &= \begin{bmatrix} -1 \\ 0 \\ 0 \\ 1 \end{bmatrix} \\
\mathbf{A}_m^p &= \begin{bmatrix} \frac{31}{24} & \frac{81}{32} & -\frac{11}{24} & \frac{17}{384} \\ -\frac{26}{3} & \frac{9}{2} & \frac{2}{3} & \frac{1}{24} \\ \frac{53}{8} & -\frac{303}{32} & \frac{39}{8} & \frac{91}{128} \\ -\frac{64}{3} & 24 & -\frac{64}{3} & \frac{28}{3} \end{bmatrix} & \mathbf{A}_q^p &= \begin{bmatrix} -\frac{1309}{384} \\ \frac{83}{24} \\ -\frac{351}{128} \\ \frac{28}{3} \end{bmatrix} & \mathbf{A}_p^p &= \begin{bmatrix} \frac{37}{128} \\ -\frac{3}{8} \\ \frac{37}{128} \\ -1 \end{bmatrix} \\
& & \mathbf{A}_q^q &= \begin{bmatrix} -1 \\ -1 \\ -1 \\ -1 \end{bmatrix} & \mathbf{A}_p^q &= \begin{bmatrix} -\frac{1}{4} \\ -\frac{1}{2} \\ -\frac{3}{4} \\ -1 \end{bmatrix}
\end{aligned} \tag{C.4}$$

C.2 Error estimate for a nodal time interpolation

This section gives a simple proof of the fact that the nodal time interpolation $\mathbf{F}(\alpha)$ of a function $\mathbf{F}(\alpha)$ on the master element $\mathcal{I}_\alpha = [0, 1]$, which is given by

$$\mathbf{F}(\alpha) = \sum_{I=1}^{k+1} M_I(\alpha) \mathbf{F}(\alpha_I), \tag{C.5}$$

with $k + 1$ equidistant nodes $\alpha_I = I/(k + 1)$, $I = 1, \dots, k + 1$ and $k + 1$ Lagrangian shape functions of the form (3.7) is of the accuracy $\mathcal{O}(h_n^k)$ (compare [44, 82]). The approximation is of the accuracy $\mathcal{O}(h_n^k)$ if the residual error $\mathbf{R}_F = -\mathbf{F} + \mathbf{F}$ is of the accuracy order $\mathcal{O}(h_n^{k+1})$. Taking Taylor's theorem into account, the nodal values $\mathbf{F}(\alpha_I)$ can be written

as

$$\mathbf{F}(\alpha_I) = \sum_{i=0}^k \frac{h_n^i}{i!} \frac{d^i \mathbf{F}(\alpha)}{dt^i} [\alpha_I - \alpha]^i + \mathcal{O}(h_n^{k+1}), \quad (\text{C.6})$$

where the time step size h_n is related to $h_n = dt/d\alpha$ by definition. We subtract the exact function $\mathbf{F}(\alpha)$ from the approximated function $\mathbf{F}(\alpha)$ and obtain the residual error

$$\mathbf{R}_F = \mathbf{F}(\alpha) [c_0 - 1] + \sum_{i=1}^k \frac{h_n^i}{i!} \frac{d^i \mathbf{F}(\alpha)}{dt^i} c_i + \mathcal{O}(h_n^{k+1}), \quad (\text{C.7})$$

where we have introduced the coefficients

$$c_i = \sum_{I=1}^{k+1} M_I(\alpha) [\alpha_I - \alpha]^i, \quad i = 0, \dots, k. \quad (\text{C.8})$$

If the approximation is of order $\mathcal{O}(h_n^k)$ then the terms of the order $\mathcal{O}(h_n^I)$, $I = 1, \dots, k$, have to vanish, which implies the matrix equation $\mathbf{A}(\alpha) \mathbf{w}(\alpha) = \mathbf{b}$ with

$$\mathbf{A} = \begin{bmatrix} (\alpha_1 - \alpha)^0 & \dots & (\alpha_{k+1} - \alpha)^0 \\ (\alpha_1 - \alpha)^1 & \dots & (\alpha_{k+1} - \alpha)^1 \\ \vdots & & \vdots \\ (\alpha_1 - \alpha)^k & \dots & (\alpha_{k+1} - \alpha)^k \end{bmatrix} \quad \mathbf{w} = \begin{bmatrix} M_1(\alpha) \\ M_2(\alpha) \\ \vdots \\ M_{k+1}(\alpha) \end{bmatrix} \quad \mathbf{b} = \begin{bmatrix} 1 \\ 0 \\ \vdots \\ 0 \end{bmatrix} \quad (\text{C.9})$$

Multiplying this matrix equation from the left by the matrix $\mathbf{B}(\alpha)$ of the form

$$\mathbf{B} = \begin{bmatrix} \binom{0}{0} \alpha^0 & \dots & \binom{0}{k} \alpha^{-k} \\ \vdots & & \vdots \\ \binom{k}{0} \alpha^k & \dots & \binom{k}{k} \alpha^0 \end{bmatrix} \quad (\text{C.10})$$

we obtain an equivalent linear system of equations of the form $\mathbf{v}(\alpha) = \mathbf{V} \mathbf{w}(\alpha)$, with the matrix $\mathbf{V} = \mathbf{B} \mathbf{A}$ and the vector $\mathbf{v}(\alpha) = \mathbf{B}(\alpha) \mathbf{b} = [1 \ \alpha \ \dots \ \alpha^k]^T$. The components V_{IJ} , $I, J = 1, \dots, k+1$, of the matrix \mathbf{V} then read

$$V_{IJ} = \sum_{i=1}^{k+1} \binom{I-1}{i-1} \alpha^{(I-1)-(i-1)} [\alpha_J - \alpha]^{i-1} = [\alpha + \alpha_J - \alpha]^{I-1} = \alpha_J^{I-1}. \quad (\text{C.11})$$

Hence this matrix is the Vandermonde matrix $\mathbf{V}(\alpha_1, \dots, \alpha_{k+1}) = \begin{bmatrix} \mathbf{v}(\alpha_1) & \dots & \mathbf{v}(\alpha_{k+1}) \end{bmatrix}$. Taking Section 3.2.2 into account, the matrix \mathbf{w} consequently includes the Lagrangian shape functions (3.7). The linear algebraic system is therefore fulfilled which leads to a residual error $\mathbf{R}_F = \mathcal{O}(h_n^{k+1})$.

C.3 Accuracy of the cG(k) method at the time nodes

In this section, we prove that the cG(k) method is of the order $\mathcal{O}(h_n^{2k})$ accurate at the time nodes in the master element (compare [82]). To this end we write the cG(k) method applied to a general Hamiltonian system in the following form:

$$\sum_{J=1}^k \int_0^1 \tilde{M}_I M'_J \, d\alpha \, \mathbf{z}_J - h_n \int_0^1 \tilde{M}_I(\alpha) \mathbb{J} \nabla H(\mathbf{z}(\alpha)) \, d\alpha = \mathbf{0}, \quad I = 1, \dots, k. \quad (\text{C.12})$$

The unknowns are represented by the vector $\mathbf{x}_z = (\mathbf{z}_2, \dots, \mathbf{z}_{k+1})$. By using the calculation rules in Appendix B, the equations can be expressed in matrix notation as

$$\left[(\mathbf{A}')^{-1} \mathbf{b}' \right] \otimes \mathbf{z}_1 + \mathbf{x}_z - h_n \int_0^1 \left[(\mathbf{A}')^{-1} \tilde{\mathbf{w}} \right] \otimes \mathbb{J} \nabla H(\mathbf{z}(\alpha)) \, d\alpha. \quad (\text{C.13})$$

As an intermediate step, we prove the relation $(\mathbf{A}')^{-1} \mathbf{b}' = -\mathbf{e}_k$, where $\mathbf{e}_k = (1 \dots 1) \in \mathbb{R}^k$ is a column vector. This equation is equivalent to the equation $\mathbf{b}' = -\mathbf{A}' \mathbf{e}_k$. Employing the definitions (3.28), the right hand side results in

$$-\mathbf{A}' \mathbf{e}_k = - \begin{bmatrix} \int_0^1 \tilde{M}_1 (M'_2 + \dots + M'_{k+1}) \, d\alpha \\ \vdots \\ \int_0^1 \tilde{M}_k (M'_2 + \dots + M'_{k+1}) \, d\alpha \end{bmatrix} \quad (\text{C.14})$$

Differentiating the completeness condition for the polynomials M_I , $I = 1, \dots, k+1$, with respect to α , one obtains $-M'_1 = M'_2 + \dots + M'_{k+1}$. Taking this equation into consideration, the proof is complete.

We apply the proved relation in equation (C.13) and obtain

$$\mathbf{x}_z = \mathbf{e}_k \otimes \mathbf{z}_1 + h_n \int_0^1 \left[(\mathbf{A}')^{-1} \tilde{\mathbf{w}} \right] \otimes \mathbb{J} \nabla H(\mathbf{z}(\alpha)) \, d\alpha. \quad (\text{C.15})$$

In the computational setting, we use Gaussian quadrature for calculating the integrals in equation (C.15). The cG(k) method therefore determines a vector \mathbf{x}_z including approximated values to the actual nodal values $\mathbf{z}_I = \mathbf{z}(\alpha_I)$, $I = 2, \dots, k+1$:

$$\mathbf{x}_z = \mathbf{e}_k \otimes \mathbf{z}_1 + h_n \sum_{l=1}^k \left[(\mathbf{A}')^{-1} \tilde{\mathbf{w}} \right] \otimes \mathbb{J} \nabla H(\mathbf{z}(\xi_l)) w_l. \quad (\text{C.16})$$

The residual error $\mathbf{R}_x = \mathbf{x} - \mathbf{x}_z$ of the approximated nodal values is due to the accuracy of the Gaussian quadrature of the order $\mathcal{O}(h_n^{2k+1})$. The nodal values \mathbf{x}_z are consequently of order $\mathcal{O}(h_n^{2k})$ accurate.

Appendix D

The assembly operator

In finite element methods, some matrices are usually calculated on the element level. The obtained element matrices are then combined into a global matrix by an operation called *matrix assembly*. This operation is often indicated by the so-called *assembly operator* \mathbf{A} (see [76]). The assembly of element vectors \mathbf{b}_e or of element square matrices \mathbf{A}_e , $e = 1, \dots, n_{el}$, to a global vector \mathbf{b} or to a global square matrix \mathbf{A} is defined by

$$\mathbf{b} = \mathbf{A} \mathbf{b}_e = \sum_{e=1}^{n_{el}} \mathbf{L}_e^T \mathbf{b}_e, \quad \text{and} \quad \mathbf{A} = \mathbf{A} \mathbf{A}_e = \sum_{e=1}^{n_{el}} \mathbf{L}_e^T \mathbf{A}_e \mathbf{L}_e, \quad (\text{D.1})$$

respectively, where the matrices \mathbf{L}_e are called the *connectivity matrices* which are Boolean matrices only consisting of the integers 0 and 1 (see [17]). Hence if the element square matrices \mathbf{A}_e are symmetric then the global square matrix \mathbf{A} is also symmetric:

$$\mathbf{A}^T = \sum_{e=1}^{n_{el}} [\mathbf{L}_e^T \mathbf{A}_e \mathbf{L}_e]^T = \sum_{e=1}^{n_{el}} [\mathbf{A}_e \mathbf{L}_e]^T \mathbf{L}_e = \sum_{e=1}^{n_{el}} \mathbf{L}_e^T \mathbf{A}_e^T \mathbf{L}_e = \sum_{e=1}^{n_{el}} \mathbf{L}_e^T \mathbf{A}_e \mathbf{L}_e = \mathbf{A}. \quad (\text{D.2})$$

Bibliography

- [1] Abraham R. and Marsden J.E. *Foundations of Mechanics*. Addison-Wesley, New York, 2nd edition, 1978.
- [2] Abraham R., Marsden J.E., and Ratiu T.S. *Manifolds, Tensor Analysis and Applications*. Springer, 2nd edition, 1988.
- [3] Allen M.P. and Tildesley D.J. *The molecular theory of gases and liquids*. Wiley, New York, 1967.
- [4] Apostol T.M. *Calculus*, volume 1. Xerox College Publishing, Lexington, Massachusetts, 2nd edition, 1967.
- [5] Armero F. and Romero I. On the Formulation of High-frequency Dissipativ Time-Stepping Algorithmns for Nonlinear Dynamics. Part I: Low-order Methods for Two Model Problems and Nonlinear Elastodynamics.
- [6] Armero F. and Romero I. On the Formulation of High-frequency Dissipativ Time-Stepping Algorithmns for Nonlinear Dynamics. Part II: Second Order Methods.
- [7] Arnold V.I. *Geometrical Methods in the Theory of Ordinary Differential Equations*. Springer, 2nd edition, 1988.
- [8] Arnold V.I. *Mathematical Methods of Classical Mechanics*. Springer, 2nd edition, 1989.
- [9] Arnold V.I. *Dynamical Systems*, volume 3. Springer, 2nd edition, 1991.
- [10] Ascher U.M. and Bader G. Stability of Collocation at Gaussian Points. *SIAM J. Numer. Anal.*, 23(2):412–422, 1986.
- [11] Ascher U.M. and Reich S. On Some Difficulties in Integrating Highly Oscillatory Hamiltonian Systems. *Lecture Notes in Computational Science and Engineering*, (4):281–296, 1998.
- [12] Ascher U.M. and Reich S. The Midpoint Scheme and Variants for Hamiltonian Systems: Advantages and Pitfalls. *SIAM J. Sci. Comput.*, 21(3):1045–1065, 1999.
- [13] Atkinson K.E. *An Introduction to Numerical Analysis*. Wiley, New York, 1978.

-
- [14] Bathe K.J. *Finite Element Procedures in Engineering Analysis*. Prentice-Hall, New Jersey, 1982.
- [15] Bauchau O.A. and Theron N.J. Energy decaying scheme for non-linear beam models. *Comput. Methods Appl. Mech. Engrg.*, 134:37–56, 1996.
- [16] Bauchau O.A. and Joo T. Computational schemes for non-linear elasto-dynamics. *International Journal for Numerical Methods in Engineering*, 45:693–719, 1999.
- [17] Belytschko T., Wing K.L., and Brian M. *Nonlinear Finite Elements for Continua and Structures*. Wiley, Chichester, 2000.
- [18] Betsch P. *Computational Methods for Flexible Multibody Dynamics*. UKL/LTM T 02-02, University of Kaiserslautern, 2002.
- [19] Betsch P. and Steinmann P. Conservation Properties of a Time FE Method. Part I: Time-Stepping Schemes for N-Body Problems. *Int. J. Numer. Meth. Engrg.*, 49:599–638, 2000.
- [20] Betsch P. and Steinmann P. Conservation Properties of a Time FE Method. Part II: Time-Stepping Schemes for Nonlinear Elastodynamics. *Int. J. Numer. Meth. Engrg.*, 50:1931–1955, 2001.
- [21] Betsch P. and Steinmann P. Conservation Properties of a Time FE Method. Part III: Mechanical Systems with Holonomic Constraints. *Int. J. Numer. Methods Engrg.*, 53:2271–2304, 2002.
- [22] Betsch P. and Steinmann P. Inherently Energy Conserving Time Finite Elements for Classical Mechanics. *Journal of Computational Physics*, 160:88–116, 2000.
- [23] Bonet J. and Wood R.D. *Nonlinear continuum mechanics for finite element analysis*. Cambridge University Press, Cambridge, 1997.
- [24] Boothby W.M. *An Introduction to Differentiable Manifolds and Riemannian Geometry*. Academic Press, New York, 1975.
- [25] Burrage K. High Order Algebraically Stable Runge-Kutta Methods. *BIT*, (18):373–383, 1978.
- [26] Butcher J.C. Implicit Runge-Kutta Processes. *Math. Comp.*, (18):50–64, 1964.
- [27] Chung J. and Hulbert G.M. A time integration algorithm for structural dynamics with improved numerical dissipation: The generalized- α method. *Journal of Applied Mechanics*, 60:371–375, 1993.
- [28] Collatz L. *Numerical Treatment of Differential Equations*. Springer, Berlin, 1960.
- [29] Cooper G.J. Interpolation and Quadrature Methods for Ordinary Differential Equations. *Math. Comp.*, (22):69–76, 1968.

-
- [30] Cooper G.J. Stability of Runge-Kutta Methods for Trajectory Problems. *Journal of Numerical Analysis*, (7):1–13, 1987.
- [31] Courant R. and Hilbert D. *Methoden der mathematischen Physik*. Springer, 4th edition, 1993.
- [32] Crisfield M.A. A Consistent Co-rotational Formulation for Non-linear, Three-Dimensional, Beam-Elements. *Comp. Meth. Appl. Mech. Engrg.*, 81:131–150, 1990.
- [33] Crisfield M.A. *Nonlinear Finite Elements Analysis of Solids and Structures*, volume 1. Wiley, New York, 1991.
- [34] Crisfield M.A. *Nonlinear Finite Elements Analysis of Solids and Structures*, volume 2. Wiley, New York, 1997.
- [35] Crisfield M.A. and Shi J. A Co-rotational Element/Time-Integration Strategy for Non-linear Dynamics. *Int. J. Numer. Meth. Engrg.*, 37:1897–1913, 1994.
- [36] Crisfield M.A. and Shi J. An Energy Conserving Co-rotational Procedure for Non-linear Dynamics with Finite Elements. *Nonlinear Dynamics*, 9:37–52, 1996.
- [37] Dahlquist G. A special stability problem for linear multistep methods. *BIT*, (3):27–43, 1963.
- [38] Dahlquist G. and Björck Å. *Numerical Methods*. Prentice Hall, Englewood Cliffs, N.J., 1974.
- [39] De Frutos J. and Sanz-Serna J. M. An Easily Implementable Fourth-Order Method for the Time Integration of Wave Problems. *Journal of Computational Physics*, (103):160–168, 1992.
- [40] Dekker K. and Verwer J.G. *Stability of Runge-Kutta methods for stiff nonlinear differential equations*. North-Holland, Amsterdam, 1984.
- [41] Dennis J. E. and Schnabel R. B. *Numerical Methods for Unconstrained Optimization and Nonlinear Equations*. SIAM, 1996.
- [42] Douglas J. Jr. and Dupont T. Galerkin methods for parabolic equations. *SIAM J. Numer. Anal.*, (7):575–626, 1970.
- [43] Ehle B.L. High Order A-Stable Methods for the Numerical Solution of Systems of Differential Equations. *BIT*, (8):276–278, 1968.
- [44] Eriksson K., Estep D., Hansbo P., and Johnson C. *Computational Differential Equations*. Cambridge University Press, 1996.
- [45] Fairweather G. *finite element galerkin methods for differential equations*. Dekker, New York, 1978.
- [46] Föllinger O. *Optimale Regelung und Steuerung*. Oldenbourg, München, 1994.

-
- [47] Fox C. *An Introduction to the Calculus of Variations*. Dover, Mineola, 1987.
- [48] French D.A. and Schaeffer J.W. Continuous Finite Element Methods Which Preserve Energy Properties for Nonlinear Problems. *Applied Mathematics and Computation*, (39):271–295, 1990.
- [49] Garcia Archilla B., Sanz-Serna J.M., and Skeel R.D. Long-time-step Methods for Oscillatory Differential Equations. *SIAM J. Sci. Comput.*, 20(3):930–963, 1998.
- [50] Goldstein H. *Classical Mechanics*. Addison-Wesley, Reading, Massachusetts, 2nd edition, 1980.
- [51] Gonzalez O. *Design and Analysis of Conserving Integrators for Nonlinear Hamiltonian Systems with Symmetry*. PhD Dissertation, 1996.
- [52] Gonzalez O. Time Integration and Discrete Hamiltonian Systems. *Journal of Nonlinear Science*, 6:449–467, 1996.
- [53] Gonzalez O. Exact Energy and Momentum Conserving Algorithms for General Models in Nonlinear Elasticity. *Comput. Methods Appl. Mech. Engrg.*, (190):1763–1783, 2000.
- [54] Gonzalez O. and Simo J. C. On the Stability of Symplectic and Energy-Momentum Algorithms for Nonlinear Hamiltonian Systems with Symmetry. *Comput. Methods Appl. Mech. Engrg.*, (134):197–222, 1996.
- [55] Göttlicher B. *Effiziente Finite-Element-Modellierung gekoppelter starrer und flexibler Strukturbereiche bei transienten Einwirkungen*. PhD Dissertation, 2002.
- [56] Greenspan D. *Discrete Models*. Addison-Wesley, 1973.
- [57] Greenspan D. Conservative Numerical Methods for $\ddot{x} = f(x)$. *Journal of Computational Physics*, 56:28–41, 1984.
- [58] Greenspan D. Completely Conservative, Covariant Numerical Methodology. *Computers and Mathematics with Applications*, 29(4):37–43, 1995.
- [59] Grigorieff R.D. *Numerik gewöhnlicher Differentialgleichungen*, volume 1. B. G. Teubner Stuttgart, 1972.
- [60] Grigorieff R.D. *Numerik gewöhnlicher Differentialgleichungen*, volume 2. B. G. Teubner Stuttgart, 1977.
- [61] Grimm V. *Exponentielle Integratoren als Lange-Zeitschritt-Verfahren für oszillatorische Differentialgleichungen zweiter Ordnung*. PhD Dissertation, 2002.
- [62] Groß M. Time-Stepping Schemes for Nonlinear Hamiltonian Systems Based on the Discontinuous Galerkin Method. Diploma Thesis, UKL/LTM report U00-02, 2000.
- [63] Groß M., Betsch P., and Steinmann P. Comparison of Galerkin Methods applied to Classical Mechanics. UKL/LTM report J00-07, 2000.

-
- [64] Hairer E. and Wanner G. *Solving Ordinary Differential Equations: Stiff Problems*, volume 2. Springer, 1991.
- [65] Hairer E., Nørsett S., and Wanner G. *Solving Ordinary Differential Equations: Non-stiff Problems*, volume 2. Springer, 1991.
- [66] Hamming R. W. *Numerical Methods for Scientists and Engineers*. McGraw-Hill, 2nd edition, 1973.
- [67] Hansbo P. A Note on Energy Conservation for Hamiltonian Systems Using Continuous Time Finite Elements. *Commun. Numer. Meth. Engrg.*, (17):863–869, 2001.
- [68] Henrici P. *Discrete Variable Methods in Ordinary Differential Equations*. Wiley, New York, 1962.
- [69] Hestenes M.R. *Calculus of Variations and Optimal Control Theory*. Wiley, New York, 1966.
- [70] Hinton E., Rock T., and Zienkiewicz O.C. A note on Mass Lumping and Related Processes in the Finite Element Method. *Earthquake Engineering and Structural Dynamics*, (4):245–249, 1976.
- [71] Hirschfelder J.O., Curtiss C.F., and Bird R.B. *The molecular theory of gases and liquids*. Wiley, New York, 1967.
- [72] Hoff C. and Pahl P.J. Development of an implicit method with numerical dissipation from a generalized single-step algorithm for structural dynamics. *Computer Methods in Applied Mechanics and Engineering*, 67:367–385, 1988.
- [73] Hoffman K. and Kunze R. *Linear Algebra*. Prentice-Hall, 2th edition, 1971.
- [74] Holzapfel G.A. *Nonlinear Solid Mechanics*. Wiley, 2000.
- [75] Holzmann G., Meyer H., and Schumpich G. *Technische Mechanik*, volume 2. Teubner, 7th edition, 1991.
- [76] Hughes T. J. R. *The Finite Element Method*. Dover, Mineola, New York, 2000.
- [77] Hughes T. J. R., Caughey T. K., and Liu W. K. Finite-Element Methods for Nonlinear Elastodynamics which Conserve Energy. *Journal of Applied Mechanics*, 45:366–370, 1978.
- [78] Hughes T.J.R. and Hulbert G.M. Space-time finite element methods for elastodynamics: Formulations and error estimates. *Comput. Meth. Appl. Mech. Engrg.*, 66:339–363, 1988.
- [79] Hulbert G.M. Time finite element methods for structural dynamics. *International Journal for Numerical Methods in Engineering*, 33:307–331, 1992.
- [80] Hulbert G.M. A unified set of single-step asymptotic annihilation algorithms for structural dynamics. *Comput. Meth. Appl. Mech. Engrg.*, 113:1–9, 1994.

-
- [81] Hulme B. L. Discrete Galerkin and Related One-Step Methods for Ordinary Differential Equations. *Mathematics of Computation*, 26(120):881–891, 1972.
- [82] Hulme B. L. One-Step Piecewise Polynomial Galerkin Methods for Initial Value Problems. *Mathematics of Computation*, 26(118):415–426, 1972.
- [83] Isaacson E. and Keller H.B. *Analyse numerischer Verfahren*. Harri Deutsch, 1973.
- [84] Iserles A. On the global error of discretization methods for highly-oscillatory ordinary differential equations. *BIT*, (42):561–599, 2002.
- [85] Iserles A. Think globally, act locally: solving highly-oscillatory ordinary differential equations. *Appl. Num. Anal.*, (43):145–160, 2002.
- [86] Johnson C. *Numerical Studies of Partial Differential Equations by the Finite Element Method*. Cambridge University Press, 1987.
- [87] Johnson C. Discontinuous Galerkin finite element methods for second order hyperbolic problems. *Computer Methods in Applied Mechanics and Engineering*, 107:117–129, 1993.
- [88] Johnson C., Nävert U., and Pitkäranta J. Finite element methods for linear hyperbolic problems. *Computer Methods in Applied Mechanics and Engineering*, 45:285–312, 1984.
- [89] Kane C., Marsden J.E., and Ortiz M. Symplectic-energy-momentum preserving variational integrators. *Journal of Mathematical Physics*, 40(7):3353–3371, 1999.
- [90] Kane C., Marsden J.E., Ortiz M., and West M. Variational integrators and the Newmark algorithm for conservative and dissipative mechanical systems. *Int. J. Numer. Meth. Engrg.*, (49):1295–1325, 2000.
- [91] Klingbeil E. *Variationsrechnung*. BI-Wissenschaftsverlag, Mannheim, 1988.
- [92] Kowalsky H.-J. *Lineare Algebra*. de Gruyter, 9th edition, 1979.
- [93] Kuypers F. *Klassische Mechanik*. VCH-Verlag, 2nd edition, 1988.
- [94] LaBudde R. A. and Greenspan D. Discrete Mechanics - A General Treatment. *Journal of Computational Physics*, 15:134–167, 1974.
- [95] LaBudde R. A. and Greenspan D. Energy and Momentum Conserving Methods of Arbitrary Order for the Numerical Integration of Equations of Motion, I. Motion of a Single Particle. *Numer. Math.*, 25:323–346, 1976.
- [96] LaBudde R. A. and Greenspan D. Energy and Momentum Conserving Methods of Arbitrary Order for the Numerical Integration of Equations of Motion, II. Motion of a System of Particles. *Numer. Math.*, 26:1–16, 1976.
- [97] Lancaster P. *Theory of matrices*. Academic Press, New York, 1969.

-
- [98] Lasaint P. and Raviart P.A. On a finite element method for solving the neutron transport equation. In Carl de Boor, editor, *Mathematical Aspects of Finite Elements in Partial Differential Equations*, pages 89–123. Academic Press, 1974.
- [99] Laursen T. A. and Meng X. N. A New Solution Procedure for Application of Energy-Conserving Algorithms to General Constitutive Models in Nonlinear Elastodynamics. *Comput. Methods Appl. Mech. Engrg.*, 190:6309–6322, 2001.
- [100] Lew A., Marsden J.E., Ortiz M., and West M. Asynchronous Variational Integrators. *Arch. Rational Mech. Anal.*, 167(2):85–146, 2003.
- [101] Lorenz F. *Lineare Algebra*, volume 1. Wissenschaftsverlag, 3rd edition, 1991.
- [102] Lubich Ch. Integration of stiff mechanical systems by Runge-Kutta methods. *ZAMP*, (44):1022–1053, 1993.
- [103] Malvern L.E. *Introduction to the Mechanics of a Continuous Medium*. Prentice-Hall, Englewood Cliffs, N.J., 1969.
- [104] Marsden J.E. *Lectures on Mechanics*. Cambridge University Press, 1992.
- [105] Marsden J.E. and Hughes T.J.R. *Mathematical Foundations of Elasticity*. Dover, New York, 1994.
- [106] Marsden J.E. and Ratiu T.S. *Introduction to Mechanics and Symmetry*. Springer, New York, 1999.
- [107] Neumann J. and Schweizerhof K. Analysis of shell structures under transient loading using adaptivity in time and space. In *European Conference on Computational Mechanics*, 1999.
- [108] Neumann J. and Schweizerhof K. Analysis of Shell Structures under Transient Loading using Adaptivity in Time and Space. *Computers and Structures*, (79):2117–2131, 2001.
- [109] Oden J.T. *Finite Elements of Nonlinear Continua*. McGraw-Hill, 1972.
- [110] Ogden R.W. *Non-Linear Elastic Deformations*. Wiley, Chichester, 1984.
- [111] Oliva W.M. *Geometric Mechanics*. Springer, New York, 2002.
- [112] Peng X. and Crisfield M.A. A Consistent Co-rotational Formulation for Shells Using The Constant Stress/ Constant Moment Triangle. *Int. J. Numer. Meth. Engrg.*, 35:1829–1847, 1992.
- [113] Podio Guidugli P. A Primer in Elasticity. *Journal of Elasticity*, 58(1), 2000.
- [114] Powell M.J.D. *Approximation theory and methods*. Cambridge University Press, Cambridge, 1981.

-
- [115] Reich S. *Dynamical Systems, Numerical Integration, and Exponentially Small Estimates*. Preprint SC 98-19, 1998.
- [116] Richtmyer R.B. and Morton K.W. *Difference Methods for Initial-Value Problems*. Interscience, New York, 2nd edition, 1967.
- [117] Ruge P. Hybrid time-finite-elements with time-step-adaption by discontinuity control. *Computational Mechanics*, 17:392–397, 1996.
- [118] Sanz Serna J.M. Runge-Kutta Schemes for Hamiltonian Systems. *BIT*, 28:877–883, 1988.
- [119] Schwarz H. *Numerische Mathematik*. B. G. Teubner Stuttgart, 3rd edition, 1993.
- [120] Simo J. C. and Gonzalez O. Assessment of Energy-Momentum and Symplectic Schemes for Stiff Dynamical Systems. In *American Society of Mechanical Engineers*, New Orleans, Louisiana, 1993. ASME Winter Annual Meeting.
- [121] Simo J. C. and Gonzalez O. Recent Results On The Numerical Integration Of Infinite-Dimensional Hamiltonian Systems. In Hughes T.J.R., Onate E., and Zienkiewicz O.C., editors, *Recent Developments in Finite Element Analysis*, pages 255–271, Barcelona, Spain, 1994. International Center of Numerical Methods in Engineering.
- [122] Simo J.C., Lewis D., and Marsden J.E. Stability of Relative Equilibria. Part I: The Reduced Energy-Momentum Method. *Arch. Rational Mech. Anal.*, (115):15–59, 1991.
- [123] Simo J.C., Tarnow N., and Wong K.K. Exact Energy-Momentum Conserving Algorithms and Symplectic Schemes for Nonlinear Dynamics. *Comput. Methods Appl. Mech. Engrg.*, (100):63–116, 1992.
- [124] Simo J.C., Posbergh T.A., and Marsden J.E. Stability of Relative Equilibria. Part II: Application to Nonlinear Elasticity. *Arch. Rational Mech. Anal.*, (115):61–100, 1991.
- [125] Simo J.C. and Tarnow N. The Discrete Energy-Momentum Method. Conserving Algorithms for Nonlinear Elastodynamics. *Z. angew. Math. Phys.*, (43):757–792, 1992.
- [126] Simo J.C. and Tarnow N. A New Energy and Momentum Conserving Algorithm for The Non-Linear Dynamics of Shells. *Int. J. Numer. Methods Engrg.*, 37:2527–2549, 1994.
- [127] Simo J.C. and Wong K.K. Unconditionally Stable Algorithms For Rigid Body Dynamics That Exactly Preserve Energy and Momentum. *Int. J. Numer. Methods Engrg.*, 31:19–52, 1991.
- [128] Stoer J. *Numerische Mathematik*, volume 1. Springer, 7th edition, 1994.

-
- [129] Stoer J. and Bulirsch R. *Numerische Mathematik*, volume 2. Springer, 3rd edition, 1990.
- [130] Strang G. and Fix G.J. *An Analysis of the Finite Element Method*. Prentice-Hall, Englewood Cliffs, N.J., 1973.
- [131] Stroud A.H. *Numerical Quadrature and Solution of Ordinary Differential Equations*. Springer, 1974.
- [132] Stuart A. M. and Humphries A. R. *Dynamical Systems and Numerical Analysis*. Cambridge University Press, 1998.
- [133] Sunyk R. *On Aspects of Mixed Continuum-Atomistic Material Modelling*. PhD Dissertation, 2003.
- [134] Sussman G.J. and Wisdom J. Chaotic evolution of the solar system. *Science*, (257):56–62, 1992.
- [135] Swartz B. and Wendroff B. Generalized Finite-Difference Schemes. *Math. Comp.*, (23):37–49, 1969.
- [136] Tarnow N. *Energy and Momentum Conserving Algorithms for Hamiltonian Systems in the Nonlinear Dynamics of Solids*. PhD Dissertation, 1993.
- [137] Tarnow N. and Simo J. C. How to render second order time-stepping algorithms fourth order accurate while retaining the stability and conservation properties. *Comput. Meth. Appl. Mech. Engrg.*, (115):233–252, 1994.
- [138] Thomee V. *Galerkin Finite Element Methods for Parabolic Problems*. Springer, Berlin, 1997.
- [139] Weisstein E.W. *CRC Concise Encyclopedia of Mathematics*. CRC, 2nd edition, 2002.
- [140] Wendlandt J.M. Mechanical Integrators Derived from a Discrete Variational Principle. *Physica D*, (106):223–246, 1997.
- [141] Wood W.L. *Practical Time-stepping Schemes*. Oxford University Press, New York, 1990.
- [142] Wriggers P. *Nichtlineare Finite-Elemente-Methoden*. Springer, 2001.
- [143] Wright K. Some Relationships between Implicit Runge-kutta, Collocation and Lanczos τ Methods, and their Stability Properties. *BIT*, (10):217–227, 1970.
- [144] Zeidler E. *Teubner-Taschenbuch der Mathematik*, volume 1. B. G. Teubner Stuttgart, 1996.
- [145] Zhong G. and Kang F. On the Approximation of Linear Hamiltonian Systems. *Journal of Computational Mathematics*, 6(1):88–97, 1988.

-
- [146] Zhong G. and Marsden J.E. Lie Poisson Hamilton Jacobi Theory and Lie Poisson Integrators. *Physics Letters A*, 133(3):134–139, 1988.
- [147] Zhong H.G. and Crisfield M.A. An Energy Conserving Co-rotational Procedure for the Dynamics of Shell Structures. *Engrg. Comput.*, 15(5):552–576, 1998.
- [148] Zienkiewicz O.C. and Taylor R.L. *The Finite Element Method*. McGraw-Hill, New York, 1991.

Lebenslauf

Name: Michael Groß
Geburtsdatum: 10.7.1971
Geburtsort: Rockenhausen
Anschrift: 67728 Münchweiler, Rosenstraße 9
Familienstand: verheiratet

Schulbildung: 1977-1979 Grundschule, Münchweiler
1979-1981 Campschule, Abu Kammash, Libyen
1981-1986 Hauptschulabschluß, Hauptschule Winnweiler
1986-1989 Fachschulreife,
Meisterschule für Handwerker, Kaiserslautern
1989-1992 Hochschulreife,
Technisches Gymnasium, Kaiserslautern

Hochschulbildung: 1992-1994 Informatik, TU Kaiserslautern
1994-2000 Diplom, Maschinenbau, TU Kaiserslautern,
Vertiefungsrichtung *Theoretische Grundlagen*
2000-2004 Wissenschaftlicher Mitarbeiter,
Lehrstuhl für Technische Mechanik (LTM),
TU Kaiserslautern
2004 Promotion, Maschinenbau, TU Kaiserslautern

Berufsausbildung: 1986-1989 Gesellenprüfung als Elektromechaniker,
Meisterschule für Handwerker, Kaiserslautern

Praktika: 1985 Berufsvorbereitungspraktikum,
Zentrale Elektronik-Werkstatt, TU Kaiserslautern
1989 Berufsausbildungspraktikum,
MD Papier GmbH, Dachau
1997 Hochschulpraktikum,
Bereich *Versuch Ottomotoren*, BMW Group